THÈSE POUR OBTENIR LE GRADE DE DOCTEUR
DE L'UNIVERSITÉ DE MONTPELLIER

En Mathématiques et modélisation

École doctorale I2S - Information, Structures, Systèmes

Unité de recherche IMAG - Institut Montpelliérain Alexander Grothendieck

Numerical study of dispersive shallow water models

Présentée par Meriem ZEFZOUF

Le 05/07/2022

Sous la direction de Fabien MARCHE

Devant le jury composé de

Fabien MARCHE	MC	Université de Montpellier	Directeur
Bruno KOOBUS	Pr	Université de Montpellier	Président du jury
Bijan MOHAMMADI	Pr	Université de Montpellier	Examinateur
Maria KAZAKOVA	MC	Université de Savoie	Examinatrice
Daniel LE ROUX	Pr	Université de Lyon 1	Rapporteur
Lisl WEYNANS	MC	Université de Bordeaux	Rapporteur

UNIVERSITÉ DE MONTPELLIER

Remerciements

Tout d'abord, je tiens à exprimer ma plus profonde gratitude à mon directeur de thèse: Fabien Marche. Avec sa gentillesse et son expérience, il m'a bien guidé et apporté son soutien tout au long de la préparation de la thèse. Je le remercie vivement pour sa gentillesse, ses encouragements et ses conseils.

Je tiens à remercier chaque membre de jury de ma thèse. Je remercie chaleureusement Daniel Le Roux et Lisl Weynans d'avoir accepté de rapporter ma thèse et pour leurs précieuses remarques qui ont enrichi ce manuscrit. De plus, je voudrais remercier Bruno Koobus d'avoir accepté de présider le jury, ainsi que Maria Kazakova et Bijan Mohammadi d'avoir accepter de participer au jury de thèse.

Merci à mes collègues de bureau, Corina keller, Alvaro Mateos Gonzalez, Daniel Castanon Quiroz, Stéven Devaux, Alan Pinoy, Florent Miralles et Hermes Lanjoinie, qui m'ont donné un environment agréable de travail.

Merci aux doctorants et post-doctorants, Juliette Veuillez, Ivan Raskin, Nathan Lombard, Victor Moulard, Daniel Castanan Quiroz, Saghar Heidari, Marien Harbot, Ali Haidar, Ibrahim Bouzalmat, Tran Trung Ngheim, Tom Ferragut, Zakaria Bouchegoura, Abdolrahim Ibrahim, Gwanael Peltier, André Harnist, Tiffany Cherchi, Tanguy Lefort, Pablo Montealegre et tous les autres. Je leurs souhaite à toutes et à tous bonne continuation, et bonne chance à celles et à ceux qui soutiendront dans un avenir proche.

Je remercie vivement l'équipe internationale, Samia Louchene, Thiziri Moulla, Zaineb Smida, Radia Bouabdallah, ainsi que Antonia Jabbour et Morgane Garreau pour les bons moments passés ensemble. Je leur souhaite une très bonne continuation.

Je remercie chaleureusement ma meilleure amie Sara Maouche, ta connaisance était l'une des belles choses qui m'arrivée en France.

Un grand merci a mes amies Noubough Alhaj sleiman et Ahlem Derridj pour leur soutien, leur temps et leurs encouragements.

J'adresse mes sincères remerciements à mes enseignants de l'université El Arbi Ben M'Hidi,

d'Oum Bouaghi, notamment Hadjou Ibrahim et Merazga Nabil, qui m'ont permis de voir les mathématiques autrement grâce a leurs grandes compétences, merci à Dehilis Sofiane, qui m'as aidé pour inscrire au master que j'ai failli rater, merci à Oussaeif Taki Eddine qui m'a beaucoup aidé à choisir mon sujet de thèse et qui m'as encouragé de travailler sur ce thème de recherche, merci à Namir Ghoraf, merci à Sihem Guerarra et merci à tous les autres. Vous m'avez appris tout ce qu'il fallait pour pouvoir enseigner à mon tour. Merci pour vos cours, votre temps, votre pédagogie, votre gentillesse et vos conseils.

Mille mercis à ma mère, pour tout ce qu'elle a fait pour moi. Je remercie du fond du coeur mes soeurs et mes frères pour leurs encouragements.

Finallement, j'adresse mes pensée à mon meilleur enseignant Diar Ahmed, qui est partit trop vite, sans que je puisse lui dire adieu. Sa présence était une source de force, de motivation, de joie pour moi. Adorable, joyeux, très gentil, très généreux, un enseignant qui faisait ses cours dans la bonne humeur, très proche de ces étudiants et il n'hésite jamais à les aider. J'aurais voulu partager au moins un dernier instant avec lui. Je ne l'oublira jamais. L'absence reste l'absence, les souvenirs demeurent. Ils nous aident à reprendre courage.

Résumé. Dans le contexte actuel de réchauffement climatique, il est important de disposer d'outils mathématiques performants et précis permettant de modéliser et simuler les phénomènes naturels extrêmes dont la fréquence d'occurrence augmente. En particulier, l'étude des risques liés à la propagation et aux transformations des vagues en milieu littoral devient fondamentale. Pour y parvenir, il est nécessaire de mettre au point et d'étudier : i) d'une part des modèles mathématiques bien posés, traduisant avec fidélité les processus physiques impliqués, ii) d'autre part des méthodes numériques adaptées aux particularités des modèles proposés et permettant de réaliser des simulations numériques pertinentes.
Ainsi, nous nous intéressons dans cette thèse au régime d'écoulement particulier "shallow water" et travaillons avec des modèles asymptotiques formant des systèmes d'équations aux dérivées partielles dispersives, incluant des effets fortement non-linéaires. Nous procédons à la conception et à l'analyse de formulations discrètes de type éléments-finis discontinus pour des modèles de type Green-Naghdi, incluant de nouveaux termes avec vorticité générale, permettant de prendre en compte les interactions non-linéaires entre vagues et courants.

Abstract. In the current context of global warming, the development of new strategies for preventing risks of coastal submersion associated with storms becomes crucial. Such strategies should rely on accurate numerical simulations. To achieve this, it is necessary on one hand to work with suitable mathematical models, with a good description of all the physical processes at stake, and on the other hand to design new numerical methods able to capture the particular assets of the models. Hence, the goal of this work is to contribute to the development of new numerical tools dedicated to the approximations of several shallow water asymptotics with weakly dispersive and fully nonlinear effects: namely the Green-naghdi equations and the rotational Green-Naghdi equations which include new terms able to account for nonlinear wave-current interactions. We develop two new discrete formulations belonging to the family of discontinuous Galerkin schemes: one for the elliptic problem associated with the Green-Naghdi dispersive terms, which is proved to be coercive, leading to an invertible matrix, and one for the rotational Green-Naghdi equations, ensuring the positivity of the water height and the enstrophy.

Contents

1 Introduction **9**
- 1.1 Modélisation . . . 9
- 1.2 Discrétisation . . . 14

2 Derivations and Notations **19**
- 2.1 Derivation of shallow water models . . . 19
  - 2.1.1 Vertically averaged free surface Euler equations . . . 19
  - 2.1.2 Irrotational flows . . . 23
  - 2.1.3 Rotational flows . . . 29
  - 2.1.4 Solitary wave solutions for rotational SGN equations . . . 50
- 2.2 Introduction to DG methods . . . 51
  - 2.2.1 Preliminary notations, definitions and results . . . 52
  - 2.2.2 Diffusion-reaction problem . . . 55
  - 2.2.3 Shallow Water equations . . . 59

3 Main results **63**
- 3.1 A new SWIP-DG formulation for SGN equations . . . 63
- 3.2 A robust SWIP-DG formulation for rotational SGN equations . . . 67

4 A New SWIP-Discontinuous Galerkin formulation for the SGN equations **73**
- 4.1 Introduction . . . 74
- 4.2 The Serre-Green-Naghdi equations . . . 76
- 4.3 Discrete formulations . . . 80
  - 4.3.1 Setting and notations . . . 80
  - 4.3.2 Symmetric and Weighted interior Penalty discrete bilinear form . . . 81
  - 4.3.3 Discrete gradient and Laplace operators . . . 82
  - 4.3.4 The discrete problem . . . 83
  - 4.3.5 Interface fluxes and well-balancing . . . 84
  - 4.3.6 Time discretization . . . 85
  - 4.3.7 Positivity of the water height . . . 85
  - 4.3.8 Well-posedness of the discrete elliptic sub-problem . . . 86
  - 4.3.9 Arbitrary order well-balancing property . . . 92
- 4.4 Numerical validations . . . 93
  - 4.4.1 Solitary wave propagation . . . 93
  - 4.4.2 Head-on collision of solitary waves . . . 94

4.4.3 One dimensional dispersive dam-break problem . . . 94
4.4.4 Reflection of solitary waves at vertical walls . . . 96
4.4.5 Shoaling of solitary waves . . . 98
4.5 Conclusion . . . 101

5 Discontinuous Galerkin approximations of rotational SGN equations 103
5.1 Introduction . . . 104
5.2 Serre-Green-Naghdi equations with vorticity . . . 106
5.2.1 The Serre-Green-Naghdi equations for irrotationnal flows . . . 106
5.2.2 Serre-Green-Naghdi equations for rotational flows . . . 107
5.2.3 Reformulation of the SGNV equations . . . 110
5.3 Discrete formulations . . . 111
5.3.1 Setting and notations . . . 111
5.3.2 The semi-discrete problems . . . 113
5.3.3 Interface fluxes . . . 114
5.3.4 Time discretization . . . 115
5.3.5 Main properties . . . 116
5.4 Numerical validation and applications . . . 121
5.4.1 Rotational solitary wave with constant vorticity . . . 121
5.4.2 Rotational solitary wave with general vorticity . . . 121
5.4.3 Collision of rotational solitary waves . . . 123
5.4.4 Shoaling of rotational solitary waves . . . 125
5.4.5 Run-up of rotational solitary waves . . . 128

6 Conclusion et perspectives 131
.

Chapter 1

Introduction

1.1 Modélisation

Les zones littorales proposent une richesse environnementale indéniable. Elles sont toutefois soumises a de fortes pressions de développement, une croissance démographique considérable et une augmentation des activités économiques et récréatives. Tout ceci, rapporté à la fragilité des environnements terrestres et marins , doit entrainer une réflexion dans la perspective de la prédiction de la vulnérabilité dans un contexte de réchauffement climatique, et d'un développement durable.
La notion de *vulnérabilité induite par les changements climatiques* est définie par le GIEC (Groupe d'experts Intergouvernemental sur l'Evolution du Climat) comme étant la combinaison de la sensibilité aux variations climatiques, la probabilité d'un changement climatique adverse et la capacité d'adaptation du système. Pour chacune de ces composantes, des indices peuvent êtres construits et combinés. Cependant, des challenges importants restent encore à relever, en particulier l'impact d'un changement climatique adverse et l'interprétation de la vulnérabilité au travers de situations variées. Comme mis en évidence par le GIEC dans le cadre d'études à l'échelle globale, les systèmes côtiers devraient être fortement vulnérables aux changements climatiques. Dans ces zones, les phénomènes d'érosion et de submersion marine sont parmi les conséquences les plus importantes de la remontée du niveau marin, et à ce titre, les côtes métropolitaines françaises sont particulièrement vulnérables.
Il est donc important d'identifier et d'estimer des indicateurs de vulnérabilité à l'érosion et la submersion marine pour les côtes basses, de l'avant-plage à l'arrière pays, face au changement climatique. Et c'est un problème extrêmement difficile, multi-disciplinaire, à la hauteur des enjeux en question, puisque le système côtier doit être défini dans son ensemble par sa morphologie, ses caractéristiques physiques, l'occupation et l'utilisation de son espace, avec des échelles temporelles qui vont du court-terme (échelle des tempêtes) au long-terme (décennies), tandis que les échelles spatiales iront de quelques dizaines de mètres à plusieurs dizaines de kilomètres.
Le mathématicien a un rôle important à jouer dans le processus de définition de tels indicateurs et la modélisation mathématique en ingénierie côtière et littorale est un domaine de recherche très actif, faisant l'objet de développements théoriques importants, motivés entre autre par la nécessité de mieux comprendre les mécanismes des phénomènes océaniques et d'anticiper leurs impacts sur les côtes, afin d'essayer d'aboutir à une gestion plus efficace des zones littorale. En ce sens, la construction de modèles hydrodynamiques littoraux est particulièrement importante, puisque de

tels modèles sont amenés à jouer un rôle clé dans l'évaluation de la vulnérabilité des côtes aux inondations et à l'érosion.

De façon générale, la description du mouvement des ondes à la surface libre d'un fluide incompressible sous l'influence de la gravité peut se faire au moyen des équations d'Euler à surface libre, dont l'étude théorique à fait l'objet de nombreux travaux [45, 100, 168, 169, 175]. De telles équations tridimensionnelles pour lesquelles le domaine de calcul fait implicitement parti des inconnues du problème, puisque la surface libre évolue au cours du temps, sont toutefois difficiles a mettre en oeuvre pour modéliser et simuler l'ensemble des processus qui interviennent aux échelles spatiales et temporelles évoquées au dessus. Il est donc nécessaire d'exhiber certaines caractéristiques permettant de particulariser les écoulements littoraux, et d'étudier des modèles mathématiques construits en prenant en compte ces particularités, en espérant ainsi simplifier, en un sens à préciser ultérieurement, le modèle d'Euler initial.
Ainsi, la notion d'écoulement en zone littorale est intimement liée à la notion d'*écoulement en eaux peu profondes*, ou encore *shallow water flow* selon la terminologie anglo-saxonne. L'hypothèse *shallow water* usuelle en mécanique des fluides fait référence au fait que l'échelle caractéristique des composantes horizontales de la vitesse de la masse d'eau est grande devant celle de la composante verticale. En mécanique, la prise en compte de cette hypothèse revient à proposer de s'affranchir du calcul de la composante verticale de la vitesse par intégration de celle-ci sur la colonne d'eau dans les équations décrivant l'écoulement considéré. Comme nous le verrons, ceci n'empêche pas de calculer une composante verticale a priori non nulle via l'équation de continuité, sachant qu'elle doit rester "petite", en un sens que nous serons à même de préciser également ultérieurement. Une autre conséquence de l'hypothèse est que les composantes horizontales de la vitesse sont susceptibles d'être constantes sur la verticale puisqu'elles sont intégrées.
En mathématique, le domaine de la *modélisation et de l'analyse asymptotique* permet de prendre en compte ces variations d'échelles au sein des modèles d'équations. Ainsi, dans les chapitres suivants, nous nous concentrons sur le régime d'écoulement *shallow water*, qui est défini en introduisant d'une part une échelle de longueur λ caractéristique des variations horizontales d'un fluide dans un tel domaine, et d'autre part une échelle de profondeur d'eau typique H_0, permettant d'obtenir le paramètre sans dimension suivant :

$$\mu := \frac{H_0^2}{\lambda^2},$$

aussi appelé *paramètre de dispersion* dans la littérature. Un écoulement sera dit vérifiant l'hypothèse *shallow water* lorsque le paramètre de dispersion vérifie :

$$\mu \ll 1.$$

Une autre caractéristique importante des écoulements littoraux est la non-linéarité des transformations des vagues, depuis la zone de *shoaling*, associée au redressement et raidissement des vagues, avant le déferlement, lorsque la profondeur diminue) au jet de rive, en passant bien entendu par le point de déferlement et la zone de surf. En effet, l'utilisation de modèles simplifiés linéaires ne permet pas de traduire la dynamique observée durant ces différentes étapes entre l'arrivée de la houle en zone intermédiaire et le phénomène de *run-up* sur la plage ou contre une structure de protection. Ceci justifie en particulier l'introduction d'un deuxième paramètre sans dimension,

important pour l'étude qui va suivre, à savoir le paramètre de non-linéarité :

$$\varepsilon := \frac{a_0}{H_0},$$

où a_0 est une grandeur caractéristique permettant de quantifier l'amplitude des vagues observées en surface. Prendre en compte l'ensemble des non-linéarités observées dans un tel écoulement revient ainsi à laisser à ε la possibilité de devenir grand:

$$\varepsilon = O(1), \tag{1.1}$$

alors qu'un écoulement caractérisé par de faibles valeurs de ε, à savoir

$$\varepsilon \ll 1,$$

sera qualifié de *faiblement non-linéaire*.

Les équations de *Saint-Venant*, décrites de manière heuristique en 1871 dans [143], et aussi appelées *Nonlinear Shallow Water equations* (NSW) en anglais, représentent aujourd'hui certainement le modèle non-linéaire de type shallow water le plus utilisé. Ces équations se présentent sous la forme d'un *système de lois de conservations hyperboliques non-linéaires du premier ordre*, couplant l'évolution temporelle de l'élévation de la surface à la composante horizontale moyenné verticalement de la vitesse. L'étude de ces équations a grandement bénéficié de l'énorme intérêt suscité par cette grande et importante famille d' Equations aux Dérivées Partielles (EDP) auprès d'un grand nombre de chercheurs depuis la seconde moitié du vingtième siècle [102]. Les équations NSW sont utilisées pour modéliser un grand nombre de phénomènes : écoulements littoraux, écoulements fluviaux, ruissellement, inondation ou encore des ruptures de barrages. En ce qui concerne leur application en océanographie littorale, il a été montré que ces équations permettaient de décrire de manière très précise le phénomène de déferlement des vagues dans la zone de surf, où la vague déferlée est assimilée à un ressaut hydraulique (onde de choc), se propageant à une vitesse calculée par les relations de Rankine-Hugoniot associée au système. Se forme alors un profil caractéristique de vague déferlée dans la zone de surf, dit *en dents de scie*, se propageant jusqu'au rivage avec une diminution d'amplitude due à la dissipation d'énergie au travers l'onde de choc. De tels transferts d'énergie sont en effet représentés de manière très fine par la structure hyperbolique du système et la diminution de l'entropie associée. A noter que les équations de Saint-Venant linéaires sont bien entendues plus simples à étudier et la théorie des systèmes hyperboliques linéaires est complète, contrairement aux systèmes non-linéaires, mais elles ne permettent pas de décrire l'ensemble des processus, hautement non-linéaires, observés dans la zone de surf.
Dans le Chapitre 2, nous procédons à la dérivation complète des équations NSW à partir des équations d'Euler à surface libre, par un procédé de développement asymptotique et d'intégration selon la direction verticale, et nous observons que la dérivation de telles équations revient à négliger les termes d'ordre μ au sein du développement asymptotique, tout en retenant la non-linéarité des processus (1.1).

Toutefois, aussi pertinentes et efficaces en terme de modélisation et simulation que soient les équations NSW, et même si l'expérience pratique tend à montrer qu'elles peuvent être utilisées

avec succès dans des configurations d'écoulements parfois à la limite de leur domaine de validité, les équations NSW ne peuvent pas modéliser convenablement les processus observables en *zone de shoaling*, juste en amont de la zone de déferlement. Cette limitation est justement liée à la nature hyperbolique des équations NSW et à la négligence des termes d'ordre μ dans le processus de construction de l'asymptotique. En effet, la prise en compte de ces termes d'ordre μ dans les équations revient à modéliser certains *effets de dispersion* correspondant, d'une certaine manière, à une description implicite (et partielle) de la variabilité verticale de l'écoulement. La dispersion est un phénomène bien connu en mécanique ondulatoire, correspondant à une situation de propagation d'ondes au sein d'un *media* où des longueurs d'onde différentes se propagent à des vitesses différentes. Ce phénomène joue bien entendu un rôle primordial dans l'étude de la propagation en zone littorale, lorsque la profondeur de l'écoulement conditionne fortement sa dynamique globale. En particulier, dans l'étude des vagues au voisinage du déferlement, la dispersion permet de venir contrebalancer les effets non-linéaires des transformations des ondes de surface, induisant ainsi un phénomène de déformation caractéristique des vagues (raidissement des vagues) associé à la diminution de la profondeur, à l'approche du point de déferlement. Ainsi, en un certain sens, la prise en compte des effets dispersifs dans les équations permets d'étendre le domaine de validité des équations NSW, depuis la zone de surf jusqu'à la zone de levée.
Ainsi, de nombreuses équations de type shallow-water, non-linéaires et faiblement dispersives ont été introduites puis étudiées dans la littérature, telles les équations de KdV [151] ou encore de Boussinesq [24, 131]. Les équations de type Boussinesq ont la particularité de prendre en compte les termes d'ordre μ ($\mu \ll 1$) dans la dérivation, tout en introduisant une hypothèse de *faible non-linéarité* : le paramètre ε est supposé du même ordre de grandeur que μ, ce qui permet de simplifier la dérivation et d'obtenir des équations certes plus complexes que NSW, mais toutefois moins complexes que celles construites sans simplification. Notons également que ces équations peuvent être *optimisées* assez facilement, en introduisant des termes d'un ordre asymptotique négligeable, mais qui permettent de corriger les propriétés dispersives des équations pour les faire correspondre avec celles des équations d'Euler sur une plus large gamme de longueur d'onde, voir par exemple [112, 126]. Mais même avec de telles optimisations, il a été observé que les équations de type Boussinesq n'étaient en général pas suffisamment non-linéaires pour permettre une représentation fidèle des profils de vagues au voisinage du déferlement [75]. Ainsi, l'objectif est de construire un modèle qui prenne en compte les effets dispersifs au premier ordre ($\mu \ll 1$), sans limiter l'ordre de grandeur des non-linéarités modélisées ($\varepsilon = O(1)$). De telles équations ont été obtenues dans [147] en 1953 dans le cas 1d, puis dans [74] en 1976 dans le cas 2d. Ces équations, dites de Serre-Green-Naghdi (SGN), représentent ainsi une étape supplémentaire dans la dérivation d'un modèle adapté à l'océanographie littorale, en supprimant l'hypothèse de faible non-linéarité utilisée pour dériver Boussinesq. Citons aussi les dérivations proposées dans [152], [117] et [146]. Notons également qu'une justification mathématique du modèle SGN a été faite dans [5].

Enfin, il est important de noter que même si les équations SGN améliorent considérablement la modélisation des processus hydrodynamiques littoraux en comparaison avec NSW, il demeure certaines situations importantes pour lesquelles les équations SGN ne permettent pas de retranscrire la totalité des processus physiques qui dominent les caractéristiques observables d'un écoulement. En effet, comme il sera rappelé dans le Chapitre 2, ces équations ont été dérivées avec une hypothèse d'écoulement irrotationnel, c'est à dire sans vorticité, ce qui est cohérent avec une perspective

générale d'étude d'écoulements variant peu dans la direction verticale. Il en est, bien entendu, de même pour les équations NSW ou de Boussinesq. Cependant, dans certaines circonstances (non exceptionnelles), les effets rotationnels peuvent être importants par rapport aux effets non-linéaires et/ou dispersifs déjà modélisés dans SGN, et deviennent donc non négligeables. C'est, par exemple le cas lorsque la vorticité est générée par une dissipation anisotrope de l'énergie due au déferlement des vagues sur des topographies présentant des variations longitudinales. C'est également le cas lorsqu'un champ de vorticité (un courant) vient interagir, de façon non-linéaire, avec les vagues. La vorticité est en effet une clé importante pour comprendre les échanges d'énergie contrôlant les processus physiques au sein de telles interactions. Mentionnons par exemple [72, 121, 130, 155, 156, 174] pour des études et descriptions concernant les interactions entre courants et vagues.
Concernant les modèles, la prise en compte d'une vorticité non nulle, ou au moins de courants de cisaillements, directement au sein des modèles évoqués précédemment, qui sont intégrés selon la verticale, est un problème difficile. Ainsi, plusieurs stratégies visant à décrire la dynamique verticale d'une onde de gravité à la surface d'un fluide en écoulement de type shallow water ont été proposées dans la littérature. Elles sont toutes, en quelque sorte, des stratégies "de contournement" du caractère trop restrictif de l'hypothèse théorique d'écoulement irrotationnel par rapport aux observations. Parmi ces différentes stratégies nous trouvons par exemple: (i) la superposition de plusieurs modèles shallow water sur la verticale en gérant les zones de contacts (modèles dits *multi-couches*, voir par exemple [10, 11, 70]), (ii) des paramétrisation du cisaillement vertical des vitesses (approche dite "quasi-3d", voir par exemple [133]), (iii) des modèles dits *non-hydrostatiques*, voir par exemple [2, 110], (iv) introduction de termes de type *tensions de radiation* afin de décrire l'action des courants comme un forçage sur les vagues (voire par exemple [108]).
Concernant la dérivation de modèles shallow wate prenant en compte la vorticité, mentionnons [35], où des modèles de type Boussinesq et GN avec cisaillement uniforme sont obtenus, [87] pour un modèle à vorticité constante, [123, 160] dans le cas 1d, où la vorticité est responsable de la présence d'un terme supplémentaire dans l'équation de la quantité de mouvement, couplée à l'équation de transport de la vorticité, [181] où un modèle SGN avec termes rotationels est dérivé, ou encore [140] pour un modèle dispersif généralisant SGN au cas des écoulements à cisaillement. Dans [92] l'effet d'un courant cisaillé vertical sur une onde scélérate bi-dimensionnelle est étudié en utilisant une approche basée sur des équations généralisées de Whitham avec un tourbillon constant, et un modèle approximatif de type NSW en présence de tourbillons est ensuite dérivé dans [91]. Citons également [18] où un ensemble d'équations non linéaires en eau peu profonde avec un tourbillon constant est également proposé.
Récemment, une théorie générale est proposée dans [27] avec une généralisation rigoureuse de SGN en présence de vorticité. Ainsi, la dynamique tri-dimensionnelle d'un écoulement shallow water avec vorticité peut être décrite à l'aide d'équations bi-dimensionelles, en utilisant une approche inspirée de la théorie de la turbulence standard, mais sans avoir besoin de modèles de fermeture, grace à la nature asymptotique de SGN. Dans [101], le système SGN rotationel est en outre étudié analytiquement pour obtenir des familles de solutions de type ondes solitaires. Ce sont les modèles SGN avec ou sans vorticité que nous nous proposons d'étudier dans cette thèse.

1.2 Discrétisation

La résolution numérique d'EDP est un domaine qui a naturellement connu de très grands développements depuis la deuxième moitié du vingtième siècle, suivant l'évolution de la puissance de calcul des ordinateurs. Différentes stratégies de discrétisation ont été introduites au fil des années, en tenant compte des particularités des différentes familles d'EDP étudiées. Les méthodes de Différences-Finies (DF) permettent de construire des approximations d'opérateurs différentiels sur des maillages à topologie cartésienne, à partir du développement de Taylor de la solution aux noeuds de la grille de calcul, qui doit donc être suffisamment régulière. Même si ils sont simples à mettre en oeuvre, et s'adaptent facilement à des opérateurs différentiels d'ordre élevé, les schémas DF souffrent d'un certains nombre de limitations inhérentes à l'utilisation de grilles cartésiennes et à la nécessité pour la solution cherchée d'être très régulière. Les méthodes DF sont donc en général peu adaptées aux problèmes impliquant des géométries complexes, ou aux calculs de solutions à faible régularité. Certaines améliorations ont été proposées, telles que les *Différences Finies Généralisées* [76] ou encore l'utilisation de méthodes de type *Frontières Immergées* [120], pour prendre en compte des géométries de frontières plus complexes.

Les méthodes de type Elements-Finis (EF) classiques ont connu un très fort développement dans les années 50, tout d'abord pour des EDP de nature elliptique ou parabolique, essentiellement en mécanique des structures et sous l'impulsion d'ingénieurs, avant d'être étendues à de très nombreux autres domaines d'applications et de voir leurs fondements théoriques solidement établis. Les ingrédients clés des méthodes EF sont d'une part les propriétés d'interpolation des Elements-Finis, et d'autre part l'introduction d'un cadre mathématique fonctionnel rigoureux pour étudier la solution du problème. Un exposé détaillé des principales méthodes EF peut être trouvé dans [68]. Les méthodes EF ont aussi été étendues à certains modèles hyperboliques à l'aide de techniques de stabilisation appropriées, voir par exemple [84]. Parmi les inconvénients identifiés des méthodes EF, notons la nécessité d'assembler et d'inverser la matrice de masse, qui est généralement une matrice pleine dont l'inversion peut être coûteuse.
Les méthodes Volumes-Finis (VF) ont d'abord été développées pour des EDP de nature hyperbolique, avant d'être également étendues à certains problèmes de nature elliptique ou parabolique. L'idée de base, pour des EDP contenant des termes en $\nabla \cdot ()$, est d'utiliser le théorème de flux-divergence pour expliciter les intégrales de volume en intégrales de surface, nommées *flux*. Ces flux sont ensuite évalués aux interfaces entre les volumes finis à l'aide d'une fonction de flux numérique approximants. Puisque le flux entrant dans un volume donné est égal au flux sortant du volume adjacent, de telles méthodes VF sont dites *conservatives* et donc bien adaptées à la résolution de lois de conservation. Des exposés détaillés des méthodes VF peuvent être trouvés dans [105, 158]. Les méthodes EF et VF permettent, en particulier, d'utiliser des maillages non-structurés et même, dans certains cas, des maillages généraux (polyèdriques). Elles sont donc bien mieux adaptées que les schémas DF aux traitement de problèmes avec des géométries complexes. Par ailleurs, ces méthodes autorisent le calcul de solutions présentant possiblement une régularité plus faible qu'avec les méthodes DF, s'appuyant sur des formulations faibles (VF) ou variationnelles (EF). Parmi les inconvénients souvents mentionnés pour les schémas VF, citons le fait que pour obtenir un ordre d'approximation élevé sur des solutions régulières, il est nécessaire d'utiliser de grands stencils, qui peuvent augmenter le coût de calcul et diminuer la robustesse, et aussi réduire l'efficacité parallèle de l'algorithme.

Les bases des méthodes de type *Discontinuous Galerkin* ont été introduites dans les années 70 pour la résolution d'un problème de transport de neutrons [134]. Plus tard, ces méthodes ont été largement développées pour de nombreux problèmes hyperboliques linéaires et non-linéaires, voir par exemple [37, 40], mais aussi pour de nombreux problèmes elliptiques (essentiellement linéaires) et même dispersifs, avec par exemple les méthodes dites *Local Discontinuous Galerkin* (LDG) [39, 41], les méthodes *Interior Penalty Discontinuous Galerkin* (IPDG) qui reposent sur des conditions de continuité imposées faiblement à la solution ou à ses dérivées à travers les interfaces [165], [54], [8], [14], [141]. Une analyse unifiée des méthodes DG pour les problèmes elliptiques est également proposée dans [9]. DG a même été appliquée à des problèmes paraboliques, voir par exemple [86], [67], [65, 66], et plus récemment [113]. Pour les équations de Navier-Stokes compressibles, une extension des méthodes DG a été proposée dans [15] puis d'autres travaux ont suivis.

Cette famille de méthodes possède des caractéristiques communes présentes en partie dans les méthodes EF et VF. Les méthodes DG peuvent être considérées comme une approche FV d'ordre élevé où la solution approchée est exprimée par un polynôme au lieu de fonctions constantes, ou comme des méthodes EF supportant des discontinuités dans les espaces de test en ce qu'elle construit une solution approchée polynomiale par morceaux sur le maillage et discontinue entre les éléments. Ils utilisent des fonctions de base qui sont des fonctions polynomiales sur l'élément mais qui sont discontinues à travers ses frontières. L'échange d'informations entre deux éléments s'effectue à travers les interfaces uniquement au moyen de flux numériques, comme pour les méthodes VF. Chaque cellule est associée à un espace d'approximation local, qui peut être choisi indépendamment des cellules voisines. Un exposé détaillé des principaux aspects mathématiques des méthodes DG peut être trouvé dans [50].

Les équations shallow water ont fait l'objet de très nombreuses études numériques, depuis les équations NSW jusqu'aux équations faiblement dispersives de type Boussinesq et plus récemment SGN. Au cours des dernières décennies, il y a eu beaucoup d'intérêt pour la construction de formulations discrètes des équations NSW à la fois en dimension un et deux de surface. Les équations NSW ont été étudiées pour des problèmes d'océanographie ou d'hydraulique, à l'aide d'un grand nombre de schémas numériques, à savoir, parmi de nombreuses références, des méthodes DF [28, 109], des méthodes VF [4, 94, 142], des méthodes WENO [125, 161], des méthodes EF [81, 83, 124, 159], des méthodes à Distribution de Résidus (DR) [135] ou encore des méthodes DG [3, 47, 145].
La plupart des travaux se sont concentrés sur l'un des deux aspects suivants : i) construire des schémas satisfaisant des propriétés de *well-balancing* pour états stationnaires au repos [13, 173] ou plus généraux [116, 170]. De telles propriétés sont en effet importantes pour pouvoir prendre en compte avec précision et stabilité les variations de la topographie dans les calculs, ii) préserver la positivité de la hauteur d'eau lors de l'évolution. C'est une propriété de stabilité non-linéaire très importante, qui a fait l'objet de nombreuses études pour les diverses méthodes citées plus haut, voir par exemple [12, 17, 32]. A noter que la construction de schémas VF satisfaisant à la fois le *well-balancing* et la positivité de la hauteur d'eau et qui soit d'ordre élevé est un problème difficile.

La construction de méthodes numériques pour les équations de Boussinesq a également fait

l'objet de nombreux travaux. Ces équations ont la particularité de faire intervenir des dérivées partielles d'ordre strictement supérieur à deux, ou bien encore des dérivées croisées temps/espaces, qui compliquent fortement la résolution numérique. La présence dans ces équations [1, 129]

Les équations SGN apportent encore une nouvelle difficulté en comparaison avec les équations de Boussinesq: la présence de termes fortement non-linéaires, et une structure analytique globalement plus compliquée, qui s'avère entrainer un coût de calcul globalement plus important que pour les équations de Boussinesq, à méthodes/maillages équivalents. Les premiers travaux numériques concernaient des méthodes DF, par exemple [6, 164].
Les méthodes FV ont été également appliquées aux équations SGN, pour nouvelle difficulté d'approcher numériquement les termes non-linéaires à l'aide d'inconnues constantes par élément. Une approche VF a par exemple été proposée sur fond plat dans [104], ainsi que des méthodes hybrides VF/DF dans [21, 36, 132], WENO/DF [29, 97] ou encore VF/EF [90]. L'idée de tells approches hybrides consiste à découpler le modèle SGN en deux sous modèles: une partie hyperbolique, traitée par une méthode VF en s'inspirant de travaux déjà développés pour NSW, et une partie dispersive, contenant les termes d'ordre élevés, qui est traité par une méthode plus adaptée.
Des applications de méthodes EF peuvent également être trouvées, voir par exemple [118, 119, 167].
L'approximation numérique des équations SGN par des méthodes DG a été considérée récemment. Les méthodes DG apparaissent comme particulièrement adaptées à la discrétisation des équations SGN. En effet, les méthodes DG offrent un cadre théorique très général permettant de construire des espaces d'approximation adaptés à de nombreux types d'opérateurs différentiels locaux, dont des opérateurs d'ordre élevé. Le traitement des opérateurs non-linéaires peut-être également effectué par une méthode de collocation, en essayant au besoin de limiter l'aliasing par les techniques usuelles utilisée par exemples dans les méthodes spectrales ou éléments-spectraux. De plus, les méthodes DG sont très robustes au voisinage des discontinuités et des forts gradients, tout en permettant d'utiliser des approximations très précises dans les zones où la solution est régulière. Enfin, les méthodes DG peuvent être efficacement parallélisées, ce qui est important pour pouvoir effectuer des simulations à des échelles réalistes (passage à l'échelle).
C'est dans cette optique qu'une première stratégie de discrétisation DG/LDG a été proposée d'abord dans le cas 1d[62] puis en 2d dans [59]. Le traitement de la partie elliptique a ensuite été amélioré dans [51] avec une reformulation des équations permettant d'utiliser une méthode *Symmetric Interior Penalty* (SIP), qui mène à une matrice globale symétrique pour la partie elliptique des équations. Toutefois, même si cette dernière approche est plus performante et robuste, elle souffre toutefois encore d'une importante limitation: il ne parait pas possible de prouver la coercivité de la forme bilinéaire discrète introduite dans [51]. Et en effet, il est possible d'exhiber des cas test manufacturés où la matrice résultant de cette discrétisation est singulière.
C'est donc dans cette perspective que ce situe la première partie des travaux présentés dans cette thèse de doctorat. Présentée au Chapitre 4 de ce manuscript, l'objectif de cette première partie est d'introduire et étudier théoriquement une nouvelle forme bilinéaire symétrique pour équations SGN, permettant de lever cette dernière limitation. Une présentation synthétique de ces travaux est fournie au Chapitre 3.

Enfin, il existe très peu de travaux numériques concernant les modèles SGN prenant en compte la vorticité. Une approche hybride WENO-DF a été utilisée dans [98] pour simuler la propagation

d'ondes solitaires. Un modèle SGN "étendu" en rapport avec celui étudié ici est introduit et utilisé dans [89] en 1d puis dans [137] en 2d. Dans ce modèle, une équation additionnelle sur l'évolution de l'enstrophie $\mathfrak{e}$, mais avec des termes sources additionnels qui sont paramétrisés, est ajoutée aux modèle SGN, afin de modéliser le déferlement et la génération de vorticité. Les méthodes numériques utilisées sont toutefois une extension directe de [59], sans analyse théorique supplémentaires des schémas.
Cette direction de recherche fait donc l'objet de la deuxième partie des travaux présentés dans ce manuscript, avec la construction d'une formulation discrète DG pour les équations SGN a vorticité générale de [25]. Une présentation des principales propriétés de cette nouvelle méthode est fournie dans le Chapitre 3, alors que l'article correspondant est placé dans le Chapitre 5.

Chapter 2

Derivations and Notations

This Chapter is organized as follows. In §2.1, we detail the derivation of various asymptotic shallow water equations from the free surface Euler equations. In §2.1.1 we derive the vertically averaged free surfce Euler equations. In §2.1.2, we aim to derive most known shallow water models, namely, NSW equations, Boussinesq equations, SGN equations in irrotational flows. In §2.1.3, we take non-zero vorticity to derive the SGN equations with constant vorticity in §2.1.3.1, and the SGN equations with general vorticity in §2.1.3.2. We present in §2.1.4, the solitary wave exact solution of SGN equations in presence of vorticity. §2.2 is devoted to the mathematical and numerical analysis of basic elliptic and hyperbolic problems, we introduce the main ingredients needed in the following Chapters.

2.1 Derivation of shallow water models

In this section, we detail the derivation of various shallow water asymptotics from the Euler equations with free surface and the classical irrotational flow assumption. The derivation process is mostly reproduced from [25], with an emphasize put on the 1d case and a more comprehensive presentation of all the computation details, which are generally skipped in [25] for the sake of simplicity. This is also the opportunity to introduce the notations used within all this manuscript.

2.1.1 Vertically averaged free surface Euler equations

Let x, z, and t denote, respectively, the horizontal, vertical, and time coordinates. Denoting by $\zeta(t,x)$ the free surface elevation with respect to its rest state, by $-H_0 + b(x)$ a parametrization of the bottom's variations, by $H(t,x) \coloneqq H_0 + \zeta(t,x) - b(x)$ the water depth, and by $\eta(t,x) \coloneqq H(t,x) + b(x)$ the total free surface elevation. The fluid domain is defined as,

$$\Omega_t = \{(x,z) \in \mathbb{R}^{d+1}, -H_0 + b(x) < z < \zeta(t,x)\}. \tag{2.1}$$

We denote by $\mathbf{U}(t,x,z) \in \mathbb{R}^{d+1}$ the velocity of the fluid, and by $v(t,x,z) \in \mathbb{R}^d$ and $w(t,x,z)$ its horizontal and vertical component respectively, with $\bar{v}$ the vertically averaged horizontal component of v. We write $P(t,x,z) \in \mathbb{R}$ for the pressure at the point $(x,z) \in \Omega_t$, the acceleration of gravity is denoted by $-ge_z$, when $g > 0$ and e_z is the unit upward vector in the vertical direction and the density of the fluid is written ρ. In an incompressible, homogeneous, irrotational and inviscid

fluid under the influence of gravity, the propagation of surface waves is governed by the Euler equations with nonlinear boundary conditions at the surface and at the bottom. The free surface Euler equations can be written as follows,

$$\partial_t \mathbf{U} + \mathbf{U} \cdot \nabla_{x,z} \mathbf{U} = -\frac{1}{\rho} \nabla_{x,z} P - g e_z \quad \text{in} \quad \Omega_t, \tag{2.2a}$$

$$\nabla_{x,z} \cdot \mathbf{U} = 0 \quad \text{in} \quad \Omega_t, \tag{2.2b}$$

$$\nabla_{x,z} \times \mathbf{U} = 0 \quad \text{in} \quad \Omega_t, \tag{2.2c}$$

$$\partial_t \zeta - \mathbf{U}_{|\zeta} \cdot N = 0 \quad \text{on} \quad \{z = \zeta(t,x)\}, \tag{2.2d}$$

$$P_{|\zeta} = P_{atm} = \text{cst} \quad \text{on} \quad \{z = \zeta(t,x)\}, \tag{2.2e}$$

$$\mathbf{U}_{|-H_0+b} \cdot N_b = 0, \tag{2.2f}$$

with

$$\mathbf{U}_{|\zeta} = \mathbf{U}(t,x,\zeta(t,x)) \quad \text{and} \quad N = (-\partial_x \zeta, 1)^T, \tag{2.3a}$$

$$\mathbf{U}_{|-H_0+b} = \mathbf{U}(t,x,-H_0+b) \quad \text{and} \quad N_b = (-\partial_x b, 1)^T. \tag{2.3b}$$

We emphasize that (2.2c) is the irrotationality condition, which is fundamental in the proposed derivation, and which will be removed in §2.1.3. The difficulty of solving the system (2.2a)-(2.2f) appears in the fact that the fluid domain is time-varying with a kinematic boundary at the surface. To deal with this issue, several equivalent formulations were proposed in the literature, such as a Lagrangian formulation in [42] or Zakharov's Hamiltonian formulation [176]. We aim in this chapter to detail a derivation process that starts directly from (2.2a)-(2.2f) with a vertical integration.

From now on, we set $d = 1$. To reformulate the free surface Euler equations in elevation-velocity form, one starts with denoting that any function $u(t,.)$ defined in the fluid domain Ω_t may be decomposed as an vertically averaged component $\bar{u}$ and a zero mean component u^*, as follows,

$$u(t,x,z) = \overline{u}(t,x) + u^*(t,x,z), \tag{2.4}$$

with,

$$\overline{u}(t,x) = \frac{1}{H} \int_{-H_0+b}^{\zeta} u(t,x,z) dz, \quad u^*(t,x,z) = u(t,x,z) - \overline{u}(t,x) \quad \text{and} \quad \int_{-H_0+b}^{\zeta} u^* = 0. \tag{2.5}$$

We have thus,

$$v(t,x,z) = \bar{v}(t,x) + v^*(t,x,z), \tag{2.6}$$

with $\bar{v}(t,x)$ and $v^*(t,x,z)$ are defined as in (2.5). We also recall the Leibniz integration formula,

$$\int_{\varsigma(x)}^{\iota(x)} \partial_x u(t,x,z) dz = \partial_x \int_{\varsigma(x)}^{\iota(x)} u(t,x,z) dz - u_{|\iota} \frac{\partial \iota}{dx} + u_{|\varsigma} \frac{\partial \varsigma}{dx}. \tag{2.7}$$

Integrating vertically (2.2b), one gets

$$w_{|\zeta} - w_{|-H_0+b} = -\partial_x \int_{-H_0+b}^{\zeta} v dz + v_{|\zeta} \partial_x \zeta - v_{|-H_0+b} \partial_x b,$$

and using the boundary conditions (2.2d)-(2.2f) and (2.6), we obtain the mass conservation equation

$$\partial_t \zeta + \partial_x (H\bar{v}) = 0. \tag{2.8}$$

Vertically averaging the horizontal component of (2.2a), one obtains

$$\int_{-H_0+b}^{\zeta} \partial_t v dz + \int_{-H_0+b}^{\zeta} v\partial_x v dz + \int_{-H_0+b}^{\zeta} w\partial_z v dz = -\frac{1}{\rho}\int_{-H_0+b}^{\zeta} \partial_x P dz. \tag{2.9}$$

Then, we look at each term separately

$$\begin{aligned} \int_{-H_0+b}^{\zeta} \partial_t v dz &= \partial_t \int_{-H_0+b}^{\zeta} v dz - v_{|\zeta}\partial_t\zeta + v_{|-H_0+b}\partial_t b, \\ &= \partial_t(H\bar{v}) - v_{|\zeta}\partial_t\zeta, \end{aligned} \tag{2.10}$$

integrating by part and using the incompressible condition (2.2b), one obtains

$$\begin{aligned} \int_{-H_0+b}^{\zeta} w\partial_z v dz &= [wv]_{-H_0+b}^{\zeta} - \int_{-H_0+b}^{\zeta} v\partial_z w dz, \\ &= [wv]_{-H_0+b}^{\zeta} + \int_{-H_0+b}^{\zeta} v\partial_x v dz, \\ &= w_{|\zeta} v_{|\zeta} - w_{|-H_0+b} v_{|-H_0+b} + \int_{-H_0+b}^{\zeta} v\partial_x v dz, \end{aligned}$$

from (2.2d)-(2.2f), one obtains

$$\int_{-H_0+b}^{\zeta} w\partial_z v dz = v_{|\zeta}\partial_t\zeta + v_{|\zeta}^2\partial_x\zeta - v_{|-H_0+b}^2\partial_x b + \int_{-H_0+b}^{\zeta} v\partial_x v dz, \tag{2.11}$$

plugging (2.10) and (2.11) in (2.9), one deduces

$$\partial_t(H\bar{v}) + 2\int_{-H_0+b}^{\zeta} v\partial_x v + v_{|\zeta}^2\partial_x\zeta - v_{|-H_0+b}^2\partial_x b + \frac{1}{\rho}\int_{-H_0+b}^{\zeta} \partial_x P dz = 0, \tag{2.12}$$

using (2.7), we get

$$2\int_{-H_0+b}^{\zeta} v\partial_x v = \int_{-H_0+b}^{\zeta} \partial_x(v^2) dz = \partial_x\Big(\int_{-H_0+b}^{\zeta} v^2 dz\Big) - v_{|\zeta}^2\partial_x\zeta + v_{|-H_0+b}^2\partial_x b. \tag{2.13}$$

Replacing (2.13) in (2.12), one obtains

$$\begin{cases} \partial_t\zeta + \partial_x(H\bar{v}) = 0, \\ \partial_t(H\bar{v}) + \partial_x\Big(\int_{-H_0+b}^{\zeta} v^2\, dz\Big) + \frac{1}{\rho}\int_{-H_0+b}^{\zeta} \partial_x P\, dz = 0. \end{cases} \tag{2.14}$$

Using (2.6), and making use of the assumption that the vertical average of v^* vanishes, we can therefore write

$$\int_{-H_0+b}^{\zeta} v^2 dz = H\bar{v}^2 + \mathbf{R} \quad \text{with} \quad \mathbf{R} := \int_{-H_0+b}^{\zeta} |v^*|^2. \tag{2.15}$$

For the last term of (2.14), integrating the vertical component of the free surface Euler equations (2.2a), and using (2.2e), one readily gets

$$P = P_{atm} + \rho g(\zeta - z) + \int_z^\zeta P_{nh}, \tag{2.16}$$

where

$$P_{nh} = \rho \int_z^\zeta \Big(\partial_t w + v\partial_x w + w\partial_z w\Big). \tag{2.17}$$

Plugging (2.15)-(2.16) in (2.14), we get the vertically averaged Euler equations

$$\begin{cases} \partial_t \zeta + \partial_x(H\bar{v}) = 0, \\ \partial_t(H\bar{v}) + \partial_x(H\bar{v}^2) + gH\partial_x\zeta + \partial_x\Big(\int_{-H_0+b}^{\zeta} |v^*|^2\Big) + \frac{1}{\varepsilon}\int_{-H_0+b}^{\zeta} \partial_x P_{nh} = 0. \end{cases} \tag{2.18}$$

From now, our goal is to express the two last terms in the second equations of (2.18), respectively called in the following *Reynolds-like tensor* and *non-hydrostatic pressure component* defined in (2.17), in terms of ζ and $\bar{v}$, through asymptotic expansions under the shallow water assumption.

The next step is to introduce nondimensionalized equations, relying on the two parameters μ and ε defined in the Introduction section. Let also introduce a typical amplitude a_{bott} of the bottom variations, and the associated dimensionless parameter fo the topography variations

$$\beta := \frac{a_{\text{bott}}}{H_0}. \tag{2.19}$$

Dimensionless variables are introduced as follows,

$$\tilde{x} := \frac{x}{\lambda}, \quad \tilde{z} := \frac{z}{H_0}, \quad \tilde{\zeta} := \frac{\zeta}{a}, \quad \tilde{b} := \frac{b}{a_{\text{bott}}},$$
$$\tilde{v} := \frac{v}{a\sqrt{g/H_0}}, \quad \tilde{w} := \frac{w}{a\lambda/H_0\sqrt{g/H_0}}, \quad \tilde{t} := \frac{t}{\lambda/\sqrt{gH_0}}, \quad \tilde{P} := \frac{P}{\rho g H_0}.$$

We focus in the following on the shallow water regime ($\mu \ll 1$). Within this regime, various sub-regimes can be identified depending on the assumptions made on the nonlinearity parameter ε: small amplitude regime ($\varepsilon \ll 1$) and large amplitude regime ($\varepsilon = O(1)$), the topography parameter β: small amplitude bottom variations ($\beta \ll 1$) and large amplitude ($\beta = O(1)$). The *shallow water* scaling corresponds to the configuration where the wave length λ of the flow is large compared to the typical depth H_0. Dropping the $\tilde{}$, the system (2.2a)-(2.2c) can be written in dimensionless form as follows,

$$\begin{aligned} \partial_t \mathbf{U}^\mu + \frac{\varepsilon}{\mu}\mathbf{U}^\mu \cdot \nabla^\mu_{x,z}\mathbf{U}^\mu &= -\frac{1}{\varepsilon}(\nabla^\mu_{x,z}P + e_z) \quad \text{in } \Omega_t, \\ \nabla^\mu_{x,z} \cdot \mathbf{U}^\mu &= 0 \quad \text{in } \Omega_t, \\ \nabla^\mu_{x,z} \times \mathbf{U}^\mu &= 0 \quad \text{in } \Omega_t, \end{aligned} \tag{2.20}$$

where $\mathbf{U}^\mu$ is the nondimensionalized velocity and Ω_t now stands for the dimensionless fluid domain, defined as

$$\Omega_t = \{(x,z) \in \mathbb{R}^{d+1}, \quad -1 + \beta b(x) < z < \varepsilon\zeta(t,x)\}.$$

Dimensionless form of the boundary conditions at the surface is given by,

$$\partial_t \zeta + \partial_x (H\bar{v}) = 0 \quad \text{and} \quad P_{atm} = 0. \tag{2.21}$$

At the bottom,

$$\mathbf{U}^{\mu}_{|-1+\beta b} \cdot N^{\mu}_{\beta b} = 0, \tag{2.22}$$

with,

$$\mathbf{U}^{\mu}_{|-1+\beta b}(t,x) = \mathbf{U}^{\mu}(t,x,-1+\beta b) \quad \text{and} \quad N^{\mu}_{\beta b} = (-\varepsilon\sqrt{\mu}\partial_x b, 0, 1)^T. \tag{2.23}$$

Dimensionless version of H and $\bar{v}$ are given by,

$$H(t,x) \coloneqq 1 + \varepsilon\zeta(t,x) - \beta b(x), \quad \bar{v}(t,x) = \frac{1}{H}\int_{-1+\beta b}^{\varepsilon\zeta} v(t,x,z)dz,$$

dimensionless form of the horizontal velocity is defined by,

$$v(t,x,z) = \bar{v}(t,x) + \sqrt{\mu}v^*(t,x,z), \tag{2.24}$$

and dimensionless averaged Euler equations are written as,

$$\begin{cases} \partial_t \zeta + \partial_x (H\bar{v}) = 0, \\ \partial_t (H\bar{v}) + \varepsilon\partial_x (H\bar{v}^2) + H\partial_x \zeta + \varepsilon\mu\partial_x (\int_{-1+\beta b}^{\varepsilon\zeta} |v^*|^2) + \frac{1}{\varepsilon}\int_{-1+\beta b}^{\varepsilon\zeta} \partial_x P_{nh} = 0, \end{cases} \tag{2.25}$$

with,

$$P_{nh} = \rho \int_z^{\varepsilon\zeta} (\partial_t w + v\partial_x w + \frac{\varepsilon}{\mu} w\partial_z w). \tag{2.26}$$

2.1.2 Irrotational flows

Let begin with irrotational flows: the effect of vorticity are neglected.

Asymptotic expansion of the velocity field

We can describe the asymptotic expansion of the velocity through the incompressibility and irrotationality conditions, given in the dimensionless form by,

$$\begin{cases} \mu\partial_x v + \partial_z w = 0, \\ \sqrt{\mu}\partial_z v - \sqrt{\mu}\partial_x w = 0, \\ w_{|-1+\beta b} - \mu\beta\partial_x v_{|-1+\beta b} = 0. \end{cases} \tag{2.27}$$

Replacing (2.24) into (2.27), with $\partial_z \bar{v} = 0$, we obtain

$$\mu\partial_x \bar{v} + \mu^{3/2}\partial_x v^* + \partial_z w = 0, \tag{2.28a}$$

$$\mu\partial_z v^* - \sqrt{\mu}\partial_x w = 0, \tag{2.28b}$$

$$w_{|-1+\beta b} - \mu\beta\partial_x b\Big(\bar{v}_{|-1+\beta b} + \sqrt{\mu}v^*_{|-1+\beta b}\Big) = 0. \tag{2.28c}$$

Integrating (2.28a) over the vertical and using (2.7), we get

$$\int_{-1+\beta b}^{z} \partial_z w = -\mu \int_{-1+\beta b}^{z} \partial_x \bar{v} - \mu^{3/2} \int_{-1+\beta b}^{z} \partial_x v^*,$$
$$w = -\mu \partial_x \int_{-1+\beta b}^{z} \bar{v} - \mu^{3/2} \partial_x \int_{-1+\beta b}^{z} v^* - \mu\beta \partial_x b \Big(\bar{v}_{|-1+\beta b} + \sqrt{\mu} v^*_{|-1+\beta b} \Big) + w_{|-1+\beta b},$$

from (2.28c), yields

$$w = -\mu \partial_x \Big[(1 + z - \beta b)\bar{v} \Big] - \mu^{3/2} \partial_x \int_{-1+\beta b}^{z} v^*. \tag{2.29}$$

Replacing (2.29) in (2.28b), and integrating over the vertical, yields

$$\begin{aligned} v^* &= -\frac{1}{\sqrt{\mu}} \int_{z}^{\varepsilon\zeta} \partial_x w + v^*_{|\varepsilon\zeta}, \\ v^* &= -\frac{1}{\sqrt{\mu}} \Big(\int_{z}^{\varepsilon\zeta} \partial_x w \Big)^*, \\ v^* &= \sqrt{\mu} \Big(\int_{z}^{\varepsilon\zeta} \partial_x^2 [(1 + z' - \beta b)\bar{v}] dz' \Big)^* + \mu \Big(\int_{z}^{\varepsilon\zeta} \partial_x^2 \int_{-1+\beta b}^{z} v^* \Big)^*. \end{aligned} \tag{2.30}$$

Introducing the operators $T[\varepsilon\zeta, \beta b]$ and $T^*[\varepsilon\zeta, \beta b]$ as follows,

$$T[\varepsilon\zeta, \beta b]w = \int_{z}^{\varepsilon\zeta} \partial_x^2 \int_{-1+\beta b}^{z'} w \quad \text{and} \quad T^*[\varepsilon\zeta, \beta b]w = (T[\varepsilon\zeta, \beta b]w)^*. \tag{2.31}$$

Hence, (2.30) can be given as follows,

$$(1 - \mu T^*[\varepsilon\zeta, \beta b])v^* = \sqrt{\mu} T^*[\varepsilon\zeta, \beta b]\bar{v}. \tag{2.32}$$

One can compute,

$$T^*[\varepsilon\zeta, \beta b]\bar{v} = -\frac{1}{2}((1 + z - \beta b)^2 - \frac{H^2}{3})\partial_x^2 \bar{v} + \beta(z - \varepsilon\zeta + \frac{1}{2}H)\Big[\partial_x b \partial_x \bar{v} + \partial_x(\partial_x b \bar{v}) \Big]. \tag{2.33}$$

Applying $(1 + \mu T^*)$ to (2.32) and using (2.33), one obtains

$$\begin{aligned} v^* &= \sqrt{\mu} T^*[\varepsilon\zeta, \beta b]\bar{v} + O(\mu^{3/2}), \\ v^* &= \frac{-\sqrt{\mu}}{2}((1 + z - \beta b)^2 - \frac{H^2}{3})\partial_x^2 \bar{v} + \sqrt{\mu}\beta(z - \varepsilon\zeta + \frac{1}{2}H)[\partial_x b \partial_x \bar{v} + \partial_x(\partial_x b \bar{v})]. \end{aligned} \tag{2.34}$$

From (2.24),(2.29) and (2.34), one deduces the approximations for the horizontal and vertical velocity fields up to $O(\mu^2)$ terms,

$$v = \bar{v} - \mu\frac{1}{2}((1 + z - \beta b)^2 - \frac{H^2}{3})\partial_x^2 \bar{v} + \mu\beta(z - \varepsilon\zeta + \frac{1}{2}H)[\partial_x b \partial_x \bar{v} + \partial_x(\partial_x b \bar{v})] + O(\mu^2), \tag{2.35a}$$

$$w = -\mu \partial_x [(1 + z - \beta b)\bar{v}] + O(\mu^2). \tag{2.35b}$$

Computation of the Reynolds-like tensor contribution

From the definitions (2.15) and using (2.34), one deduces under the dimensionless variables,

$$\varepsilon\mu\partial_x \mathbf{R} = \varepsilon\mu\partial_x \int_{-1+\beta b}^{\varepsilon\zeta} |v^*|^2 = \varepsilon\mu^2\partial_x \int_{-1+\beta b}^{\varepsilon\zeta} \left(T^*[\varepsilon\zeta, \beta b]\bar{v}\right)^2 = O(\mu^2). \tag{2.36}$$

Thus, one observes that the contribution of Reynolds tensor is above the overall $O(\mu^2)$ precision of the models in irrotational case and can therefore be neglected.

2.1.2.1 NSW equations

Owing to (2.35a) and (2.35b), we get the approximations for horizontal and vertical velocity up to $O(\mu)$, as follows

$$v = \bar{v} + O(\mu) \quad \text{and} \quad w = O(\mu). \tag{2.37}$$

From the definitions (2.26) and (2.37), one deduces

$$\frac{1}{\varepsilon}\int_{-1+\beta b}^{\varepsilon\zeta} \partial_x P_{nh} = O(\mu). \tag{2.38}$$

Plugging (2.36) and (2.38) into (2.25), with dropping the $O(\mu)$ terms one obtains the NSW equations in nondimensionalized form,

$$\begin{cases} \partial_t\zeta + \partial_x(H\bar{v}) = 0, \\ \partial_t(H\bar{v}) + \varepsilon\partial_x(H\bar{v}^2) + H\partial_x\zeta = 0. \end{cases} \tag{2.39}$$

2.1.2.2 The Boussinesq equations

Deriving the Boussinesq equations required keeping the terms of order μ, together with an additional assumptions, namely an assumption of *weak nonlinearity*, that stands for a smallness condition on ε, and a smallness assumption on the topography variations,

$$\varepsilon = O(\mu) \quad \text{and} \quad \beta = O(\mu). \tag{2.40}$$

Note that based on the above assumptions one can observe that terms of size $O(\varepsilon\mu)$ and $O(\beta\mu)$ can be regarded as $O(\mu^2)$, so they are dropped. Using (2.35a)-(2.35b) with (2.40), one obtains the approximations for horizontal velocity up to $O(\mu)$ and vertical velocity up to $O(\mu^2)$, as follows

$$v = \bar{v} + O(\mu) \quad \text{and} \quad w = -\mu\partial_x[(1+z)\bar{v}] + O(\mu^2). \tag{2.41}$$

Using (2.41) with (2.26) and (2.40), we get

$$\begin{aligned}\frac{1}{\varepsilon}\int_{-1+\beta b}^{\varepsilon\zeta}\partial_x P_{nh} &= \int_{-1+\beta b}^{\varepsilon\zeta}\partial_x\int_z^{\varepsilon\zeta}\Big(\partial_t w+\varepsilon v\partial_x w+\frac{\varepsilon}{\mu}w\partial_z w\Big),\\ &= -\mu\int_{-1+\beta b}^{\varepsilon\zeta}\partial_x\int_z^{\varepsilon\zeta}\partial_t(\partial_x((1+z)\bar v))\\ &\quad-\varepsilon\mu\int_{-1+\beta b}^{\varepsilon\zeta}\partial_x\int_z^{\varepsilon\zeta}\bar v\partial_x(\partial_x((1+z)\bar v))\\ &\quad+\varepsilon\mu\int_{-1+\beta b}^{\varepsilon\zeta}\partial_x\int_z^{\varepsilon\zeta}\partial_x((1+z)\bar v)\partial_z(\partial_x((1+z)\bar v)),\\ &= -\mu\int_{-1+\beta b}^{\varepsilon\zeta}\partial_x\int_z^{\varepsilon\zeta}\partial_t(\partial_x((1+z)\bar v))+O(\mu^2),\end{aligned}\tag{2.42}$$

one computes,

$$\begin{aligned}-\mu\int_{-1+\beta b}^{\varepsilon\zeta}\partial_x\int_z^{\varepsilon\zeta}\partial_t\big(\partial_x((1+z)\bar v)\big) &= -\mu\int_{-1+\beta b}^{\varepsilon\zeta}\partial_x\int_z^{\varepsilon\zeta}\partial_t\Big((1+z)\partial_x\bar v\Big),\\ &= -\mu\int_{-1+\beta b}^{\varepsilon\zeta}\partial_x\int_z^{\varepsilon\zeta}\Big((1+z)\partial_x(\partial_t\bar v)\Big),\\ &= -\mu\int_{-1+\beta b}^{\varepsilon\zeta}\partial_x\Big(\partial_x(\partial_t\bar v)\Big(\frac{H^2}{2}-\frac{(1+z)^2}{2}\Big)\Big),\\ &= \mu\int_{-1+\beta b}^{\varepsilon\zeta}\Big(\partial_t(\partial_x(\partial_t\bar v))\frac{H^2}{2}-\partial_x(\partial_t\bar v)H\partial_x H+\partial_x(\partial_x(\partial_t\bar v))\frac{(1+z)^2}{2}\Big),\\ &= -\partial_x(\partial_x(\partial_t\bar v))\frac{H^3}{3}-\partial_x(\partial_t\bar v)H^2\partial_x H,\end{aligned}\tag{2.43}$$

thus,

$$-\mu\int_{-1+\beta b}^{\varepsilon\zeta}\partial_x\int_z^{\varepsilon\zeta}\partial_t(\partial_x((1+z)\bar v)) = -\frac{\mu}{3}\partial_x^2(\partial_t\bar v)+O(\mu^2).\tag{2.44}$$

Plugging this relation in (2.25) and dropping the $O(\mu^2)$ terms, one obtains the Boussinesq equations,

$$\begin{cases}\partial_t\zeta+\partial_x(H\bar v)=0,\\ (1-\frac{\mu}{3}\partial_x^2)\partial_t\bar v+\varepsilon\bar v\partial_x\bar v+H\partial_x\zeta=0.\end{cases}\tag{2.45}$$

We observe that, when compared with the NSW equations, the Boussinesq equations differs through the occurrence of a second order linear operator acting on the time derivative of the velocity, in the momentum conservation equation.

2.1.2.3 The Serre-Green-Naghdi equations

If one wants to focus on fully nonlinear flows, and remove the weak nonlinearity assumption made to derive the Boussinesq equations, we need to compute again the pressure term contributions.

From (2.35a) and (2.35b), we obtain the approximation for the horizontal velocity up to $O(\mu)$ and for vertical velocity up to $O(\mu^2)$ as follows,

$$v(t,x,z) = \bar{v}(t,x) + O(\mu), \quad w(t,x,z) = -\mu\partial_x[(1+z-\beta b)\bar{v}] + O(\mu^2). \tag{2.46}$$

From (2.26) and (2.46), we have

$$\begin{aligned}
\frac{1}{\varepsilon}\int_{-1+\beta b}^{\varepsilon\zeta}\partial_x P_{nh} &= \int_{-1+\beta b}^{\varepsilon\zeta}\partial_x\int_z^{\varepsilon\zeta}\Big(\partial_t w + \varepsilon v\partial_x w + \frac{\varepsilon}{\mu}w\partial_z w\Big),\\
&= \int_{-1+\beta b}^{\varepsilon\zeta}\partial_x\int_z^{\varepsilon\zeta}\partial_t(-\mu\partial_x[(1+z-\beta b)\bar{v}])\\
&- \int_{-1+\beta b}^{\varepsilon\zeta}\partial_x\int_z^{\varepsilon\zeta}\varepsilon\bar{v}\,\partial_x(-\mu[(1+z-\beta b)\bar{v}])\\
&- \varepsilon\int_{-1+\beta b}^{\varepsilon\zeta}\partial_x\int_z^{\varepsilon\zeta}\partial_x[(1+z-\beta b)\bar{v}]\partial_z(-\mu\partial_x[(1+z-\beta b)\bar{v}]).
\end{aligned} \tag{2.47}$$

Let compute each term explicitly,

First term - We have,

$$\begin{aligned}
\int_z^{\varepsilon\zeta}\partial_t w &= \int_z^{\varepsilon\zeta}\Big(-\mu(1+z-\beta b)\partial_x(\partial_t\bar{v}) + \mu\beta\partial_x b\partial_t\bar{v}\Big)dz,\\
&= -\mu\partial_x(\partial_t\bar{v})\Big(\frac{H^2}{2} - \frac{(1+z-\beta b)^2}{2}\Big) + \mu\beta\partial_x b\partial_t\bar{v}(\varepsilon\zeta - z),
\end{aligned}$$

moreover,

$$\begin{aligned}
\partial_x\int_z^{\varepsilon\zeta}\partial_t w &= \Big(\mu\beta\partial_x^2 b\partial_t\bar{v} + \mu\beta\partial_x b\partial_x(\partial_t\bar{v})\Big)(\varepsilon\zeta - z) + \mu\beta\partial_x b\partial_t\bar{v}\partial_x H\\
&+ \mu\beta^2(\partial_x b)^2\partial_t\bar{v} - \mu\partial_x(\partial_x(\partial_t\bar{v}))\frac{H^2}{2} - \mu\partial_x(\partial_t\bar{v})H\partial_x H\\
&+ \mu\partial_x(\partial_x(\partial_t\bar{v}))\frac{(1+z-\beta b)^2}{2} - \mu\beta\partial_x b\partial_x(\partial_t\bar{v})(1+z-\beta b).
\end{aligned}$$

Finally, after straightforward computations we get

$$\begin{aligned}
\int_{-1+\beta b}^{\varepsilon\zeta}\partial_x\int_z^{\varepsilon\zeta}\partial_t w &= -\frac{\mu}{3}\partial_x(H^3\partial_x(\partial_t\bar{v}))\\
&+ \frac{\mu\beta}{2}\Big[\partial_x(H^2\partial_x b\partial_t\bar{v}) - H^2\partial_x b\partial_x(\partial_t\bar{v})\Big] + \mu H\beta^2(\partial_x b)^2\partial_t\bar{v}.
\end{aligned} \tag{2.48}$$

Second term - We have,

$$\begin{aligned}
\int_z^{\varepsilon\zeta}\varepsilon\bar{v}\partial_x w &= -\varepsilon\mu\bar{v}\partial_x^2\bar{v}\Big(\frac{H^2}{2} - \frac{(1+z-\beta b)^2}{2}\Big)\\
&+ \Big(2\varepsilon\mu\beta\partial_x b\bar{v}\partial_x\bar{v} + \varepsilon\mu\beta\partial_x^2 b\bar{v}^2\Big)(\varepsilon\zeta - z),
\end{aligned}$$

moreover,

$$\begin{aligned}\partial_x \int_z^{\varepsilon\zeta} \varepsilon\bar{v}\partial_x w &= (2\varepsilon\mu\beta\partial_x b\bar{v}\partial_x\bar{v} + \varepsilon\mu\beta\partial_x^2 b\bar{v}^2)\varepsilon\partial_x\zeta \\ &+ \Big(2\varepsilon\mu\beta\partial_x b(\partial_x\bar{v})^2 + 2\varepsilon\mu\beta\partial_x b\bar{v}\partial_x^2\bar{v} + 4\varepsilon\mu\beta\partial_x^2 b\bar{v}\partial_x\bar{v} + \varepsilon\mu\beta\partial_x^3 b\bar{v}^2\Big)(\varepsilon\zeta - z) \\ &- (\varepsilon\mu\bar{v}\partial_x^3\bar{v} + \varepsilon\mu\partial_x\bar{v}\partial_x^2\bar{v})\Big(\frac{H^2}{2} - \frac{(1+z-\beta b)^2}{2}\Big) - \varepsilon\mu\bar{v}\partial_x^2\bar{v}\big[H\partial_x H + \beta\partial_x b(1+z-\beta b)\big],\end{aligned}$$

hence, using the fact that $\varepsilon\partial_x\zeta = \partial_x H + \partial_x b$, we get

$$\begin{aligned}\int_{-1+\beta b}^{\varepsilon\zeta}\partial_x\int_z^{\varepsilon\zeta}\varepsilon\bar{v}\partial_x w &= -\varepsilon\mu\bar{v}\partial_x^3\bar{v}\frac{H^3}{3} - \varepsilon\mu\bar{v}\partial_x^2\bar{v}H^2\partial_x H - \mu\partial_x\bar{v}\partial_x^2\bar{v}\frac{H^3}{3} \\ &+ 2H^2\varepsilon\mu\beta\partial_x^2 b\bar{v}\partial_x\bar{v} + 2\varepsilon\mu\beta\partial_x b\bar{v}\partial_x\bar{v}H\partial_x H + 2\varepsilon\mu\beta^2(\partial_x b)^2\bar{v}\partial_x\bar{v}H + \varepsilon\mu\beta\partial_x^3 b\bar{v}^2\frac{H^2}{2} \\ &+ \varepsilon\mu\beta\partial_x b\bar{v}\partial_x^2\bar{v}\frac{H^2}{2} + \varepsilon\mu\beta\partial_x^2 b\bar{v}^2 H\partial_x H + \varepsilon\beta^2\mu\partial_x^2 b\partial_x b\bar{v}^2 H + \varepsilon\beta\mu H^2(\partial_x\bar{v})^2\partial_x b.\end{aligned} \tag{2.49}$$

Third term - We have,

$$\int_z^{\varepsilon\zeta} w\partial_z w = \varepsilon\mu(\partial_x\bar{v})^2\Big(\frac{H^2}{2} - \frac{(1+z-\beta b)^2}{2}\Big) - \varepsilon\mu\beta\partial_x b\bar{v}\partial_x\bar{v}(\varepsilon\zeta - z),$$

moreover,

$$\begin{aligned}\partial_x\int_z^{\varepsilon\zeta} w\partial_z w &= \varepsilon\mu\partial_x((\partial_x\bar{v})^2)\frac{H^2}{2} + \varepsilon\mu(\partial_x\bar{v})^2 H\partial_x H - \varepsilon\mu\beta^2(\partial_x b)^2\bar{v}\partial_x\bar{v} \\ &+ \varepsilon\mu\beta\partial_x b(\partial_x\bar{v})^2(1+z-\beta b) - \varepsilon\mu\beta\partial_x b(\partial_x\bar{v})^2(\varepsilon\zeta - z) - \varepsilon\mu\beta\partial_x b\bar{v}\partial_x\bar{v}\partial_x H \\ &- \varepsilon\mu\beta\partial_x b\bar{v}\partial_x^2\bar{v}(\varepsilon\zeta - z) - \varepsilon\mu\beta\partial_x^2 b\bar{v}\partial_x\bar{v}(\varepsilon\zeta - z) - \varepsilon\mu\partial_x((\partial_x\bar{v})^2)\frac{(1+z-\beta b)^2}{2},\end{aligned}$$

using the fact that $\varepsilon\partial_x\zeta = \partial_x H + \beta\partial_x b$, we infer

$$\begin{aligned}\int_{-1+\beta b}^{\varepsilon\zeta}\partial_x\int_z^{\varepsilon\zeta} w\partial_z w &= \varepsilon\mu\partial_x((\partial_x\bar{v})^2)\frac{H^3}{2} + \varepsilon\mu(\partial_x\bar{v})^2 H^2\partial_x H \\ &+ \varepsilon\mu\beta\partial_x b(\partial_x\bar{v})^2\frac{H^2}{2} - \varepsilon\mu\beta\partial_x b(\partial_x\bar{v})^2\frac{H^2}{2} - \varepsilon\mu\beta\partial_x b\bar{v}\partial_x^2\bar{v}\frac{H^2}{2} \\ &- \varepsilon\mu\beta\partial_x^2 b\bar{v}\partial_x\bar{v}\frac{H^2}{2} - \varepsilon\mu\beta\partial_x b\bar{v}\partial_x\bar{v}H\partial_x H - \varepsilon\mu H\beta^2(\partial_x b)^2\bar{v}\partial_x\bar{v} - \varepsilon\mu\partial_x((\partial_x\bar{v})^2)\frac{H^3}{6},\end{aligned} \tag{2.50}$$

regrouping the above calculations (2.48)-(2.50) and after some computations, we finally get

$$\frac{1}{\varepsilon}\int_{-1+\beta b}^{\varepsilon\zeta}\partial_x P_{nh} = \mu\mathbf{T}[H,\beta b][\partial_t(H\bar{v}) + \varepsilon\partial_x(H\bar{v}^2)] + \varepsilon\mu H\mathcal{Q}_1[H,\beta b](\bar{v}). \tag{2.51}$$

So that the resulting SGN equations read as follows,

$$\begin{cases}\partial_t\zeta + \partial_x(H\bar{v}) = 0, \\ (1+\mu\mathbf{T}[H,\beta b])[\partial_t(H\bar{v}) + \varepsilon\partial_x(H\bar{v}^2)] + H\partial_x\zeta + \varepsilon\mu H\mathcal{Q}_1[H,\beta b](\bar{v}) = 0,\end{cases} \tag{2.52}$$

where the linear operator $\mathbf{T}[H,\beta b]\cdot$ and the quadratic form $Q_1[H,\beta b](\cdot)$ are defined for all smooth enough scalar-valued functions u by,

$$\mathbf{T}[H,\beta b]u \coloneqq H\mathcal{T}[H,\beta b]\frac{u}{H}, \tag{2.53}$$

$$\mathcal{T}[H,\beta b]u = -\frac{1}{3H}\partial_x(H^3\partial_x u) + \frac{\beta}{2H}\Big[\partial_x(H^2\partial_x bu) - H^2\partial_x b\partial_x u\Big] + \beta^2(\partial_x b)^2 u, \tag{2.54}$$

$$Q_1[H,\beta b](u) = \frac{2}{3H}\partial_x(H^3(\partial_x u)^2) + \beta H(\partial_x u)^2\partial_x b + \frac{\beta}{2H}\partial_x(H^2u^2\partial_x^2 b) + \beta^2u^2\partial_x b\partial_x^2 b. \tag{2.55}$$

Note that these operators may be also expressed as follows,

$$\mathcal{T}[H,\beta b]u \coloneqq \mathcal{R}_1[H,\beta b](\partial_x u) + \mathcal{R}_2[H,\beta b](u\partial_x b), \tag{2.56}$$

$$Q_1[H,\beta b](u) \coloneqq -2\mathcal{R}_1[H,\beta b]((\partial_x u)^2) + \beta\mathcal{R}_2[H,\beta b](u^2\partial_x^2 b), \tag{2.57}$$

with,

$$\mathcal{R}_1[H,\beta b]u \coloneqq -\frac{1}{3H}\partial_x(H^3u) - \frac{H}{2}\beta u\partial_x b, \qquad \mathcal{R}_2[H,\beta b]u \coloneqq \frac{1}{2H}\partial_x(H^2u) + \beta u\partial_x b.$$

2.1.3 Rotational flows

We turn on considering the case of non-zero vorticity and derive the corresponding SGN-like equations. Starting again from the free surface Euler equations, condition (2.2c) is now replaced by,

$$\operatorname{curl}\mathbf{U} = \boldsymbol{\omega}, \tag{2.58}$$

which gives in nondimensionalized form,

$$\operatorname{curl}^\mu\mathbf{U}^\mu = \mu\boldsymbol{\omega}_\mu \quad \text{with} \quad \boldsymbol{\omega}_\mu = \begin{bmatrix} \frac{1}{\sqrt{\mu}}(\partial_z v - \partial_x w) \\ -\partial_x v \end{bmatrix}. \tag{2.59}$$

Also, system (2.20) has now to be supplemented with the vorticity evolution equation,

$$\partial_t\boldsymbol{\omega}_\mu + \frac{\varepsilon}{\mu}\mathbf{U}^\mu\cdot\nabla^\mu_{x,z}\boldsymbol{\omega}_\mu = \frac{\varepsilon}{\mu}\boldsymbol{\omega}_\mu\cdot\nabla^\mu_{x,z}\mathbf{U}^\mu, \tag{2.60}$$

where,

$$\mathbf{U}^\mu = (\sqrt{\mu}v, 0, w)^T \quad \text{and} \quad \nabla^\mu_{x,z} = (\sqrt{\mu}\partial_x, 0, \partial_z)^T. \tag{2.61}$$

Note also that the Reynolds-like tensor (which turns out to be a scalar number when $d = 1$) can no longer be neglected within the asymptotic expansion's accuracy.

Asymptotic expansion of the velocity field

Proceeding as in the irrotational case, the relations (2.27) can be written as,

$$\begin{cases} \mu\partial_x v + \partial_z w = 0, \\ \sqrt{\mu}\partial_z v - \sqrt{\mu}\partial_x w = \mu\boldsymbol{\omega}_{\mu,h}, \\ \partial_x v = \boldsymbol{\omega}_{\mu,v}, \\ w_{|-1+\beta b} - \mu\beta\partial_x v_{|-1+\beta b} = 0. \end{cases} \tag{2.62}$$

Plugging (2.24) into (2.62), one deduces

$$\begin{cases} \mu\partial_x\bar{v} + \mu^{3/2}\partial_x v^* + \partial_z w = 0, \\ \sqrt{\mu}\partial_z v^* - \sqrt{\mu}\partial_x w = \mu\boldsymbol{\omega}_{\mu,h}, \\ \partial_x\bar{v} + \sqrt{\mu}\partial_x v^* = \boldsymbol{\omega}_{\mu,v}, \\ w_{|-1+\beta b} - \mu\beta\partial_x b(\bar{v}_{|-1+\beta b} + \sqrt{\mu}v^*_{|-1+\beta b}) = 0, \end{cases} \tag{2.63}$$

where $\boldsymbol{\omega}_{\mu,h}$ and $\boldsymbol{\omega}_{\mu,v}$ denotes respectively the horizontal and vertical components of the vorticity $\boldsymbol{\omega}_\mu$. The first and the third equations of (2.63), give

$$w = -\mu\partial_x[(1+z-\beta b)\bar{v}] - \mu^{3/2}\partial_x\int_{-1+\beta b}^{z} v^*. \tag{2.64}$$

Integrating vertically the second equation of (2.63) with (2.64), yields

$$\begin{aligned} v^* &= -\frac{1}{\sqrt{\mu}}\Big(\int_z^{\varepsilon\zeta}\partial_x w\Big)^* - \Big(\int_z^{\varepsilon\zeta}\boldsymbol{\omega}_{\mu,h}\Big)^*, \\ v^* &= \sqrt{\mu}\Big(\int_z^{\varepsilon\zeta}\partial_x^2[(1+z'-\beta b)\bar{v}]dz'\Big)^* + \mu\Big(\int_z^{\varepsilon\zeta}\partial_x^2\int_{-1+\beta b}^{z} v^*\Big)^* + \Big(-\int_z^{\varepsilon\zeta}\boldsymbol{\omega}_{\mu,h}\Big)^*. \end{aligned} \tag{2.65}$$

Introducing the operators $T[\varepsilon\zeta,\beta b]$ and $T^*[\varepsilon\zeta,\beta b]$ as in (2.31), together with the vertically dependent component of the shear velocity,

$$v^*_{\mathrm{sh}} = -\Big(\int_z^{\varepsilon\zeta}\boldsymbol{\omega}_{\mu,h}\Big)^*, \tag{2.66}$$

expression (2.65) can be given under the form,

$$(1-\mu T^*[\varepsilon\zeta,\beta b])v^* = v^*_{\mathrm{sh}} + \sqrt{\mu}T^*[\varepsilon\zeta,\beta b]\bar{v}. \tag{2.67}$$

Applying $(1+\mu T^*[\varepsilon\zeta,\beta b])$ to (2.67), yields

$$v^* = v^*_{\mathrm{sh}} + \sqrt{\mu}T^*[\varepsilon\zeta,\beta b]\bar{v} + \mu T^*[\varepsilon\zeta,\beta b]v^*_{\mathrm{sh}} + O(\mu^{\frac{3}{2}}). \tag{2.68}$$

Finally, using (2.64) and (2.68), we obtain

$$v = \bar{v} + \sqrt{\mu}v^*_{\mathrm{sh}} + O(\mu), \tag{2.69a}$$

$$v = \bar{v} + \sqrt{\mu}v^*_{\mathrm{sh}} + \mu T^*[\varepsilon\zeta,\beta b]\bar{v} + \mu^{\frac{3}{2}}T^*[\varepsilon\zeta,\beta b]v^*_{\mathrm{sh}} + O(\mu^2), \tag{2.69b}$$

$$w = -\mu\partial_x[(1+z-\beta b)\bar{v}] - \mu^{\frac{3}{2}}\partial_x\int_{-1+\beta b}^{z} v^*_{\mathrm{sh}} + O(\mu^2). \tag{2.69c}$$

We also remark that the Reynolds-like tensor in the presence of vorticity may now be decomposed as follows,

$$\mathbf{R} = E + \frac{1}{2}\int_{-1+\beta b}^{\varepsilon\zeta}(v^*-v^*_{\mathrm{sh}})(v^*+v^*_{\mathrm{sh}}) \quad \text{with} \quad E = \int_{-1+\beta b}^{\varepsilon\zeta}(v^*_{\mathrm{sh}})^2. \tag{2.70}$$

Owing to (2.68) and dropping $O(\mu^2)$ terms, one deduces

$$\varepsilon\mu\partial_x\mathbf{R} = \varepsilon\mu\partial_x\int_{-1+\beta b}^{\varepsilon\zeta}|v^*_{\mathrm{sh}}|^2 + 2\varepsilon\mu^{\frac{3}{2}}\partial_x\int_{-1+\beta b}^{\varepsilon\zeta}v^*_{\mathrm{sh}}T^*[\varepsilon\zeta,\beta b]\bar{v}. \tag{2.71}$$

Now, one can proceed to the derivation of SGN-like models in the presence of vorticity. We distinguish two situations: the case of a constant vorticity, and the case of a general vorticity.

2.1.3.1 SGN equations with constant vorticity

Assuming that the vorticity is constant, we have $\boldsymbol{\omega}_\mu = (0, \omega, 0)^T$ with $\omega = \partial_z v^* - \partial_x w = cst$. We obtain the following expressions respectively for the shear velocity and the vertical velocity,

$$v^*_{\text{sh}} = -\Big(\int_z^{\varepsilon\zeta} \omega \Big)^* = -((\varepsilon\zeta - z) - \frac{1}{2}H)\omega, \tag{2.72a}$$

$$w = -\mu\partial_x((1 + z - \beta b)\bar{v}) + \frac{\mu^{\frac{3}{2}}\omega}{2}\partial_x((\varepsilon\zeta - z)(z + 1 - \beta b)). \tag{2.72b}$$

Computation of the Reynolds-like tensor contribution

Replacing (2.68) and (2.72a) in (2.70), and dropping the $O(\mu^2)$, the Reynolds-like tensor contribution can be formulated in terms of ζ and $\bar{v}$ as follows,

$$\begin{aligned}
\varepsilon\mu\partial_x \mathbf{R} &= \varepsilon\mu\partial_x \int_{-1+\beta b}^{\varepsilon\zeta} |v^*_{\text{sh}}|^2 + 2\varepsilon\mu^{\frac{3}{2}}\partial_x \int_{-1+\beta b}^{\varepsilon\zeta} v^*_{\text{sh}} T[\varepsilon\zeta, \beta b]\bar{v}, \\
&= \varepsilon\mu\omega^2\partial_x \int_{-1+\beta b}^{\varepsilon\zeta} ((\varepsilon\zeta - z) - \frac{1}{2}H)^2 \\
&- 2\varepsilon\mu^{\frac{3}{2}}\omega\partial_x \int_{-1+\beta b}^{\varepsilon\zeta} ((\varepsilon\zeta - z) - \frac{1}{2}H) \int_z^{\varepsilon\zeta} \partial_x^2((1 + z' - \beta b)\bar{v}), \\
&= \frac{\varepsilon\mu}{12}\omega^2\partial_x(H^3) + \partial_x^2\bar{v}\Big(\frac{H^2}{2} - \frac{(1 + z - \beta b)^2}{2}\Big)\Big) \\
&- 2\varepsilon\mu^{\frac{3}{2}}\omega\partial_x \int_{-1+\beta b}^{\varepsilon\zeta} ((\varepsilon\zeta - z) - \frac{1}{2}H)\Big((-\beta\partial_x^2 b\bar{v} - 2\beta\partial_x b\partial_x\bar{v})(\varepsilon\zeta - z), \\
&= \frac{\varepsilon\mu}{12}\omega^2\partial_x(H^3) - \frac{\varepsilon\mu^{\frac{3}{2}}}{12}\omega\partial_x\big[H^3(H\partial_x^2\bar{v} - 2\beta\bar{v}\partial_x^2 b - 4\beta\partial_x\bar{v}\partial_x b)\big].
\end{aligned} \tag{2.73}$$

Computation of the pressure contribution

Using (2.26), (2.69b), (2.72a) and (2.72b), the contribution of the pressure to (2.18) can be formulated depending only on the variables ζ and $\bar{v}$.

$$\begin{aligned}
\frac{1}{\varepsilon}\int_{-1+\beta b}^{\varepsilon\zeta} \partial_x P_{nh} &= \int_{-1+\beta b}^{\varepsilon\zeta} \partial_x \int_z^{\varepsilon\zeta} \Big(\partial_t w + \varepsilon v\partial_x w + \frac{\varepsilon}{\mu} w\partial_z w\Big) \\
&= \int_{-1+\beta b}^{\varepsilon\zeta} \partial_x \int_z^{\varepsilon\zeta} \partial_t\Big(- \mu\partial_x((1 + z - \beta b)\bar{v})\Big) \\
&+ \int_{-1+\beta b}^{\varepsilon\zeta} \partial_x \int_z^{\varepsilon\zeta} \varepsilon\bar{v}\partial_x\Big(- \mu\partial_x((1 + z - \beta b)\bar{v})\Big) \\
&+ \frac{\varepsilon}{\mu}\Big(- \mu\partial_x((1 + z - \beta b)\bar{v})\Big)\partial_z\Big(- \mu\partial_x((1 + z - \beta b)\bar{v})\Big) + \varrho + O(\mu^2), \\
&= \mu\mathbf{T}[H, \beta b]\big[\partial_t(H\bar{v}) + \varepsilon\partial_x(H\bar{v}^2)\big] + \mu\varepsilon H\boldsymbol{Q}_1[H, \beta b](\bar{v}) + \varrho + O(\mu^2),
\end{aligned} \tag{2.74}$$

where,

$$
\begin{aligned}
\varrho = &\int_{-1+\beta b}^{\varepsilon\zeta} \partial_x \int_z^{\varepsilon\zeta} \partial_t \Big(\frac{\mu^{\frac{3}{2}}\omega}{2} \partial_x \big((\varepsilon\zeta - z)(1 + z - \beta b) \big) \Big) \\
&+ \int_{-1+\beta b}^{\varepsilon\zeta} \partial_x \int_z^{\varepsilon\zeta} \Big(\varepsilon\sqrt{\mu} v_{\mathrm{sh}}^* \partial_x (-\mu \partial_x ((1 + z - \beta b)\bar{v})) \Big) \\
&+ \int_{-1+\beta b}^{\varepsilon\zeta} \partial_x \int_z^{\varepsilon\zeta} \varepsilon\bar{v} \partial_x \Big(\frac{\mu^{\frac{3}{2}}\omega}{2} \partial_x ((\varepsilon\zeta - z)(z + 1 - \beta b)) \Big) \\
&+ \int_{-1+\beta b}^{\varepsilon\zeta} \partial_x \int_z^{\varepsilon\zeta} (\varepsilon \frac{\mu^{\frac{3}{2}}\omega}{2} \partial_x ((\varepsilon\zeta - z)(1 + z - \beta b))) \partial_z \Big(- \mu \partial_x ((1 + z - \beta b)\bar{v}) \Big) \\
&+ \int_{-1+\beta b}^{\varepsilon\zeta} \partial_x \int_z^{\varepsilon\zeta} \varepsilon \big(- \partial_x ((1 + z - \beta b)\bar{v}) \big) \partial_z \Big(\frac{\mu^{\frac{3}{2}}\omega}{2} \partial_x ((\varepsilon\zeta - z)(1 + z - \beta b)) \Big), \\
&= \int_{-1+\beta b}^{\varepsilon\zeta} \partial_x \int_z^{\varepsilon\zeta} (\varrho_1 + \cdots + \varrho_5).
\end{aligned}
$$

Let compute each term explicitly,

First term - We have,

$$
\begin{aligned}
\int_z^{\varepsilon\zeta} \varrho_1 &= \frac{\mu^{\frac{3}{2}}\omega}{2} \int_z^{\varepsilon\zeta} \Big((1 + z - \beta b)\partial_x(\partial_t H) - \varepsilon\beta \partial_x b \partial_t \zeta \Big), \\
&= \frac{\mu^{\frac{3}{2}}\omega}{2} \Big(\partial_x(\partial_t H) \Big(\frac{H^2}{2} - \frac{(1 + z - \beta b)^2}{2} \Big) - \beta \partial_x b \partial_t H (\varepsilon\zeta - z) \Big),
\end{aligned}
$$

then,

$$
\begin{aligned}
\partial_x \int_z^{\varepsilon\zeta} \varrho_1 = \frac{\mu^{\frac{3}{2}}\omega}{2} \Big(&\partial_x(\partial_x(\partial_t H)) \frac{H^2}{2} + \partial_x(\partial_t H) H \partial_x H \\
&- \partial_x(\partial_x(\partial_t H)) \frac{(1 + z - \beta b)^2}{2} + \partial_x(\partial_t H) \beta \partial_x b (1 + z - \beta b) \\
&- (\beta \partial_x^2 b \partial_t H + \beta \partial_x b \partial_x(\partial_t H))(\varepsilon\zeta - z) - \beta \partial_x b \partial_t H \partial_x H - (\beta \partial_x b)^2 \partial_t H \Big).
\end{aligned}
$$

Finally we get the expression of the first term,

$$
\begin{aligned}
\int_{-1+\beta b}^{\varepsilon\zeta} \partial_x \int_z^{\varepsilon\zeta} \varrho_1 = &\frac{\mu^{\frac{3}{2}}\omega}{6} \partial_x(\partial_x(\partial_t H)) H^3 - \frac{\mu^{\frac{3}{2}}\omega}{2} \beta \partial_x b H \partial_t H \partial_x H - \frac{\mu^{\frac{3}{2}}\omega}{2} (\beta \partial_x b)^2 H \partial_t H \\
&+ \frac{\mu^{\frac{3}{2}}\omega}{2} \partial_x(\partial_t H) H^2 \partial_x H - \frac{\mu^{\frac{3}{2}}\omega}{4} \beta \partial_x^2 b H^2 \partial_t H - \frac{\mu^{\frac{3}{2}}\omega}{4} \beta \partial_x b \partial_x(\partial_t H) H^2.
\end{aligned}
$$

Second term - We have,

$$\int_z^{\varepsilon\zeta} \varrho_2 = \int_z^{\varepsilon\zeta} \varepsilon\mu^{\frac{3}{2}}\Big(\partial_x^2\zeta(1+z-\beta b) - 2\varepsilon\partial_x\zeta\beta\partial_x b - \beta\partial_x^2 b(\varepsilon\zeta - z)\Big),$$
$$= \mu^{\frac{3}{2}}\Big(\varepsilon\bar{v}\partial_x^2\zeta\Big(\frac{H^2}{2} - \frac{(1+z-\beta b)^2}{2}\Big) - (2\varepsilon\bar{v}\partial_x\zeta\beta\partial_x b + \beta\partial_x^2 b\bar{v}\frac{(\varepsilon\zeta - z)}{2})(\varepsilon\zeta - z)\Big),$$

moreover,

$$\partial_x\int_z^{\varepsilon\zeta}\varrho_2 = \varepsilon\mu^{\frac{3}{2}}\bar{v}\partial_x^2\zeta[H\partial_x H + \beta\partial_x b(1+z-\beta b)]$$
$$+ (\varepsilon\mu^{\frac{3}{2}}\partial_x\bar{v}\partial_x^2\zeta + \varepsilon\mu^{\frac{3}{2}}\bar{v}\partial_x^3\zeta)\Big(\frac{H^2}{2} - \frac{(1+z-\beta b)^2}{2}\Big)$$
$$- 2\mu^{\frac{3}{2}}\bar{v}\varepsilon^2(\partial_x\zeta)^2\beta\partial_x b - \mu^{\frac{3}{2}}(\beta\partial_x^3 b\bar{v} + \beta\partial_x^2 b\partial_x v)\frac{(\varepsilon\zeta - z)^2}{2}$$
$$- 2\varepsilon\mu^{\frac{3}{2}}(\partial_x\bar{v}\partial_x\zeta\beta\partial_x b + \bar{v}\partial_x^2\zeta\beta\partial_x b + \bar{v}\partial_x\zeta\beta\partial_x^2 b + \beta\partial_x^2 b\partial_x\zeta\bar{v})(\varepsilon\zeta - z).$$

Integrationg over z, we obtain the expression of the second term

$$\int_{-1+\beta b}^{\varepsilon\zeta}\partial_x\int_z^{\varepsilon\zeta}\varrho_2 = \frac{\varepsilon\mu^{\frac{3}{2}}\omega}{2}\Big(\varepsilon\partial_x\bar{v}\partial_x^2\zeta\frac{H^3}{2} + \varepsilon\bar{v}\partial_x^3\zeta\frac{H^3}{6}$$
$$- \frac{1}{2}\varepsilon\bar{v}\partial_x^2\zeta\beta\partial_x bH^2 - \frac{3}{2}\varepsilon\partial_x\zeta\bar{v}\beta\partial_x^2 bH^2 - \beta\partial_x^3 b\bar{v}\frac{H^3}{6}$$
$$- 2\bar{v}\varepsilon^2(\partial_x\zeta)^2\beta\partial_x bH + \varepsilon\bar{v}\partial_x^2\zeta H^2\varepsilon\partial_x H - \beta\partial_x^2 b\partial_x\bar{v}\frac{H^3}{6} - \partial_x\bar{v}\varepsilon\partial_x\zeta\beta\partial_x bH^2\Big).$$

Third term - We have,

$$\int_z^{\varepsilon\zeta}\varrho_3 = \int_z^{\varepsilon\zeta}\Big((1+z-\beta b-\frac{1}{2}H)\big(\beta\partial_x^2 b\bar{v} + 2\beta\partial_x b\partial_x\bar{v} - (1+z-\beta b)\partial_x^2\bar{v}\big)\Big),$$
$$= -\partial_x^2\bar{v}\Big(\frac{H^3}{12} - \frac{(1+z-\beta b)^3}{3}\Big)$$
$$+ \partial_x^2\bar{v}\Big(\frac{H}{4}(1+z-\beta b)^2\Big) + (\beta\partial_x^2 b\bar{v} + 2\beta\partial_x b\partial_x\bar{v})\Big(\frac{H^2}{8} - \frac{(1+z-\beta b-\frac{1}{2}H)^2}{2}\Big),$$

then,

$$\partial_x\int_z^{\varepsilon\zeta}\varrho_3 = -\partial_x^3\bar{v}\Big(\frac{H^3}{12} - \frac{(1+z-\beta b)^3}{3} + \frac{H}{4}(1+z-\beta b)^2\Big)$$
$$+ (\beta\partial_x^3 b\bar{v} + 3\beta\partial_x^2 b\partial_x\bar{v} + 2\beta\partial_x b\partial_x^2\bar{v})\Big(\frac{H^2}{8} - \frac{(1+z-\beta b-\frac{1}{2}H)}{2}\Big)$$
$$+ (\beta\partial_x^2 b\bar{v} + 2\beta\partial_x b\partial_x\bar{v})\Big(\frac{H}{4}\partial_x H + (\beta\partial_x b + \frac{1}{2}\partial_x H)(1+z-\beta b-\frac{H}{2})\Big)$$
$$- \partial_x^2\bar{v}\Big(\frac{H^2}{4}\partial_x H + \beta\partial_x b(1+z-\beta b)^2 + \frac{1}{4}\partial_x H(1+z-\beta b)^2 - \frac{H}{2}\beta\partial_x b(1+z-\beta b)\Big),$$

thus,

$$\int_{-1+\beta b}^{\varepsilon\zeta}\partial_x\int_z^{\varepsilon\zeta}\varrho_3=\varepsilon\mu^{\frac{3}{2}}\omega\Big((\beta\partial_x^3b\bar{v}+3\beta\partial_x^2b\partial_x\bar{v})\frac{H^3}{12}+\frac{2}{12}\beta\partial_xb\partial_x^2\bar{v}H^3 \\ +\frac{H^2}{4}\partial_xH(\beta\partial_x^2b\bar{v}+2\beta\partial_xb\partial_x\bar{v})-\partial_x^3\bar{v}\frac{H^4}{12}-\partial_x^2\bar{v}(\frac{H^3}{12}\partial_xH+\beta\partial_xb\frac{H^3}{12})\Big).$$

Fourth term - We have,

$$\int_z^{\varepsilon\zeta}\varrho_4=\frac{\varepsilon\mu^{\frac{3}{2}}\omega}{2}\int_z^{\varepsilon\zeta}\Big(-\varepsilon\partial_x\zeta\partial_x\bar{v}(z+1-\beta b)+\beta\partial_xb\partial_x\bar{v}(\varepsilon\zeta-z)\Big), \\ =\frac{\varepsilon\mu^{\frac{3}{2}}\omega}{2}\Big(-\varepsilon\partial_x\zeta\partial_x\bar{v}\Big(\frac{H^2}{2}-\frac{(1+z-\beta b)^2}{2}\Big)+\beta\partial_xb\partial_x\bar{v}\frac{(\varepsilon\zeta-z)^2}{2}\Big),$$

moreover,

$$\partial_x\int_z^{\varepsilon\zeta}\varrho_4=\frac{\varepsilon\mu^{\frac{3}{2}}\omega}{2}\Big(-\varepsilon\partial_x\zeta\partial_x\bar{v}(H\partial_xH+\beta\partial_xb(z+1-\beta b)) \\ -(\varepsilon\partial_x^2\zeta\partial_x\bar{v}+\varepsilon\partial_x\zeta\partial_x^2\bar{v})\Big(\frac{H^2}{2}-\frac{(1+z-\beta b)^2}{2}\Big) \\ +((\beta\partial_x^2b\partial_x\bar{v}+\beta\partial_xb\partial_x^2\bar{v})\frac{(\varepsilon\zeta-z)}{2}+\beta\partial_xb\partial_x\bar{v}\varepsilon\partial_x\zeta)(\varepsilon\zeta-z)\Big).$$

Finally we obtain the expression of fourth term,

$$\int_{-1+\beta b}^{\varepsilon\zeta}\partial_x\int_z^{\varepsilon\zeta}\varrho_4=-\frac{\varepsilon^2\mu^{\frac{3}{2}}\omega}{2}\partial_x^2\zeta\partial_x\bar{v}\frac{H^3}{3} \\ +\frac{\varepsilon\mu^{\frac{3}{2}}\omega}{2}\Big(-\varepsilon\partial_x\zeta\partial_x^2\bar{v}\frac{H^3}{3}-\varepsilon\partial_x\zeta\partial_x\bar{v}H^2\partial_xH+\beta\partial_x^2b\partial_x\bar{v}\frac{H^3}{6}+\beta\partial_xb\partial_x^2\bar{v}\frac{H^3}{6}\Big).$$

Fifth term - We have,

$$\int_z^{\varepsilon\zeta}\varrho_5=\frac{\varepsilon\mu^{\frac{3}{2}}\omega}{2}\Big((\beta\partial_xb\bar{v}\varepsilon\partial_x\zeta+(\beta\partial_xb)^2\bar{v})(\varepsilon\zeta-z) \\ -(\beta\partial_xb\partial_x\bar{v}+\varepsilon\partial_x\zeta\partial_x\bar{v})\Big(\frac{H^2}{2}-\frac{(z+1-\beta b)^2}{2}\Big)\Big),$$

again,

$$\partial_x\int_z^{\varepsilon\zeta}\varrho_5=\frac{\varepsilon\mu^{\frac{3}{2}}\omega}{2}\Big(-(\beta\partial_xb\partial_x\bar{v}+\varepsilon\partial_x\zeta\partial_x\bar{v})(H\partial_xH+\beta\partial_xb(z+1-\beta b)) \\ +(\beta\partial_xb)^2\partial_x\bar{v})(\varepsilon\zeta-z)+\beta\partial_xb\bar{v}\varepsilon^2(\partial_x\zeta)^2+(\beta\partial_xb)^2\bar{v}\varepsilon\partial_x\zeta \\ +(\beta\partial_x^2b\bar{v}\varepsilon\partial_x\zeta+\beta\partial_xb\partial_x\bar{v}\varepsilon\partial_x\zeta+\beta\partial_xb\bar{v}\varepsilon\partial_x^2\zeta+2\beta^2\partial_xb\partial_x^2b\bar{v} \\ -\Big(\beta\partial_x^2b\partial_x\bar{v}+\beta\partial_xb\partial_x^2\bar{v}+\varepsilon\partial_x^2\zeta\partial_x\bar{v}+\varepsilon\partial_x\zeta\partial_x^2\bar{v}\Big)\Big(\frac{H^2}{2}-\frac{(z+1-\beta b)^2}{2}\Big)\Big),$$

then,

$$\int_{-1+\beta b}^{\varepsilon\zeta}\partial_x\int_z^{\varepsilon\zeta}\varrho_5=\frac{\varepsilon\mu^{\frac{3}{2}}\omega}{2}(\beta\partial_x^2b\bar{v}\varepsilon\partial_x\zeta+\varepsilon\partial_x^2\zeta\partial_x\bar{v})$$
$$+\frac{\varepsilon\mu^{\frac{3}{2}}\omega}{2}\Big((\beta\partial_xb\partial_x\bar{v}\varepsilon\partial_x\zeta+\beta\partial_xb\bar{v}\varepsilon\partial_x^2\zeta+2\beta^2\partial_xb\partial_x^2b\bar{v}+\frac{H^2}{2}(\beta\partial_xb)^2\partial_x\bar{v})$$
$$+H[\beta\partial_xb\bar{v}\varepsilon^2(\partial_x\zeta)^2+(\beta\partial_xb)^2\bar{v}\varepsilon\partial_x\zeta]-[\beta\partial_x^2b\partial_x\bar{v}+\beta\partial_xb\partial_x^2\bar{v}$$
$$+\varepsilon\partial_x\zeta\partial_x^2\bar{v}]\frac{H^3}{3}-(\beta\partial_xb\partial_x\bar{v}+\varepsilon\partial_x\zeta\partial_x\bar{v})(H^2\partial_xH+\beta\partial_xb\frac{H^2}{2})\Big)\Big).$$

Using the fact that $\partial_t\zeta+\bar{v}\varepsilon\partial_x\zeta=\beta\bar{v}\partial_xb-H\partial_x\bar{v}$ and collecting the above computations, we get the contribution of the pressure term as follows,

$$\frac{1}{\varepsilon}\int_{-1+\beta b}^{\varepsilon\zeta}\partial_xP_{nh}=\mu\mathbf{T}[H,\beta b][\partial_t(H\bar{v})+\varepsilon\partial_x(H\bar{v}^2)]+\varepsilon\mu HQ_1[H,\beta b](\bar{v})$$
$$-\varepsilon\frac{\mu^{\frac{3}{2}}\omega}{2}H\mathcal{T}[H,\beta b](\beta\bar{v}\partial_xb-H\partial_x\bar{v})-\varepsilon\frac{\mu^{\frac{3}{2}}\omega}{12}\partial_x(H^4\partial_x^2\bar{v}+6H^3\partial_x\zeta\partial_x\bar{v}) \tag{2.75}$$
$$+\beta\frac{\mu^{\frac{3}{2}}}{12}[\omega H^2\partial_x\bar{v}(H\partial_x^2b-6\partial_x\zeta\partial_xb)+3\beta H\bar{v}\partial_xb(H\partial_x^2b+2\partial_xb\partial_x\zeta)].$$

Gathering the expression of Reynolds-like tensor (2.73) and the contribution of the pressure (2.75), we obtain

$$\varepsilon\mu\partial_x\int_{-1+\beta b}^{\varepsilon\zeta}|v^*|^2+\frac{1}{\varepsilon}\int_{-1+\beta b}^{\varepsilon\zeta}\partial_xP_{nh}=\mu\mathbf{T}[H,\beta b][\partial_t(H\bar{v})+\varepsilon\partial_x(H\bar{v}^2)]+\varepsilon\mu HQ_1[H,\beta b](\bar{v})$$
$$+\varepsilon\mu\partial_xE-\varepsilon\mu^{\frac{3}{2}}HC[H](v^\#,\bar{v})+\varepsilon\beta\mu^{\frac{3}{2}}HC_b[H](v^\#,\bar{v}).$$

Replacing these terms into (2.25) and denoting $v^\#=H\omega$, we obtain the SGN equations with constant vorticity in one-dimensional framework as follows,

$$\begin{cases}\partial_t\zeta+\partial_x(H\bar{v})=0,\\(1+\mu\mathbf{T}[H,\beta b])[\partial_t(H\bar{v})+\varepsilon\partial_x(H\bar{v}^2)]+H\partial_x\zeta+\varepsilon\mu HQ_1[H,\beta b](\bar{v})+\varepsilon\mu\partial_xE\\+\varepsilon\mu^{3/2}HC[H](v^\#,\bar{v})+\varepsilon\beta\mu^{3/2}HC_b[H](v^\#,\bar{v})=0,\end{cases} \tag{2.76}$$

where:

1. the linear operator $\mathbf{T}[H,\beta b]\cdot$ and the quadratic form $Q_1[H,\beta b](\cdot)$ are defined as in (2.54)-(2.55),
2. the second order term $E=\frac{1}{12}H^3\omega^2$ can be calculated easily, since $\omega=cst$,
3. the nonlinear interactions between the vertical dependence of the velocity field and the vertical dependence coming from the dispersive effects lead to the term $HC[H](v^\#,\bar{v})$, which is defined as follows,

$$HC[H](v^\#,\bar{v})=-\frac{1}{6}\partial_x(2H^3v^\#\partial_x^2\bar{v}+\partial_x(H^3v^\#)\partial_xv^\#), \tag{2.77}$$

4. the last term appearing in the momentum equations of (2.76) is defined as,

$$HC_b[H](v^\#,\bar{v}) = \frac{1}{3}\big(\partial_x(H^2 v^\# \partial_x^2 b\bar{v}) + H^2 v^\# \partial_x^2 b \partial_x \bar{v}\big). \tag{2.78}$$

Assuming an additional smallness assumption on the topography, such that $\varepsilon\beta\mu^{3/2} = O(\mu^2)$, one can neglect this last term and the model (2.76) becomes,

$$\begin{cases} \partial_t\zeta + \partial_x(H\bar{v}) = 0, \\ (1+\mu\mathbf{T}[H,\beta b])[\partial_t(H\bar{v}) + \varepsilon\partial_x(H\bar{v}^2)] + H\partial_x\zeta + \varepsilon\mu H\mathcal{Q}_1[H,\beta b](\bar{v}) + \varepsilon\mu\partial_x E \\ +\varepsilon\mu^{3/2} HC[H](v^\#,\bar{v}) = 0. \end{cases} \tag{2.79}$$

This model is numerically studied in Chapter 5, together with the model with general vorticity derived in the next subsection.

2.1.3.2 SGN equations with a general vorticity

In the presence of a non-constant vorticity, the situation is of course more complicated. According to [27], looking for a closure equation for E, leads to a cascade of equations involving interaction terms of increasing orders. Keeping only those orders below the overall $O(\mu^2)$ precision of the model allows to obtain a closed form without introducing additional turbulence models. In order to simplify the computations, we consider the previous medium amplitude bottom variations assumption,

$$\beta = O(\sqrt{\mu}). \tag{2.80}$$

Computation of the Reynolds-like tensor contribution

Proceeding as for (2.73) with dropping $O(\mu^2)$ terms, we have

$$\begin{aligned} \varepsilon\mu\partial_x\int_{-1+\beta b}^{\varepsilon\zeta}|v^*|^2 &= \varepsilon\mu\partial_x\int_{-1+\beta b}^{\varepsilon\zeta}|v^*_{\mathrm{sh}}|^2 + 2\varepsilon\mu^{\frac{3}{2}}\partial_x\int_{-1+\beta b}^{\varepsilon\zeta} v^*_{\mathrm{sh}} T[\varepsilon\zeta,\beta b]\bar{v} \\ &= \varepsilon\mu\partial_x\int_{-1+\beta b}^{\varepsilon\zeta}|v^*_{\mathrm{sh}}|^2 + 2\varepsilon\mu^{\frac{3}{2}}\partial_x\int_{-1+\beta b}^{\varepsilon\zeta} v^*_{\mathrm{sh}}\int_z^{\varepsilon\zeta}\partial_x^2((1+z'-\beta b)\bar{v}), \end{aligned}$$

and from the identity,

$$2\int_{-1+\beta b}^{\zeta} v^*_{\mathrm{sh}}\int_z^{\varepsilon\zeta}\partial_x^2((1+z'-\beta b)\bar{v}) = -\int_{-1+\beta b}^{\varepsilon\zeta}\int_z^{\varepsilon\zeta} v^*_{\mathrm{sh}}\partial_x^2((1+z'-\beta b)\bar{v}), \tag{2.81}$$

we get,

$$\varepsilon\mu\partial_x\int_{-1+\beta b}^{\varepsilon\zeta}|v^*|^2 = \varepsilon\mu\partial_x\int_{-1+\beta b}^{\varepsilon\zeta}|v^*_{\mathrm{sh}}|^2 - \varepsilon\mu^{\frac{3}{2}}\partial_x\int_{-1+\beta b}^{\varepsilon\zeta}\int_z^{\varepsilon\zeta} v^*_{\mathrm{sh}}\partial_x^2((1+z'-\beta b)\bar{v}). \tag{2.82}$$

Introducing,

$$v^\# := -\frac{24}{H^3}\int_{-1+\beta b}^{\varepsilon\zeta}\int_z^{\varepsilon\zeta}\int_{-1+\beta b}^{z} v^*_{\mathrm{sh}}, \tag{2.83}$$

one computes that,

$$\int_{-1+\beta b}^{\varepsilon\zeta}\int_{z}^{\varepsilon\zeta} v_{\rm sh}^{*}\partial_x^2((1+z'-\beta b)\bar{v}) = \frac{H^3}{12}v^{\#}\partial_x^2\bar{v} + O(\beta), \tag{2.84}$$

and we deduce, under the medium amplitude bottom variations assumption (2.80) that,

$$\varepsilon\mu\partial_x\int_{-1+\beta b}^{\varepsilon\zeta}|v^{*}|^2 = \varepsilon\mu\partial_x\int_{-1+\beta b}^{\varepsilon\zeta}|v_{\rm sh}^{*}|^2 - \varepsilon\frac{\mu^{\frac{3}{2}}}{12}\partial_x(H^3v^{\#}\partial_x^2\bar{v}) + O(\mu^2). \tag{2.85}$$

An equation for the shear velocity

Let derive an approximate equation solved by the shear velocity $v_{\rm sh}^{*}$ defined in (2.66), starting from the equation on the horizontal component of the vorticity,

$$\partial_t\boldsymbol{\omega}_{\mu,h} + \varepsilon v\partial_x\boldsymbol{\omega}_{\mu,h} + \frac{\varepsilon}{\mu}w\partial_z\boldsymbol{\omega}_{\mu,h} = \varepsilon\boldsymbol{\omega}_{\mu,h}\partial_x v + \frac{\varepsilon}{\sqrt{\mu}}\boldsymbol{\omega}_{\mu,v}\partial_z v. \tag{2.86}$$

Recalling that we have,

$$\begin{aligned} v &= \bar{v} + \sqrt{\mu}v_{\rm sh}^{*} + O(\mu),\\ w &= -\mu\partial_x[(1+z-\beta b)\bar{v}] - \mu^{\frac{3}{2}}\partial_x\int_{-1+\beta b}^{z} v_{\rm sh}^{*} + O(\mu^2), \end{aligned} \tag{2.87}$$

one can compute,

$$\begin{aligned} \varepsilon v\partial_x\boldsymbol{\omega}_{\mu,h} &= \varepsilon\bar{v}\partial_x\boldsymbol{\omega}_{\mu,h} + \varepsilon\sqrt{\mu}v_{\rm sh}^{*}\partial_x\boldsymbol{\omega}_{\mu,h},\\ \frac{\varepsilon}{\mu}w\partial_z\boldsymbol{\omega}_{\mu,h} &= -\varepsilon\partial_x[(1+z-\beta b)\bar{v}]\partial_z\boldsymbol{\omega}_{\mu,h} - \varepsilon\sqrt{\mu}\Big(\partial_x\int_{-1+\beta b}^{z} v_{\rm sh}^{*}\Big)\partial_z\boldsymbol{\omega}_{\mu,h},\\ \varepsilon\boldsymbol{\omega}_{\mu,h}\partial_x v &= \varepsilon\boldsymbol{\omega}_{\mu,h}\partial_x\bar{v} + \varepsilon\sqrt{\mu}\boldsymbol{\omega}_{\mu,h}\partial_x v_{\rm sh}^{*}, \end{aligned} \tag{2.88}$$

and as we have $\boldsymbol{\omega}_{\mu,v} = -\partial_x v = -\partial_x\bar{v} - \sqrt{\mu}\partial_x v_{\rm sh}^{*}$ and $\partial_z v = \sqrt{\mu}\partial_z v_{\rm sh}^{*} = \sqrt{\mu}\boldsymbol{\omega}_{\mu,h}$, we obtain

$$\frac{\varepsilon}{\sqrt{\mu}}\boldsymbol{\omega}_{\mu,v}\partial_z v = -\varepsilon\boldsymbol{\omega}_{\mu,h}\partial_x\bar{v} - \varepsilon\sqrt{\mu}\boldsymbol{\omega}_{\mu,h}\partial_x v_{\rm sh}^{*}. \tag{2.89}$$

Replacing the above calculations in (2.86), we obtain

$$\begin{aligned} \partial_t\boldsymbol{\omega}_{\mu,h} + \varepsilon\bar{v}\partial_x\boldsymbol{\omega}_{\mu,h} - \varepsilon\partial_x[(1+z-\beta b)\bar{v}]\partial_z\boldsymbol{\omega}_{\mu,h}&\\ = \varepsilon\sqrt{\mu}\Big\{-v_{\rm sh}^{*}\partial_x\boldsymbol{\omega}_{\mu,h} + \partial_x\Big(\int_{-1+\beta b}^{z} v_{\rm sh}^{*}\Big)\partial_z\boldsymbol{\omega}_{\mu,h}\Big\} + O(\varepsilon\mu).& \end{aligned} \tag{2.90}$$

Dropping $O(\varepsilon\sqrt{\mu})$ terms, we infer

$$\partial_t\boldsymbol{\omega}_{\mu,h} + \varepsilon\bar{v}\partial_x\boldsymbol{\omega}_{\mu,h} - \varepsilon\partial_x[(1+z-\beta b)\bar{v}]\partial_z\boldsymbol{\omega}_{\mu,h} = O(\varepsilon\sqrt{\mu}). \tag{2.91}$$

Integrating equation (2.90) on z and using (2.7) and (2.66), we get

$$\begin{aligned}\int_z^{\varepsilon\zeta} \partial_t \boldsymbol{\omega}_{\mu,h} &= \partial_t \int_z^{\varepsilon\zeta} \boldsymbol{\omega}_{\mu,h} - \varepsilon\partial_t\zeta\boldsymbol{\omega}_{\mu,h_{|\varepsilon\zeta}},\\ &= -\partial_t v_{\text{sh}} - \varepsilon\partial_t\zeta\boldsymbol{\omega}_{\mu,h_{|\varepsilon\zeta}},\end{aligned}$$

$$\begin{aligned}\int_z^{\varepsilon\zeta} \bar{v}\partial_x\boldsymbol{\omega}_{\mu,h} &= \bar{v}\int_z^{\varepsilon\zeta} \partial_x\boldsymbol{\omega}_{\mu,h},\\ &= \bar{v}[\partial_x \int_z^{\varepsilon\zeta} \boldsymbol{\omega}_{\mu,h} - \varepsilon\partial_x\zeta\boldsymbol{\omega}_{\mu,h_{|\varepsilon\zeta}}],\\ &= -\bar{v}\partial_x v_{\text{sh}} - \varepsilon\bar{v}\partial_x\zeta\boldsymbol{\omega}_{\mu,h_{|\varepsilon\zeta}},\end{aligned}$$

$$\begin{aligned}\int_z^{\varepsilon\zeta} \partial_x[(1+z-\beta b)\bar{v}]\partial_z\boldsymbol{\omega}_{\mu,h} &= \int_z^{\varepsilon\zeta} \partial_z\big\{\partial_x[(1+z-\beta b)\bar{v}]\boldsymbol{\omega}_{\mu,h}\big\}\\ &\quad - \int_z^{\varepsilon\zeta} \partial_z\big\{\partial_x[(1+z-\beta b)\bar{v}]\big\}\boldsymbol{\omega}_{\mu,h},\\ &= \Big[\partial_x[(1+z-\beta b)\bar{v}]\boldsymbol{\omega}_{\mu,h}\Big]_z^{\varepsilon\zeta} - \int_z^{\varepsilon\zeta} \partial_z\Big\{\partial_x[(1+z-\beta b)\bar{v}]\Big\}\boldsymbol{\omega}_{\mu,h}.\end{aligned}$$

We also have,

$$\partial_z\Big\{\partial_x[(1+z-\beta b)\bar{v}]\Big\} = \partial_z\{-\beta\partial_x b\bar{v} + (1+z-\beta b)\partial_x\bar{v}\} = \partial_x\bar{v}, \tag{2.92}$$

and thus,

$$\begin{aligned}\int_z^{\varepsilon\zeta} \partial_x[(1+z-\beta b)\bar{v}]\partial_z\boldsymbol{\omega}_{\mu,h} &= \Big[\partial_x[(1+z-\beta b)\bar{v}]\boldsymbol{\omega}_{\mu,h}\Big]_z^{\varepsilon\zeta} - \int_z^{\varepsilon\zeta} \boldsymbol{\omega}_{\mu,h}\partial_x\bar{v},\\ &= \Big[\partial_x[(1+z-\beta b)\bar{v}]\boldsymbol{\omega}_{\mu,h}\Big]_z^{\varepsilon\zeta} + v_{\text{sh}}\partial_x\bar{v},\\ &= \Big[\big(-\beta\partial_x b\bar{v} + (1+z-\beta b)\partial_x\bar{v}\big)\boldsymbol{\omega}_{\mu,h}\Big]_z^{\varepsilon\zeta} + v_{\text{sh}}\partial_x\bar{v},\\ &= \big\{-\beta\partial_x b\bar{v}(\boldsymbol{\omega}_{\mu,h_{|\varepsilon\zeta}} - \boldsymbol{\omega}_{\mu,h}) + H\partial_x\bar{v}\boldsymbol{\omega}_{\mu,h_{|\varepsilon\zeta}} - (1+z-\beta b)\partial_x\bar{v}\boldsymbol{\omega}_{\mu,h}\big\} + v_{\text{sh}}\partial_x\bar{v}.\end{aligned}$$

Integrating the right-hand side terms in (2.90), we get

$$\begin{aligned}\int_z^{\varepsilon\zeta} \Big(\partial_x \int_{-1+\beta b}^{z} v_{\text{sh}}^*\Big)\partial_z\boldsymbol{\omega}_{\mu,h} &= \int_z^{\varepsilon\zeta} \partial_z\Big\{\Big(\partial_x \int_{-1+\beta b}^{z} v_{\text{sh}}^*\Big)\boldsymbol{\omega}_{\mu,h}\Big\}\\ &\quad - \int_z^{\varepsilon\zeta} \partial_z\Big\{\Big(\partial_x \int_{-1+\beta b}^{z} v_{\text{sh}}^*\Big)\Big\}\boldsymbol{\omega}_{\mu,h},\\ &= \Big[\Big(\partial_x \int_{-1+\beta b}^{z} v_{\text{sh}}^*\Big)\boldsymbol{\omega}_{\mu,h}\Big]_z^{\varepsilon\zeta} - \int_z^{\varepsilon\zeta} \partial_x\Big\{\Big(\underbrace{\partial_z \int_{-1+\beta b}^{z} v_{\text{sh}}^*}_{= v_{\text{sh}}^* - v_{\text{sh}_{|-1+\beta b}}^*}\Big)\Big\}\boldsymbol{\omega}_{\mu,h},\end{aligned}$$

using (2.66) and the decomposition (2.4), one gets

$$\begin{aligned} v^*_{\mathrm{sh}_{|-1+\beta b}} &= -\Big(\int_{-1+\beta b}^{\varepsilon\zeta} \boldsymbol{\omega}_{\mu,h}\Big)^*, \\ &= -\Big(\int_{-1+\beta b}^{\varepsilon\zeta} \boldsymbol{\omega}_{\mu,h}\Big) + \frac{1}{H}\int_{-1+\beta b}^{\varepsilon\zeta}\Big(\underbrace{\int_{-1+\beta b}^{\varepsilon\zeta} \boldsymbol{\omega}_{\mu,h}}_{\text{does not depend on } z}\Big), \\ &= -\Big(\int_{-1+\beta b}^{\varepsilon\zeta} \boldsymbol{\omega}_{\mu,h}\Big) + \Big(\int_{-1+\beta b}^{\varepsilon\zeta} \boldsymbol{\omega}_{\mu,h}\Big) = 0, \end{aligned} \tag{2.93}$$

and,

$$\Big[\Big(\partial_x \int_{-1+\beta b}^{z} v^*_{\mathrm{sh}}\Big)\boldsymbol{\omega}_{\mu,h}\Big]_z^{\varepsilon\zeta} = \Big(\partial_x \int_{-1+\beta b}^{\varepsilon\zeta} v^*_{\mathrm{sh}}\Big)\boldsymbol{\omega}_{\mu,h_{|\varepsilon\zeta}} - \Big(\partial_x \int_{-1+\beta b}^{z} v^*_{\mathrm{sh}}\Big)\boldsymbol{\omega}_{\mu,h}, \tag{2.94}$$

still using the decomposition (2.4), we infer

$$\int_{-1+\beta b}^{\varepsilon\zeta} v^*_{\mathrm{sh}} = 0, \tag{2.95}$$

thus,

$$\int_z^{\varepsilon\zeta}\Big(\partial_x \int_{-1+\beta b}^{z} v^*_{\mathrm{sh}}\Big)\partial_z\boldsymbol{\omega}_{\mu,h} = -\Big(\partial_x \int_{-1+\beta b}^{z} v^*_{\mathrm{sh}}\Big)\boldsymbol{\omega}_{\mu,h} - \int_z^{\varepsilon\zeta} \boldsymbol{\omega}_{\mu,h}\partial_x v^*_{\mathrm{sh}}.$$

Gathering the above calculations, we obtain

$$\begin{aligned} &-\partial_t v_{\mathrm{sh}} - \varepsilon\partial_t\zeta\boldsymbol{\omega}_{\mu,h_{|\varepsilon\zeta}} - \varepsilon\bar{v}\partial_x v_{\mathrm{sh}} - \varepsilon\bar{v}\partial_x\zeta\boldsymbol{\omega}_{\mu,h_{|\varepsilon\zeta}} - \varepsilon v_{\mathrm{sh}}\partial_x\bar{v} \\ &\quad - \Big\{-\beta\partial_x b\bar{v}\boldsymbol{\omega}_{\mu,h_{|\varepsilon\zeta}} + \beta\partial_x b\bar{v}\boldsymbol{\omega}_{\mu,h_{|\varepsilon\zeta}} + H\partial_x\bar{v}\boldsymbol{\omega}_{\mu,h_{|\varepsilon\zeta}} - (1+z-\beta b)\partial_x\bar{v}\boldsymbol{\omega}_{\mu,h}\Big\} \\ &\quad = \varepsilon\sqrt{\mu}\Big\{-\int_z^{\varepsilon\zeta} v^*_{\mathrm{sh}}\partial_x\boldsymbol{\omega}_{\mu,h} - \Big(\partial_x\int_{-1+\beta b}^{z} v^*_{\mathrm{sh}}\Big)\boldsymbol{\omega}_{\mu,h} - \int_z^{\varepsilon\zeta}\boldsymbol{\omega}_{\mu,h}\partial_x v^*_{\mathrm{sh}}\Big\} + O(\varepsilon\mu), \end{aligned} \tag{2.96}$$

moreover,

$$\begin{aligned} &\partial_t v_{\mathrm{sh}} + \varepsilon\bar{v}\partial_x v_{\mathrm{sh}} + \varepsilon v_{\mathrm{sh}}\partial_x\bar{v} \\ &\quad + \varepsilon(\partial_t\zeta + \varepsilon\bar{v}\partial_x\zeta - \beta\partial_x b\bar{v} + H\partial_x\bar{v})\boldsymbol{\omega}_{\mu,h_{|\varepsilon\zeta}} + \varepsilon\Big(\beta\partial_x b\bar{v} - \partial_x\bar{v}(1+z-\beta b)\Big)\boldsymbol{\omega}_{\mu,h} \\ &\quad = \varepsilon\sqrt{\mu}\Big\{\int_z^{\varepsilon\zeta} v^*_{\mathrm{sh}}\partial_x\boldsymbol{\omega}_{\mu,h} + \Big(\partial_x\int_{-1+\beta b}^{z} v^*_{\mathrm{sh}}\Big)\boldsymbol{\omega}_{\mu,h} + \int_z^{\varepsilon\zeta}\boldsymbol{\omega}_{\mu,h}\partial_x v^*_{\mathrm{sh}}\Big\} + O(\varepsilon\mu), \end{aligned} \tag{2.97}$$

using the mass conservation equation, we obtain

$$\begin{aligned} (\partial_t\zeta + \varepsilon\bar{v}\partial_x\zeta - \beta\partial_x b\bar{v} + H\partial_x\bar{v})\boldsymbol{\omega}_{\mu,h_{|\varepsilon\zeta}} &= (\partial_t\zeta + \bar{v}\partial_x(1+\varepsilon\zeta-\beta b) + H\partial_x\bar{v})\boldsymbol{\omega}_{\mu,h_{|\varepsilon\zeta}}, \\ &= (\partial_t\zeta + \partial_x(H\bar{v}))\boldsymbol{\omega}_{\mu,h_{|\varepsilon\zeta}} = 0, \end{aligned} \tag{2.98}$$

we have also,

$$\begin{aligned} \Big(\beta\partial_x b\bar{v} - \partial_x\bar{v}(1+z-\beta b)\Big)\boldsymbol{\omega}_{\mu,h} &= \Big(-\partial_x(1+z-\beta b)\bar{v} - (1+z-\beta b)\partial_x\bar{v}\Big)\boldsymbol{\omega}_{\mu,h}, \\ &= -\partial_x[(1+z-\beta b)\bar{v}]\boldsymbol{\omega}_{\mu,h}. \end{aligned}$$

Thus,

$$\begin{aligned}
&\partial_t v_{\mathrm{sh}} + \varepsilon\bar{v}\partial_x v_{\mathrm{sh}} + \varepsilon v_{\mathrm{sh}}\partial_x\bar{v} - \varepsilon\partial_x[(1+z-\beta b)\bar{v}]\boldsymbol{\omega}_{\mu,h} \\
&\quad = \varepsilon\sqrt{\mu}\Big\{\int_z^{\varepsilon\zeta} v_{\mathrm{sh}}^*\partial_x\boldsymbol{\omega}_{\mu,h} + \Big(\partial_x\int_{-1+\beta b}^{z} v_{\mathrm{sh}}^*\Big)\boldsymbol{\omega}_{\mu,h} + \int_z^{\varepsilon\zeta}\boldsymbol{\omega}_{\mu,h}\partial_x v_{\mathrm{sh}}^*\Big\} + O(\varepsilon\mu), \qquad (2.99)\\
&\quad = \varepsilon\sqrt{\mu}C + O(\varepsilon\mu),
\end{aligned}$$

with,

$$C = \int_z^{\varepsilon\zeta} v_{\mathrm{sh}}^*\partial_x\boldsymbol{\omega}_{\mu,h} + \Big(\partial_x\int_{-1+\beta b}^{z} v_{\mathrm{sh}}^*\Big)\boldsymbol{\omega}_{\mu,h} + \int_z^{\varepsilon\zeta}\boldsymbol{\omega}_{\mu,h}\partial_x v_{\mathrm{sh}}^*, \qquad (2.100)$$

using the fact that $\boldsymbol{\omega}_{\mu,h} = \partial_z v_{\mathrm{sh}}^*$, one can simplifie C-expression (2.100) as follows,

$$\begin{aligned}
C &= \int_z^{\varepsilon\zeta} v_{\mathrm{sh}}^*\partial_x(\partial_z v_{\mathrm{sh}}^*) + \int_z^{\varepsilon\zeta}\partial_x v_{\mathrm{sh}}^*\partial_z v_{\mathrm{sh}}^* + \Big(\partial_x\int_{-1+\beta b}^{z} v_{\mathrm{sh}}^*\Big)\boldsymbol{\omega}_{\mu,h},\\
&= \int_z^{\varepsilon\zeta}\Big[v_{\mathrm{sh}}^*\partial_z(\partial_x v_{\mathrm{sh}}^*) + \partial_x v_{\mathrm{sh}}^*\partial_z v_{\mathrm{sh}}^*\Big] + \Big(\partial_x\int_{-1+\beta b}^{z} v_{\mathrm{sh}}^*\Big)\boldsymbol{\omega}_{\mu,h},\\
&= \int_z^{\varepsilon\zeta}\partial_z(v_{\mathrm{sh}}^*\partial_x v_{\mathrm{sh}}^*) + \Big(\partial_x\int_{-1+\beta b}^{z} v_{\mathrm{sh}}^*\Big)\boldsymbol{\omega}_{\mu,h}, \qquad (2.101)\\
&= \Big[v_{\mathrm{sh}}^*\partial_x v_{\mathrm{sh}}^*\Big]_z^{\varepsilon\zeta} + \Big(\partial_x\int_{-1+\beta b}^{z} v_{\mathrm{sh}}^*\Big)\partial_z v_{\mathrm{sh}}^*,\\
&= (v_{\mathrm{sh}}^*\partial_x v_{\mathrm{sh}}^*)_{|\varepsilon\zeta} - v_{\mathrm{sh}}^*\partial_x v_{\mathrm{sh}}^* + \Big(\partial_x\int_{-1+\beta b}^{z} v_{\mathrm{sh}}^*\Big)\partial_z v_{\mathrm{sh}}^*,
\end{aligned}$$

owing to $v_{\mathrm{sh}}^* = v_{\mathrm{sh}} - \bar{v}_{\mathrm{sh}}$ and $v_{\mathrm{sh}_{|\varepsilon\zeta}} = 0$, we get

$$(v_{\mathrm{sh}}^*\partial_x v_{\mathrm{sh}}^*)_{|\varepsilon\zeta} = ((v_{\mathrm{sh}} - \bar{v}_{\mathrm{sh}})\partial_x(v_{\mathrm{sh}} - \bar{v}_{\mathrm{sh}}))_{|\varepsilon\zeta} = \bar{v}_{\mathrm{sh}}\partial_x\bar{v}_{\mathrm{sh}}, \qquad (2.102)$$

so we get,

$$C = -v_{\mathrm{sh}}^*\partial_x v_{\mathrm{sh}}^* + \bar{v}_{\mathrm{sh}}\partial_x\bar{v}_{\mathrm{sh}} + \Big(\partial_x\int_{-1+\beta b}^{z} v_{\mathrm{sh}}^*\Big)\partial_z v_{\mathrm{sh}}^*, \qquad (2.103)$$

still using $v_{\mathrm{sh}}^* = v_{\mathrm{sh}} - \bar{v}_{\mathrm{sh}}$, we get

$$-v_{\mathrm{sh}}^*\partial_x v_{\mathrm{sh}}^* + \bar{v}_{\mathrm{sh}}\partial_x\bar{v}_{\mathrm{sh}} = -v_{\mathrm{sh}}^*\partial_x v_{\mathrm{sh}} + v_{\mathrm{sh}}\partial_x\bar{v}_{\mathrm{sh}}, \qquad (2.104)$$

thus,

$$C = -v_{\mathrm{sh}}^*\partial_x v_{\mathrm{sh}} + v_{\mathrm{sh}}\partial_x\bar{v}_{\mathrm{sh}} + \Big(\partial_x\int_{-1+\beta b}^{z} v_{\mathrm{sh}}^*\Big)\partial_z v_{\mathrm{sh}}^*. \qquad (2.105)$$

Finally, we obtain the following equation for the shear velocity

$$\begin{aligned}
&\partial_t v_{\mathrm{sh}} + \varepsilon\bar{v}\partial_x v_{\mathrm{sh}} + \varepsilon v_{\mathrm{sh}}\partial_x\bar{v} - \varepsilon\partial_x[(1+z-\beta b)\bar{v}]\partial_z v_{\mathrm{sh}} \\
&\qquad = \varepsilon\sqrt{\mu}\Big\{ - v_{\mathrm{sh}}^*\partial_x v_{\mathrm{sh}} + v_{\mathrm{sh}}\partial_x\bar{v}_{\mathrm{sh}} + \Big(\partial_x\int_{-1+\beta b}^{z} v_{\mathrm{sh}}^*\Big)\partial_z v_{\mathrm{sh}}^*\Big\} + O(\varepsilon\mu). \qquad (2.106)
\end{aligned}$$

Dropping the $O(\varepsilon\mu)$-terms we get lower order version of (2.106),

$$\partial_t v_{\rm sh} + \varepsilon\bar{v}\partial_x v_{\rm sh} + \varepsilon v_{\rm sh}\partial_x\bar{v} - \varepsilon\partial_x[(1+z-\beta b)\bar{v}]\partial_z v_{\rm sh} = O(\varepsilon\sqrt{\mu}). \tag{2.107}$$

Now, we want to obtain an equation of $\bar{v}_{\rm sh}$. Integrating (2.106) over z and using (2.7) we have

$$\begin{aligned}\int_{-1+\beta b}^{\varepsilon\zeta}\partial_t v_{\rm sh} &= \partial_t\int_{-1+\beta b}^{\varepsilon\zeta} v_{\rm sh} - \varepsilon\partial_t\zeta v_{{\rm sh}_{|\varepsilon\zeta}},\\ &= \partial_t(H\bar{v}_{\rm sh}) - \varepsilon\partial_t\zeta\underbrace{v_{{\rm sh}_{|\varepsilon\zeta}}}_{=0}.\end{aligned} \tag{2.108}$$

Recalling that,

$$v_{\rm sh} = -\int_z^{\varepsilon\zeta}\boldsymbol{\omega}_{\mu,h}, \qquad \text{we have thus} \qquad v_{{\rm sh}_{|\varepsilon\zeta}} = -\int_{\varepsilon\zeta}^{\varepsilon\zeta}\boldsymbol{\omega}_{\mu,h} = 0, \tag{2.109}$$

and,

$$\begin{aligned}\int_{-1+\beta b}^{\varepsilon\zeta}\bar{v}\partial_x v_{\rm sh} &= \bar{v}\partial_x(H\bar{v}_{\rm sh}) + \bar{v}\beta\partial_x b v_{{\rm sh}_{|-1+\beta b}},\\ \int_{-1+\beta b}^{\varepsilon\zeta} v_{\rm sh}\partial_x\bar{v} &= H\bar{v}_{\rm sh}\partial_x\bar{v},\\ \int_{-1+\beta b}^{\varepsilon\zeta}\partial_x[(1+z-\beta b)\bar{v}]\partial_z v_{\rm sh} &= \int_{-1+\beta b}^{\varepsilon\zeta}\partial_z\Big\{\partial_x[(1+z-\beta b)\bar{v}]v_{\rm sh}\Big\}\\ &\quad - \int_{-1+\beta b}^{\varepsilon\zeta}\partial_z\Big\{\partial_x[(1+z-\beta b)\bar{v}]\Big\}v_{\rm sh},\\ &= \int_{-1+\beta b}^{\varepsilon\zeta}\partial_z\Big\{\partial_x[(1+z-\beta b)\bar{v}]v_{\rm sh}\Big\} - H\bar{v}_{\rm sh}\partial_x\bar{v},\\ &= \Big[(-\beta\partial_x b\bar{v} + (1+z-\beta b)\partial_x\bar{v})v_{\rm sh}\Big]_{-1+\beta b}^{\varepsilon\zeta} - H\bar{v}_{\rm sh}\partial_x\bar{v},\\ &= \beta\partial_x b\bar{v}v_{{\rm sh}_{|-1+\beta b}} - H\bar{v}_{\rm sh}\partial_x\bar{v}.\end{aligned} \tag{2.110}$$

Integrating on z the terms of C-expression (2.105) and using $v_{\rm sh} = \bar{v}_{\rm sh} + v^*_{\rm sh}$, we infer

$$\begin{aligned}\int_{-1+\beta b}^{\varepsilon\zeta} v^*_{\rm sh}\partial_x v_{\rm sh} &= \int_{-1+\beta b}^{\varepsilon\zeta} v^*_{\rm sh}\partial_x\bar{v}_{\rm sh} + \int_{-1+\beta b}^{\varepsilon\zeta} v^*_{\rm sh}\partial_x v^*_{\rm sh},\\ &= \partial_x\bar{v}_{\rm sh}\underbrace{\int_{-1+\beta b}^{\varepsilon\zeta} v^*_{\rm sh}}_{=0} + \int_{-1+\beta b}^{\varepsilon\zeta} v^*_{\rm sh}\partial_x v^*_{\rm sh},\\ &= \int_{-1+\beta b}^{\varepsilon\zeta} v^*_{\rm sh}\partial_x v^*_{\rm sh}.\end{aligned} \tag{2.111}$$

Integrating the second term of (2.105), yields

$$\int_{-1+\beta b}^{\varepsilon\zeta} v_{\mathrm{sh}}\partial_x\bar{v}_{\mathrm{sh}} = H\bar{v}_{\mathrm{sh}}\partial_x\bar{v}_{\mathrm{sh}}, \tag{2.112}$$

then using (2.7) and $v_{\mathrm{sh}_{|-1+\beta b}} = 0$, we infer

$$\begin{aligned}
\int_{-1+\beta b}^{\varepsilon\zeta}\Big(\partial_x\int_{-1+\beta b}^{z} v_{\mathrm{sh}}^*\Big)\partial_z v_{\mathrm{sh}}^* &= \int_{-1+\beta b}^{\varepsilon\zeta}\partial_z\Big\{\Big(\partial_x\int_{-1+\beta b}^{z} v_{\mathrm{sh}}^*\Big)v_{\mathrm{sh}}^*\Big\} \\
&\quad - \int_{-1+\beta b}^{\varepsilon\zeta}\partial_z\Big\{\Big(\partial_x\int_{-1+\beta b}^{z} v_{\mathrm{sh}}^*\Big)\Big\}v_{\mathrm{sh}}^*, \\
&= \underbrace{\Big[\Big(\partial_x\int_{-1+\beta b}^{z} v_{\mathrm{sh}}^*\Big)v_{\mathrm{sh}}^*\Big]_{-1+\beta b}^{\varepsilon\zeta}}_{=0} - \int_{-1+\beta b}^{\varepsilon\zeta}\partial_x\Big(\partial_z\int_{-1+\beta b}^{z} v_{\mathrm{sh}}^*\Big)v_{\mathrm{sh}}^*, \\
&= -\int_{-1+\beta b}^{\varepsilon\zeta} v_{\mathrm{sh}}^*\partial_x v_{\mathrm{sh}}^*,
\end{aligned}$$

one can deduce,

$$-\int_{-1+\beta b}^{\varepsilon\zeta} v_{\mathrm{sh}}^*\partial_x v_{\mathrm{sh}} + \int_{-1+\beta b}^{\varepsilon\zeta}\Big(\partial_x\int_{-1+\beta b}^{z} v_{\mathrm{sh}}^*\Big)\partial_z v_{\mathrm{sh}}^* = -\partial_x\int_{-1+\beta b}^{\varepsilon\zeta}(v_{\mathrm{sh}}^*)^2, \tag{2.113}$$

reprouping the computations of C-expression terms, we deduce

$$C = H\bar{v}_{\mathrm{sh}}\partial_x\bar{v}_{\mathrm{sh}} - \partial_x\int_{-1+\beta b}^{\varepsilon\zeta}(v_{\mathrm{sh}}^*)^2, \tag{2.114}$$

gathering the above calculations, one gets

$$\begin{aligned}
&\partial_t(H\bar{v}_{\mathrm{sh}}) + \varepsilon\bar{v}\partial_x(H\bar{v}_{\mathrm{sh}}) \\
&\qquad + \varepsilon\beta\bar{v}\partial_x b v_{\mathrm{sh}_{|-1+\beta b}} + \varepsilon H\bar{v}_{\mathrm{sh}}\partial_x\bar{v} - \varepsilon\beta\partial_x b\bar{v}v_{\mathrm{sh}_{|-1+\beta b}} \\
&\qquad + \varepsilon H\bar{v}_{\mathrm{sh}}\partial_x\bar{v} = \varepsilon\sqrt{\mu}\Big\{H\bar{v}_{\mathrm{sh}}\partial_x\bar{v}_{\mathrm{sh}} - \partial_x\int_{-1+\beta b}^{\varepsilon\zeta}(v_{\mathrm{sh}}^*)^2\Big\} + O(\varepsilon\mu),
\end{aligned} \tag{2.115}$$

thus,

$$\begin{aligned}
&\partial_t(H\bar{v}_{\mathrm{sh}}) + \varepsilon\bar{v}\partial_x(H\bar{v}_{\mathrm{sh}}) + \varepsilon H\bar{v}_{\mathrm{sh}}\partial_x\bar{v} \\
&\qquad + \varepsilon H\bar{v}_{\mathrm{sh}}\partial_x\bar{v} = \varepsilon\sqrt{\mu}\Big\{H\bar{v}_{\mathrm{sh}}\partial_x\bar{v}_{\mathrm{sh}} - \partial_x\int_{-1+\beta b}^{\varepsilon\zeta}(v_{\mathrm{sh}}^*)^2\Big\} + O(\varepsilon\mu),
\end{aligned} \tag{2.116}$$

using the mass conservation equation $\partial_t H + \partial_x(H\bar{v}) = 0$, one can simplifie

$$\begin{aligned}
\partial_t(H\bar{v}_{\mathrm{sh}}) + \varepsilon\bar{v}\partial_x(H\bar{v}_{\mathrm{sh}}) + \varepsilon H\bar{v}_{\mathrm{sh}}\partial_x\bar{v} &= \partial_t H\bar{v}_{\mathrm{sh}} + H\partial_t\bar{v}_{\mathrm{sh}} + \varepsilon\bar{v}\partial_x H\bar{v}_{\mathrm{sh}} + \varepsilon H\bar{v}\partial_x\bar{v}_{\mathrm{sh}} + \varepsilon H\bar{v}_{\mathrm{sh}}\partial_x\bar{v}, \\
&= \bar{v}_{\mathrm{sh}}\underbrace{(\partial_t H + \partial_x(H\bar{v}))}_{=0} + H\partial_t\bar{v}_{\mathrm{sh}} + \varepsilon\bar{v}H\partial_x\bar{v}_{\mathrm{sh}}, \\
&= H\partial_t\bar{v}_{\mathrm{sh}} + \varepsilon H\bar{v}\partial_x\bar{v}_{\mathrm{sh}},
\end{aligned}$$

we obtain,

$$H\partial_t\bar{v}_{\rm sh} + \varepsilon H\bar{v}\partial_x\bar{v}_{\rm sh} + \varepsilon H\bar{v}_{\rm sh}\partial_x\bar{v} = \varepsilon\sqrt{\mu}\Big\{H\bar{v}_{\rm sh}\partial_x\bar{v}_{\rm sh} - \partial_x\int_{-1+\beta b}^{\varepsilon\zeta}(v^*_{\rm sh})^2\Big\} + O(\varepsilon\mu). \tag{2.117}$$

Dividing by H we obtain the following equation for the average shear velocity $\bar{v}_{\rm sh}$,

$$\partial_t\bar{v}_{\rm sh} + \varepsilon\bar{v}\partial_x\bar{v}_{\rm sh} + \varepsilon\bar{v}_{\rm sh}\partial_x\bar{v} + \varepsilon\sqrt{\mu}\Big\{\frac{1}{H}\partial_x\int_{-1+\beta b}^{\varepsilon\zeta}(v^*_{\rm sh})^2 - \bar{v}_{\rm sh}\partial_x\bar{v}_{\rm sh}\Big\} = O(\varepsilon\mu). \tag{2.118}$$

Dropping $O(\varepsilon\mu)$ terms we get lower order version of (2.118),

$$\partial_t\bar{v}_{\rm sh} + \varepsilon\bar{v}\partial_x\bar{v}_{\rm sh} + \varepsilon\bar{v}_{\rm sh}\partial_x\bar{v} = O(\varepsilon\sqrt{\mu}). \tag{2.119}$$

Taking the difference between (2.118) and (2.106) and using (2.104) with the fact that $\partial_z v_{\rm sh} = \partial_z v^*_{\rm sh}$ and dropping $O(\varepsilon\mu)$ we obtain the following evolution equation on $v^*_{\rm sh}$,

$$\begin{aligned}&\partial_t v^*_{\rm sh} + \varepsilon\bar{v}\partial_x v^*_{\rm sh} + \varepsilon v^*_{\rm sh}\partial_x\bar{v}\\ &\quad + \varepsilon\sqrt{\mu}\Big\{v^*_{\rm sh}\partial_x v^*_{\rm sh} - \frac{1}{H}\partial_x\int_{-1+\beta b}^{\varepsilon\zeta}(v^*_{\rm sh})^2\Big\} = \varepsilon\partial_x\Big[\int_{-1+\beta b}^{z}(\bar{v} + \sqrt{\mu}v^*_{\rm sh})\Big]\partial_z v^*_{\rm sh}.\end{aligned} \tag{2.120}$$

Dropping $O(\varepsilon\sqrt{\mu})$ terms we get a lower order evolution equation for $v^*_{\rm sh}$,

$$\partial_t v^*_{\rm sh} + \varepsilon\bar{v}\partial_x v^*_{\rm sh} + \varepsilon v^*_{\rm sh}\partial_x\bar{v} - \varepsilon\partial_x[(1+z-\beta b)\bar{v}]\partial_z v^*_{\rm sh} = O(\varepsilon\sqrt{\mu}). \tag{2.121}$$

Computation of the pressure contribution

As for (2.74), we write

$$\begin{aligned}\frac{1}{\varepsilon}\int_{-1+\beta b}^{\varepsilon\zeta}\partial_x P_{nh} &= \int_{-1+\beta b}^{\varepsilon\zeta}\partial_x\int_{z}^{\varepsilon\zeta}\Big(\partial_t w + \varepsilon v\partial_x w + \frac{\varepsilon}{\mu}w\partial_z w\Big)\\ &= \mu\mathbf{T}[H,\beta b][\partial_t(H\bar{v}) + \varepsilon\partial_x(H\bar{v}^2)] + \varepsilon\mu HQ_1[H,\beta b](\bar{v}) + \mu^{\frac{3}{2}}\varrho_{3/2} + O(\mu^2).\end{aligned} \tag{2.122}$$

To calculate $\varrho_{3/2}$ we introduce the operator $\tilde{\mathcal{T}}[\varepsilon\zeta,\beta b]$ as follows,

$$\tilde{\mathcal{T}}[\varepsilon\zeta,\beta b]w = -\frac{1}{H}\int_{-1+\beta b}^{\varepsilon\zeta}\partial_x\int_{z}^{\varepsilon\zeta}\partial_x\int_{-1+\beta b}^{z}w, \tag{2.123}$$

with $\tilde{\mathcal{T}}[\varepsilon\zeta,\beta b]\overline{w} = \mathcal{T}[\varepsilon\zeta,\beta b]w$ when $w = \overline{w}$.

$$\begin{aligned}\varrho_{3/2} &= H\tilde{\mathcal{T}}[\varepsilon\zeta,\beta b]\partial_t v^*_{\rm sh}\\ &\quad + \varepsilon\int_{-1+\beta b}^{\varepsilon\zeta}\partial_x\int_{z}^{\varepsilon\zeta}\Big(\bar{v}\partial_x(-\partial_x\int_{-1+\beta b}^{z}v^*_{\rm sh}) + v^*_{\rm sh}\partial_x(-\partial_x((1+z'-\beta b)\bar{v}))\Big)\\ &\quad + \varepsilon\int_{-1+\beta b}^{\varepsilon\zeta}\partial_x\int_{z}^{\varepsilon\zeta}\Big(-\partial_x((1+z'-\beta b)\bar{v})(-\partial_x v^*_{\rm sh}) - \int_{-1+\beta b}^{z}\partial_x v^*_{\rm sh}(-\partial_x\bar{v})\Big).\end{aligned} \tag{2.124}$$

According to (2.80) the contribution of order $O(\mu^{3/2}\beta)$ may be neglected. We obtain,

$$\begin{aligned}\varrho_{3/2} &= H\tilde{\mathcal{T}}[\varepsilon\zeta,\beta b][\partial_t v^*_{\rm sh} + \varepsilon\bar{v}\partial_x v^*_{\rm sh} + \varepsilon\bar{v}\partial_x v^*_{\rm sh}] + 2\varepsilon\int_{-1}^{\varepsilon\zeta}\partial_x\int_z^{\varepsilon\zeta}(\partial_x\bar{v})\partial_x\int_{-1}^{z'} v^*_{\rm sh}\\ &\quad - \varepsilon\int_{-1}^{\varepsilon\zeta}\partial_x\int_z^{\varepsilon\zeta} v^*_{\rm sh}\partial_x^2((1+z')\bar{v}) + \varepsilon\int_{-1}^{\varepsilon\zeta}\partial_x\int_z^{\varepsilon\zeta}(\partial_x v^*_{\rm sh})\partial_x((1+z')\bar{v}).\end{aligned} \tag{2.125}$$

Applying $\tilde{\mathcal{T}}[\varepsilon\zeta,\beta b]$ to (2.120) up to $O(\sqrt{\mu})$ terms, we get

$$\begin{aligned}H\tilde{\mathcal{T}}[\varepsilon\zeta,\beta b][\partial_t v^*_{\rm sh} + \varepsilon\bar{v}\partial_x v^*_{\rm sh} + \varepsilon v^*_{\rm sh}\partial_x\bar{v}] &= -\varepsilon\int_{-1}^{\zeta}\partial_x\int_z^{\varepsilon\zeta}\partial_x\int_{-1}^{z'}\partial_x[(1+z)\bar{v}]\partial_z v^*_{\rm sh}\\ &= -\varepsilon\int_{-1}^{\zeta}\partial_x\int_z^{\varepsilon\zeta}\partial_x\int_{-1}^{z'}\partial_x\bar{v}v^*_{\rm sh} - \varepsilon\int_{-1}^{\zeta}\partial_x\int_z^{\varepsilon\zeta}\partial_x[\partial_x((1+z')\bar{v})v^*_{\rm sh}].\end{aligned} \tag{2.126}$$

Thus,

$$\begin{aligned}H\tilde{\mathcal{T}}[\varepsilon\zeta,\beta b][\partial_t v^*_{\rm sh} + \varepsilon\bar{v}\partial_x v^*_{\rm sh}] &= -2H\tilde{\mathcal{T}}[\varepsilon\zeta,\beta b](v^*_{\rm sh}\partial_x\bar{v})\\ &\quad - \varepsilon\int_{-1}^{\zeta}\partial_x\int_z^{\varepsilon\zeta} v^*_{\rm sh}\partial_x^2((1+z')\bar{v}) - \varepsilon\int_{-1}^{\zeta}\partial_x\int_z^{\varepsilon\zeta}\partial_x((1+z')\bar{v})\partial_x v^*_{\rm sh}.\end{aligned} \tag{2.127}$$

Plugging the above relation into $\varrho_{3/2}$, we get

$$\begin{aligned}\varrho_{3/2} &= -2H\tilde{\mathcal{T}}[\varepsilon\zeta,\beta b](v^*_{\rm sh}\partial_x\bar{v})\\ &\quad + 2\varepsilon\int_{-1}^{\zeta}\partial_x\int_z^{\varepsilon\zeta}(\partial_x\bar{v})\partial_x\int_{-1}^{z'} v^*_{\rm sh} - 2\varepsilon\int_{-1}^{\zeta}\partial_x\int_z^{\varepsilon\zeta} v^*_{\rm sh}\partial_x^2((1+z')\bar{v}).\end{aligned} \tag{2.128}$$

Using (2.84) together with the identities,

$$\begin{aligned}-8H\tilde{\mathcal{T}}[\varepsilon\zeta,\beta b](v^*_{\rm sh}\partial_x\bar{v}) &= -\frac{1}{3}\partial_x(H^3\partial_x(v^\#\partial_x\bar{v})) - \partial_x(H^2\partial_x H v^\#\partial_x\bar{v}) + O(\beta),\\ -4\partial_x\int_{-1}^{\varepsilon\zeta}\int_z^{\varepsilon\zeta}\int_{-1}^{z'}\partial_x\bar{v}\partial_x v^*_{\rm sh} &= \partial_x\Big(\big(\frac{H^2\partial_x H}{2}v^\# + \frac{H^3}{6}\partial_x v^\#\big)\partial_x\bar{v}\Big) + O(\beta),\end{aligned} \tag{2.129}$$

we finally get,

$$\varrho_{3/2} = -\frac{1}{4}\partial_x(H^3 v^\#\partial_x^2\bar{v}) - \frac{1}{6}\partial_x(\partial_x(H^3 v^\#)\partial_x\bar{v}). \tag{2.130}$$

Gathering the above computations and dropping $O(\mu^2)$ terms we obtain the following equation,

$$\begin{aligned}&(1+\mu\mathbf{T}[H,\beta b])[\partial_t(H\bar{v}) + \varepsilon\partial_x(H\bar{v}^2)]\\ &\qquad + H\partial_x\zeta + \varepsilon\mu H\mathcal{Q}_1[H,\beta b](\bar{v}) + \varepsilon\mu\partial_x E + \varepsilon\mu^{\frac{3}{2}}HC[H](v^\#,\bar{v}) = 0,\end{aligned}$$

with,

$$E = \int_{-1+\beta b}^{\varepsilon\zeta}(v^*_{\rm sh})^2 \quad\text{and}\quad v^\# = -\frac{24}{H^3}\int_{-1+\beta b}^{\varepsilon\zeta}\int_z^{\varepsilon\zeta}\int_{-1+\beta b}^{z} v^*_{\rm sh}, \tag{2.131}$$

and $C[H](v^\#,\bar{v})$ is defined as in (2.77).

Closure equation for $v^{\#}$

Since $v^{\#}$ appears only in the $O(\mu^{\frac{3}{2}})$ terms in (2.1.3.2), we only need to derive an equation for $v^{\#}$ at order $O(\sqrt{\mu})$ to keep the overall $O(\mu^2)$ precision of (2.1.3.2).

Applying the triple integration operator $\int_{-1+\beta b}^{\varepsilon\zeta}\int_{z}^{\varepsilon\zeta}\int_{-1+\beta b}^{z}$ to (2.119), we obtain

$$\int_{-1+\beta b}^{\varepsilon\zeta}\int_{z}^{\varepsilon\zeta}\int_{-1+\beta b}^{z}\Big(\partial_t v^*_{\rm sh}+\varepsilon\bar v\partial_x v^*_{\rm sh}+\varepsilon v^*_{\rm sh}\partial_x\bar v-\varepsilon\partial_x[(1+z-\beta b)\bar v]\partial_z v^*_{\rm sh}\Big)=O(\varepsilon\sqrt{\mu}),$$

let computing each term,

$$\int_{-1+\beta b}^{\varepsilon\zeta}\int_{z}^{\varepsilon\zeta}\int_{-1+\beta b}^{z}\partial_t v^*_{\rm sh}=\partial_t\int_{z}^{\varepsilon\zeta}\int_{-1+\beta b}^{z}v^*_{\rm sh}=\frac{-1}{24}\partial_t(H^3v^{\#}),$$

still owing to (2.7),

$$\begin{aligned}\int_{-1+\beta b}^{\varepsilon\zeta}\int_{z}^{\varepsilon\zeta}\int_{-1+\beta b}^{z}\varepsilon\bar v\partial_x v^*_{\rm sh}&=\varepsilon\int_{-1+\beta b}^{\varepsilon\zeta}\int_{z}^{\varepsilon\zeta}\bar v\partial_x\int_{-1+\beta b}^{z}v^*_{\rm sh}+\underbrace{\varepsilon\beta\partial_x b\bar v v^*_{\rm sh_{|-1+\beta b}}}_{=0},\\&=\varepsilon\int_{-1+\beta b}^{\varepsilon\zeta}\bar v\partial_x\int_{z}^{\varepsilon\zeta}\int_{-1+\beta b}^{z}v^*_{\rm sh}=\varepsilon\bar v\partial_x\int_{-1+\beta b}^{\varepsilon\zeta}\int_{z}^{\varepsilon\zeta}\int_{-1+\beta b}^{z}v^*_{\rm sh},\\&=-\frac{1}{24}\bar v\partial_x(H^3v^{\#}),\end{aligned}$$

$$\int_{-1+\beta b}^{\varepsilon\zeta}\int_{z}^{\varepsilon\zeta}\int_{-1+\beta b}^{z}\varepsilon v^*_{\rm sh}\partial_x\bar v=-\frac{1}{24}H^3v^{\#}\partial_x\bar v,$$

$$\begin{aligned}-\varepsilon\int_{-1+\beta b}^{\varepsilon\zeta}\int_{z}^{\varepsilon\zeta}\int_{-1+\beta b}^{z}&\partial_x[(1+z-\beta b)\bar v]\partial_z v^*_{\rm sh}\\&=-\varepsilon\int_{-1+\beta b}^{\varepsilon\zeta}\int_{z}^{\varepsilon\zeta}\int_{-1+\beta b}^{z}\Big(-\beta\partial_x b\bar v+(1+z-\beta b)\partial_x\bar v\Big)\partial_z v^*_{\rm sh},\\&=-\varepsilon\int_{-1+\beta b}^{\varepsilon\zeta}\int_{z}^{\varepsilon\zeta}\int_{-1+\beta b}^{z}(1+z-\beta b)\partial_x\bar v\partial_z v^*_{\rm sh}+O(\beta),\\&=-\varepsilon\partial_x\bar v\int_{-1+\beta b}^{\varepsilon\zeta}\int_{z}^{\varepsilon\zeta}\int_{-1+\beta b}^{z}(1+z-\beta b)\partial_z v^*_{\rm sh}+O(\beta),\\&=-\varepsilon\partial_x\bar v\int_{-1+\beta b}^{\varepsilon\zeta}\int_{z}^{\varepsilon\zeta}\underbrace{\int_{-1+\beta b}^{z}(1+z-\beta b)\partial_z v^*_{\rm sh}}_{:=\varrho_1}+O(\beta),\end{aligned}$$

one can compute,

$$\begin{aligned}\varrho_1 &= \int_{-1+\beta b}^{z} \partial_z\Big\{(1+z-\beta b)v_{\text{sh}}^*\Big\} - \int_{-1+\beta b}^{z} \partial_z\Big\{(1+z-\beta b)\Big\}v_{\text{sh}}^*,\\ &= \Big[(1+z-\beta b)v_{\text{sh}}^*\Big]_{-1+\beta b}^{\varepsilon\zeta} - \int_{-1+\beta b}^{z} v_{\text{sh}}^* = (1+z-\beta b)v_{\text{sh}}^* - \int_{-1+\beta b}^{z} v_{\text{sh}}^*,\end{aligned}$$

thus,

$$\int_z^{\varepsilon\zeta} \varrho_1 = \int_z^{\varepsilon\zeta} (1+z-\beta b)v_{\text{sh}}^* - \int_z^{\varepsilon\zeta}\int_{-1+\beta b}^{z} v_{\text{sh}}^*,$$

so,

$$\begin{aligned}\int_{-1+\beta b}^{\varepsilon\zeta}\int_z^{\varepsilon\zeta} \varrho_1 &= \int_{-1+\beta b}^{\varepsilon\zeta}\int_z^{\varepsilon\zeta} (1+z-\beta b)v_{\text{sh}}^* - \int_{-1+\beta b}^{\varepsilon\zeta}\int_z^{\varepsilon\zeta}\int_{-1+\beta b}^{z} v_{\text{sh}}^*,\\ &= \frac{H^3}{24}v^{\#} + \int_{-1+\beta b}^{\varepsilon\zeta}\int_z^{\varepsilon\zeta} (1+z-\beta b)v_{\text{sh}}^*,\end{aligned}$$

integrating by parts, we get

$$\begin{aligned}\int_z^{\varepsilon\zeta} (1+z-\beta b)v_{\text{sh}}^* &= \Big[(\int_{-1+\beta b}^{z} v_{\text{sh}}^*)(1+z-\beta b)\Big]_z^{\varepsilon\zeta} - \int_z^{\varepsilon\zeta}(\int_{-1+\beta b}^{z} v_{\text{sh}}^*),\\ &= -(\int_{-1+\beta b}^{z} v_{\text{sh}}^*)(1+z-\beta b) - \int_z^{\varepsilon\zeta}(\int_{-1+\beta b}^{z} v_{\text{sh}}^*).\end{aligned}$$

Moreover,

$$\int_{-1+\beta b}^{\varepsilon\zeta}\int_z^{\varepsilon\zeta} (1+z-\beta b)v_{\text{sh}}^* = \frac{H^3}{24}v^{\#} - \int_{-1+\beta b}^{\varepsilon\zeta}(\int_{-1+\beta b}^{z} v_{\text{sh}}^*)(1+z-\beta b),$$

integrating on z again,

$$\int_{-1+\beta b}^{\varepsilon\zeta}\int_{-1+\beta b}^{\varepsilon\zeta}\int_z^{\varepsilon\zeta} (1+z-\beta b)\partial_z v_{\text{sh}}^* = \frac{2H^3}{24}v^{\#} - \int_{-1+\beta b}^{\varepsilon\zeta}(\int_{-1+\beta b}^{z} v_{\text{sh}}^*)(1+z-\beta b),$$

integrating by parts again,

$$\begin{aligned}-\int_{-1+\beta b}^{\varepsilon\zeta}(\int_{-1+\beta b}^{z} v_{\text{sh}}^*)(1+z-\beta b) &= -\int_{-1+\beta b}^{\varepsilon\zeta}\Big(\int_z^{\varepsilon\zeta}\int_{-1+\beta b}^{z} v_{\text{sh}}^*\Big),\\ &= \frac{H^3}{24}v^{\#}.\end{aligned}$$

moreover,

$$-\int_{-1+\beta b}^{\varepsilon\zeta}\int_z^{\varepsilon\zeta}\int_{-1+\beta b}^{z} (1+z-\beta b)\partial_z v_{\text{sh}}^* = \frac{3H^3}{24}v^{\#},$$

guthering the above integrations, we obtain

$$\partial_t(H^3 v^{\#}) + \varepsilon\bar{v}\partial_x(H^3 v^{\#}) + \varepsilon H^3 v^{\#}\partial_x\bar{v} = -3\varepsilon H^3 v^{\#}\partial_x\bar{v} + O(\varepsilon\sqrt{\mu}), \tag{2.132}$$

thus,

$$\begin{aligned} &H^3\partial_t v^{\#} + v^{\#}\partial_t(H^3) \\ &\qquad + \varepsilon H^3\bar{v}\partial_x v^{\#} + \varepsilon\bar{v}\partial_x(H^3)v^{\#} + \varepsilon H^3 v^{\#}\partial_x\bar{v} + 3\varepsilon H^3 v^{\#}\partial_x\bar{v} = O(\varepsilon\sqrt{\mu}), \end{aligned} \tag{2.133}$$

owing to the mass conservation equation $\partial_t H + \partial_x(H\bar{v}) = 0$, we get

$$\frac{1}{3}v^{\#}\partial_t(H^3) + \frac{1}{3}v^{\#}\partial_x(H^3)\bar{v} + (H^3 v^{\#})\partial_x\bar{v} = O(\varepsilon\sqrt{\mu}). \tag{2.134}$$

Dividing on H^3 we obtain the following evolution equation on $v^{\#}$, we infer

$$\partial_t v^{\#} + \varepsilon\bar{v}\partial_x v^{\#} + \varepsilon v^{\#}\partial_x\bar{v} = O(\varepsilon\sqrt{\mu}). \tag{2.135}$$

Closure equation for E

E appears in term of order $O(\mu)$, we need a closure equation for E at order $O(\mu)$ to keep the presicion of the model. Multiplying (2.120) by v^*_{sh}, we get

$$\begin{aligned} &v^*_{\mathrm{sh}}\partial_t v^*_{\mathrm{sh}} + \varepsilon\bar{v}v^*_{\mathrm{sh}}\partial_x v^*_{\mathrm{sh}} + \varepsilon(v^*_{\mathrm{sh}})^2\partial_x\bar{v} \\ &+ \varepsilon\sqrt{\mu}\Big\{(v^*_{\mathrm{sh}})^2\partial_x v^*_{\mathrm{sh}} - \frac{1}{H}v^*_{\mathrm{sh}}\Big(\partial_x\int_{-1+\beta b}^{\varepsilon\zeta}(v^*_{\mathrm{sh}})^2\Big)\Big\} = \varepsilon\partial_x\Big[\int_{-1+\beta b}^{z}(\bar{v}+\sqrt{\mu}v^*_{\mathrm{sh}})\Big]v^*_{\mathrm{sh}}\partial_z v^*_{\mathrm{sh}}. \end{aligned} \tag{2.136}$$

Let compute each term explicitly,

First term - We have,

$$\begin{aligned} \int_{-1+\beta b}^{\varepsilon\zeta} v^*_{\mathrm{sh}}\partial_t v^*_{\mathrm{sh}} &= \frac{1}{2}\int_{-1+\beta b}^{\varepsilon\zeta}\partial_t(v^*_{\mathrm{sh}})^2, \\ &= \frac{1}{2}\partial_t\int_{-1+\beta b}^{\varepsilon\zeta}(v^*_{\mathrm{sh}})^2 - \frac{1}{2}\varepsilon\partial_t\zeta\underbrace{(v^*_{\mathrm{sh}})^2_{|\varepsilon\zeta}}_{=0} = \frac{1}{2}\partial_t E. \end{aligned} \tag{2.137}$$

Second term - We have,

$$\begin{aligned} \int_{-1+\beta b}^{\varepsilon\zeta}\varepsilon\bar{v}v^*_{\mathrm{sh}}\partial_x v^*_{\mathrm{sh}} &= \frac{\varepsilon\bar{v}}{2}\int_{-1+\beta b}^{\varepsilon\zeta}\partial_x(v^*_{\mathrm{sh}})^2, \\ &= \frac{\varepsilon\bar{v}}{2}\Big[\partial_x\int_{-1+\beta b}^{\varepsilon\zeta}(v^*_{\mathrm{sh}})^2 - \varepsilon\partial_x\zeta\underbrace{(v^*_{\mathrm{sh}})^2_{|\varepsilon\zeta}}_{=0} + \beta\partial_x b\underbrace{(v^*_{\mathrm{sh}})^2_{|-1+\beta b}}_{=0}\Big], \\ &= \frac{\varepsilon\bar{v}}{2}\partial_x E. \end{aligned} \tag{2.138}$$

Third term - We have,

$$\int_{-1+\beta b}^{\varepsilon\zeta}\varepsilon(v^*_{\mathrm{sh}})^2\partial_x\bar{v} = \varepsilon E\partial_x\bar{v}. \tag{2.139}$$

Fourth term - We have,

$$\varepsilon\sqrt{\mu}\int_{-1+\beta b}^{\varepsilon\zeta}(v_{\rm sh}^*)^2\partial_x v_{\rm sh}^* = \frac{1}{3}\varepsilon\sqrt{\mu}\int_{-1+\beta b}^{\varepsilon\zeta}\partial_x(v_{\rm sh}^*)^3 = \frac{1}{3}\varepsilon\sqrt{\mu}\partial_x F. \tag{2.140}$$

$$\int_{-1+\beta b}^{\varepsilon\zeta} v_{\rm sh}^*\Big(\frac{1}{H}\partial_x\int_{-1+\beta b}^{\varepsilon\zeta}(v_{\rm sh}^*)^2\Big) = \frac{1}{H}\partial_x E\underbrace{\int_{-1+\beta b}^{\varepsilon\zeta} v_{\rm sh}^*}_{=0} = 0. \tag{2.141}$$

Fifth term - We have,

$$\begin{aligned}\partial_x\int_{-1+\beta b}^{z}(\bar v+\sqrt{\mu}v_{\rm sh}^*) &= \int_{-1+\beta b}^{z}\Big[\partial_x\bar v+\sqrt{\mu}\partial_x v_{\rm sh}^*-\beta\partial_x b(\bar v+\sqrt{\mu}v_{\rm sh}^*)_{|-1+\beta b}\Big],\\ &= \int_{-1+\beta b}^{z}\Big[\partial_x\bar v+\sqrt{\mu}\partial_x v_{\rm sh}^*-\beta\partial_x b\bar v\Big],\end{aligned}$$

moreover,

$$\begin{aligned}&\varepsilon\int_{-1+\beta b}^{\varepsilon\zeta} v_{\rm sh}^*\partial_x\Big[\int_{-1+\beta b}^{z}(\bar v+\sqrt{\mu}v_{\rm sh}^*)\Big]\partial_z v_{\rm sh}^*\\ &\quad= \varepsilon\int_{-1+\beta b}^{\varepsilon\zeta} v_{\rm sh}^*\Big[\int_{-1+\beta b}^{z}\big[\partial_x\bar v+\sqrt{\mu}\partial_x v_{\rm sh}^*-\beta\partial_x b\bar v\big]\Big]\partial_z v_{\rm sh}^*,\\ &\quad= \frac{\varepsilon}{2}\int_{-1+\beta b}^{\varepsilon\zeta} v_{\rm sh}^*\Big[\int_{-1+\beta b}^{z}\big[\partial_x\bar v+\sqrt{\mu}\partial_x v_{\rm sh}^*\big]\Big]\partial_z v_{\rm sh}^*-\varepsilon\beta\partial_x b\bar v\int_{-1+\beta b}^{\varepsilon\zeta} v_{\rm sh}^*\partial_z v_{\rm sh}^*,\\ &\quad= \varrho_1+\varrho_2,\end{aligned} \tag{2.142}$$

integrating by parts and owing to (2.7), we get

$$\begin{aligned}\varrho_1 &= \underbrace{\frac{\varepsilon}{2}\Big[\Big(\int_{-1+\beta b}^{\varepsilon\zeta}(\partial_x\bar v+\sqrt{\mu}\partial_x v_{\rm sh}^*)\Big)(v_{\rm sh}^*)^2\Big]_{-1+\beta b}^{\varepsilon\zeta}}_{=0}-\frac{\varepsilon}{2}\int_{-1+\beta b}^{\varepsilon\zeta}(\partial_x\bar v+\sqrt{\mu}\partial_x v_{\rm sh}^*)(v_{\rm sh}^*)^2,\\ &= -\frac{\varepsilon}{2}\int_{-1+\beta b}^{\varepsilon\zeta}(v_{\rm sh}^*)^2\partial_x\bar v-\frac{\varepsilon\sqrt{\mu}}{2}\int_{-1+\beta b}^{\varepsilon\zeta}(v_{\rm sh}^*)^2\partial_x v_{\rm sh}^*,\\ &= -\frac{\varepsilon}{2}E\partial_x\bar v-\frac{1}{6}\varepsilon\sqrt{\mu}\partial_x F,\end{aligned}$$

we also have,

$$\begin{aligned}\varrho_2 = -\varepsilon\beta\partial_x b\bar v\int_{-1+\beta b}^{\varepsilon\zeta} v_{\rm sh}^*\partial_z v_{\rm sh}^* &= -\frac{1}{2}\varepsilon\beta\partial_x b\bar v\int_{-1+\beta}^{\varepsilon\zeta}\partial_x(v_{\rm sh}^*)^2,\\ &= -\frac{1}{2}\varepsilon\beta\partial_x b\bar v\underbrace{(v_{\rm sh}^*)^2]_{-1+\beta b}^{\varepsilon\zeta}}_{=0} = 0.\end{aligned} \tag{2.143}$$

Regrouping the above calculations, we obtient the following evolution equation for E,

$$\partial_t E+\varepsilon\bar v\partial_x E+3\varepsilon E\partial_x\bar v+\varepsilon\sqrt{\mu}\partial_x F = 0. \tag{2.144}$$

with,

$$F = \int_{-1+\beta b}^{\varepsilon\zeta} (v_{\rm sh}^*)^3. \tag{2.145}$$

Closure equation for F

From (2.144), one deduces that we need to determine an evolution equation for F up to $O(\sqrt{\mu})$ terms.

Multiplying (2.121) by $(v_{\rm sh}^*)^2$, we get

$$(v_{\rm sh}^*)^2\partial_t v_{\rm sh}^* + \varepsilon\bar{v}(v_{\rm sh}^*)^2\partial_x v_{\rm sh}^* + \varepsilon(v_{\rm sh}^*)^3\partial_x\bar{v} - \varepsilon\partial_x[(1+z-\beta b)\bar{v}](v_{\rm sh}^*)^2\partial_z v_{\rm sh}^* = O(\sqrt{\mu}), \tag{2.146}$$

integrating this equation on z and using (2.7), we compute

$$\begin{aligned}
\int_{-1+\beta b}^{\varepsilon\zeta} (v_{\rm sh}^*)^2\partial_t v_{\rm sh}^* &= \frac{1}{3}\int_{-1+\beta b}^{\varepsilon\zeta} \partial_t (v_{\rm sh}^*)^3 = \frac{1}{3}\partial_t F,\\
\int_{-1+\beta b}^{\varepsilon\zeta} \varepsilon\bar{v}(v_{\rm sh}^*)^2\partial_x v_{\rm sh}^* &= \frac{1}{3}\varepsilon\bar{v}\partial_x F,\\
\int_{-1+\beta b}^{\varepsilon\zeta} \varepsilon\partial_x\bar{v}(v_{\rm sh}^*)^3 &= \varepsilon F\partial_x\bar{v},
\end{aligned} \tag{2.147}$$

then,

$$\begin{aligned}
\int_{-1+\beta b}^{\varepsilon\zeta} \partial_x[(1+z-\beta b)\bar{v}](v_{\rm sh}^*)^2\partial_z v_{\rm sh}^* &= \frac{1}{3}\int_{-1+\beta b}^{\varepsilon\zeta} \partial_x[(1+z-\beta b)\bar{v}]\partial_z(v_{\rm sh}^*)^3,\\
&= \frac{1}{3}\int_{-1+\beta b}^{\varepsilon\zeta} \partial_z\Big\{\partial_x[(1+z-\beta b)\bar{v}](v_{\rm sh}^*)^3\Big\} - \frac{1}{3}\int_{-1+\beta b}^{\varepsilon\zeta} \partial_z\Big\{\partial_x[(1+z-\beta b)\bar{v}]\Big\}(v_{\rm sh}^*)^3,\\
&= \frac{1}{3}\underbrace{\Big[\partial_x[(1+z-\beta b)\bar{v}](v_{\rm sh}^*)^3\Big]_{-1+\beta b}^{\varepsilon\zeta}}_{=0} - \frac{1}{3}\int_{-1+\beta b}^{\varepsilon\zeta} \partial_x\Big\{\underbrace{\partial_z[(1+z-\beta b)\bar{v}]}_{=\partial_x\bar{v}}\Big\}(v_{\rm sh}^*)^3,\\
&= -\frac{1}{3}F\partial_x\bar{v}.
\end{aligned}$$

Gathering the above computations with dropping $O(\sqrt{\mu})$ terms, we obtient evolution equation on F

$$\partial_t F + \varepsilon\bar{v}\partial_x F + 4\varepsilon F\partial_x\bar{v} = 0. \tag{2.148}$$

Finally, we obtain the SGN equations with a general vorticity, under the assumption $\beta = O(\sqrt{\mu})$, in one-dimensional horizontal case. These equations are given as follows,

$$\begin{cases}
\partial_t\zeta + \partial_x(H\bar{v}) = 0,\\
(1+\mu\mathbf{T}[H,\beta b])[\partial_t(H\bar{v}) + \varepsilon\partial_x(H\bar{v}^2)] + H\partial_x\zeta + \varepsilon\mu H\mathcal{Q}_1[H,\beta b](\bar{v}) + \varepsilon\mu\partial_x E\\
+\varepsilon\mu^{3/2}HC[H](v^{\#},\bar{v}) = 0,\\
\partial_t v^{\#} + \varepsilon\partial_x(\bar{v}v^{\#}) = 0,\\
\partial_t E + \varepsilon\bar{v}\partial_x E + 3\varepsilon E\partial_x\bar{v} + \varepsilon\sqrt{\mu}\partial_x F = 0,\\
\partial_t F + \varepsilon\bar{v}\partial_x F + 4\varepsilon F\partial_x\bar{v} = 0.
\end{cases} \tag{2.149}$$

We observe that if F is initially equal to zero, then one can remove F from (2.149) to obtain a simplified model,

$$\begin{cases} \partial_t\zeta + \partial_x(H\bar{v}) = 0, \\ (1+\mu\mathbf{T}[H,\beta b])[\partial_t(H\bar{v}) + \varepsilon\partial_x(H\bar{v}^2)] + H\partial_x\zeta + \varepsilon\mu H\mathcal{Q}_1[H,\beta b](\bar{v}) + \varepsilon\mu\partial_x E \\ +\varepsilon\mu^{3/2}HC[H](v^\#,\bar{v}) = 0, \\ \partial_t v^\# + \varepsilon\partial_x(\bar{v}v^\#) = 0, \\ \partial_t E + \varepsilon\bar{v}\partial_x E + 3\varepsilon E\partial_x\bar{v} = 0. \end{cases} \tag{2.150}$$

Anticipating on the design of a suitable discrete formulation, let introduce the new variables $\mathfrak{e} = H^{-3}E$ and $\mathfrak{v}^\sharp = H^{-1}v^\sharp$, in order to obtain the following model, which will be numerically studied in Chapter 5,

$$\begin{cases} \partial_t\zeta + \partial_x(H\bar{v}) = 0, \\ (1+\mu\mathbf{T}[H,\beta b])[\partial_t(H\bar{v}) + \varepsilon\partial_x(H\bar{v}^2)] + H\partial_x\zeta + \varepsilon\mu H\mathcal{Q}_1[H,\beta b](\bar{v}) + \varepsilon\mu\partial_x(H^3\mathfrak{e}) \\ +\varepsilon\mu^{3/2}C[H](H\mathfrak{v}^\sharp,\bar{v}) = 0, \\ \partial_t(H\mathfrak{v}^\sharp) + \varepsilon\partial_x(H\bar{v}\mathfrak{v}^\sharp) = 0, \\ \partial_t(H\mathfrak{e}) + \varepsilon\partial_x(H\bar{v}\mathfrak{e}) = 0. \end{cases} \tag{2.151}$$

2.1.4 Solitary wave solutions for rotational SGN equations

In this section, we adapt the results of [101] to the model (2.151). It is well known in the irrotational flow and in the flat bottom case, that irrotational SGN equations admit solitary wave solutions of amplitude εH_0, which have known formula in a closed form,

$$\eta(t,x) = H_0 + \varepsilon H_0\,\mathrm{sech}^2(k(x-ct)), \quad q(t,x) = c(\eta(t,x) - H_0), \tag{2.152}$$

with $k := \sqrt{\frac{3\varepsilon}{4H_0^2(1+\varepsilon)}}$ and $c := \sqrt{gH_0(1+\varepsilon)}$.

For rotational flows, the situation is quite different and the existence of smooth solitary waves for the model (2.151) may depend on some conditions. Considering $b = 0$, (2.151) can be written as an (ODE) system as follows,

$$\begin{cases} \zeta_t + (H\bar{v})_x = 0, \\ \bar{v}_t + g\partial_x\zeta + \bar{v}\partial_x\bar{v} + \frac{1}{H}E_x - \frac{1}{6H}[2H^3v^\#\bar{v}_{xx} + (H^3v^\#)_x\bar{v}_x]_x = \frac{1}{3}\frac{1}{H}[H^3(\bar{v}_{xt} + \bar{v}\bar{v}_{xx} - \bar{v}_x^2)]_x \\ v_t^\# + (\bar{v}v^\#)_x = 0, \\ \left(\frac{E}{H^3}\right)_t + \bar{v}\left(\frac{E}{H^3}\right)_x = 0. \end{cases} \tag{2.153}$$

Definition 2.1. *A solitary wave of speed c for (2.153) is a mapping*

$$(t,x) \in \mathbb{R} \mapsto (\zeta,\bar{v},v^\#,E)(t,x) = (\underline{\zeta},\underline{\bar{v}},\underline{v}^\#,\underline{E})(x-ct),$$

such that there exists $H \in C^2(\mathbb{R})$ *and* $E_\infty > 0$, $v_\infty^\# \in \mathbb{R}$ *such that,*

$$\underline{\zeta} = H - H_0, \quad \overline{v} = c\frac{H - H_0}{H}, \quad \underline{v}^\# = \frac{H}{H_0}v_\infty^\#, \quad \underline{E} = \frac{H^3}{H_0^3}E_\infty, \tag{2.154}$$

with $c \in \mathbb{R}$, $\underline{\zeta}$ *and* $\overline{v}$ *vanishing at infinity, over a current that might not vanish at infinity,*

$$\lim_{\mp\infty}(\underline{\zeta}, \underline{v}) = 0 \quad \textit{and} \quad \lim_{\mp\infty}(\underline{v}^\#, \underline{E}) = (v_\infty^\#, E_\infty),$$

and H *solves the ODE,*

$$\frac{1}{3}c(cH_0^2 - v_\infty^\# H^2)H_{xx} = \frac{H - H_0}{2H}(2c^2H_0 - gH(H + H_0)) - (\frac{H^3}{H_0^3} - 1)E_\infty + \frac{c^2}{3}H_0^2\frac{H_x^2}{H}, \tag{2.155}$$

on $\mathbb{R}$ *and satisfies* $\lim_{\mp\infty} H = H_0$.

The following Proposition gives the criteria of the existence of smooth solitary waves in the sense of Definition 2.1.

Proposition 2.2. *(Existence of smooth solitary waves). Let* $E_\infty > 0, v_\infty^\# \in \mathbb{R}$. *Let also* $H_{\max} > H_0$.

1. *Up to translations, there can be at most two solitary waves of maximal height* $H_{\max}$ *for* (2.153)*; if they exist, they have opposite speed* $\mp\underline{c}$, *with*

$$\underline{c} = \left(gH_{\max} + \frac{H_{\max}(H_{\max} + 2H_0)}{H_0^3}E_\infty\right)^{\frac{1}{2}}. \tag{2.156}$$

2. *The solitary wave of speed* $\underline{c}$ *(respectively,* $-\underline{c}$*) exists if and only if the following conditions holds,*

$$\underline{c}(\underline{c}H_0^2 - v_\infty^\# H_{\max}^2) > 0, \qquad (\textit{respectively}, \quad -\underline{c}(-\underline{c}H_0^2 - v_\infty^\# H_{\max}^2) > 0). \tag{2.157}$$

   The profile of the solitary wave H *then attains its maximal value at a unique point* $x_{\max}$ *and it is symmetric with respect to the axis* $x = x_{\max}$ *and decaying on the half-line* $x > x_{\max}$.

Proof. The proof is detailed in [101].

□

Remark 2.3. *Taking* $E_\infty = v_\infty^\# = 0$ *in the statement of Proposition 2.2, we get the same solitary wave as in the irrotational case.*

2.2 Introduction to DG methods

The goal of this section is to recall the basic concepts needed for the construction and analyze of a DG formulation for a diffusion-reaction problem and the construction of a DG formulation for the NSW equations. The sections concerning elliptic problems are borrowed from [50]. These discrete formulations may be regarded as the starting points for the construction of the more elaborated formulations that will be detailed in Chapter 4 and Chapter 5.

2.2.1 Preliminary notations, definitions and results

Abstract linear stationary problem

Let V be an Hilbert space, a is a bounded bilinear form on $V \times V$ and f a bounded linear form on V. We consider the following problem,

$$\text{find } u \in V, \quad \forall v \in V, \quad a(u,v) = (f,v), \tag{2.158}$$

where $(\cdot,\cdot)$ refers to the L^2-scalar product.

The existence and uniqueness of the solution of (2.158) is given by the Lax-Milgram lemma,

Lemma 2.4. *(Lax-Milgram). Assume that a is coercive on V,*

$$\exists C_{sta} > 0, \forall v \in V, \quad a(v,v) \geq C_{sta}\|v\|_V^2.$$

Then the problem (2.158) *is well-posed.*

Proof. see, e.g., [50, Lemma 1.4]. □

Discrete setting

Let Ω be an open and convex set of $\mathbb{R}^d$ of boundary $\partial\Omega$. Let $\mathcal{T}_h$ be a partition of the computational domain Ω such that $\overline{\Omega} = \cup_{T\in\mathcal{T}_h}\overline{T}$. When $d = 1$, Ω and T are respectively open and close intervals of $\mathbb{R}$. Let x refer to the spatial coordinates in Ω. The meshsize is defined as the real number $h \coloneqq \max_{T\in\mathcal{T}} h_T$, where h_T denotes the diameter of T. We denote the set of interfaces of $\mathcal{T}_h$ by $\mathcal{F}_h^{\mathrm{i}}$, such that for all $F \in \mathcal{F}_h^{\mathrm{i}}$ and for two distinct mesh elements T_1 and T_2, then $F = \partial T_1 \cap \partial T_2$ and the set of boundary faces is denoted by $\mathcal{F}_h^{\mathrm{b}}$, for $T \in \mathcal{T}_h$, $F \in \mathcal{F}_h^{\mathrm{b}}$ then, $F = \partial T \cap \partial\Omega$. Moreover, we denote $\mathcal{F}_h \coloneqq \mathcal{F}_h^{\mathrm{i}} \cup \mathcal{F}_h^{\mathrm{b}}$ the set of mesh faces. We define n_T a.e. on ∂T as the unit outward normal to T. For any mesh element $T \in \mathcal{T}_h$, the set $F_T \coloneqq \{F \in \mathcal{F}_h \mid F \subset \partial T\}$ collects the mesh faces composing the boundary of T. The maximum number of mesh faces composing the boundary of mesh elements is denoted by $N_\partial \coloneqq \max_{T\in\mathcal{T}_h} \mathrm{card}(\mathcal{F}_T)$. Let φ be a sufficiently regular function defined on Ω, that is smooth enough suh that for all $T \in \mathcal{T}_h$, the restriction $\varphi_{|T}$ of φ to the open set T can be defined up to the boundary ∂T. Then, for all $F \in \mathcal{F}_h$, the average and the jump of φ are given by, respectively,

$$\{\!\{\varphi\}\!\}_F \coloneqq \frac{1}{2}(\varphi_{|T_1} + \varphi_{|T_2}), \quad [\![\varphi]\!]_F \coloneqq \varphi_{|T_1} - \varphi_{|T_2}. \tag{2.159}$$

For the boundary face $F \in \mathcal{F}_h^{\mathrm{b}}$, we set $\{\!\{\varphi\}\!\}_F = [\![\varphi]\!]_F \coloneqq v_{|T}$. In what follows, the subscript F is dropped from both $\{\!\{\varphi\}\!\}_F$ and $[\![\varphi]\!]_F$ when no confusion is possible. For a positive integer $k \geq 1$, we define the broken polynomial space as follows,

$$\mathbb{P}^k(\mathcal{T}_h) \coloneqq \{v \in L^2(\Omega) |\ \forall T \in \mathcal{T}_h, v_{|T} \in \mathbb{P}^k(T)\}, \tag{2.160}$$

where $\mathbb{P}^k(T)$ denotes the space of polynomials in T of total degree at most k. For a positive integer m, the broken Sobolev space is defined as follows,

$$W^{m,p}(\mathcal{T}_h) \coloneqq \{v \in L^p(\Omega) \mid \forall T \in \mathcal{T}_h,\ v_{|T} \in W^{m,p}(T)\}. \tag{2.161}$$

We introduce the following inner products for regular enough scalar-valued functions v, w:

$$(v,w)_\Omega \coloneqq \int_\Omega v(x)w(x)dx, \quad (v,w)_T \coloneqq \int_T v(x)w(x)dx \quad \forall T \in \mathcal{T}_h, \quad (v,w)_F \coloneqq (vw)(x_F) \quad \forall F \in \mathcal{F}_h,$$

and we denote respectively by $\|v\|_\Omega = (v,v)_\Omega^{\frac{1}{2}}$, $\|v\|_T = (v,v)_T^{\frac{1}{2}}$ and $\|v\|_F = (v,v)_F^{\frac{1}{2}}$ the corresponding L^2 norms.

We recall the definition of the so called *broken gradient* that acts on broken Sobolev spaces,

Definition 2.5. *The broken gradient $\partial_x^h : W^{1,p}(\mathcal{T}_h) \to L^p(\Omega)$ is defined such that,*

$$\forall v \in W^{1,p}(\mathcal{T}_h),\ \forall T \in \mathcal{T}_h, \quad (\partial_x^h v)_{|T} \coloneqq \partial_x(v_{|T}). \tag{2.162}$$

In the following, we drop the index h in the broken gradient when this operator appears inside an integral over a fixed mesh element $T \in \mathcal{T}_h$. Let also recall the following discrete trace inequality,

Lemma 2.6. *(Discrete trace inequality). For all $v_h \in \mathbb{P}^k(\mathcal{T}_h)$, all $T \in \mathcal{T}_h$, and all $F \in \mathcal{F}_T$,*

$$h_T^{\frac{1}{2}} \|v_h\|_F \le C_{tr} \|v_h\|_T, \tag{2.163}$$

where C_{tr} depends only on k, the horizontal surface dimension and the mesh regularity parameters. Summing over $F \in \mathcal{F}_T$, one deduces from (2.163) and the Cauchy-Schwarz inequality that,

$$h_T^{\frac{1}{2}} \|v_h\|_{\partial T} \le C_{tr} N_\partial^{\frac{1}{2}} \|v_h\|_T. \tag{2.164}$$

Proof. see, e.g., [50, Lemma 1.46]. □

Now, let consider the following general discrete problem,

$$\text{find } v_h \in \mathbb{P}^k(\mathcal{T}_h),\ \forall w_h \in \mathbb{P}^k(\mathcal{T}_h), \quad a_h(v_h, w_h) = (f, w_h)_\Omega, \tag{2.165}$$

where a_h is a discrete bilinear form defined on $\mathbb{P}^k(\mathcal{T}_h) \times \mathbb{P}^k(\mathcal{T}_h)$ and $f \in L^2(\Omega)$.

The well-posedness of (2.165) may be achieved relying on a discrete counterpart of the Lax-Milgram lemma, provided that the discrete bilinear form enjoys some discrete coercivity, consistency and boundedness properties, which are defined in the following. Following the strategy introduced in [50], to get the consistency, we need to extend the bilinear form to $V_* \times \mathbb{P}^k(\mathcal{T}_h)$ where V_* is a subspace of V, in order to be able to plug the exact solution in the first argument of the bilinear form. In practice, one can define the bilinear form on $\mathbb{P}^k(\mathcal{T}_h)$ and provide some additional assumptions on the exact solution. For the boundedness property, we need to extend the bilinear form to $V_{*_h} \times \mathbb{P}^k(\mathcal{T}_h)$, with $V_{*_h} \coloneqq V_* + \mathbb{P}^k(\mathcal{T}_h)$.

Definition 2.7. *1. We say that the discrete bilinear form a_h enjoys discrete coercivity on $\mathbb{P}^k(\mathcal{T}_h)$ with respect to the norm $|||\cdot|||$ if the following property holds,*

$$\exists C_{sta} > 0,\ \forall v_h \in \mathbb{P}^k(\mathcal{T}_h), \quad a_h(v_h, v_h) \ge C_{sta} |||v_h|||^2. \tag{2.166}$$

2. *We say that the discrete problem (2.165) is consistent with (2.158) if for the exact solution* $\mathfrak{p} \in V_*$*, we have*

$$a_h(\mathfrak{p}, w_h) = \big(f, w_h\big)_\Omega, \quad \forall w_h \in \mathbb{P}^k(\mathcal{T}_h). \tag{2.167}$$

3. *We say that the discrete bilinear form* a_h *is bounded in* $V_{*_h} \times \mathbb{P}^k(\mathcal{T}_h)$ *if there exists* $C_{bnd} > 0$ *such that the following inequality holds,*

$$\forall (v_h, w_h) \in V_{*_h} \times \mathbb{P}^k(\mathcal{T}_h), \quad |a_h(v_h, w_h)| \leq C_{bnd} |||v_h|||_* |||w_h|||. \tag{2.168}$$

We can now state the main result concerning the convergence of the discrete formulation,

Theorem 2.8. *(Abstract error estimate). Let consider* $\mathfrak{p}$ *and* $\mathfrak{p}_h$*, respectively solutions of (2.158) and (2.165). We assume that the discrete bilinear form* a_h *is coercive, consistent with the continuous bilinear form and bounded. Then, the following error estimate holds,*

$$|||\mathfrak{p} - \mathfrak{p}_h||| \leq C \inf_{y_h \in \mathbb{P}^k(\mathcal{T}_h)} |||\mathfrak{p} - y_h|||_*, \tag{2.169}$$

with $C = 1 + C_{sta}^{-1} C_{bnd}$.

Proof. see [50, theorem 1.35]. □

The following lemmas will also be useful in the following,

Lemma 2.9. *(Optimality of* L^2*-orthogonal projection). Let* π_h *be the* L^2*-orthogonal projection onto* $\mathbb{P}^k(\mathcal{T}_h)$*. Then, for all* $s \in \{0, ..., k+1\}$ *and all* $v \in H^s(T)$*, there holds*

$$|v - \pi_h v|_{H^m(T)} \leq C'_{app} h_T^{s-m} |v|_{H^s(T)} \quad \forall m \in \{0, ..., s\}, \tag{2.170}$$

where C'_{app} *is independent of both* T *and* h*.*

Proof. see, e.g., [50, Lemma 1.58]. □

Lemma 2.10. *In addition to the hypotheses of Lemma 2.9, assume that* $s \geq 1$*. Then, for all* $h \in \mathcal{H}$*, all* $T \in \mathcal{T}_h$*, and all* $F \in \mathcal{F}_T$*, there holds*

$$\|v - \pi_h v\|_F \leq C''_{app} h_T^{s-\frac{1}{2}} |v|_{H^s(T)}, \tag{2.171}$$

and if $s \geq 2$*,*

$$\|\partial_x (v - \pi_h v)_{|T} \cdot n_T\|_F \leq C'''_{app} h_T^{s-\frac{1}{2}} |v|_{H^s(T)}, \tag{2.172}$$

where C'''_{app} *and* C'''_{app} *are independent of both* T *and* h*.*

From the error estimate (2.169), one deduces that the following inequality holds,

$$|||u - u_h||| \leq \inf_{y_h \in V_h} |||u - y_h|||_* \leq |||u - \pi_h u|||_*. \tag{2.173}$$

2.2.2 Diffusion-reaction problem

We now recall the analysis of the simplest DG formulation in the simple case of a diffusion-reaction problem with homogeneous Dirichlet boundary conditions.

The continuous problem

Let consider the diffusion-reaction problem with Dirichlet boundary conditions,

$$\begin{aligned} -\Delta \mathfrak{p} + \delta \mathfrak{p} &= f \quad \text{in} \quad \Omega, \\ \mathfrak{p} &= 0 \quad \text{on} \quad \partial\Omega, \end{aligned} \tag{2.174}$$

with the source term $f \in L^2(\Omega)$ and the reaction coefficient $\delta \in L^\infty(\Omega)$. This problem may be classically written in the equivalent form,

$$\text{Find } \mathfrak{p} \in H_0^1(\Omega) \quad \forall v \in H_0^1(\Omega) \quad a(\mathfrak{p}, v) = \big(f, v\big)_\Omega, \tag{2.175}$$

where a is a bounded bilinear form defined on $H_0^1(\Omega) \times H_0^1(\Omega)$, defined as follows

$$\forall v, w \in H_0^1(\Omega) \quad a(v, w) \coloneqq \big(\partial_x v, \partial_x w\big)_\Omega + \big(\delta v, w\big)_\Omega. \tag{2.176}$$

It is classical that problem (2.175) is well-posed, which is a straightforward consequence of Lax-Milgram lemma.

The discrete problem

We consider the following discrete problem: find $\mathfrak{p}_h \in \mathbb{P}^k(\mathcal{T}_h)$, such that for all $w_h \in \mathbb{P}^k(\mathcal{T}_h)$, we have

$$a_h(\mathfrak{p}_h, w_h) = \big(f, w_h\big)_\Omega, \tag{2.177}$$

with,

$$\begin{aligned} a_h(v_h, w_h) = &\sum_{T \in \mathcal{T}_h} \big(\partial_x v_h, \partial_x w_h\big)_T - \sum_{F \in \mathcal{F}_h} \big(\big(\{\!\{\partial_x^h v_h\}\!\}, [\![w_h]\!]\big)_F + \big([\![v_h]\!], \{\!\{\partial_x^h w_h\}\!\}\big)_F\big) \\ &+ \sum_{F \in \mathcal{F}_h} \frac{\xi}{h_F} \big([\![v_h]\!], [\![w_h]\!]\big)_F + \sum_{T \in \mathcal{T}_h} \big(\delta v_h, w_h\big)_T, \end{aligned} \tag{2.178}$$

where ξ is a user-defined parameter to be specified later. This discrete bilinear form is called *Symmetric Interior Penalty* (SIP) form in the literature. In the following, we recall that (2.178) is consistent and enjoys some discrete coercivity property, provided that the penalty coefficient ξ is large enough, so that the corresponding discrete problem (2.177) is well-posed. Let begin with the consistency property,

Proposition 2.11. *(Consistency)*

$$\forall \phi_h \in \mathbb{P}^k(\mathcal{T}_h), \quad a_h(\mathfrak{p}, \phi_h) = \big(f, \phi_h\big)_\Omega. \tag{2.179}$$

Proof. To check the consistency of the discret problem, we set $v_h \coloneqq \mathfrak{p}$ in (2.178), to obtain

$$a_h(\mathfrak{p}, w_h) = \sum_{T\in\mathcal{T}_h} \big(\partial_x \mathfrak{p}, \partial_x w_h\big)_T - \sum_{F\in\mathcal{F}_h} \big(\partial_x \mathfrak{p}, [\![w_h]\!]\big)_F + \sum_{T\in\mathcal{T}_h} \big(\delta\mathfrak{p}, w_h\big)_T, \tag{2.180}$$

and after an integration by parts,

$$a_h(\mathfrak{p}, w_h) = -\sum_{T\in\mathcal{T}_h} \big(\Delta\mathfrak{p}, w_h\big)_T + \sum_{T\in\mathcal{T}_h} \big(\delta\mathfrak{p}, w_h\big)_T, \tag{2.181}$$

so that $a_h(\cdot,\cdot)$ is consistent in the following sense,

$$a_h(\mathfrak{p}, w_h) = \big(f, w_h\big)_\Omega, \quad \forall w_h \in \mathbb{P}^k(\mathcal{T}_h). \tag{2.182}$$

□

In order to formulate the discrete stability result, let introduce the following norm, for all $v_h \in \mathbb{P}^k(\mathcal{T}_h)$,

$$|||v_h||| \coloneqq \Big(\|\partial_x^h v_h\|_\Omega^2 + \|\delta^{\frac{1}{2}} v_h\|_\Omega^2 + |v_h|_{j,\kappa}^2\Big)^{\frac{1}{2}}, \tag{2.183}$$

with the jumps seminorm,

$$|v_h|_{j,\kappa} = \Big(\sum_{F\in\mathcal{F}_h} \frac{1}{h_F} \|[\![v_h]\!]\|_F^2\Big)^{\frac{1}{2}}. \tag{2.184}$$

Before addressing the discrete coercivity, we need some bounds on the boundary terms, which are addressed in the following Lemma.

Lemma 2.12. *For all* $(v_h, w_h) \in (\mathbb{P}^k(\mathcal{T}_h))^2$,

$$\Big|\sum_{F\in\mathcal{F}_h} \big(\{\!\{\partial_x^h v_h\}\!\}, [\![w_h]\!]\big)_F\Big| \le \Big(\sum_{T\in\mathcal{T}_h}\sum_{F\in\mathcal{F}_T} h_F \|\partial_x^h v_{h|T}\cdot n_F\|_F^2\Big)^{\frac{1}{2}} |w_h|_{j,\kappa}. \tag{2.185}$$

Proof. For all $F \in \mathcal{F}_h^i$ with $F = \partial T_1 \cap \partial T_2$, let introduce the following convenient shortcuts $a_i = \partial_x^h v_{h|T_i}\cdot n_F, i \in \{1,2\}$. The Cauchy-Schwarz inequality, yields

$$\begin{aligned}\big(\{\!\{\partial_x^h v_h\}\!\}, [\![w_h]\!]\big)_F &= \big(\frac{1}{2}(a_1+a_2), [\![w_h]\!]\big)_F \\ &\le \Big(\frac{1}{2} h_F(\|a_1\|_F^2 + \|a_2\|_F^2)\Big)^{\frac{1}{2}} \times \frac{1}{h_F}\|[\![w_h]\!]\|_F.\end{aligned}$$

Moreover, for all $F \in \mathcal{F}_h^b$ with $F = \partial T_1 \cap \partial\Omega$,

$$\big(\{\!\{\partial_x^h v_h\}\!\}, [\![w_h]\!]\big)_F \le h_F^{\frac{1}{2}} \|\partial_x^h v_{|T}\cdot n_F\|_F \times \Big(\frac{1}{h_F}\Big)^{\frac{1}{2}} \|[\![w_h]\!]\|_F.$$

Summing over mesh faces, using the Cauchy-Schwarz inequality, and regrouping the face contributions for each mesh element yields the assertion. □

Proposition 2.13. *(Discrete coercivity). For all $\xi > \underline{\xi} := C_{tr}^2 N_\partial$, where C_{tr} results from the discrete trace inequality (2.163), the bilinear form defined by (2.178) is coercive on $\mathbb{P}^k(\mathcal{T}_h)$ with respect to the $|||\cdot|||$-norm, i.e.,*

$$\exists C_\xi > 0, \quad \forall v_h \in \mathbb{P}^k(\mathcal{T}_h), \quad a_h(v_h, v_h) \geq C_\xi |||v_h|||^2,$$

where C_ξ depends on ξ and C_{tr}.

Proof. Let $v_h \in \mathbb{P}^k(\mathcal{T}_h)$, owing to the discrete trace inequality (2.163), we have

$$\begin{aligned}\sum_{T\in\mathcal{T}_h}\sum_{F\in\mathcal{F}_T} h_F \left\|\partial_x^h v_{h|T}\cdot n_F\right\|_F^2 &\leq \sum_{T\in\mathcal{T}_h} h_T \left\|\partial_x^h v_{h|T}\cdot n_F\right\|_{\partial T}^2,\\ &\leq C_{tr}^2 N_\partial \left\|\partial_x^h v_h\right\|_\Omega^2,\end{aligned}$$

and we infer from (2.185) that,

$$|\sum_{F\in\mathcal{F}_h} \left(\{\!\{\partial_x^h v_h\}\!\}, [\![v_h]\!]\right)_F| \leq C_{tr} N_\partial^{\frac{1}{2}} \left\|\partial_x^h v_h\right\|_\Omega |v_h|_{j,\kappa}.$$

As a result,

$$a_h(v_h, v_h) \geq \left\|\partial_x^h v_h\right\|_\Omega^2 - 2C_{tr} N_\partial^{\frac{1}{2}} \left\|\partial_x^h v_h\right\|_\Omega |v_h|_{j,\kappa} + \xi |v_h|_{j,\kappa}^2.$$

We now use the following inequality: let σ be a positive real numbers, let $\xi \geq \sigma^2$, then

$$\forall (x,y) \in \mathbb{R}^2, \quad x^2 - 2\sigma xy + \xi y^2 \geq \frac{\xi - \sigma^2}{1+\xi}(x^2+y^2). \tag{2.186}$$

Applying this inequality with $\sigma := C_{tr} N_\partial^{\frac{1}{2}}$, $x := \left\|\partial_x^h v_h\right\|_\Omega$, $y := |v_h|_{j,\kappa}$, we infer,

$$a_h(v_h, v_h) \geq \min(1, C_\xi) |||v_h|||^2,$$

with $C_\xi = \frac{\xi - C_{tr} N_\partial^{\frac{1}{2}}}{1+\xi}$. □

A straightforward consequence of the Lax-Milgram lemma is that the discrete problem (2.177) is well-posed. In order to study the convergence, we assume that the exact solution $\mathfrak{p}$ is such that,

$$\mathfrak{p} \in V_{*h} := H_0^1(\Omega) \cap H^2(\Omega) + \mathbb{P}^k(\mathcal{T}_h), \tag{2.187}$$

and we define on V_{*h} the norm,

$$|||v_h|||_* := \left(|||v_h|||^2 + \sum_{T\in\mathcal{T}_h} h_T \|\partial_x v_{h|T}\cdot n_T\|_{\partial T}^2\right)^{\frac{1}{2}}. \tag{2.188}$$

Proposition 2.14. *(Boundedness) There is C_{bnd}, independent of h, such that*

$$\forall (v_h, w_h) \in V_{*h} \times \mathbb{P}^k(\mathcal{T}_h), \quad a_h(v_h, w_h) \leq C_{bnd} |||v_h|||_* |||w_h|||. \tag{2.189}$$

Proof. Let $(v_h, w_h) \in V_{*h} \times \mathbb{P}^k(\mathcal{T}_h)$. We observe that,

$$\begin{aligned} a_h(v_h, w_h) = &\sum_{T\in\mathcal{T}_h} \big(\partial_x v_h, \partial_x w_h\big)_T - \sum_{F\in\mathcal{F}_h} \big(\{\!\{\partial_x v_h\}\!\}, [\![w_h]\!]\big)_F - \sum_{F\in\mathcal{F}_h} \big([\![v_h]\!], \{\!\{\partial_x w_h\}\!\}\big)_F \\ &+ \sum_{F\in\mathcal{F}_h} \xi\big(\frac{1}{h_F}[\![v_h]\!], [\![w_h]\!]\big)_F + \sum_{T\in\mathcal{T}_h} \big(\delta v_h, w_h\big)_T, \\ &\coloneqq \varrho_1 + \cdots + \varrho_5. \end{aligned} \tag{2.190}$$

Using the Cauchy-Schwarz inequality, yields

$$\begin{aligned} |\varrho_1| \le \|\partial_x v_h\|_\Omega \|\partial_x w_h\|_\Omega \le |||v_h||| \, |||w_h|||, \\ |\varrho_4| \le \xi |v_h|_{j,\kappa} |w_h|_{j,\kappa} \le \xi |||v_h||| \, |||w_h|||, \end{aligned} \tag{2.191}$$

owing to the bound (2.185) and since $h_F \simeq h_T$, one obtains

$$|\varrho_2| \le \Big(\sum_{T\in\mathcal{T}_h} h_T \|\partial_x v_{h|T} \cdot n_T\|^2_{\partial T} \Big)^{\frac{1}{2}} |w_h|_{j,\kappa} \le |||v_h|||_* |w_h|_{j,\kappa} \le |||v_h|||_* |||w_h|||, \tag{2.192}$$

by definition of the $|||\cdot|||_*$-norm, still using (2.185) and proceeding as in the proof of proposition 2.13, yields

$$|\varrho_3| \le C_{tr} N_\partial^{1/2} |||v_h||| \, |||w_h|||, \tag{2.193}$$

using again the Cauchy-Schwarz inequality, we infer

$$|\varrho_5| \le \|\delta^{\frac{1}{2}} v_h\|_\Omega \|\delta^{\frac{1}{2}} w_h\|_\Omega \le |||v_h||| \, |||w_h|||, \tag{2.194}$$

gathering the above bounds yields (2.192) with $C_{bnd} = 3 + \xi + C_{tr} N_\partial^{1/2}$.

□

A straightforward consequence of the above results together with Theorem 2.8 is the following error estimate,

Proposition 2.15. *Let $\mathfrak{p} \in V_{*h}$ and $\mathfrak{p}_h$ be the solutions of (2.175) and (2.177), respectively, with a_h defined by (2.178). Then, there is C, independent of h, such that*

$$|||\mathfrak{p} - \mathfrak{p}_h||| \le C \inf_{v_h \in \mathbb{P}^k(\mathcal{T}_h)} |||\mathfrak{p} - \mathfrak{p}_h|||_*. \tag{2.195}$$

To infer a convergence result from (2.195), we assume that the exact solution is smooth enough and use lemmata 2.9 and 2.10.

Lemma 2.16. *Assuming $\mathfrak{p} \in H^{k+1}(\Omega)$, in addition to the assumptions of proposition 2.15. Then, there holds*

$$|||\mathfrak{p} - \mathfrak{p}_h||| \le C_\mathfrak{p} h^k, \tag{2.196}$$

with $C_\mathfrak{p} = C\|\mathfrak{p}\|_{H^{k+1}(\Omega)}$ and C independent of h.

Proof. Taking $v_h = \pi\mathfrak{p}$, the L^2-orthogonal projection of $\mathfrak{p}$ onto $\mathbb{P}^k(\mathcal{T}_h)$, we get

$$\begin{aligned}
|||\mathfrak{p} - \pi_h\mathfrak{p}|||_* = &\sum_{T\in\mathcal{T}_h} \|\partial_x(\mathfrak{p} - \pi_h\mathfrak{p})\|_T^2 + \sum_{F\in\mathcal{F}_h} \frac{1}{h_F} \left\|[\![\mathfrak{p} - \pi_h\mathfrak{p}]\!]\right\|_F^2 \\
&+ \sum_{T\in\mathcal{T}_h} h_T \left\|\partial_x^h(\mathfrak{p} - \pi_h\mathfrak{p})_{|T} \cdot n_T\right\|_{\partial T}^2 + \sum_{T\in\mathcal{T}_h} \left\|\delta^{\frac{1}{2}}(\mathfrak{p} - \pi_h\mathfrak{p})\right\|_T^2, \\
&:= \varrho_1 + \varrho_2 + \varrho_3 + \varrho_4.
\end{aligned}$$

Using Cauchy-Schwarz inequality and lemma 2.9 with $m = 1$ and $s = k + 1$, we infer

$$\varrho_1 \leq \sum_{T\in\mathcal{T}_h} C_{app}'^2 h_T^{2k} \|\mathfrak{p}\|_{H^{k+1}(T)}^2,$$

triangular inequality, discrete trace inequality (2.163) and lemma 2.10, give

$$\varrho_2 \leq \sum_{T\in\mathcal{T}_h} \frac{1}{h_T} \sum_{F\in F_T} \|\mathfrak{p} - \pi_h\mathfrak{p}\|_F^2 \leq \sum_{T\in\mathcal{T}_h} N_\partial C_{app}''^2 h_T^{2k} \|\mathfrak{p}\|_{H^{k+1}(T)}^2,$$

owing to the trace inequality and lemma 2.9 with $m = 1$ and $s = k + 1$, yields

$$\varrho_3 \leq \sum_{T\in\mathcal{T}_h} \left\|\partial_x(\mathfrak{p} - \pi_h\mathfrak{p})_{|T}\right\|_T^2 \leq \sum_{T\in\mathcal{T}_h} C_{tr}^2 C_{app}'^2 N_\partial h_T^{2k} \|\mathfrak{p}\|_{H^{k+1}(T)}^2,$$

Cauchy-Schwarz inequality and lemma 2.9 with $m = 0$ and $s = k + 1$, give

$$\varrho_4 \leq \sum_{T\in\mathcal{T}_h} C_{app}'^2 h_T^{2(k+1)} \|\mathfrak{p}\|_{H^{k+1}(T)}^2,$$

gathering the above bounds yields the assertion with,

$$C_\mathfrak{p} = \left(C_{app}' + N_\partial^{\frac{1}{2}} C_{app}'' + N_\partial^{\frac{1}{2}} C_{app}' C_{tr} + C_{app}' h\right). \tag{2.197}$$

□

2.2.3 Shallow Water equations

In this section, we recall the construction of DG approximations for the weak solutions of the NSW equations, as introduced in [61]. Setting $b = 0$ for the sake of simplicity, the NSW equations (2.198) obtained at the beginning of this Chapter may be alternatively written as follows,

$$\begin{cases} \partial_t H + \partial_x q = 0, \\ \partial_t q + \partial_x(H\bar{v}^2) + gH\partial_x H = 0, \end{cases} \tag{2.198}$$

where we have set $q = H\bar{v}$. This system can be written in a compact general conservative form as follows,

$$\partial_t \mathbf{w} + \partial_x \mathbb{F}(\mathbf{w}) = 0, \tag{2.199}$$

where $\mathbb{F}(\mathbf{w}) : \Omega \longrightarrow \mathbb{R}^2 \times \mathbb{R}$ is the flux function, which reads

$$\mathbb{F}(\mathbf{w}) \coloneqq \begin{pmatrix} q \\ \mathcal{F}(\mathbf{w}) \end{pmatrix}, \tag{2.200}$$

and the nonlinear flux is,

$$\mathcal{F}(\mathbf{w}) \coloneqq H\bar{v}^2 + \frac{1}{2}gH^2.$$

Multiplying (2.199) by test functions $\phi \in \mathbb{P}^k(\mathcal{T}_h)$ and integrating over a given element T_i, with the flux term being integrated by parts, one obtains

$$\int_{T_i} \partial_t \mathbf{w}\phi - \int_{T_i} \mathbb{F}(\mathbf{w})\partial_x \phi + \int_{\partial T_i} \mathbb{F}(\mathbf{w}) \cdot n_{\partial T_i}\phi = 0, \tag{2.201}$$

where ∂T_i is the boundary of T_i and $n_{\partial T_i}$ its unit outward normal. The local approximated vector solution $\mathbf{w}_h \in \mathbb{P}^k(\mathcal{T}_h)$ is expressed as a polynomial of order k on each element T_i,

$$\mathbf{w}_h(t,x) = \sum_{l=1}^{N_d} \mathbf{w}_i^l(t)\phi_i^l(x), \quad \forall x \in T_i, \forall t \in [0, t_{max}], \tag{2.202}$$

where $\{\phi_i^l\}_{l=1}^{N_d}$ is a polynomial basis for $\mathbb{P}^k(T)$, and $\{\mathbf{w}_i^l(t)\}_{l=1}^{N_d}$ are the local expansion coefficient vectors with $\mathbf{w}_i^l(t) = (\eta_i^l, q_i^l)$. Many choices are possible for the expansion basis, and we choose to use a nodal approach: $\{\phi_i^l\}_{l=1}^{N_d}$ will refer to the interpolant Lagrangian expansion basis, with $N_d = k + 1$. Thus, a discrete formulation of (2.201) is obtained by replacing the exact solution $\mathbf{w}(t,x)$ by the approximation $\mathbf{w}_h(t,x)$ and the test function ϕ by the expansion basis functions,

$$\int_{T_i} \Big(\sum_{l=1}^{N_d} \partial_t \mathbf{w}_i^l \phi_i^l\Big)\phi_i^m - \int_{T_i} \mathbb{F}(\mathbf{w}_h)\partial_x \phi_i^m + \int_{\partial T_i} \mathbb{F}(\mathbf{w}_h) \cdot n_{\partial T_i}\phi_i^m = 0, \quad 1 \le m \le N_d. \tag{2.203}$$

Noting that we have,

$$\int_{\partial T_i} \mathbb{F}(\mathbf{w}_h) \cdot n_{\partial T_i}\phi_i^m = \sum_{F \in \mathcal{F}_T} \big(\widehat{\mathbb{F}}_{TF}, \phi_i^m\big)_F, \tag{2.204}$$

we obtain the following discrete formulation,

$$\sum_{l=1}^{N_d} \partial_t \mathbf{w}_i^l \int_{T_i} \phi_i^l \phi_i^m - \int_{T_i} \mathbb{F}(\mathbf{w}_h)\partial_x \phi_i^m + \sum_{F \in \mathcal{F}_T} \big(\widehat{\mathbb{F}}_{TF}, \phi_i^m\big)_F = 0, \quad 1 \le m \le N_d. \tag{2.205}$$

Hence, the DG approximation of (2.199) reads,

find $(\eta_h, q_h) \in (\mathbb{P}^k(\mathcal{T}_h))^2$ such that, for all $\varphi_h \in \mathbb{P}^k(\mathcal{T}_h)$,

$$\big(\partial_t \mathbf{w}_h, \varphi_h\big)_\Omega + \big(\mathcal{A}_h(\mathbf{w}_h), \varphi_h\big)_\Omega = 0, \tag{2.206}$$

where

1. the discrete nonlinear operator $\mathcal{A}_h$ in (2.206) is defined by,

$$\big(\mathcal{A}_h(\mathbf{w}_h),\varphi_h\big)_\Omega = -\sum_{T\in\mathcal{T}_h}\big(\mathbb{F}(\mathbf{w}_h),\partial_x\varphi_h\big)_T + \sum_{T\in\mathcal{T}_h}\sum_{F\in\mathcal{F}_T}\big(\widehat{\mathbb{F}}_{TF},\varphi_h\big)_F, \tag{2.207}$$

2. $\widehat{\mathbb{F}}_{TF}$ is a numerical approximation of the normal face fluxes $\mathbb{F}(\mathbf{w}_h)\cdot n_{TF}$ which is chosen to be the Lax-Friedrichs flux. Denoting by $\mathbf{w}^-$ and $\mathbf{w}^+$, respectively, the interior and exterior traces of $\mathbf{w}_h$ on F, with respect to the element T. The global Lax-Friedrichs flux is given by,

$$\widehat{\mathbb{F}}_{TF} = \frac{1}{2}\big(\mathbb{F}(\mathbf{w}^-)\cdot\overrightarrow{n}_{TF} + \mathbb{F}(\mathbf{w}^+)\cdot\overrightarrow{n}_{TF} - a(\mathbf{w}^+ - \mathbf{w}^-)\big), \tag{2.208}$$

with $a \coloneqq \max_{T\in\mathcal{T}_h}\sigma_T$ and

$$\sigma_T \coloneqq \max_{\partial T}\left(\left|\frac{q_{h|T}}{H_{h|T}}\cdot n_T\right| + \sqrt{gH_{h|T}}\right). \tag{2.209}$$

2.2.3.1 Time discretization

Supplementing (2.199) with an initial datum $\mathbf{w}(0,.) = \mathbf{w}^0$, the time stepping is carried out using the explicit SSP-RK schemes of. For $k < 3$, we consider SSP-RK schemes of order $(k+1)$. For instance, writing the discrete formulations (2.205) in the operator form,

$$\partial_t\mathbf{w}_h + \mathcal{A}_h(\mathbf{w}_h) = 0, \tag{2.210}$$

we advance from time level n to $(n+1)$ as follows with the third-order scheme as follows,

$$\begin{aligned}
\mathbf{w}_h^{n,1} &= \mathbf{w}_h^n - \Delta t^n\mathcal{A}_h(\mathbf{w}_h^n),\\
\mathbf{w}_h^{n,2} &= \frac{1}{4}(3\mathbf{w}_h^n + \mathbf{w}_h^{n,1}) - \frac{1}{4}\Delta t^n\mathcal{A}_h(\mathbf{w}_h^{n,1}),\\
\mathbf{w}_h^{n+1} &= \frac{1}{3}(\mathbf{w}_h^n + 2\mathbf{w}_h^{n,2}) - \frac{2}{3}\Delta t^n\mathcal{A}_h(\mathbf{w}_h^{n,2}),
\end{aligned}$$

where $\mathbf{w}_h^{n,i}$, $1\le i\le 2$, are the intermediate stages, Δt^n is obtained from the CFL condition (5.40), and the discrete initial data $\mathbf{w}_h^0$ is defined either as the L^2-projection or interpolation on $(\mathbb{P}^k(\mathcal{T}_h))^2$ of $\mathbf{w}_0$. For $k\ge 3$, the five stages fourth order SSP-RK scheme of [150] is used (the details are omitted for the sake of simplicity). The corresponding time step Δt^n is computed adaptively using the following CFL condition (see [38]),

$$\Delta t^n < \frac{1}{2k+1}\min_{T\in\mathcal{T}_h}\left(\frac{h_T}{\sigma_T}\right), \tag{2.211}$$

with,

$$\sigma_T \coloneqq \max_{\partial T}\left(\left|\frac{q_{h|T}}{H_{h|T}}\cdot \mathrm{n}_T\right| + \sqrt{gH_{h|T}}\right).$$

Chapter 3

Main results

In the previous Chapter, we recall the complete derivation of various shallow water models, in the particular case $d = 1$, including the NSW equations, the Boussinesq equations and the SGN equations without and with vorticity. These various models may be regarded as a hierarchy of increasing complexity set of equations towards a more complete description of the whole range of hydrodynamical processes in nearshore oceanography. Having such a hierarchy available, one has to investigate now the construction of discrete formulations allowing to compute the time evolution of approximate solutions to these models.
To this end, we have highlighted in the introductory Chapter 2 §2.1 that DG methods may be particularly well suited, as they allow enough flexibility, efficiency, and accuracy to successfully address the numerous difficulties associated with such highly nonlinear and dispersive equations. To highlight such flexibility, and to introduce the main ideas of the design and analysis of DG methods, we also recall in Chapter 2, §2.2 the construction and analysis of basic arbitrary order accuracy DG approximations for some model problems: the diffusion-reaction problem, which is an elliptic problem, and the NSW equations, which is a nonlinear hyperbolic problem.
And indeed, several recently published studies have shown successful applications of various DG formulations to NSW, Boussinesq and SGN equations. However, there are still several limitations, which are addressed in this thesis. This Chapter is dedicated to a summarized presentation of these works, with a particular emphasize put on the specific improvements and novelties.

3.1 A new SWIP-DG formulation for SGN equations

Let focus first on the classical SGN equations without vorticity. As already mentioned in Chapter 2, the construction of fully discontinuous Finite-Element formulations for the SGN equations is investigated first in [59, 60]. In these preliminary works, DG methods based on LDG approximations for higher-order derivatives is built for the optimized SGN equations of [97]. However, the particular SGN equations of [97] relies on a simpler second order elliptic operator. This simpler structure is of course exploited in [59, 60].
However, the corresponding discretization matrices obtained in [59, 60] are not symmetric due to the nature of the LDG formulations. Additionally, the LDG strategy requires the introduction of many auxiliary variables to formulate the higher-order differential operators as systems of first-

order operators and generate some computational overhead and complexity.
These drawbacks are partially addressed in [51], where the elliptic operator associated with the classical SGN equations is reformulated as a symmetric diffusion-reaction like problem, as follows:

$$H(1+\mathcal{T}[H,b])w = -\frac{1}{3}\partial_x\Big(\underbrace{H^3}_{\kappa(H)}\partial_x w\Big) + \underbrace{\Big(H+\frac{1}{2}\partial_x(H^2\partial_x b)+H(\partial_x b)^2\Big)}_{\delta(H,b)}w. \tag{3.1}$$

Such an operator may be discretized with a SIP-DG method inspired from the one recalled in Chapter 2 §2.2. There is however several major differences:

1. the second order term and the reaction term in (3.1) have variable (non-homogeneous) coefficients κ and δ, defined with respect to the water height H and the topography b,
2. writing the associated discrete formulation, the water height is approximated by a broken polynomial and as a consequence, the discrete version of these coefficients are discontinuous by construction,
3. the water height may exhibit strong variations, leading to strong gradients values in the vicinity of the waves breaking area.

These particular and constraining features justify the introduction of a specific stability enforcement at the mesh interfaces, and the method proposed in [51] falls into the particular family of *Symmetric Weighted Interior Penalty*-DG method (SWIP-DG), see [52] for details. The discrete bilinear form associated with (3.1), with the notations introduced in Chapter2, reads as follows:

$$\begin{aligned} a_h^{(1)}(\kappa,\delta;v_h,w_h) \coloneqq & \sum_{T\in\mathcal{T}_h}\big(\kappa\partial_x v_h,\partial_x w_h\big)_T + \sum_{F\in\mathcal{F}_h}\xi\big(\frac{\gamma_{\kappa,F}}{h_F}[\![v_h]\!],[\![w_h]\!]\big)_F + \sum_{T\in\mathcal{T}_h}\big(\delta v_h,w_h\big)_T \\ & - \sum_{F\in\mathcal{F}_h}\Big(\big(\{\!\{\kappa\partial_x^h v_h\}\!\}_\omega,[\![w_h]\!]\big)_F + \big([\![v_h]\!],\{\!\{\kappa\partial_x^h w_h\}\!\}_\omega\big)_F\Big). \end{aligned} \tag{3.2}$$

We observe the symmetry of the interface terms

$$\sum_{F\in\mathcal{F}_h}\Big(\big(\{\!\{\kappa\partial_x^h v_h\}\!\}_\omega,[\![w_h]\!]\big)_F + \big([\![v_h]\!],\{\!\{\kappa\partial_x^h w_h\}\!\}_\omega\big)_F\Big).$$

We also emphasize that the terms

$$\sum_{F\in\mathcal{F}_h}\xi\big(\frac{\gamma_{\kappa,F}}{h_F}[\![v_h]\!],[\![w_h]\!]\big)_F,$$

are called the *interior penalty terms*, which are added to obtain the discrete stability. Using this discrete formulation, one is able to use iterative methods for sparse linear systems in order to solve the linear system associated with this new discretization and this is a real improvement.
However, this formulation still suffers from a major drawback: the reaction term $H+\frac{1}{2}\partial_x(H^2\partial_x b)+H(\partial_x b)^2$ in (3.1) may not be always positive, as it depends on $\partial_x b$. A straightforward consequence is that the discrete coercivity property of the associated discrete bilinear form can not been proved

as in 2 §2.2.

The goal of Chapter 4 is to alleviate such a limitation and introduce a new DG formulation for the SGN equations for which it is possible to ensure the stability of the discrete bilinear form.

To achieve this, a reformulation of the SGN equations is proposed as follows:

$$\begin{aligned} \partial_x \mathbf{w} + \partial_x \mathbb{F}(\mathbf{w}, b) + \mathbb{D}(\mathbf{w}, \mathfrak{p}) &= \mathbb{B}(\mathbf{w}, \partial_x b), \\ \partial_x \left(-\kappa(H)\partial_x \mathfrak{p}\right) - \beta(H, \partial_x b)\partial_x \mathfrak{p} + \partial_x \left(\beta(H, \partial_x b)\mathfrak{p}\right) + \delta(H, \partial_x b)\mathfrak{p} &= \mathbb{Q}[H, b](\eta, \bar{v}), \end{aligned} \tag{3.3}$$

where we have, in particular, $\delta(H, \partial_x b) \coloneqq H(\partial_x b)^2 + H$ and the other coefficients $\kappa(H)$ and $\beta(H, \partial_x b)$ are defined in Chapter 4. We emphasize that the coupling between the first (hyperbolic) and the second (elliptic) equations is achieved through the introduction of an auxiliary variable $\mathfrak{p}$.

Looking specifically at the elliptic problem and comparing the formulation

$$H(1 + \mathcal{T}[H, b])w = \partial_x \left(-\kappa[H]\partial_x w\right) - \beta[H, \partial_x b]\partial_x w + \partial_x \left(\beta[H, \partial_x b]w\right) + H\left((\partial_x b)^2 + 1\right) w, \tag{3.4}$$

with (3.1), we observe two major differences: (i) assuming that $H \geq 0$, the reaction-like coefficient of the new formulation, namely $H((\partial_x b)^2 + 1)$, is always positive, (ii) there are two additional first-order convection-like terms, namely $\beta[H, \partial_x b]\partial_x w$ and $\partial_x(\beta[H, \partial_x b]w)$ with coefficients $\beta[H, \partial_x b]$ which sign doesn't matter for the stability analysis of the upcoming DG formulation.

Relying on this reformulation, we introduce a new discrete bilinear form, still belonging to the family of *Symmetric Weighted Interior Penalty*-DG methods, and which reads as follows:

$$\begin{aligned} a_h(\kappa, \beta, \delta; v_h, w_h) \coloneqq & \sum_{T \in \mathcal{T}_h} \left(\kappa \partial_x v_h, \partial_x w_h\right)_T + \sum_{F \in \mathcal{F}_h} \xi \left(\frac{\gamma_{\kappa,F}}{h_F} [\![v_h]\!], [\![w_h]\!]\right)_F + \sum_{T \in \mathcal{T}_h} \left(\delta v_h, w_h\right)_T \\ & - \sum_{F \in \mathcal{F}_h} \left(\left(\{\!\{\kappa \partial_x^h v_h\}\!\}_\omega, [\![w_h]\!]\right)_F + \left([\![v_h]\!], \{\!\{\kappa \partial_x^h w_h\}\!\}_\omega\right)_F \right) \\ & - \sum_{T \in \mathcal{T}_h} \left(\beta v_h, \partial_x w_h\right)_T - \sum_{T \in \mathcal{T}_h} \left(\partial_x v_h, \beta w_h\right)_T \\ & + \sum_{F \in \mathcal{F}_h} \left(\left(\{\!\{\beta v_h\}\!\}_\omega, [\![w_h]\!]\right)_F + \left([\![v_h]\!], \{\!\{\beta w_h\}\!\}_\omega\right)_F \right). \end{aligned} \tag{3.5}$$

We observe that this new discrete bilinear form is indeed symmetric and we emphasize that this is a highly non-trivial feature for any DG formulations with advection-like operators. In the proposed formulation, this symmetry is obtained thanks to the reformulation (3.3). Indeed, we observe that the two new advection-like terms in (3.4) lead to two new surface integral terms in (3.5):

$$\sum_{T \in \mathcal{T}_h} \left(\beta v_h, \partial_x w_h\right)_T + \sum_{T \in \mathcal{T}_h} \left(\partial_x v_h, \beta w_h\right)_T,$$

together with the corresponding interface terms,

$$\sum_{F\in\mathcal{F}_h} \left(\left(\{\!\{\beta v_h\}\!\}_\omega, [\![w_h]\!] \right)_F + \left([\![v_h]\!], \{\!\{\beta w_h\}\!\}_\omega \right)_F \right). \tag{3.6}$$

Concerning the consistency, we have the following result, which is proved in Chapter 4:

Proposition 3.1. *(Consistency)*

$$\forall \phi_h \in \mathbb{P}^k(\mathcal{T}_h), \quad a_h(\kappa(H), \beta(H, \partial_x b), \delta(H, \partial_x b); \mathfrak{p}, \phi_h) = \left(\mathbb{Q}[H, b](\eta, \bar{v}), \phi_h \right)_\Omega.$$

Looking at the penalty terms in (3.5), we emphasize that they now have the liability to counterbalance, in the discrete coercivity study, the signs of both the "usual" interface terms and the new interface terms (3.6). In order to formulate the discrete stability result, let introduce the following norm, for all $v_h \in \mathbb{P}^k(\mathcal{T}_h)$,

$$|||v_h||| := \left(\left\| \kappa(H_h)^{\frac{1}{2}} \partial_x^h v_h \right\|_\Omega^2 + \left\| (H_h^{\frac{1}{2}} \partial_x b_h) v_h \right\|_\Omega^2 + \left\| H_h^{\frac{1}{2}} v_h \right\|_\Omega^2 + |v_h|_{j,\kappa}^2 \right)^{1/2}, \tag{3.7}$$

with the jumps seminorm

$$|v_h|_{j,\kappa} = \left(\sum_{F\in\mathcal{F}_h} \frac{\gamma_{k,F}}{h_F} \left\| [\![v_h]\!] \right\|_F^2 \right)^{1/2}. \tag{3.8}$$

We establish the following stability results:

Proposition 3.2. *(Discrete coercivity) For all $\xi > \underline{\xi}$ (with $\underline{\xi}$ defined in Chapter 4), the bilinear form defined by (3.5) is coercive on $\mathbb{P}^k(\mathcal{T}_h)$ with respect to the $|||\cdot|||$-norm, i.e.,*

$$\exists C_\xi > 0, \quad \forall v_h \in \mathbb{P}^k(\mathcal{T}_h), \quad a_h(\kappa[H_h], \beta[H_h, \nabla b_h], \delta[H_h, \nabla b_h]; v_h, v_h) \geq C_\xi |||v_h|||^2.$$

In order to formulate the error estimate result, we assume that the bilinear form (3.5) is extended to $V_{*_h} \times \mathbb{P}^k(\mathcal{T}_h)$, with $V_{*_h} := H^2(\Omega) + \mathbb{P}^k(\mathcal{T}_h)$.

let introduce the following norm, for all $v_h \in \mathbb{P}^k(\mathcal{T}_h)$,

$$|||v_h|||_* := \left(|||v_h|||^2 + \sum_{T\in\mathcal{T}_h} h_T \left\| \kappa(H_h)_{|T}^{\frac{1}{2}} \partial_x^h v_{h|T} \cdot n_T \right\|_{\partial T}^2 + \sum_{T\in\mathcal{T}_h} h_T \left\| (H_h^{\frac{1}{2}} \partial_x b_h)_{|T} v_{h|_T} \cdot n_{|T} \right\|_{\partial T}^2 \right)^{1/2}, \tag{3.9}$$

As a complement to the submitted paper [177], we also establish the following error estimate:

Theorem 3.3. *(Error estimate) Let* $\mathfrak{p} \in V_{*_h}$ *solve* (4.15b). *Let* $\mathfrak{p}_h \in \mathbb{P}^k(\mathcal{T}_h)$ *solve the discrete problem with* a_h *defined by* (3.5) *and penality parameter as in proposition* (4.8). *Then, there is* C, *independant of* h, κ *and* χ, *such that*

$$|||\mathfrak{p} - \mathfrak{p}_h||| \leq C \inf_{v_h \in \mathbb{P}^k(\mathcal{T}_h)} |||\mathfrak{p} - \mathfrak{p}_h|||_* \tag{3.10}$$

Moreover, if $\mathfrak{p} \in H^{k+1}(\Omega)$,

$$|||\mathfrak{p} - \mathfrak{p}_h||| \leq C_{\kappa,\chi} C_{\mathfrak{p}} h^k, \tag{3.11}$$

with

$$\begin{aligned} C_{\mathfrak{p}} &= C \, \|\mathfrak{p}\|_{H^{k+1}(\Omega)}, \\ C_{\kappa,\chi} &= C_{\max}(\bar{\kappa}^{\frac{1}{2}} + \bar{\chi} h + \bar{H}_h^{\frac{1}{2}} h + \overline{\kappa}^{\frac{1}{2}} + \overline{\chi} h), \end{aligned} \tag{3.12}$$

and

$$\begin{aligned} \overline{\kappa} &:= \|\kappa[H_h]\|_{L^\infty(\Omega)}, \ \overline{\chi} := \|\chi[H_h, \nabla b_h]\|_{L^\infty(\Omega)}, \ \overline{H} := \|H_h\|_{L^\infty(\Omega)}, \\ C_{\max} &= \max(C'_{app}, N_\partial^{1/2} \min(\kappa_1, \kappa_2)^{1/2} C''_{app}, N_\partial^{1/2} C'''_{app}, C_{tr} N_\partial^{1/2} C'_{app}). \end{aligned} \tag{3.13}$$

We finally emphasize that this new formulation for the SGN equations may be extended to the $d = 2$ situation, by switching to 2d differential operators in the proposed formulation.

3.2 A robust SWIP-DG formulation for rotational SGN equations

In Chapter 5, we investigate the design of DG formulations for the SGN equations with vorticity (2.151). To our knowledge, the only numerical discretization for these equations was proposed in [101], with a hybrid WENO-DF discretization. Let also mention the recent works [89, 137] in which related models with a modified time-evolution equation on the enstrophy $\mathfrak{e}$, with calibrated source terms to model wave breaking, are considered. However, these works focus on the issue of wave-breaking and not on the stability of the numerical methods, which are straightforwardly adapted from [59]. The system under study reads as follows:

$$\begin{cases} \partial_t \zeta + \partial_x(H\bar{v}) = 0, \\ (1 + \mu \mathbf{T}[H, \beta b])[\partial_t(H\bar{v}) + \varepsilon \partial_x(H\bar{v}^2)] + H\partial_x \zeta + \varepsilon\mu H Q_1[H, \beta b](\bar{v}) + \varepsilon\mu\partial_x(H^3\mathfrak{e}) \\ +\varepsilon\mu^{3/2} C[H](H\mathfrak{v}^\sharp, \bar{v}) = 0, \\ \partial_t(H\mathfrak{v}^\sharp) + \varepsilon\partial_x(H\bar{v}\mathfrak{v}^\sharp) = 0, \\ \partial_t(H\mathfrak{e}) + \varepsilon\partial_x(H\bar{v}\mathfrak{e}) = 0. \end{cases} \tag{3.14}$$

Starting from the formulation of Chapter 4 for the (irrotational) SGN equations, there are some major novelties in equations (3.14) that introduce additional challenges: (i) there are two new variables, namely $\mathfrak{e}$ and $\mathfrak{v}^\sharp$, which are occurring in the momentum conservation equation. This entails some modifications in the coupling strategy, between the hyperbolic part of the model, and the elliptic part. In particular, the new enstrophy variable $\mathfrak{e}$ occurs in the definition of the associated nonlinear flux, (ii) the enstrophy variable $\mathfrak{e}$ is defined as a non-negative quantity. The proposed new DG formulation should ensure that this non-negativity is preserved at the discrete level.

The goal of Chapter 5 is to design a new fully discontinuous discrete formulation for (3.14) that accounts for these features.

Let introduce an augmented vector of state variables, and the corresponding nonlinear flux vector, as follows

$$\mathbf{w} = \begin{pmatrix} \zeta \\ H\bar{v} \\ H\mathfrak{v}^\sharp \\ H\mathfrak{e} \end{pmatrix}, \quad \mathbb{F}(\mathbf{w}) = \begin{pmatrix} H\bar{v} \\ \mathcal{F}(\mathbf{w}) \\ H\bar{v}\mathfrak{v}^\sharp \\ H\bar{v}\mathfrak{e} \end{pmatrix}, \tag{3.15}$$

with

$$\mathcal{F}(\mathbf{w}) \coloneqq H\bar{v}^2 + \frac{1}{2}gH^2 + H^3\mathfrak{e}, \tag{3.16}$$

so that as in the previous section, the rotational SGN equations (2.151) may be formulated in a compact form as follows:

$$\begin{cases} \partial_t \mathbf{w} + \partial_x \mathbb{F}(\mathbf{w}) + \mathbb{D}(\mathbf{w}, \mathfrak{p}) = \mathbb{B}(\mathbf{w}, b), & \text{(3.17a)} \\ \partial_x\Big(-\kappa(H)\partial_x\mathfrak{p}\Big) - \beta(H, \partial_x b)\partial_x\mathfrak{p} + \partial_x\Big(\beta(H, \partial_x b)\,\mathfrak{p}\Big) + \delta(H, \partial_x b)\mathfrak{p} = \mathbb{Q}(\mathbf{w}, b). & \text{(3.17b)} \end{cases}$$

The state vector $\mathbf{w}$ is assumed to take values in a convex and open set $\mathcal{U}$ defined as

$$\mathcal{U} = \{(H, H\bar{v}, H\mathfrak{v}^\sharp, H\mathfrak{e}) \in \mathbb{R}^4,\ H \geq 0, \mathfrak{e} \geq 0\}, \tag{3.18}$$

and focusing on the first-order and homogeneous part of (5.19), which reads as

$$\partial_t \mathbf{w} + \partial_x \mathbb{F}(\mathbf{w}) = 0, \tag{3.19}$$

the computation of $\mathbb{F}'(\mathbf{w})$ shows that the corresponding system is strictly hyperbolic as soon as $H > 0$, with the following eigenvalues:

$$\lambda_1 = \bar{v} - (gH + 3H^2\mathfrak{e})^{\frac{1}{2}}, \quad \lambda_2 = \lambda_3 = \bar{v}, \quad \lambda_4 = \bar{v} + (gH + 3H^2\mathfrak{e})^{\frac{1}{2}}. \tag{3.20}$$

The inclusion of the term $H^3\mathfrak{e}$ in the definition of the nonlinear flux (3.16) is mainly motivated by the fact that the resulting wave-speeds (3.20) are very similar to the propagation speed of the rotational solitary waves (2.156) and as a consequence, such a choice may ensure that realistic wave speeds are effectively accurately approximated in the transport part of the proposed new DG formulation.

The first step to achieve the design of an arbitrary-order DG scheme for equations (2.151) is the construction of a robust lowest-order FV scheme. Such a FV scheme should rely on a new HLLC-type Riemann solver for the homogeneous hyperbolic system (3.19).
More precisely, we consider an approximate Riemann solver at interface F consisting of 2 finite external wave-speeds λ_F^-, λ_F^+ and an additional intermediate wave $\lambda_F^\star$ (note that in the following, the subscript F may be avoided when no confusion is possible). We denote by $\mathbf{w}_L^\star$ and $\mathbf{w}_R^\star$ the intermediate states to the left and to the right of the wave $\lambda^\star$ respectively. The 3 wave speeds are

therefore separating 4 constant states $\mathbf{w}_L$, $\mathbf{w}_L^\star$, $\mathbf{w}_R^\star$ and $\mathbf{w}_R$, leading to the following approximate solver:

$$\hat{\mathbf{w}}(\xi, \mathbf{w}_L, \mathbf{w}_R) = \begin{cases} \mathbf{w}_L & \text{if } \xi \leq \lambda^-, \\ \mathbf{w}_L^\star & \text{if } \lambda^- \leq \xi \leq \lambda^\star, \\ \mathbf{w}_R^\star & \text{if } \lambda^\star \leq \xi \leq \lambda^+, \\ \mathbf{w}_R & \text{if } \lambda^+ \leq \xi, \end{cases} \tag{3.21}$$

with $\xi = \frac{x - x_F}{t - t^n}$. Assuming that λ^- and λ^+ are given by some estimates under the form

$$\lambda^- = \bar{v}_L - \frac{s_L}{H_L}, \quad \lambda^+ = \bar{v}_R + \frac{s_R}{H_R}, \tag{3.22}$$

the definition of the 8 components of the 2 unknown intermediate states $\mathbf{w}_L^\star$ and $\mathbf{w}_R^\star$, together with the intermediate wave speed $\lambda^\star$, are needed. To achieve this, we build a system made of the consistency condition for the discharge $H\bar{v}$, together with the jump conditions across each wave for the variables $H, H\mathfrak{v}^\sharp$ and $H\mathfrak{e}$ and we exhibit the corresponding solution in (5.36)-(5.38). This solution satisfies the following preliminary robustness result:

Proposition 3.4. *Consider the approximate Riemann solver (5.36)-(5.38), together with the wave-speed estimates (3.22). Then, with suitable values of s_L and s_R defined in (5.44)-(5.45), the approximate Riemann solver (5.36)-(5.38) preserves the invariant domain $\mathcal{U}$:*

$$\mathbf{w}_L, \mathbf{w}_R \in \mathcal{U} \quad \Rightarrow \quad \hat{\mathbf{w}}(\xi, \mathbf{w}_L, \mathbf{w}_R) \in \mathcal{U} \text{ for any value of } \xi.$$

This robustness result is then used to build a robust lowest-order FV scheme accordingly. Indeed, once the intermediate states are known, the corresponding fluxes can be computed as follows:

$$\mathbb{F}_h(\mathbf{w}_L, \mathbf{w}_R) = \begin{cases} \mathbb{F}(\mathbf{w}_L) & \text{if } 0 \leq \lambda^-, \\ \mathbb{F}(\mathbf{w}_L) + \lambda^-(\mathbf{w}_L^\star - \mathbf{w}_L) & \text{if } \lambda^- \leq 0 \leq \lambda^\star, \\ \mathbb{F}(\mathbf{w}_R) + \lambda^+(\mathbf{w}_R^\star - \mathbf{w}_R) & \text{if } \lambda^\star \leq 0 \leq \lambda^+, \\ \mathbb{F}(\mathbf{w}_R) & \text{if } \lambda^+ \leq 0. \end{cases} \tag{3.23}$$

Hence, a FV scheme built upon this HLLC interface preserves the positivity of H and $\mathfrak{e}$:

Proposition 3.5. *The lowest-order FV numerical scheme obtained by setting $k = 0$ and $\varphi_h = 1$ in (2.206), with interface numerical fluxes (3.23) and a first-order Euler time discretization, preserves the invariant domain $\mathcal{U}$ under the following CFL-like condition:*

$$\Delta t^n = \min_{T \in \mathcal{T}_h} \left(\frac{h_T}{\lambda_T} \right), \quad \lambda_T := \max_{F \in \mathcal{F}_T} \left(|\lambda_F^-|, |\lambda_F^+| \right). \tag{3.24}$$

The last step is to consider an arbitrary order of approximation $k \geq 1$. Setting $\varphi_h = 1$ in (2.206), using a first-order Euler time discretization and denoting by $\bar{\mathbf{w}}_T^n$ the mean values of $\mathbf{w}_h$ at discrete time t^n on mesh element T, the fully discrete formulation satisfied by the state vector averages reads as follows:

$$\frac{h_T}{\Delta t^n}(\bar{\mathbf{w}}_T^{n+1} - \bar{\mathbf{w}}_T^n) + \sum_{F \in \mathcal{F}_T} \mathbb{F}_h(\mathbf{w}_F^-, \mathbf{w}_F^+)\mathbf{n}_{TF} = 0, \tag{3.25}$$

where $\mathbf{w}_F^-, \mathbf{w}_F^+$ respectively stand for the interior and exterior traces of $\mathbf{w}_h$ on F, with respect to mesh element T. Let consider the τ-points Gauss-Lobatto quadrature rule $\{x_i^T,\ 1 \le i \le \tau\}$ on mesh element T (with $\tau \ge 2$), and the corresponding quadrature weights $\{\hat{w}_i,\ 1 \le i \le \tau\}$ such that $\sum_{i=1}^{q} \hat{w}_i = 1$. This quadrature rule allows to exactly compute integrals of polynomials up to degree $2\tau - 3$. In particular, choosing $\tau = \lceil (k+3)/2 \rceil$, we have:

$$\forall T \in \mathcal{T}_h, \quad \bar{\mathbf{w}}_T^n = \frac{1}{h_T} \int_T \mathbf{w}_T^n = \sum_{i=1}^{\tau} \hat{w}_i \mathbf{w}_T^n(x_i^T).$$

We have the following result:

Proposition 3.6. *Assume that for all $T \in \mathcal{T}_h$, $\bar{\mathbf{w}}_T^n \in \mathcal{U}$ and for all $i \in \{1, \dots, \tau\}, \mathbf{w}_T^n(x_i^T) \in \mathcal{U}$. Then the scheme (3.25), satisfied by the averaged values of the state vector, with interface numerical fluxes built from the approximate Riemann solver (3.23), preserves the invariant domain $\mathcal{U}$ under the following CFL-like condition:*

$$\Delta t^n \le \hat{w}_1 \min_{T \in \mathcal{T}_h} \Big(\frac{h_T}{\lambda_T} \Big), \quad \lambda_T := \max_{F \in \mathcal{F}_T} \left(|\lambda_L^F|, |\lambda_R^F| \right). \tag{3.26}$$

Gathering all these ingredients, the new DG formulation adapted to SGN equations (2.151) reads as follows:

find $\mathbf{w}_h = (\zeta_h, \bar{v}_h, v_h^\sharp, \mathfrak{e}_h, \mathfrak{p}_h) \in (\mathbb{P}^k(\mathcal{T}_h))^5$ such that, for all $(\varphi_h, \psi_h) \in (\mathbb{P}^k(\mathcal{T}_h))^2$,

$$\left(\partial_t \mathbf{w}_h, \varphi_h\right)_{\mathcal{T}_h} + \left(\mathcal{A}_h(\mathbf{w}_h, \mathfrak{p}_h), \varphi_h\right)_{\mathcal{T}_h} = 0, \tag{3.27a}$$

$$a_h(\kappa(H_h), \beta(H_h, \nabla b_h), \delta(H_h, \nabla b_h); \mathfrak{p}_h, \psi_h) = \left(\mathbb{Q}_h[H_h, b_h](\zeta_h, \bar{v}_h), \psi_h\right)_{\mathcal{T}_h}, \tag{3.27b}$$

where:

(i) the discrete bilinear form $a_h(\kappa, \beta, \delta; \cdot, \cdot)$ is the same as in the previous Chapter,

(ii) the discrete nonlinear operator $\mathcal{A}_h$ in (5.32a) is defined by

$$\left(\mathcal{A}_h(\mathbf{w}_h, \mathfrak{p}_h), \varphi_h\right)_{\mathcal{T}_h} := -\left(\mathbb{F}(\mathbf{w}_h), \partial_x^h \varphi_h\right)_{\mathcal{T}_h} + \left(\mathbb{F}_h \mathbf{n}, \varphi_h\right)_{\partial \mathcal{T}_h} + \left(\mathbb{D}_h(\mathbf{w}_h, \mathfrak{p}_h), \varphi_h\right)_{\mathcal{T}_h} - \left(\mathbb{B}(\mathbf{w}_h, b_h), \varphi_h\right)_{\mathcal{T}_h}, \tag{3.28}$$

where the interface stabilizing fluxes contribution is defined as follows

$$\left(\mathbb{F}_h \mathbf{n}, \varphi_h\right)_{\partial \mathcal{T}_h} = \sum_{T \in \mathcal{T}_h} \sum_{F \in \mathcal{F}_T} \left(\mathbb{F}_h(\mathbf{w}_F^-, \mathbf{w}_F^+) \mathbf{n}_{TF}, \varphi_h\right)_F,$$

and $\mathbb{F}_h(\mathbf{w}_F^-, \mathbf{w}_F^+)$ is defined in (3.23).

We highlight that the coupling between the transport (hyperbolic) part and the dispersive (elliptic) part of the model is achieved through the algebraic operator:

$$\left(\mathbb{D}_h(\mathbf{w}_h, \mathfrak{p}_h), \varphi_h\right)_{\mathcal{T}_h} = \left(H_h \mathfrak{p}_h - g H_h \nabla_h^k(\zeta_h) - 3 H_h^2 \nabla_h^k(H_h) \mathfrak{e}_h - H_h^3 \nabla_h^k(\mathfrak{e}_h), \varphi_h\right)_{\mathcal{T}_h}.$$

From the robustness and nonlinear stability results above, related to the homogeneous system, it is clear that this global DG formulation for the rotational SGN equations preserves the positivity of H and $\mathfrak{e}$ at the discrete level. This new scheme may be straightforwardly used in the models with enstrophy of [89, 137] for instance.

Chapter 4

A New SWIP-Discontinuous Galerkin formulation for the SGN equations

This Chapter gathers the works published in the following paper:

M. Zefzouf, F. Marche, A New Symmetric Interior Penalty Discontinuous Galerkin formulation for the Serre-Green-Naghdi equations, *Numer. Methods Partial Differ. Eq.*. (2022), 1-26. https://doi.org/10.1002/num.22942,

together with a new error estimate result.

4.1 Introduction

In an incompressible, homogeneous and inviscid fluid, the propagation of surface waves is governed by the Euler equations with nonlinear boundary conditions at the surface and at the bottom. As this problem is still complicated to solve in its full generality, both mathematically and numerically, several simpler models have been derived to describe the behavior of the solution in some physical specific regimes (see, e.g., [96] for a review). In what follows, we focus on the *shallow water* regime:

$$(\textit{shallow water regime}) \qquad \mu := \frac{H_0^2}{\lambda^2} \ll 1, \tag{4.1}$$

where H_0 refers to the typical water depth, λ the typical wave length. In this regime, the classical Nonlinear Shallow Water (NSW) equations [143] can be derived from the full water waves equations by neglecting all the terms of order $O(\mu)$, see for instance [99]. This model provides an accurate description of important unsteady processes in the surf and swash zones, such as nonlinear wave transformations, run-up and flooding due to storm waves, see for instance [19], but it neglects the dispersive effects which are fundamental for the study of wave transformations in the shoaling area and, possibly, slightly deeper water areas. Keeping these dispersive effects in the equations, and neglecting only the $O(\mu^2)$ terms, one obtains a more accurate - but mathematically and numerically more complicated - set of equations known as the Serre [147] in the horizontal surface dimension, or Green-Naghdi [74, 151], or fully nonlinear Boussinesq [163] equations for the two-dimensional case. We refer to these models here as the Serre-Green-Naghdi (SGN) equations. Note that contrary to the weakly nonlinear Boussinesq models that go back to Boussinesq himself, no smallness assumption is made on the size of the surface perturbations, the corresponding regime is said to be *fully nonlinear*:

$$(\textit{fully nonlinear / large amplitude regime}) \qquad \varepsilon := \frac{a}{H_0} = O(1), \tag{4.2}$$

where a is the typical wave's amplitude. Such equations have been mathematically justified in [5] and [85] in the one-dimensional case.

Let x, z, and t denote, respectively, the horizontal, vertical, and time coordinates. We denote by $\zeta(t,x)$ the free surface elevation with respect to its rest state, by $-H_0 + b(x)$ a parametrization of the bottom's variations and by $H := H_0 + \zeta - b$ the water depth, as shown in Figure 4.1. Denoting by u_{hor} the horizontal component of the velocity field in the fluid domain, we define the vertically averaged horizontal velocity $\overline{v} \in \mathbb{R}$ as

$$\overline{v}(t,x) := \frac{1}{H}\int_{-H_0+b}^{\zeta} u_{\text{hor}}(t,x,z)dz,$$

and we denote by $q := H\overline{v}$ the corresponding horizontal momentum. The classical SGN equations read as follows:

$$\partial_t \zeta + \partial_x(H\overline{v}) = 0, \tag{4.3a}$$

$$(1 + \mathcal{T}[H,b])\,\partial_t \overline{v} + \overline{v}\partial_x \overline{v} + g\partial_x \zeta + \mathcal{Q}[H,b](\overline{v}) = 0, \tag{4.3b}$$

where the linear operator $\mathcal{T}[H,b]\cdot$ and the quadratic form $\mathcal{Q}[H,b](\cdot)$ are defined for all smooth enough scalar-valued functions w by

$$\mathcal{T}[H,b]w \coloneqq \mathcal{R}_1[H,b](\partial_x w) + \mathcal{R}_2[H,b](w\partial_x b), \tag{4.4a}$$

$$\mathcal{Q}[H,b](w) \coloneqq \mathcal{R}_1[H,b](\partial_x(w\partial_x w) - 2(\partial_x w)^2) + \mathcal{R}_2[H,b]((w\partial_x)^2 b), \tag{4.4b}$$

where

$$\mathcal{R}_1[H,b]w \coloneqq -\frac{1}{3H}\partial_x(H^3 w) - \frac{H}{2}w\partial_x b, \qquad \mathcal{R}_2[H,b]w \coloneqq \frac{1}{2H}\partial_x(H^2 w) + w\partial_x b.$$

Considering the discrete formulations, the SGN equations have recently received attention and various numerical methods have been introduced, mostly in the surface horizontal $d = 1$ case, like Finite-Difference (FD) approaches [7], Finite-Volume (FV) [20, 36], WENO [29, 48], pseudo-spectral (PS) [63], (continuous) Finite-Element (FEM) [71, 118, 119], FV and FEM methods on hyperbolic relaxed approximating models [69, 77] and discontinuous Galerkin approaches (possibly mixed with FEM) in [51, 53, 60, 114, 127, 148]. In $d = 2$ case, several methods have been developed mostly on cartesian meshes: FD [6, 163, 182], FV [103], hybrid FV-FD [132, 149] and WENO-FD [97], PS (in the rotating case) [128] and more recently a Hybridizable-DG method [144] and a Central DG-FE method in [106]. Numerical approximations of SGN equations on general unstructured (simplicial) meshes are considered in [59, 115].
We have introduced in [51] some high-order fully discontinous Galerkin discrete formulations for the (classical) SGN equations, as well as for the asymptotically enhanced SGN models of [97] in order to optimize the dispersive properties of the classical SGN equations. In these formulations, relying on the Symmetric Weighted interior Penalty DG approach (SWIP-DG), the fully nonlinear and weakly dispersive equations are written as coupled nonlinear (pseudo) hyperbolic-elliptic problems, relying on the (non-dispersive) NSW equations supplemented by additional algebraic source terms, which fully accounts for the $O(\mu^2)$ nonlinear dispersive correction. These source terms are themselves computed as the solutions of auxiliary linear second order elliptic problems associated with the elliptic operator $1 + \mathcal{T}[H,b]$ defined in (4.4a). We observe from this work, as well as in [59, 115], that high-order DG methods are well-suited for the approximation of the solutions of SGN equations. It is generally acknowledged that DG methods exhibit several appealing features (*i.e.* local conservation, stability, a straightforward ability to handle arbitrary high-order polynomial approximations, a great geometrical discretization flexibility, compact stencils and minimal inter-element communications). Beyond these general features, using DG method provide a general and unified discrete framework allowing to accurately approximate both the hyperbolic and elliptic parts of the SGN equations. Keeping nearshore oceanography applications in mind, the robustness of DG methods in the vicinity of sharp gradients also appears to be well suited for the description of wave steepening and breaking, see for instance [137]. Such features may also allow to easily introduce adaptive algorithms (refining or coarsening a grid can be achieved without enforcing the continuity property commonly associated with the conforming FEM), together with the use of high order polynomial approximations away from breaking and run-up areas.

However, considering the SWIP-DG method of [51] for the classical SGN equations (the Model 1 of [51]), we are not able to ensure the discrete coercivity for the discrete counterpart of the elliptic operator $1 + \mathcal{T}[H,b]$ defined in (4.4a) (see Remark 3 of [51] for details). As

an answer to this drawback, we focus in this work on the construction and validation of a new Symmetric interior Penalty discontinuous Galerkin formulation that is well-posed for the elliptic operator $H\,(1+\mathcal{T}[H,b])$. This new formulation shares with the formulation introduced in [51] the appealing symmetry property and it is especially designed so that a discrete coercivity property is ensured, with a negligible computational overhead. As in [51], the stability threshold on the penalty parameter is still independent of the interface values of both H and b and it naturally allows to deal with the discontinuous nature of the discrete elliptic problem's coefficients in a stable and consistent way. Our numerical investigations show that this approach leads to an excellent agreement with data taken from several experiments.

4.2 The Serre-Green-Naghdi equations

Still focusing on the horizontal one-dimensional (1d) case, we denote by $\eta = H + b$ the total free surface elevation, as shown on Figure 4.1.

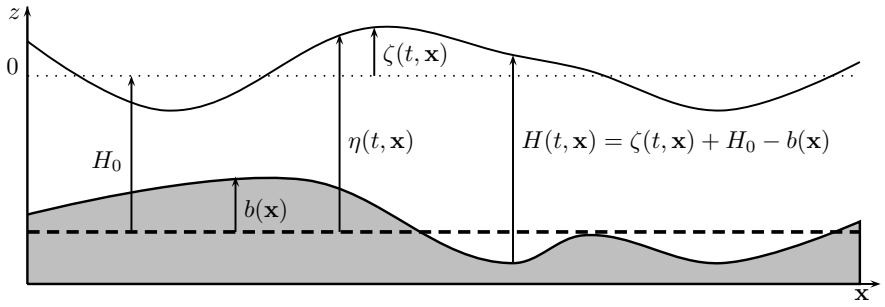


Figure 4.1: Free surface flow description and notations.

The Serre-Green-Naghdi equations, as reformulated in [20], read as follows:

$$\partial_t \eta + \partial_x q = 0, \tag{4.5a}$$

$$\partial_t q + \partial_x(\overline{v} q) = -\left(1 + \mathbf{T}[H,b]\right)^{-1} \mathbb{Q}[H,b](\eta,\overline{v}), \tag{4.5b}$$

where the linear operator $\mathbf{T}[H,b]\cdot$ and the nonlinear operator $\mathbb{Q}[H,b]$ are defined for all smooth enough scalar-valued functions w by

$$\mathbf{T}[H,b]w \coloneqq H\mathcal{T}[H,b]\frac{w}{H}, \tag{4.6}$$

$$\mathbb{Q}[H,b](\eta,\overline{v}) = gH\partial_x\eta + H\mathcal{Q}_1[H,b](\overline{v}), \tag{4.7}$$

$$\mathcal{Q}_1[H,b](w) \coloneqq -2\mathcal{R}_1[H,b]((\partial_x w)^2) + \mathcal{R}_2[H,b]((w\partial_x)^2 b). \tag{4.8}$$

This formulation has several advantages. In particular, it does not require the computation of third order derivatives and, as shown in the theoretical analysis of [5] and in our previous works [20, 29, 60], the presence of the operator $(1+\mathbf{T}[H,b])^{-1}$ makes the model robust with respect to high frequency perturbations.

In [51], in order to build a discrete formulation associated with $1 + \mathbf{T}[H, b]$ and relying on a symmetric discrete bilinear form, it is observed that, assuming that the water depth H is bounded away from zero, it holds that, for any sufficiently smooth scalar-valued function v:

$$(1+\mathbf{T}[H,b])v = H(1+\mathcal{T}[H,b])\frac{v}{H},$$

where, for any sufficiently smooth scalar-valued function w:

$$H(1+\mathcal{T}[H,b])w = -\frac{1}{3}\partial_x(H^3\partial_x w) + \left(H + \frac{1}{2}\partial_x(H^2\partial_x b) + H(\partial_x b)^2\right)w. \tag{4.9a}$$

The approximation of the right-hand side of (4.5b) may consequently be computed as the solution of a non-homogeneous diffusion-reaction-like elliptic problem, with a time-dependent reaction-like coefficient defined as $H + \frac{1}{2}\partial_x(H^2\partial_x b) + H(\partial_x b)^2$. A Symmetric Weighted interior Penalty discontinuous Galerkin (SWIP-DG) discrete bilinear form is proposed in [51], with non-homogeneous and time-dependent diffusion-like and reaction-like coefficients respectively defined from discrete approximations of $\nu[H]$ and $\beta[H, b]$. However, as already pointed out in [51], one main drawback of this formulation is that the sign of the reaction-like coefficient $H + \frac{1}{2}\partial_x(H^2\partial_x b) + H(\partial_x b)^2$ depends on the sign of $\partial_x(H^2\partial_x b)$. As a result, we are not able to ensure, for all topography configurations, a discrete coercivity property for the proposed discrete counterpart of the operator $H(1 + \mathcal{T}[H, b])$.

In order to design a new symmetric DG formulation with better properties, let recall first that SGN equations are rigorously justified in [5], in which a well-posedness result is proved for the general two-dimensional case with varying bottom using a Nash-Moser scheme. This result has also been obtained using a Picard iterative scheme in the one-dimensional case in [85].

More precisely, in the $d = 1$ case, assuming that the initial data $(\eta_0, u_0) \in H^s(\mathbb{R}) \times H^{s+1}(\mathbb{R})$ with $s > \frac{3}{2}$ (where $H^s(\mathbb{R})$ is the Sobolev space of functions $v \in L^2(\mathbb{R})$ such that their weak derivatives up to order s have a finite L^2-norm) and that $b \in C_b^\infty(\mathbb{R})$ (where $C_b^\infty(\mathbb{R})$ is the space of infinitely differentiable functions that are bounded together with all their derivatives), then there exists a maximal time $t_{\max} > 0$, uniformly bounded with respect to μ, such that SGN admits a unique solution $(\eta, u) \in C([0, t_{\max}], H^s(\mathbb{R}) \times H^{s+1}(\mathbb{R}))$. This result can be extended to finite domains and periodic boundary conditions. In particular, we recall the following result:

Proposition 4.1. *Assuming $b \in C_b^\infty(\mathbb{R})$ and $\eta \in W^{1,\infty}(\mathbb{R})$ such that*

$$\exists H_\varepsilon,\ \inf_{x\in\mathbb{R}} H = \eta - b > H_\varepsilon.$$

then the operator

$$H(1+\mathcal{T}[H,b]) \ :\ H^2(\mathbb{R}) \ \rightarrow \ L^2(\mathbb{R}),$$

is well-defined, one-to-one and onto.

Proof. The detailed proof is given in [85] for the nondimensionalized equations. Let just recall here that the following identity holds:

$$H\mathcal{T}[H,b] = (S_1[H,b])^\star H\, S_1[H,b] + (S_2[b])^\star H\, S_2[b], \tag{4.10}$$

where the first and zero order differential operators $S_1[H,b]$ and $S_2[b]$ are defined as follows:

$$S_1[H,b] = \frac{H}{\sqrt{3}}\partial_x - \frac{\sqrt{3}}{2}\partial_x b, \qquad S_2[b] = \frac{1}{2}\partial_x b,$$

with adjoint operators

$$(S_1[H,b])^\star = -\frac{1}{\sqrt{3}}\partial_x(H\cdot) - \frac{\sqrt{3}}{2}\partial_x b, \qquad (S_2[b])^\star = S_2[b].$$

Considering the bilinear form defined and continuous on $H^1(\mathbb{R}) \times H^1(\mathbb{R})$ by:

$$a(v,w) = \big(HS_1[H,b]v, S_1[H,b]w\big) + \big(HS_2[H,b]v, S_2[H,b]w\big) + \big(Hv, w\big), \tag{4.11}$$

where $(\cdot,\cdot)$ refers to the L^2-scalar product, we have:

$$a(w,w) = (H(1+\mathcal{T}[H,b])w, w) \geq H_\varepsilon \left(\|w\|^2 + \|S_1[H,b]w\|^2 + \|S_2[b]w\|^2 \right),$$

so that $H(1+\mathcal{T}[H,b])$ is one to one. We additionally have

$$H_\varepsilon \left(\|w\|^2 + \|S_1[H,b]w\|^2 + \|S_2[b]w\|^2 \right) \geq C \|w\|^2_{H^1(\mathbb{R})},$$

proving that $a(\cdot,\cdot)$ is coercive on $H^1(\mathbb{R})$ and from Lax-Milgram theorem, for all $f \in L^2(\mathbb{R})$, there exists unique $u \in H^1(\mathbb{R})$ such that, for all $w \in H^1(\mathbb{R})$, $a(u,w) = (f,w)$. □

In the following, we aim at designing a new discontinuous Galerkin formulation for SGN equations that mimics these properties. Denoting by $\mathbf{w} \coloneqq (\eta, q)$ the vector collecting the primal variables, using the following *pre-balanced* splitting (we refer the reader to [107] for details on the *pre-balanced* formulation) of the hydrostatic pressure term:

$$gH\partial_x\zeta = \frac{1}{2}g\partial_x(\eta^2 - 2\eta b) + g\eta\partial_x b, \tag{4.12}$$

recalling that for any $w \in H^2(\mathbb{R})$, we have:

$$(1+\mathbf{T}[H,b])w = \big(H + (S_1[H,b])^\star H\, S_1[H,b] + (S_2[b])^\star H\, S_2[b]\big)\frac{w}{H},$$

and introducing an auxiliary variable $\mathfrak{p}$, system (4.5) can be equivalently reformulated as follows:

$$\partial_t \mathbf{w} + \partial_x \mathbb{F}(\mathbf{w}, b) + \mathbb{D}(\mathbf{w}, b) = \mathbb{B}(\mathbf{w}, \partial_x b), \tag{4.13a}$$

$$\big(H + (S_1[H,b])^\star H\, S_1[H,b] + (S_2[b])^\star H\, S_2[b]\big)\mathfrak{p} = \mathbb{Q}[H,b](\eta,\overline{v}), \tag{4.13b}$$

where

$$\mathbb{F}(\mathbf{w},b) \coloneqq \begin{pmatrix} q \\ \mathcal{F}(\mathbf{w},b) \end{pmatrix}, \quad \mathbb{B}(\mathbf{w},\partial_x b) \coloneqq \begin{pmatrix} 0 \\ -g\eta\partial_x b \end{pmatrix}, \quad \mathbb{D}(\mathbf{w},b) \coloneqq \begin{pmatrix} 0 \\ H\mathfrak{p} - gH\partial_x\eta \end{pmatrix}, \tag{4.13c}$$

and the nonlinear *pre-balanced* flux is defined as

$$\mathcal{F}(\mathbf{w}, b) \coloneqq \overline{v} q + \frac{1}{2} g(\eta^2 - 2\eta b).$$

This last formulation highlights the fact that the SGN equations can be regarded as a dispersive correction of order $O(\mu)$ of the nonlinear hyperbolic shallow water equations. This dispersive correction is related to the source term $\mathbb{D}(\mathbf{w}, b)$ in (4.13a), and is obtained from the solution of an auxiliary scalar and linear second-order elliptic sub-problem (4.13b). Additionally observing that

$$\Big(H + S_1[H,b]^\star H\, S_1[H,b] + S_2[b]^\star H\, S_2[b]\Big) w \\ = \partial_x(-\kappa[H]\partial_x w) - \beta[H, \partial_x b]\partial_x w + \partial_x(\beta[H, \partial_x b]\, w) + \delta[H, \partial_x b] w,$$

where

$$\kappa[H] \coloneqq \frac{1}{3} H^3, \qquad \beta[H, \partial_x b] \coloneqq \frac{\sqrt{3}}{2} \kappa[H]^{\frac{1}{2}} \chi[H, \partial_x b], \qquad \delta[H, \partial_x b] \coloneqq \chi[H, \partial_x b]^2 + H, \tag{4.14a}$$

and

$$\chi[H, \partial_x b] = H^{\frac{1}{2}} \partial_x b, \tag{4.14b}$$

system (4.13) may be written as

$$\partial_t \mathbf{w} + \partial_x \mathbb{F}(\mathbf{w}, b) + \mathbb{D}(\mathbf{w}, b) = \mathbb{B}(\mathbf{w}, \partial_x b), \tag{4.15a}$$

$$\partial_x\big(-\kappa[H]\partial_x \mathfrak{p}\big) - \beta[H, \partial_x b]\partial_x \mathfrak{p} + \partial_x(\beta[H, \partial_x b]\mathfrak{p}) + \delta[H, \partial_x b]\mathfrak{p} = \mathbb{Q}[H, b](\eta, \overline{v}), \tag{4.15b}$$

which is the formulation upon which our new discrete bilinear form is designed in the next section.

Remark 4.2. *In practice, the numerical solution of (4.5) is sought in a bounded spatial domain $\Omega \subset \mathbb{R}$ (which reduce to line segments in the $d = 1$ horizontal surface dimension). To close (4.5), we have to prescribe suitable boundary conditions. Formulation (4.15) highlights that boundary conditions should be provided for the primal variables $\mathbf{w} \coloneqq (\eta, q)$ but also for the auxiliary variable $\mathfrak{p}$, for the corresponding discrete problem to be well-defined on Ω. In the following, we consider only reflexive boundary conditions, which aim at mimicking the presence of a solid-wall, and which may be obtained by enforcing :*

$$\partial_x \eta_{|\partial\Omega} = 0, \qquad q_{|\partial\Omega} = 0, \qquad \partial_x \mathfrak{p}_{|\partial\Omega} = 0. \tag{4.16}$$

All the following analysis may be reproduced in the case of periodic boundary conditions, adapting the discrete formulation accordingly.

Remark 4.3. *In the flat bottom case, SGN equations admit solitary wave solutions of amplitude εH_0, which have known formulae in a closed form:*

$$\eta(t,x) = H_0 + \varepsilon H_0 \operatorname{sech}^2(\kappa(x - ct)), \qquad q(t,x) = c\,(\eta(t,x) - H_0), \ \forall t \geq 0, \forall x \in \Omega, \tag{4.17}$$

with $\kappa \coloneqq \sqrt{\frac{3\varepsilon}{4H_0^2(1+\varepsilon)}}$ and $c \coloneqq \sqrt{gH_0(1+\varepsilon)}$.

Remark 4.4. *It is classical that the frequency dispersion of (4.5) can be improved by adding some terms of order $O(\mu^2)$ to the momentum equation, see for instance [111, 166]. Since this equation is already precise up to terms of order $O(\mu^2)$, this manipulation does not affect the precision of the model. As shown in [20], an improved version of the SGN equations reads as follows:*

$$\partial_t \eta + \partial_x q = 0, \tag{4.18a}$$

$$\partial_t q + \partial_x(\overline{v} q) + \frac{\alpha - 1}{\alpha} g H \partial_x \eta = -\left(1 + \alpha \mathbf{T}[H, b]\right)^{-1} \mathbb{Q}_\alpha[H, b](\eta, \overline{v}), \tag{4.18b}$$

with

$$\mathbb{Q}_\alpha[H, b](\eta, \overline{v}) = \frac{1}{\alpha} g H \partial_x \eta + H \boldsymbol{Q}_1[H, b](\overline{v}), \tag{4.19}$$

where α may be set to 1.159 in order to provide a better description of the wave in intermediate or even deep water, in addition to the shallow water zone. With such optimization, system (4.15) becomes:

$$\partial_t \mathbf{w} + \partial_x \mathbb{F}(\mathbf{w}, b) + \mathbb{D}_\alpha(\mathbf{w}, b) = \mathbb{B}(\mathbf{w}, \partial_x b), \tag{4.20a}$$

$$\partial_x\left(-\kappa[H]\partial_x \mathfrak{p}\right) - \beta[H, \partial_x b]\partial_x \mathfrak{p} + \partial_x(\beta[H, \partial_x b]\mathfrak{p}) + \delta[H, \partial_x b]\mathfrak{p} = \mathbb{Q}_\alpha[H, b](\eta, \overline{v}), \tag{4.20b}$$

where

$$\mathbb{D}_\alpha(\mathbf{w}, b) := \begin{pmatrix} 0 \\ H\mathfrak{p} - \frac{1}{\alpha} g H \partial_x \eta \end{pmatrix}, \tag{4.21}$$

and

$$\kappa[H] := \frac{\alpha}{3} H^3, \qquad \beta[H, \partial_x b] := \frac{\sqrt{3}}{2} \kappa[H]^{\frac{1}{2}} \chi[H, \partial_x b], \qquad \delta[H, \partial_x b] := \chi[H, \partial_x b]^2 + H, \tag{4.22}$$

$$\chi[H, \partial_x b] = \alpha^{\frac{1}{2}} H^{\frac{1}{2}} \partial_x b, \tag{4.23}$$

which is the formulation upon which our new discrete bilinear form is designed in the next section (note that choosing $\alpha = 1$ allows to recover (4.15)). The subscript index α is removed in the follwing.

4.3 Discrete formulations

In this section, we design a new discontinuous Galerkin (DG) discrete formulation for the SGN equations, as written in (4.20), supplemented with suitable boundary conditions (see Remark 4.2). For the sake of simplicity, we only consider the case of *reflexive* boundary conditions (4.16) in the following. Although we work here in one space dimension, we keep the notations as close as possible to the classical one for DG methods in higher space dimensions, both to facilitate the reader familiar with DG methods, and to make easier the extension to two space dimensions.

4.3.1 Setting and notations

Let $\Omega \subset \mathbb{R}$ denote an open segment with boundary $\partial\Omega$. We consider a partition $\mathcal{T}_h$ of Ω in $|\mathcal{T}_h|$ open disjoint segments T of boundary ∂T such that $\overline{\Omega} = \bigcup_{T \in \mathcal{T}_h} \overline{T}$. The partition is characterized by

the meshsize $h \coloneqq \max_{T\in\mathcal{T}_h} h_T$, where h_T is the length of the element T. For all $T \in \mathcal{T}_h$, we denote by n_T the unit outward normal taking values in $\{-1,1\}$ on ∂T, and by x_T its barycenter.

Mesh faces, reduced here to vertices, are collected in the set $\mathcal{F}_h$ partitioned as $\mathcal{F}_h = \mathcal{F}_h^{\mathrm{i}} \cup \mathcal{F}_h^{\mathrm{b}}$, where $\mathcal{F}_h^{\mathrm{i}}$ collects the interior vertices and $\mathcal{F}_h^{\mathrm{b}}$ the (two) boundary vertices. The abscissa of a vertex $F \in \mathcal{F}_h$ is denoted by x_F, and we let h_F denote the minimum length of the mesh elements to which F belongs. For all $T \in \mathcal{T}_h$, $\mathcal{F}_T \coloneqq \{F \in \mathcal{F}_h \mid F \subset \partial T\}$ denotes the set of vertices in ∂T and, for all $F \in \mathcal{F}_T$, n_{TF} is the unit normal to F pointing out of T. For any interior vertex $F \in \mathcal{F}_h^{\mathrm{i}}$, we choose an arbitrarily oriented but fixed unit normal n_F, and we set $\mathrm{n}_F \coloneqq \mathrm{n}_{TF}$ for all boundary vertices $F \subset \partial T \cap \partial\Omega$. The maximum number of mesh faces composing the boundary of mesh elements is denoted by

$$N_\partial = \max_{T\in\mathcal{T}_h} \mathrm{card}(\mathcal{F}_T),$$

(and we obviously have $N_\partial = 2$ in the present setting). Given an integer polynomial degree $k \geq 1$, we consider the broken polynomial space

$$\mathbb{P}^k(\mathcal{T}_h) \coloneqq \left\{v \in L^2(\Omega) \,|\, v_{|T} \in \mathbb{P}^k(T) \;\; \forall T \in \mathcal{T}_h\right\}, \tag{4.24}$$

where $\mathbb{P}^k(T)$ denotes the space of polynomials in T of total degree at most k.

For a given final computational time $t_{\max} > 0$, we consider a partition $(t^n)_{0\leq n\leq N}$ of the time interval $[0, t_{\max}]$ with $t^0 = 0$, $t^N = t_{\max}$ and $t^{n+1} - t^n =: \Delta t^n$. More details on the computation of the time step Δt^n and on the time marching algorithms are given in Section 5.3.4. For any sufficiently regular scalar-valued function of time w, we let $w^n \coloneqq w(t^n)$.

We introduce the following inner products for regular enough scalar-valued functions v, w:

$$(v,w)_\Omega \coloneqq \int_\Omega v(x)w(x)dx, \quad (v,w)_T \coloneqq \int_T v(x)w(x)dx \quad \forall T \in \mathcal{T}_h, \quad (v,w)_F \coloneqq (vw)(x_F) \quad \forall F \in \mathcal{F}_h,$$

and we denote respectively by $\|v\|_\Omega = (v,v)_\Omega^{\frac{1}{2}}$, $\|v\|_T = (v,v)_T^{\frac{1}{2}}$ and $\|v\|_F = (v,v)_F^{\frac{1}{2}}$ the corresponding L^2 norms. For all $T \in \mathcal{T}_h$, we denote p_T^k the L^2-orthogonal projector onto $\mathbb{P}^k(T)$ and $p_{\mathcal{T}_h}^k$ the L^2-orthogonal projector onto $\mathbb{P}^k(\mathcal{T}_h)$. Similarly, we denote I_T^k the element nodal interpolation into $\mathbb{P}^k(T)$. The corresponding nodal distributions in elements and edges are approximated optimal nodes introduced in [31], which have better approximation properties than equidistant distributions. The global $I_{\mathcal{T}_h}^k$ interpolation into $\mathbb{P}^k(\mathcal{T}_h)$ is obtained by gathering the local interpolating polynomials defined on each elements.

For further use, we recall the following classical discrete trace inequality (see, e.g., [50, Lemma 1.46] for proof and details related to the mesh regularity parameters):

$$\forall v_h \in \mathbb{P}^k(\mathcal{T}_h), \forall T \in \mathcal{T}_h, \forall F \in \mathcal{F}_T, \; h_T^{\frac{1}{2}} \|v_h\|_F \leq C_{tr} \|v_h\|_T, \tag{4.25}$$

where the constant C_{tr} only depends on k, the horizontal surface dimension d, and the mesh regularity parameters.

4.3.2 Symmetric and Weighted interior Penalty discrete bilinear form

Let $\kappa, \beta, \delta \in L^\infty(\Omega)$ denote uniformly bounded coefficients and set, for the sake of simplicity, $\kappa_T \coloneqq \kappa_{|T}$, $\beta_T \coloneqq \beta_{|T}$ and $\delta_T \coloneqq \delta_{|T}$ for all $T \in \mathcal{T}_h$. Following [52, 55], we define the jump and

weighted average operators such that, for a sufficiently regular function φ and an interior vertex $F \in \mathcal{F}_h^i$ such that $F \subset \partial T_1 \cap \partial T_2$ for distinct mesh elements T_1 and T_2,

$$[\![\varphi]\!]_F := \varphi_{|T_1} - \varphi_{|T_2}, \qquad \{\!\{\varphi\}\!\}_{\omega,F} := \omega_2 \varphi_{|T_1} + \omega_1 \varphi_{|T_2}, \quad \omega_i := \frac{\kappa_{T_i}}{\kappa_{T_1} + \kappa_{T_2}} \quad \forall i \in \{1,2\}. \tag{4.26}$$

In what follows, and when no confusion can arise, we omit the subscript F from both $[\![v]\!]_{\omega,F}$ and $\{\!\{v\}\!\}_{\omega,F}$. When $\kappa \equiv C$ in Ω for some real number $C > 0$, we have $\omega_1 = \omega_2 = \frac{1}{2}$, and also the subscript ω is omitted. The definition of the average and jump operators at boundary vertices depends on the selected variable, according to the prescribed boundary conditions. We refer the reader to [50, Section 4.5] for a discussion on the role of weighted averages and harmonic means in the context of heterogeneous diffusion problems.

For further use, let consider the following bilinear form $a_h(\kappa,\beta,\delta;\cdot,\cdot)$ defined on $\mathbb{P}^k(\mathcal{T}_h)\times\mathbb{P}^k(\mathcal{T}_h)$:

$$\begin{aligned} a_h(\kappa,\beta,\delta;v_h,w_h) := &\sum_{T\in\mathcal{T}_h} \left(\kappa\partial_x v_h, \partial_x w_h\right)_T + \sum_{F\in\mathcal{F}_h} \xi\left(\frac{\gamma_{\kappa,F}}{h_F}[\![v_h]\!],[\![w_h]\!]\right)_F \\ &- \sum_{F\in\mathcal{F}_h} \left(\left(\{\!\{\kappa\partial_x^h v_h\}\!\}_\omega,[\![w_h]\!]\right)_F + \left([\![v_h]\!],\{\!\{\kappa\partial_x^h w_h\}\!\}_\omega\right)_F\right) \\ &- \sum_{T\in\mathcal{T}_h} \left(\beta v_h, \partial_x w_h\right)_T - \sum_{T\in\mathcal{T}_h} \left(\partial_x v_h, \beta w_h\right)_T \\ &+ \sum_{F\in\mathcal{F}_h} \left(\left(\{\!\{\beta v_h\}\!\}_\omega,[\![w_h]\!]\right)_F + \left([\![v_h]\!],\{\!\{\beta w_h\}\!\}_\omega\right)_F\right) \\ &+ \sum_{T\in\mathcal{T}_h} \left(\delta v_h, w_h\right)_T, \end{aligned} \tag{4.27}$$

with a κ-dependent penalty parameter $\gamma_{\kappa,F}$ defined as follows: In (4.27), ξ denotes a user-defined parameter sufficiently large to ensure coercivity (see Proposition 4.8) and ∂_x^h has to be intended as the partial derivative along x localized to mesh elements of $\mathcal{T}_h$, that is, for a given function $v_h \in \mathbb{P}^k(\mathcal{T}_h)$, $(\partial_x^h v_h)_{|T} = \partial_x(v_{h|T})$.

Remark 4.5. *Taking $\beta := 0$ and $\delta := 0$ in (4.27), one obtains the Symmetric Weighted interior Penalty-DG bilinear form of [52, 55] associated with heterogeneous diffusion problems, while taking $\kappa := \frac{1}{3}H^3$, $\beta := 0$, $\delta := H + \frac{1}{2}\partial_x(H^2\partial_x b) + H(\partial_x b)^2$, one recovers the SWIP-DG method associated with $H(1 + \mathcal{T}[H,b])$ introduced in [51].*

4.3.3 Discrete gradient and Laplace operators

As in [51], in order to discretize the linear and nonlinear operators that appear in our models, we need discrete counterparts of the gradient and of the Laplacian applied to broken polynomial functions. For any $v_h \in \mathbb{P}^k(\mathcal{T}_h)$, we define the following global lifting of the jumps of v_h (see, e.g. [50, Section 4.3]):

$$\mathcal{R}_h^k([\![v_h]\!]) := \sum_{F\in\mathcal{F}_h} r_F^k([\![v_h]\!]),$$

where, for all $F \in \mathcal{F}_h$, the local lifting operator $r_F^k([\![v_h]\!]) \in \mathbb{P}^k(\mathcal{T}_h)$ is defined as the unique solution of the following problem:

$$\big(r_F^k([\![v_h]\!]), \psi_h\big)_\Omega = \big([\![v_h]\!], \{\!\{\psi_h\}\!\}\mathrm{n}_F\big)_F \qquad \forall \psi_h \in \mathbb{P}^k(\mathcal{T}_h),$$

with $\{\!\{\psi_h\}\!\}$ standard average operators given by (4.26) with $\omega_1 = \omega_2 = \frac{1}{2}$ at interior nodes and extended as described in the previous section to boundary nodes. Following [50, Section 2.3], we define the discrete gradient operator $\nabla_h^k : \mathbb{P}^k(\mathcal{T}_h) \to \mathbb{P}^k(\mathcal{T}_h)$ such that, for all $v_h \in \mathbb{P}^k(\mathcal{T}_h)$,

$$\nabla_h^k v_h \coloneqq \partial_x^h v_h - \mathcal{R}_h^k([\![v_h]\!]).$$

This gradient has better consistency properties than the broken (element-by-element) gradient ∂_x^h, as it accounts for the jumps of its argument through the second contribution; see [49, Theorem 2.2] for further insight into this point. Taking inspiration from [88, Eq. (2.10)], we also introduce the discrete Laplace operator $\Delta_h^k : \mathbb{P}^k(\mathcal{T}_h) \to \mathbb{P}^k(\mathcal{T}_h)$ such that, for all $v_h \in \mathbb{P}^k(\mathcal{T}_h)$, $\Delta_h^k(v_h)$ solves

$$-\big(\Delta_h^k v_h, \psi_h\big)_\Omega = a_h^{\mathrm{SIP}}(v_h, \psi_h) \qquad \forall \psi_h \in \mathbb{P}^k(\mathcal{T}_h),$$

where the bilinear form $a_h^{\mathrm{SIP}}(v_h, \psi_h)$ is given by (4.27) with the particular choices $\kappa \coloneqq 1$, $\beta \coloneqq 0$ and $\delta \coloneqq 0$. It can be proved that, for any $v \in H_0^1(\Omega) \cap H^{k+1}(\Omega)$, it holds

$$\inf_{v_h \in \mathbb{P}^k(\mathcal{T}_h)} \|\nabla v - \nabla_h^k v_h\| \lesssim h^k, \qquad \inf_{v_h \in \mathbb{P}^k(\mathcal{T}_h)} \|\triangle v - \Delta_h^k v_h\| \lesssim h^{k-1},$$

where $a \lesssim b$ means $a \le Cb$ with real number $C > 0$ independent of the meshsize h, and the second estimate further requires mesh quasi-uniformity.

4.3.4 The discrete problem

Let now $b_h \in \mathbb{P}^k(\mathcal{T}_h)$ denote a piecewise polynomial approximation of the topography parameterization b which can be obtained either by L^2-orthogonal projection (*i.e.* $b_h = \pi_h^k(b)$) or by interpolation (*i.e.* $b_h = \mathcal{I}_h^k(b)$). Note that any order of approximation may be used for the definition of b_h, and in what follows, we choose the same order k as for the primal variables, for the sake of simplicity, and the following shortcuts are introduced: $\nabla b_h = \nabla_h^k b_h$, $\Delta b_h = \Delta_h^k b_h$ and $\nabla^3 b_h = \nabla_h^k(\Delta_h^k b_h)$. The semi-discrete in space discontinuous Galerkin approximation of (4.20) reads:

Find $\mathbf{w}_h = (\eta_h, q_h) \in (\mathbb{P}^k(\mathcal{T}_h))^2$ and $\mathfrak{p}_h \in \mathbb{P}^k(\mathcal{T}_h)$ such that, for all $(\varphi_h, \psi_h) \in (\mathbb{P}^k(\mathcal{T}_h))^2$,

$$\big(\partial_t \mathbf{w}_h, \varphi_h\big)_\Omega + \big(\mathcal{A}_h(\mathbf{w}_h), \varphi_h\big)_\Omega = 0, \tag{4.28a}$$

$$a_h(\kappa[H_h], \beta[H_h, \nabla b_h], \delta[H_h, \nabla b_h]; \mathfrak{p}_h, \psi_h) = \big(\mathbb{Q}_h[H_h, b_h](\eta_h, u_h), \psi_h\big)_\Omega, \tag{4.28b}$$

where

1. the discrete nonlinear operator $\mathcal{A}_h$ in (4.28a) is defined by

$$\begin{aligned}\big(\mathcal{A}_h(\mathbf{w}_h), \varphi_h\big)_\Omega \coloneqq &- \sum_{T \in \mathcal{T}_h} \big(\mathbb{F}(\mathbf{w}_h, b_h), \partial_x \varphi_h\big)_T \\ &+ \sum_{T \in \mathcal{T}_h} \sum_{F \in \mathcal{F}_T} \big(\widehat{\mathbb{F}}_{TF}, \varphi_h\big)_F + \big(\mathbb{D}_h, \varphi_h\big)_\Omega - \big(\mathbb{B}(\mathbf{w}_h, \nabla b_h), \varphi_h\big)_\Omega,\end{aligned} \tag{4.29}$$

and the discrete dispersive correction is defined as follows

$$\left(\mathbb{D}_h, \varphi_h\right)_\Omega = \begin{pmatrix} 0 \\ \left(H_h \mathfrak{p}_h - \frac{1}{\alpha} g H_h \nabla_h^k \eta_h, \varphi_h\right)_\Omega \end{pmatrix}, \tag{4.30}$$

$\widehat{\mathbb{F}}_{TF}$ being a suitable approximation of the normal face fluxes $\mathbb{F}(\mathbf{w}_h, b_h)\cdot \mathrm{n}_{TF}$, see Section 4.3.5 below.

2. The discrete operators $\kappa[H_h]$, $\beta[H_h, \nabla b_h]$ and $\delta[H_h, \nabla b_h]$ are obtained according to (4.22)-(4.23), and recalled here:

$$\kappa[H_h] := \frac{\alpha}{3} H_h^3, \tag{4.31a}$$

$$\beta[H_h, \nabla b_h] := \frac{\sqrt{3}}{2} \kappa[H_h]^{\frac{1}{2}} \chi[H_h, \nabla b_h], \tag{4.31b}$$

$$\delta[H_h, \nabla b_h] := \chi[H_h, \nabla b_h]^2 + H_h, \tag{4.31c}$$

with

$$\chi[H_h, \nabla b_h] := \alpha^{\frac{1}{2}} H_h^{\frac{1}{2}} \nabla b_h. \tag{4.31d}$$

3. The discrete nonlinear operator $\mathbb{Q}_h[H_h, b_h]$ in (4.28b) is defined by

$$\mathbb{Q}_h[H_h, b_h](\eta_h, u_h) := \frac{1}{\alpha} g H_h \nabla_h^k \eta_h + H_h \mathcal{Q}_{1,h}[H_h, b_h](u_h).$$

where, for any $w_h \in \mathbb{P}^k(\mathcal{T}_h)$,

$$\begin{aligned} \mathcal{Q}_{1,h}[H_h, b_h](w_h) := {} & 2 H_h \nabla_h^k (H_h + \frac{b_h}{2})(\nabla_h^k w_h)^2 + \frac{4}{3} H_h^2 \nabla_h^k w_h \Delta_h^k w_h \\ & + H_h \Delta b_h (\nabla_h^k w_h) w_h + \left(\nabla_h^k \eta_h \Delta b_h + \frac{H_h}{2} \nabla^3 b_h\right) w_h^2. \end{aligned}$$

4.3.5 Interface fluxes and well-balancing

The high-order reconstructed numerical flux detailed in [61] is a good default choice to approximate the interface fluxes $\mathbb{F}(\mathbf{w}, b)\cdot \mathrm{n}_T$, allowing to obtain a well-balanced scheme that preserves motionless steady states for SGN equations. Considering $T \in \mathcal{T}_h$ and $F \in \mathcal{F}_T \cap \mathcal{F}_h^i$ and denoting by $\mathbf{w}^-$, $\mathbf{w}^+$, respectively, the *interior* and *exterior* traces of $\mathbf{w}_h$ on F, with respect to the element T and b^- and b^+ the *interior* and *exterior* traces of b_h on F, this numerical flux relies on reconstructed interface states $\check{\mathbf{w}}^-$, $\check{\mathbf{w}}^+, \check{b}$ such that

$$\widehat{\mathbb{F}}_{TF} = \mathbb{F}_h(\check{\mathbf{w}}^-, \check{\mathbf{w}}^+, \check{b}, \check{b}, \mathrm{n}_{TF}) + \widetilde{\mathbb{F}}_{TF}, \tag{4.32}$$

where $\mathbb{F}_h$ is the Lax-Friedrichs flux and $\widetilde{\mathbb{F}}_{TF}$ is a high-order correction term. The reader is referred to [51] for the detailed formulations.

4.3.6 Time discretization

Supplementing (4.15) with an initial datum $\mathbf{w}(0,\cdot) = \mathbf{w}^0$, the time stepping is carried out using the explicit SSP-RK schemes of [73]. For $k < 3$, we consider SSP-RK schemes of order $(k+1)$. For instance, writing the semi-discrete equation (4.28a) in the operator form

$$\partial_t \mathbf{w}_h + \mathcal{A}_h(\mathbf{w}_h) = 0,$$

we advance from time level n to $(n+1)$ as follows with the third-order scheme as follows:

$$\begin{aligned}
\mathbf{w}_h^{n,1} &= \mathbf{w}_h^n - \Delta t^n \mathcal{A}_h(\mathbf{w}_h^n),\\
\mathbf{w}_h^{n,2} &= \frac{1}{4}(3\mathbf{w}_h^n + \mathbf{w}_h^{n,1}) - \frac{1}{4}\Delta t^n \mathcal{A}_h(\mathbf{w}_h^{n,1}),\\
\mathbf{w}_h^{n+1} &= \frac{1}{3}(\mathbf{w}_h^n + 2\mathbf{w}_h^{n,2}) - \frac{2}{3}\Delta t^n \mathcal{A}_h(\mathbf{w}_h^{n,2}),
\end{aligned}$$

where $\mathbf{w}_h^{n,i}$, $1 \le i \le 2$, are the intermediate stages, Δt^n is obtained from the CFL condition (4.33), and the discrete initial data $\mathbf{w}_h^0$ is defined either as the L^2-projection or interpolation on $(\mathbb{P}^k(\mathcal{T}_h))^2$ of $\mathbf{w}_0$. For $k \ge 3$, the five stages fourth order SSP-RK scheme of [150] is used (the details are omitted for the sake of simplicity). The corresponding time step Δt^n is computed adaptively using the following CFL condition (see [38]):

$$\Delta t^n < \frac{1}{2k+1} \min_{T\in\mathcal{T}_h}\left(\frac{h_T}{\sigma_T}\right), \tag{4.33}$$

with

$$\sigma_T := \max_{\partial T}\left(\left|\frac{q_{h|T}}{H_{h|T}}\cdot \mathrm{n}_T\right| + \sqrt{gH_{h|T}}\right).$$

4.3.7 Positivity of the water height

While we choose not to focus on the issue of preserving the positivity of the water height in this paper, we emphasize that the proposed discrete formulation is compatible with the strategy of [59, 60] that ensures that the mean value of the water height remains positive, itself based on the ideas of [172, 178]. This approach is briefly recalled in the following. Let consider $H_{h|T}^n(x)$ obtained at the discrete time t^n from the fully discrete previous dG formulation and $\bar{H}_T^n$ its average. Assuming that $\forall T \in \mathcal{T}_h$, $\bar{H}_T^n \ge 0$, we want to ensure that $\forall T \in \mathcal{T}_h$, $\bar{H}_T^{n+1} \ge 0$ without destroying the order of accuracy. For each element T:

1. let $S^T = \{r_j^T\}_{j=1,..,d}$ be the set of d Legendre-Gauss-Lobatto (LGL) points on the element T, and $\{\hat{\omega}_j\}_{j=1,..,d}$ the corresponding quadrature weights. d is chosen such that the associated quadrature rule is exact for polynomials of degree k (*i.e.* $2d-3 \ge k$). We compute $m_T^n = \min_{r_i^T \in S^T} H_{h|T}^n(r_j^T)$.

2. we modify $H_{h|T}^n(x)$ in order to ensure that it is positive at the previous set of d LGL nodes. This is done using the following conservative accuracy-preserving linear scaling around the cell average:

$$\check{H}_{h|T}^n(x) = \theta_T^n(H_{h|T}^n(x) - \bar{H}_T^n) + \bar{H}_T^n\,. \tag{4.34}$$

where

$$\theta_T^n = \min\left(\frac{\bar{H}_T^n}{\bar{H}_T^n - m_T^n}, 1\right).$$

We deduce from (4.34) a modified polynomial $\check{\eta}_{h|T}^n(x)$ of order k, which is used to compute the numerical fluxes (4.32). Thus, following [172, 178], the positivity of the mean water height $\bar{H}_T^{n+1}$, as well as the positivity of H_h^n at chosen quadrature nodes, is ensured under the condition :

$$\sigma_T \frac{\Delta_t^n}{|T|} \leq \hat{w}_1. \tag{4.35}$$

In practice, we have $\hat{w}_1 = \frac{1}{6}$ for $N = 2, 3$ and $\hat{w}_1 = \frac{1}{12}$ for $N = 4, 5$. Note that new *a posteriori* strategies based on Finite-Volume subcells and local flux reconstructions are currently under investigations.

4.3.8 Well-posedness of the discrete elliptic sub-problem

We show, in this section, that the proposed discrete bilinear form in (4.28b) is symmetric, consistent with the elliptic operator $H(1 + \mathcal{T}[H, b])$ and enjoys some discrete coercivity property, provided that the penalty coefficient ξ is large enough, so that the corresponding discrete problem (4.28b) is well-posed.
From definitions (4.27) and (4.31), we have:

$$\begin{aligned}
a_h(\kappa[H_h],\beta[H_h,\nabla b_h],\delta[H_h,\nabla b_h]; v_h, w_h) :=& \sum_{T\in\mathcal{T}_h} \big(\kappa[H_h]\partial_x v_h, \partial_x w_h\big)_T + \sum_{F\in\mathcal{F}_h} \xi\big(\frac{\gamma_{\kappa,F}}{h_F}[\![v_h]\!],[\![w_h]\!]\big)_F \\
&- \sum_{F\in\mathcal{F}_h} \Big(\big(\{\!\{\kappa[H_h]\partial_x^h v_h\}\!\}_\omega, [\![w_h]\!]\big)_F + \big([\![v_h]\!], \{\!\{\kappa[H_h]\partial_x^h w_h\}\!\}_\omega\big)_F \Big) \\
&- \frac{\sqrt{3}}{2} \sum_{T\in\mathcal{T}_h} \Big(\big(\kappa[H_h]^{\frac{1}{2}}\chi[H_h,\nabla b_h]v_h, \partial_x w_h\big)_T + \big(\kappa[H_h]^{\frac{1}{2}}\chi[H_h,\nabla b_h]\partial_x v_h, w_h\big)_T \Big) \\
&+ \frac{\sqrt{3}}{2} \sum_{F\in\mathcal{F}_h} \Big(\big(\{\!\{\kappa[H_h]^{\frac{1}{2}}\chi[H_h,\nabla b_h]v_h\}\!\}_\omega, [\![w_h]\!]\big)_F + \big([\![v_h]\!], \{\!\{\kappa[H_h]^{\frac{1}{2}}\chi[H_h,\nabla b_h]w_h\}\!\}_\omega\big)_F \Big) \\
&+ \sum_{T\in\mathcal{T}_h} \big((\chi[H_h,\nabla b_h]^2 + H_h)v_h, w_h\big)_T.
\end{aligned} \tag{4.36}$$

This discrete bilinear form is obviously symmetric. In the following, we consider some smooth and uniformly bounded initial data $\mathbf{w}_0 = (\eta_0, q_0) \in C_b^\infty(\Omega) \times C_b^\infty(\Omega)$, together with $b \in C_b^\infty(\mathbb{R})$, so that the associated exact solution $\mathbf{w} = (\eta, q)$ of (4.20a), and the exact solution $\mathfrak{p}$ of the elliptic problem (4.20b) satisfy the following jump conditions:

$$\forall F \in \mathcal{F}_h, \quad [\![\mathfrak{p}]\!]_F = 0, \quad [\![H]\!]_F = 0, \quad [\![\partial_x b]\!]_F = 0. \tag{4.37}$$

Proposition 4.6. *(Consistency)*

$$\forall w_h \in \mathbb{P}^k(\mathcal{T}_h), \quad a_h(\kappa[H],\beta[H,\partial_x b],\delta[H,\partial_x b]; \mathfrak{p}, w_h) = \big(\mathbb{Q}[H,b](\eta,u), w_h\big)_\Omega.$$

Proof. We set $\alpha = 1$ in the following, for the sake of simplicity. To check the consistency of the discrete elliptic sub-problem (4.28b), we set $v_h := \mathfrak{p}$, $H_h := H$, $b_h := b$, $\nabla b_h := \partial_x b$, $\kappa := \kappa[H]$, $\beta := \beta[H, \partial_x b]$, $\delta := \delta[H, \partial_x b]$ in (4.36), to obtain:

$$\begin{aligned} a_h(\kappa[H], \beta[H, \partial_x b], \delta[H, \partial_x b]; \mathfrak{p}, w_h) = &\sum_{T \in \mathcal{T}_h} \big(\frac{1}{3} H^3 \partial_x \mathfrak{p}, \partial_x w_h\big)_T - \sum_{F \in \mathcal{F}_h} \big(\frac{1}{3} H^3 \partial_x \mathfrak{p}, [\![w_h]\!]\big)_F \\ &- \frac{1}{2} \sum_{T \in \mathcal{T}_h} \big(H^2 \partial_x b\, \mathfrak{p}, \partial_x w_h\big)_T + \frac{1}{2} \sum_{F \in \mathcal{F}_h} \big(H^2 \partial_x b\, \mathfrak{p}, [\![w_h]\!]\big)_F \\ &- \frac{1}{2} \sum_{T \in \mathcal{T}_h} \big(H^2 \partial_x b\, \partial_x \mathfrak{p}, w_h\big)_T + \sum_{T \in \mathcal{T}_h} \big(H((\partial_x b)^2 + 1)\mathfrak{p}, w_h\big)_T, \end{aligned} \tag{4.38}$$

and after integration by parts:

$$\begin{aligned} a_h(\kappa[H], \beta[H, \partial_x b], \delta[H, \partial_x b]; \mathfrak{p}, w_h) = &- \sum_{T \in \mathcal{T}_h} \big(\partial_x (\frac{1}{3} H_h^3 \partial_x \mathfrak{p}), w_h\big)_T + \frac{1}{2} \sum_{T \in \mathcal{T}_h} \big(\partial_x (H^2 \partial_x b\, \mathfrak{p}), w_h\big)_T \\ &- \frac{1}{2} \sum_{T \in \mathcal{T}_h} \big(H^2 \partial_x b\, \partial_x \mathfrak{p}, w_h\big)_T + \sum_{T \in \mathcal{T}_h} \big(H((\partial_x b)^2 + 1)\mathfrak{p}, w_h\big)_T, \end{aligned} \tag{4.39}$$

so that $a_h(\kappa, \beta, \delta; \cdot, \cdot)$ is consistent in the following sense:

$$a_h(\kappa[H], \beta[H, \partial_x b], \delta[H, \partial_x b]; \mathfrak{p}, w_h) = \big(gH\partial_x \eta + Q_1[H, b](u), w_h\big)_\Omega, \quad \forall w_h \in \mathbb{P}^k(\mathcal{T}_h).$$

□

In order to formulate the discrete stability result, let introduce the following norm, for all $v_h \in \mathbb{P}^k(\mathcal{T}_h)$,

$$|\!|\!| v_h |\!|\!| := \Big(\Big\| \kappa[H_h]^{\frac{1}{2}} \partial_x^h v_h \Big\|_\Omega^2 + \| \chi[H_h, \nabla b_h] v_h \|_\Omega^2 + \Big\| H_h^{\frac{1}{2}} v_h \Big\|_\Omega^2 + |v_h|_{j,\kappa}^2 \Big)^{1/2}, \tag{4.40}$$

with the jumps seminorm

$$|v_h|_{j,\kappa} = \Big(\sum_{F \in \mathcal{F}_h} \frac{\gamma_{k,F}}{h_F} \big\| [\![v_h]\!] \big\|_F^2 \Big)^{1/2}. \tag{4.41}$$

Before addressing the discrete coercivity, we need some bounds on the boundary terms, which are addressed in the following Lemma.

Lemma 4.7. *For all* $(v_h, w_h) \in (\mathbb{P}^k(\mathcal{T}_h))^2$,

$$\Big| \sum_{F \in \mathcal{F}_h} \big(\{\!\{ \kappa[H_h] \partial_x^h v_h \}\!\}_\omega, [\![w_h]\!] \big)_F \Big| \leq \Big(\sum_{T \in \mathcal{T}_h} \sum_{F \in \mathcal{F}_T} h_F \Big\| \kappa[H_h]^{\frac{1}{2}}_{|T} \partial_x^h v_{h|T} \cdot n_F \Big\|_F^2 \Big)^{1/2} |w_h|_{j,\kappa}, \tag{4.42a}$$

$$\Big| \sum_{F \in \mathcal{F}_h} \big(\{\!\{ \kappa[H_h]^{\frac{1}{2}} \chi[H_h, \nabla b_h] v_h \}\!\}_\omega, [\![w_h]\!] \big)_F \Big| \leq \Big(\sum_{T \in \mathcal{T}_h} \sum_{F \in \mathcal{F}_T} h_F \big\| \chi[H_h, \nabla b_h]_{|T} v_{h|T} \cdot n_F \big\|_F^2 \Big)^{1/2} |w_h|_{j,\kappa}. \tag{4.42b}$$

Proof. Inequality (4.42a) is shown in e.g., [50, proof of Lemma 4.50]). For all $F \in \mathcal{F}_h^i$ with $F = \partial T_1 \cap \partial T_2$, let introduce the following convenient shortcuts $\omega_i = \omega_{T_i,F}, \kappa_i = \kappa[H_h]_{|T_i}, \chi_i = \chi[H_h, \nabla b_h]_{|T_i}$ and $a_i = \chi_i v_{h|T_i} \cdot n_F, i \in \{1,2\}$. The Cauchy-Schwartz inequality yields

$$\begin{aligned}\left(\{\!\{\kappa[H_h]^{\frac{1}{2}}\chi[H_h,\nabla b_h]v_h\}\!\}_\omega, [\![w_h]\!]\right)_F &= \left(\omega_2\kappa_1^{\frac{1}{2}}a_1 + \omega_1\kappa_2^{\frac{1}{2}}a_2, [\![w_h]\!]\right)_F \\ &\le \left(\frac{1}{2}h_F(\|a_1\|_F^2 + \|a_2\|_F^2)\right)^{\frac{1}{2}} \\ &\times \left(2(\omega_2^2\kappa_1 + \omega_1^2\kappa_2)\frac{1}{h_F}\left\|[\![w_h]\!]\right\|_F^2\right)^{\frac{1}{2}},\end{aligned}$$

and since $2(\omega_2^2\kappa_1 + \omega_1^2\kappa_2) = \gamma_{\kappa,F}$, we infer

$$\left(\{\!\{\kappa[H_h]^{\frac{1}{2}}\chi[H_h,\nabla b_h]v_h\}\!\}_\omega, [\![w_h]\!]\right)_F \le \left(\frac{1}{2}h_F(\|a_1\|_F^2 + \|a_2\|_F^2)\right)^{\frac{1}{2}} \times \left(\frac{\gamma_{\kappa,F}}{h_F}\right)^{\frac{1}{2}}\left\|[\![w_h]\!]\right\|_F,$$

Moreover, for all $F \in \mathcal{F}_h^b$ with $F = \partial T_1 \cap \partial\Omega$,

$$\left(\{\!\{\kappa[H_h]^{\frac{1}{2}}\chi[H_h,\nabla b_h]v_h\}\!\}_\omega, [\![w_h]\!]\right)_F \le h_F^{\frac{1}{2}}\left\|\chi_T v_{|T}.n_F\right\|_F \times \left(\frac{\gamma_{\kappa,F}}{h_F}\right)^{\frac{1}{2}}\left\|[\![w_h]\!]\right\|_F.$$

Summing over mesh faces, using the Cauchy-Schwartz inequality, and regrouping the face contributions for each mesh element yields the assertion. □

Proposition 4.8. *(Discrete coercivity) For all $\xi > \underline{\xi} := 2\sqrt{3}(1 + \frac{2}{\sqrt{3}}C_{tr}^2 N_\partial)(2-\sqrt{3})^{-1}$, where C_{tr} results from the discrete trace inequality (4.25), the bilinear form defined by (4.36) is coercive on $\mathbb{P}^k(\mathcal{T}_h)$ with respect to the $|||\cdot|||$-norm, i.e.,*

$$\exists C_\xi > 0, \quad \forall v_h \in \mathbb{P}^k(\mathcal{T}_h), \quad a_h(\kappa[H_h], \beta[H_h,\nabla b_h], \delta[H_h,\nabla b_h]; v_h, v_h) \ge C_\xi |||v_h|||^2,$$

where C_ξ depends on ξ and C_{tr}.

Proof. Again, we set $\alpha = 1$ in the following. Let $v_h \in V_h$, owing to the discrete trace inequality (4.25), we have

$$\begin{aligned}\sum_{T\in\mathcal{T}_h}\sum_{F\in\mathcal{F}_T} h_F\left\|\kappa[H_h]_{|T}^{\frac{1}{2}}\partial_x^h v_{h|T}\cdot n_F\right\|_F^2 &\le C_{tr}^2 N_\partial\left\|\kappa[H_h]^{\frac{1}{2}}\partial_x^h v_h\right\|_\Omega^2, \\ \sum_{T\in\mathcal{T}_h}\sum_{F\in F_T} h_F\left\|\chi[H_h,\nabla b_h]_{|T}v_{|T}\cdot n_F\right\|_F^2 &\le C_{tr}^2 N_\partial\left\|\chi[H_h,\nabla b_h]v_h\right\|_\Omega^2,\end{aligned}$$

and we infer from (4.42a)-(4.42b) that

$$\left|\sum_{F\in\mathcal{F}_h}\left(\{\!\{\kappa[H_h]^{\frac{1}{2}}\chi[H_h,\nabla b_h]v_h\}\!\}_\omega, [\![v_h]\!]\right)_F\right| \le C_{tr}N_\partial^{\frac{1}{2}}\left\|\chi[H_h,\nabla b_h]v_h\right\|_\Omega |v_h|_{j,\kappa},$$

$$\left|\sum_{F\in\mathcal{F}_h}\left(\{\!\{\kappa[H_h]\partial_x^h v_h\}\!\}_\omega, [\![v_h]\!]\right)_F\right| \le C_{tr}N_\partial^{\frac{1}{2}}\left\|\kappa[H_h]^{\frac{1}{2}}\partial_x^h v_h\right\|_\Omega |v_h|_{j,\kappa}.$$

Using Cauchy-Schwartz and Young inequalities, we also have

$$\left|\sum_{T\in\mathcal{T}_h}\left(\kappa[H_h]^{\frac{1}{2}}\chi[H_h,\nabla b_h]\partial_x v_h, v_h\right)_T\right| \leq \frac{1}{2}\left\|\kappa[H_h]^{\frac{1}{2}}\partial_x^h v_h\right\|_\Omega^2 + \frac{1}{2}\left\|\chi[H_h,\nabla b_h]v_h\right\|_\Omega^2.$$

As a result,

$$\begin{aligned} a_h(\kappa[H_h],\beta[H_h,\nabla b_h],\delta[H_h,\nabla b_h];v_h,v_h) \geq{}& \left\|\kappa[H_h]^{\frac{1}{2}}\partial_x^h v_h\right\|_\Omega^2 - 2C_{tr}N_\partial^{\frac{1}{2}}\left\|\kappa[H_h]^{\frac{1}{2}}\partial_x^h v_h\right\|_\Omega |v_h|_{j,\kappa} \\ &+ \xi|v_h|_{j,\kappa}^2 + \left\|\chi[H_h,\nabla b_h]v_h\right\|_\Omega^2 - \sqrt{3}C_{tr}N_\partial^{\frac{1}{2}}\left\|\chi[H_h,\nabla b_h]v_h\right\|_\Omega |v_h|_{j,\kappa} \\ &- \frac{\sqrt{3}}{2}\left\|\kappa[H_h]^{\frac{1}{2}}\partial_x^h v_h\right\|_\Omega^2 - \frac{\sqrt{3}}{2}\left\|\chi[H_h,\nabla b_h]v_h\right\|_\Omega^2 + \left\|H^{\frac{1}{2}}v_h\right\|_\Omega^2. \end{aligned}$$

We now use the following inequality: let σ be a positive real numbers, let $\xi \geq 2\sigma^2$, then

$$\forall (x,y)\in\mathbb{R}^2, \qquad x^2 - 2\sigma xy + \frac{\xi}{2}y^2 \geq \frac{\xi - 2\sigma^2}{2+\xi}(x^2+y^2). \tag{4.43}$$

Applying this inequality twice, one for $\sigma_1 := C_{tr}N_\partial^{\frac{1}{2}}$, $x := \left\|\kappa[H_h]^{\frac{1}{2}}\partial_x^h v_h\right\|_\Omega$, $y := |v_h|_{j,\kappa}$, and the other for $\sigma_2 := \frac{\sqrt{3}}{2}C_{tr}N_\partial^{\frac{1}{2}}$, $x := \left\|\chi[H_h,\nabla b_h]v_h\right\|_\Omega$, $y := |v_h|_{j,\kappa}$, introducing $C_1 := (\xi - 2\sigma_1^2)(2+\xi)^{-1}$, $C_2 := (\xi - 2\sigma_2^2)(2+\xi)^{-1}$, and choosing ξ such that $C_i - \frac{\sqrt{3}}{2} > 0$, $i = 1,2$, we infer,

$$\begin{aligned} a_h(\kappa[H_h],\beta[H_h,\nabla b_h],\delta[H_h,\nabla b_h];v_h,v_h) \geq{}& (C_1 - \frac{\sqrt{3}}{2})\left\|\kappa[H_h]^{\frac{1}{2}}\partial_x^h v_h\right\|_\Omega^2 \\ &+ (C_2 - \frac{\sqrt{3}}{2})\left\|\chi[H_h,\nabla b_h]v_h\right\|_\Omega^2 + (C_1+C_2)|v_h|_{j,\kappa}^2 + \left\|H^{\frac{1}{2}}v_h\right\|_\Omega^2, \end{aligned}$$

and finally

$$a_h(\kappa[H_h],\beta[H_h,\nabla b_h],\delta[H_h,\nabla b_h];v_h,v_h) \geq C|||v_h|||^2,$$

with $C = \min(C_1 - \frac{\sqrt{3}}{2}, C_2 - \frac{\sqrt{3}}{2}, C_1 + C_2, 1) > 0$. We remark that choosing the penalty coefficient ξ large enough to enforce $C_i - \frac{\sqrt{3}}{2} > 0$ leads to $\xi > \frac{2\sqrt{3}+4\sigma_1^2}{2-\sqrt{3}}$. □

A straightforward consequence of the Lax-Milgram lemma is that the discrete problem (4.28b) is well-posed.

To establish the error estimate, we assume in spirit of [50], that the exact solution of (4.15b) satisfies the following regularity assumption:

$$\mathfrak{p} \in V_{*_h} := H^2(\Omega) + \mathbb{P}^k(\mathcal{T}_h). \tag{4.44}$$

We define on V_{*h} the norm,

$$|||v_h|||_* := \left(|||v_h|||^2 + \sum_{T\in\mathcal{T}_h} h_T\left\|\kappa[H_h]_{|T}^{\frac{1}{2}}\partial_x^h v_{h|T}\cdot n_T\right\|_{\partial T}^2 + \sum_{T\in\mathcal{T}_h} h_T\left\|\chi[H_h,\nabla b_h]_{|T}v_{h|T}\cdot n_T\right\|_{\partial T}^2\right)^{\frac{1}{2}}. \tag{4.45}$$

Lemma 4.9. *(Boundedness) There is C_{bnd}, independant of h, κ and χ, such that*

$$\forall (v_h, w_h) \in V_{*h} \times \mathbb{P}^k(\mathcal{T}_h), \quad a_h(\kappa[H_h], \beta[H_h, \nabla b_h], \delta[H_h, \nabla b_h]; v_h, w_h) \leq C_{bnd} |||v_h|||_* |||w_h|||. \tag{4.46}$$

Proof. Let $(v_h, w_h) \in V_{*h} \times \mathbb{P}^k(\mathcal{T}_h)$. We observe that

$$\begin{aligned}
a_h(\kappa[H_h], \beta[H_h, \nabla b_h], \delta[H_h, \nabla b_h]; v_h, w_h) &:= \sum_{T \in \mathcal{T}_h} \left(\kappa[H_h] \partial_x v_h, \partial_x w_h\right)_T + \sum_{F \in \mathcal{F}_h} \xi \left(\frac{\gamma_{\kappa,F}}{h_F} [\![v_h]\!], [\![w_h]\!]\right)_F \\
&- \sum_{F \in \mathcal{F}_h} \left(\left(\{\!\{ \kappa[H_h] \partial_x^h v_h \}\!\}_\omega, [\![w_h]\!] \right)_F + \left([\![v_h]\!], \{\!\{ \kappa[H_h] \partial_x^h w_h \}\!\}_\omega \right)_F \right) \\
&- \frac{\sqrt{3}}{2} \sum_{T \in \mathcal{T}_h} \left(\left(\kappa[H_h]^{\frac{1}{2}} \chi[H_h, \nabla b_h] v_h, \partial_x w_h \right)_T + \left(\kappa[H_h]^{\frac{1}{2}} \chi[H_h, \nabla b_h] \partial_x v_h, w_h \right)_T \right) \\
&+ \frac{\sqrt{3}}{2} \sum_{F \in \mathcal{F}_h} \left(\left(\{\!\{ \kappa[H_h]^{\frac{1}{2}} \chi[H_h, \nabla b_h] v_h \}\!\}_\omega, [\![w_h]\!] \right)_F + \left([\![v_h]\!], \{\!\{ \kappa[H_h]^{\frac{1}{2}} \chi[H_h, \nabla b_h] w_h \}\!\}_\omega \right)_F \right) \\
&+ \sum_{T \in \mathcal{T}_h} \left((\chi[H_h, \nabla b_h]^2 + H_h) v_h, w_h \right)_T, \\
&= \varrho_1 + \cdots + \varrho_{10}.
\end{aligned} \tag{4.47}$$

Using the Cauchy-Schwartz inequality, we get

$$|\varrho_1 + \varrho_2| \leq (1 + \xi) |||v_h||| |||w_h|||,$$

moreover, using (4.42a) and (4.42b) ,

$$|\varrho_3| \leq |||v_h|||_* |w_h|_{j,\kappa} \leq |||v_h|||_* |||w_h|||,$$

$$|\varrho_7| \leq \frac{\sqrt{3}}{2} |||v_h|||_* |w_h|_{j,\kappa} \leq \frac{\sqrt{3}}{2} |||v_h|||_* |||w_h|||,$$

by the definition of the $|||\cdot|||_*$-norm. Still owing to the bound (4.42a), (4.42b) and proceeding as in the proof of lemma 4.8 leads to

$$|\varrho_4| \leq C_{tr} N_\partial^{1/2} |v_h|_{j,\kappa} \left\| \kappa[H_h]^{\frac{1}{2}} \partial_x^h w_h \right\|_\Omega \leq C_{tr} N_\partial^{1/2} |||v_h||| |||w_h|||,$$

$$|\varrho_8| \leq \frac{\sqrt{3}}{2} C_{tr} N_\partial^{1/2} |v_h|_{j,\kappa} \left\| \chi[H_h, \nabla b_h] w_h \right\|_\Omega \leq \frac{\sqrt{3}}{2} C_{tr} N_\partial^{1/2} |||v_h||| |||w_h|||,$$

proceeding as in the lemma 4.8 we infer,

$$|\varrho_5| \leq \frac{\sqrt{3}}{2} \left\| \chi[H_h, \nabla b_h] v_h \right\|_\Omega \left\| \kappa[H_h]^{\frac{1}{2}} \partial_x^h w_h \right\|_\Omega \leq \frac{\sqrt{3}}{2} |||v_h||| |||w_h|||,$$

$$|\varrho_6| \leq \frac{\sqrt{3}}{2} \left\| \kappa[H_h]^{\frac{1}{2}} \partial_x^h v_h \right\|_\Omega \left\| \chi[H_h, \nabla b_h] w_h \right\|_\Omega \leq \frac{\sqrt{3}}{2} |||v_h||| |||w_h|||,$$

$$|\varrho_9| \leq \|\chi[H_h, \nabla b_h]v_h\|_\Omega \, \|\chi[H_h, \nabla b_h]w_h\|_\Omega \leq |||v_h||| \, |||w_h|||,$$
$$|\varrho_{10}| \leq \left\|H_h^{\frac{1}{2}} v_h\right\|_\Omega \left\|H_h^{\frac{1}{2}} w_h\right\|_\Omega \leq |||v_h||| \, |||w_h|||,$$

collecting the above bounds yields the assertion with $C_{bnd} = \left(4 + \frac{3\sqrt{3}}{2} + \xi + (1 + \frac{\sqrt{3}}{2})C_{tr}N_\partial^{1/2}\right)$. □

A straightforward consequence of theoreme 2.8 together with Lemmas 2.9 and Lemmas 2.10, is the following convergence result.

Theorem 4.10. *(Error estimate and convergence rate). Let $\mathfrak{p} \in V_*$ solve (4.15b). Let $\mathfrak{p}_h \in \mathbb{P}^k(\mathcal{T}_h)$ solve the discrete problem with a_h defined by (4.36) and penality parameter as in lemma 4.8. Then, there is C, independant of h, κ and χ, such that*

$$|||\mathfrak{p} - \mathfrak{p}_h||| \leq C \inf_{v_h \in \mathbb{P}^k(\mathcal{T}_h)} |||\mathfrak{p} - \mathfrak{p}_h|||_* \tag{4.48}$$

Moreover, if $\mathfrak{p} \in H^{k+1}(\Omega)$,

$$|||\mathfrak{p} - \mathfrak{p}_h||| \leq C_{\kappa,\chi} C_\mathfrak{p} h^k, \tag{4.49}$$

with,

$$\begin{aligned} C_\mathfrak{p} &= C \, \|\mathfrak{p}\|_{H^{k+1}(\Omega)}, \\ C_{\kappa,\chi} &= C_{\max}(\bar{\kappa}^{\frac{1}{2}} + \bar{\chi} h + \bar{H}^{\frac{1}{2}} h + \bar{\kappa}^{\frac{1}{2}} + \bar{\chi} h), \end{aligned} \tag{4.50}$$

and

$$\begin{aligned} \bar{\kappa} &:= \|\kappa[H_h]\|_{L^\infty(\Omega)}, \; \bar{\chi} := \|\chi[H_h, \nabla b_h]\|_{L^\infty(\Omega)}, \bar{H} := \|H_h\|_{L^\infty(\Omega)}, \\ C_{\max} &= \max(C'_{app}, N_\partial^{1/2} \min(\kappa_1, \kappa_2)^{1/2} C''_{app}, N_\partial^{1/2} C'''_{app}, C_{tr} N_\partial^{1/2} C'_{app}). \end{aligned} \tag{4.51}$$

Proof. The proof of (4.48) is similar to that of theoreme 2.8.

To proof (4.49) we only need to proof this inequality $|||\mathfrak{p} - \mathfrak{p}_h|||_* \leq C_{\kappa,\chi} C_\mathfrak{p} h^k$ taking $v_h = \pi\mathfrak{p}$, the L^2-orthogonal projection of $\mathfrak{p}$ onto $\mathbb{P}^k(\mathcal{T}_h)$.

$$\begin{aligned} |||\mathfrak{p} - \pi_h\mathfrak{p}|||_* = &\left\|\kappa[H_h]^{\frac{1}{2}} \partial_x^h(\mathfrak{p} - \pi_h\mathfrak{p})\right\|_\Omega^2 + \sum_{F \in \mathcal{F}_h} \frac{\gamma_{k,F}}{h_F} \left\|[\![\mathfrak{p} - \pi_h\mathfrak{p}]\!]\right\|_F^2 \\ &+ \|\chi[H_h, \nabla b_h](\mathfrak{p} - \pi_h\mathfrak{p})\|_\Omega^2 + \left\|H_h^{\frac{1}{2}} v_h\right\|_\Omega^2 \\ &+ \sum_{T \in \mathcal{T}_h} h_T \left\|\kappa[H_h]^{\frac{1}{2}} \partial_x^h(\mathfrak{p} - \pi_h\mathfrak{p})_{|T} \cdot n_T\right\|_{\partial T}^2 + \sum_{T \in \mathcal{T}_h} h_T \left\|\chi[H_h, \nabla b_h]_{|T}(\mathfrak{p} - \pi_h\mathfrak{p})_{|T} \cdot n_T\right\|_{\partial T}^2 \\ &= \varrho_1 + \cdots + \varrho_6. \end{aligned}$$

Using Cauchy-Schwartz inequality and Lemmas 2.9 with $m = 1$ and $s = k + 1$, we infer

$$\begin{aligned} \varrho_1 = \sum_{T \in \mathcal{T}_h} \left\|\kappa[H_h]^{\frac{1}{2}} \partial_x(\mathfrak{p} - \pi_h\mathfrak{p})\right\|_T^2 &\leq \|\kappa[H_h]\|_{L^\infty(\Omega)} \sum_{T \in \mathcal{T}_h} \left\|\partial_x(\mathfrak{p} - \pi_h\mathfrak{p})_{|T}\right\|_T^2, \\ &\leq \bar{\kappa} \sum_{T \in \mathcal{T}_h} C_{app}^2 h_T^{2k} \, \|\mathfrak{p}\|_{H^{k+1}(T)}^2, \end{aligned}$$

owing to triangular inequality and Lemmas 2.10, we infer

$$\begin{aligned}\varrho_2 &\leq \sum_{T\in\mathcal{T}_h}\sum_{F\in F_T}\gamma_{\kappa,F}\left\|(\mathfrak{p}-\pi_h\mathfrak{p})_{|T}\right\|_F^2\\ &\leq \sum_{T\in\mathcal{T}_h} N_\partial \min(\kappa_1,\kappa_2)C_{app}'^2 h^{2k}\left\|\mathfrak{p}\right\|^2_{H^{k+1}(T)},\end{aligned}$$

still using Cauchy-Schwarz inequality and Lemmas 2.9 with $m = 0$ and $s = k + 1$, we infer

$$\begin{aligned}\varrho_3 &= \sum_{T\in\mathcal{T}_h}\left\|\chi[H_h,\nabla b_h]_{|T}(\mathfrak{p}-\pi_h\mathfrak{p})_{|T}\right\|_T^2 \leq \bar{\chi}^2\sum_{T\in\mathcal{T}_h} C_{app}''^2 h^{2(k+1)}\left\|\mathfrak{p}\right\|^2_{H^{k+1}(T)},\\ \varrho_4 &= \sum_{T\in\mathcal{T}_h}\left\|H_h^{\frac{1}{2}}(\mathfrak{p}-\pi_h\mathfrak{p})_{|T}\right\|_T^2 \leq \bar{H}\sum_{T\in\mathcal{T}_h} C_{app}'^2 h^{2(k+1)}\left\|\mathfrak{p}\right\|^2_{H^{k+1}(T)},\end{aligned}$$

applying Cauchy-Schwarz inequality and Lemmas 2.10, yields

$$\begin{aligned}\varrho_5 &= \sum_{T\in\mathcal{T}_h}\left\|\kappa[H_h]_T^{\frac{1}{2}}\partial_x(\mathfrak{p}-\pi_h\mathfrak{p})_{|T}\cdot n_T\right\|_T^2 \leq \|\kappa[H_h]\|_{L^\infty(\Omega)}\sum_{T\in\mathcal{T}_h}\left\|\partial_x(\mathfrak{p}-\pi_h\mathfrak{p})_{|T}\right\|_T^2,\\ &\leq \bar{\kappa}\sum_{T\in\mathcal{T}_h} C_{app}'''^2 N_\partial h_T^{2k}\left\|\mathfrak{p}\right\|^2_{H^{k+1}(T)},\end{aligned}$$

using (2.163) Lemmas 2.9 with $m = 0$ and $s = k + 1$, we infer

$$\varrho_6 \leq \bar{\chi}^2\sum_{T\in\mathcal{T}_h} C_{tr}^2 N_\partial C_{app}'^2 h_T^{2(k+1)}\left\|\mathfrak{p}\right\|^2_{H^{k+1}(T)}, \tag{4.52}$$

collecting the above bounds yields the assertion. □

4.3.9 Arbitrary order well-balancing property

We have the following well-balancing result, obtained as a straightforward consequence of the well-balancing property for the (hyperbolic) shallow water equations (see for instance [61]) and the previous well-posedness result for the elliptic sub-problem:

Proposition 4.11. *The discrete formulation* (4.28) *together with the numerical fluxes* (4.32) *and a first order Euler time-marching algorithm preserves the motionless steady states, providing that the integrals of* (4.28a) *are exactly computed for the motionless steady states: For all* $n \in \mathbb{N}$ *and all* $\eta^e \in \mathbb{R}$,

$$\left(\eta_h^n \equiv \eta^e \text{ and } q_h^n \equiv 0\right) \implies \left(\eta_h^{n+1} \equiv \eta^e \text{ and } q_h^{n+1} \equiv 0\right).$$

This analysis can also be extended to the high order SSP schemes of Section 4.3.6 exploiting the fact that the intermediate stages $\mathbf{w}_h^{n,i}$ are obtained as convex combinations of forward Euler substeps; see, e.g., [171].

4.4 Numerical validations

In this section, we validate the previous discrete formulation through several benchmark problems. In all the test cases, the time step restriction is computed according to the most restrictive condition between (4.33) and (4.35). Exploiting the symmetry of the discrete bilinear form, the sparse linear systems associated with the discretization of $H(1+\alpha\mathcal{T}[H,b])$ are solved using a Cholesky methods. We set $\alpha = 1$ in the first three test cases, so that solitary waves of the form (4.17) are exact solutions. In the other test cases, we use the optimized value $\alpha = 1.159$. We consider *solid-wall* boundary conditions on the two domain's boundaries. Some numerical accuracy and convergence analysis are performed in test 1, using the L^2 norm defined, for any arbitrary scalar valued piecewise polynomial function $w_h \in \mathbb{P}^k(\mathcal{T}_h)$, as follows:

$$\|w_h\|^2_{\mathcal{T}_h} = \big(w_h, w_h\big)_{\mathcal{T}_h},$$

with

$$\big(v, w\big)_{\mathcal{T}_h} := \sum_{T\in\mathcal{T}_h} \big(v, w\big)_T.$$

4.4.1 Solitary wave propagation

In this first test, we investigate the propagation of a solitary wave as defined by (4.17), over a flat topography. Such solitary waves are exact solutions for SGN equations (4.15). The computational domain is $200\,m$ long, the reference water depth is set to $H_0 = 1m$ and the relative amplitude to $\epsilon = 0.1$. The solitary wave is initially centered at $x_0 = 80\,m$ and we compute the L^2-error between numerical results and analytic solution for η and q at $t = 0.1\,s$ on a sequence of progressively refined uniform meshes. We start from mesh containing $|\mathcal{T}_h| = 800$ elements, and the computation is performed in double precision arithmetic. The corresponding L^2-errors are gathered in Figure 4.2 and we observe a scaling that lies between $O(h^{k+\frac{1}{2}})$ and $O(h^{k+1})$.

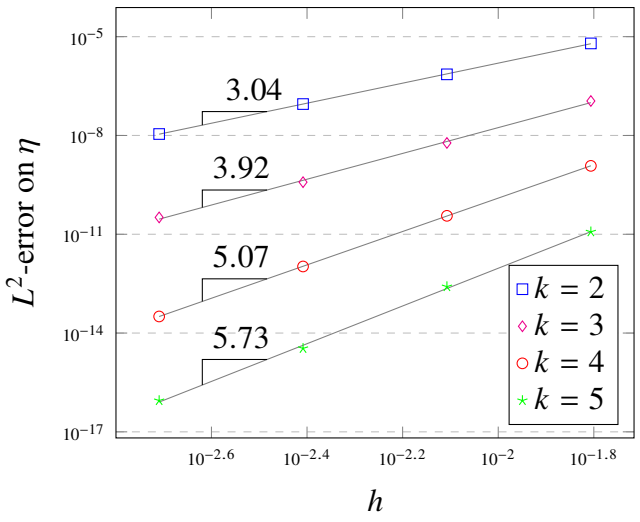


Figure 4.2: Test 1 - Solitary wave propagation: L^2-error for the total free surface elevation η at $t_{\max} = 0.1\,s$ vs. h, for polynomial orders $k = 2, 3, 4, 5$.

4.4.2 Head-on collision of solitary waves

Let consider now the head-on collision of two identical solitary waves propagating in opposite directions (see [44] for an extensive study). The collision of the two waves is associated with a change of the nonlinear dispersion characteristics and the discrete formulation has to ensure the equilibrium between amplitude and frequency dispersion in order to allow the propagation at constant shape and speed. The computational domain is defined as $\Omega = (-200\,m, 200\,m)$. The initial condition is defined with two solitary waves (4.17) of relative amplitude $\varepsilon = 0.2$ initially located at $x = -50\,m$ and $x = 50\,m$ and with opposite velocities. The number of mesh elements is set to $|\mathcal{T}_h| = 800$, corresponding to a uniform meshsize of $h = 0.5\,m$, and the polynomial order to $k = 2$. We show on Figure 4.3 some snapshots of the free surface at several times during the propagation, including a zoom on the dispersive tail generated after the collision. We observe that the maximum wave amplitude during the collision is slightly larger than twice the initial amplitude, in agreement with the results of [44, 118, 136]. The dispersive tail is very well reproduced, even with this low number of mesh elements.

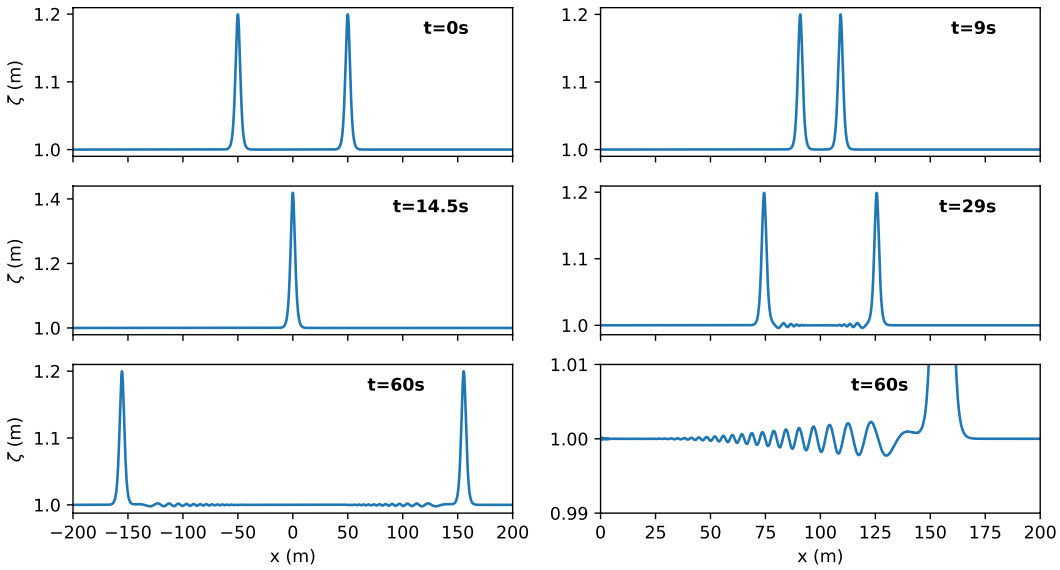


Figure 4.3: Test 2 - Head-on collision of solitary waves: snapshots of the free surface.

4.4.3 One dimensional dispersive dam-break problem

We now study the time evolution of a dispersive dam break problem over a flat bottom. We consider the computational domain $\Omega = (-300\,m,\ 300\,m)$ and the initial data is defined as :

$$H(0,x) = \frac{H_L - H_R}{2}(1 - \tanh(\frac{x}{\chi})), \quad q(0,x) = 0,$$

with $H_L = 1.8$, $H_R = 1$ and $\chi = 0.4$, and the velocity is initially uniformly set to zero, reproducing the set-up of [103] and emulating a piecewise constant initial data with a sharp variation initially

located at $x = 0$. The number of mesh elements is set to $|\mathcal{T}_h| = 1500$, corresponding to a uniform meshsize of $h = 0.4\,m$, and the polynomial order to $k = 2$. As expected, the initial discontinuity divides into a dispersive shock wave propagating to the right and a rarefaction wave propagating to the left. We show on Figures 4.4 and 4.5 the structure of the water height and the velocity at time $t = 47.5\,s$. As pointed out in [64], the analysis of Riemann invariants of the shallow-water system, coupled with the analysis of the Witham system for SGN equations, allows to approximate the values (H^*, u^*) of the mean flow dividing the rarefaction wave and the dispersive shock zones:

$$H^* = \frac{(\sqrt{H_L} + \sqrt{H_R})^2}{4}, \quad u^* = 2(\sqrt{gH^*} - \sqrt{gH_R}).$$

An asymptotic approximation of the amplitude of the lead soliton, denoted a^+ in the following, may also be obtained :

$$a^+ = \sigma_0 - \frac{1}{12}\sigma_0^2 + O(\sigma_0^3),$$

where $\sigma_0 = H_L - H_R$ denotes the initial jump value (note that the values provided in [64] are obtained with nondimensionalized equations). Numerical results are compared with these values and show very good agreement, as highlighted on Figures 4.4 and 4.5. We emphasize that, for instance, the results shown in [103] or [157] are obtained respectively with 24000 and 8000 mesh elements and second order Finite-Volume schemes, while the use of a higher-order scheme allows us to obtain very satisfying results with only 1500 mesh elements.

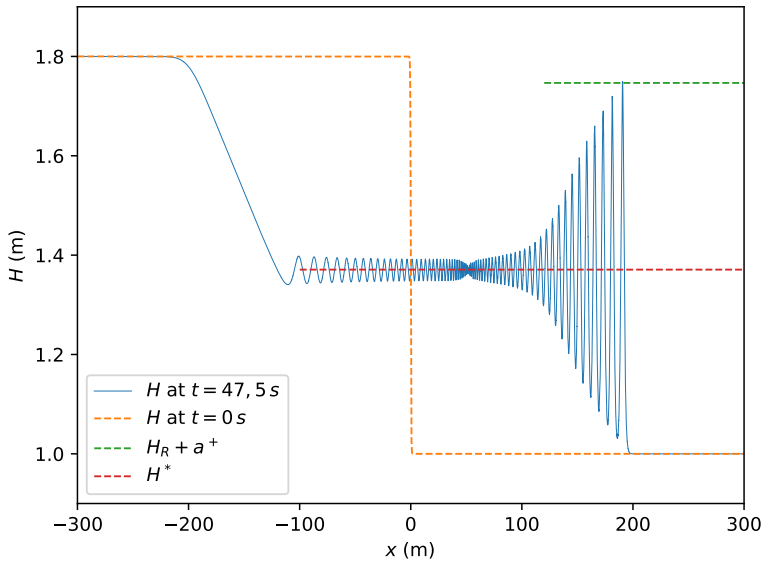


Figure 4.4: Test 3 - Dispersive dam-break: water depth profile at $t = 47.5\,s$.

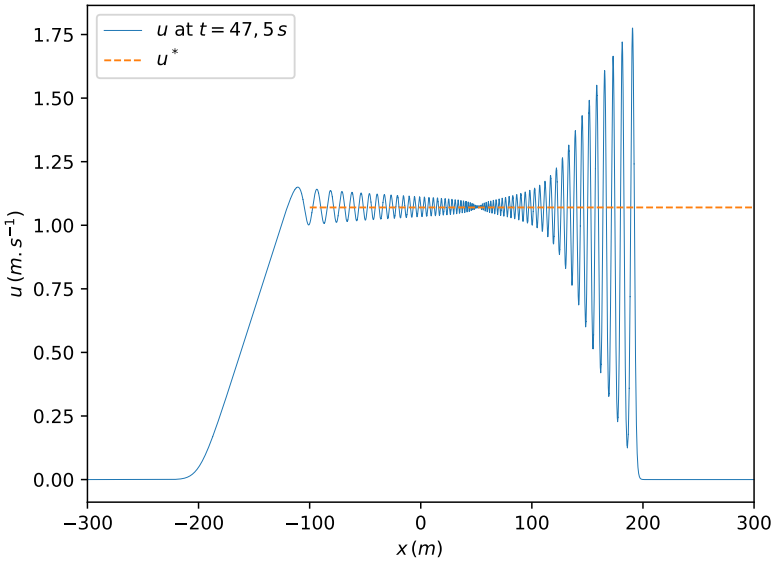


Figure 4.5: Test 3 - Dispersive dam-break: velocity profile at $t = 47.5\,s$.

4.4.4 Reflection of solitary waves at vertical walls

In this section, we focus on the propagation and reflexion of solitary waves against a vertical wall. We compare numerical results with two different sets of experimental data, coming for two different experiments and involving varying bottoms.
In the first experiment, the spatial domain is $60\,m$ long, the depth profile is piecewise linear, with a slope s defined as follows:

$$s(x) = \begin{cases} 0 & \text{if} \quad x \leq 40, \\ 1/50 & \text{if} \quad 40 \leq x \leq 60, \end{cases} \tag{4.53}$$

and terminated by a vertical solid wall located at $x = 60\,m$. The reader is referred to [162] for a complete description. The initial solitary wave, define from (4.17), is centered at $x = 10\,m$ m and is propagating from left to right. The still water depth is $H_0 = 0.7\,m$. Two runs are performed with two different initial solitary wave amplitudes, provided with relative amplitudes $\epsilon = 0.1$ and $\epsilon = 0.171$. The computational domain is uniformly discretized using $|\mathcal{T}_h| = 100$ mesh elements and the polynomial order is set to $k = 1$. Experimental data are compared with numerical results in Figure 4.6, in which time series of the surface elevation measured at a location near the solid wall ($x = 57.75$) are shown. We can observe the two expected peaks corresponding respectively to the incident and reflected waves and the discrete formulation provides a very accurate matching between simulation and experimental data, especially concerning the amplitude of the waves.

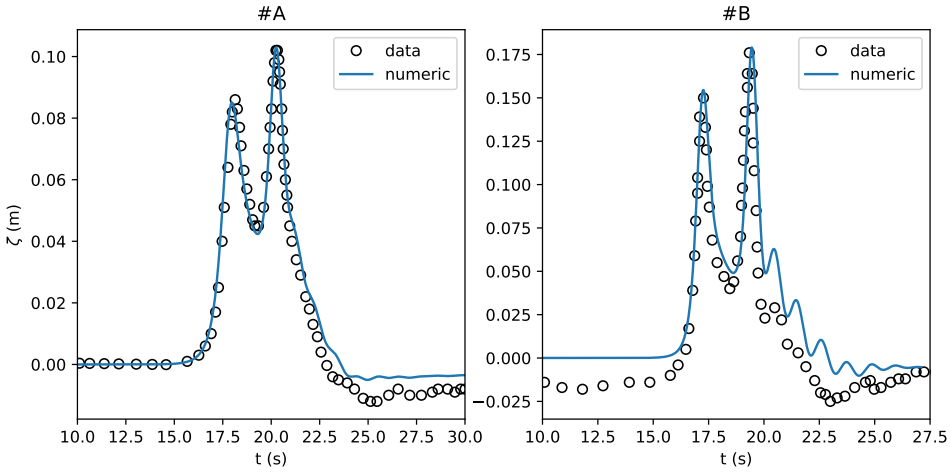


Figure 4.6: Test 4 - Reflexion of a solitary wave against a vertical wall (first test): time series of the free surface at x = 57.75 m for $\epsilon = 0.1$ (left) and $\epsilon = 0.171$ (right) - Comparison between numerical results (-) and experimental data (o).

In the second test case, we study the propagation of solitary waves over a composite beach which mimics the geometrical dimensions of the Revere Beach. The original experiment was performed in a tank by the U.S. Army corps of Engineers at the Coastal Engineering Research Center in Vicksburg, Mississippi and is depicted in details in [154]. The spatial domain is $33,23\,m$ long and the constructed beach consists of three piece-wise linear segments, terminated with a vertical wall on the left and the solitary wave is initially centered at $x = 0$, see Figure 4.7 for a sketch of the corresponding initial set-up.

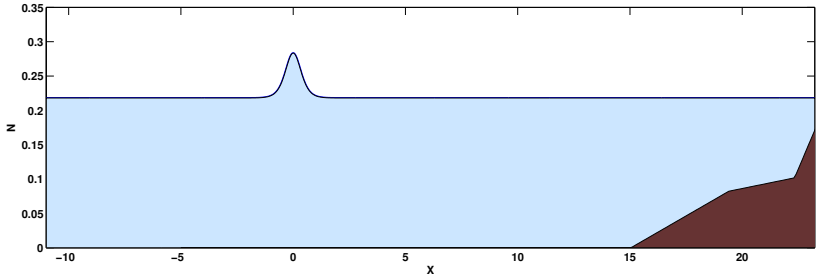


Figure 4.7: Test 5 - Reflection of a solitary wave on a composite beach: topography and initial free surface.

The slope s of the topography is defined as follows:

$$s(x) = \begin{cases} 0 \quad \text{if} \quad x \leq 15.04, \\ 1/53 \quad \text{if} \quad 15.04 \leq x \leq 19.4, \\ 1/150 \quad \text{if} \quad 19.4 \leq x \leq 22.33, \\ 1/13 \quad \text{if} \quad 22.33 \leq x \leq 23.23. \end{cases} \tag{4.54}$$

We focus here on the case (B) of the experiment $\varepsilon = 0.28$ and we provide the solitary wave of targeted height, centered at $x = 0$, as the initial condition. The computational domain is uniformly discretized using $|\mathcal{T}_h| = 100$ mesh elements and the polynomial order is set to $k = 1$. We observe the propagation, reflection on the wall at the right boundary before traveling back to the left boundary. Experimental data are provided as time series of the wave elevation at several gauges located along the wave flume. We show on Figure 4.8 the comparison between data and computed results at wave gauges 5, 7 and 9, respectively located at $x_5 = 15.04\,m$, $x_7 = 19.4\,m$ and $x_9 = 22.33\,m$ (exactly at the locations corresponding to the slope variations). We observe a very accurate agreement, the wave amplitude and celerity during the propagation and reflection are very well reproduced, even with a very low number of mesh elements.

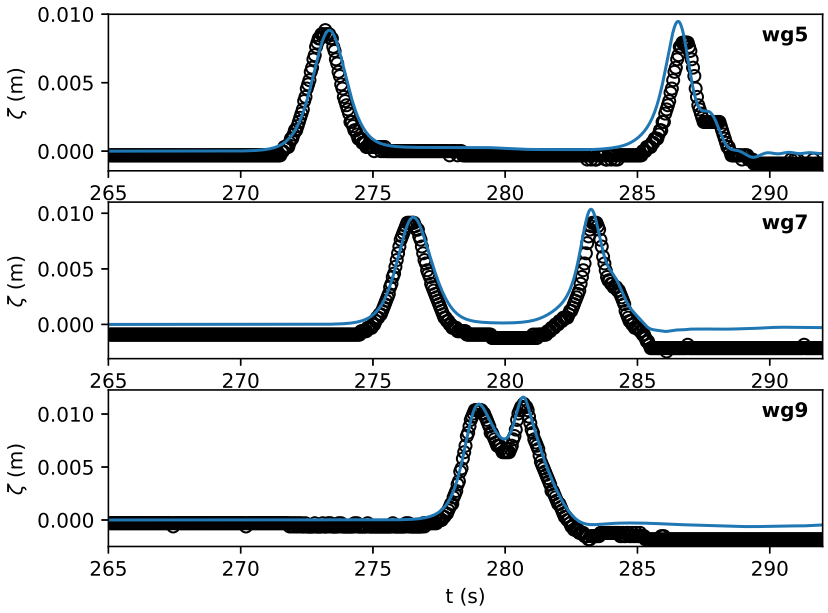


Figure 4.8: Test 5 - Reflection of a solitary wave on a composite beach: comparaison between experimental (o) data and numerical solution (-) at gauges 5,7 and 9 for case B ($\epsilon = 0.28$).

4.4.5 Shoaling of solitary waves

In this section, we investigate the dispersive properties of our model through the study of the nonlinear shoaling of solitary waves over constant bed slopes. In what follows, we numerically reproduce three different experimental configurations.
The first one relies on the data issued from the laboratory study performed at LEGI (Grenoble, France) and detailed in [78]. We consider in this test at $36\,m$ channel with constant bed slope $1:30$ and a solitary waves propagating from the left boundary, with a water level at rest $H_0 = 0.25\,m$. Measurements of the free surface are available in the vicinity of the breaking point during the simulation, at several wave gauges. We consider 4 series of experiments, involving increasing waves relative amplitudes, from $\epsilon = 0.096$ to $\epsilon = 0.534$. For each experiment, we compare the

Incident wave amplitude: $\varepsilon = 0.096$			
Gauge location (m)	2.430	2.215	1.960
Incident wave amplitude: $\varepsilon = 0.298$			
Gauge location (m)	3.980	3.765	3.510
Incident wave amplitude: $\varepsilon = 0.456$			
Gauge location (m)	4.910	4.695	4.440
Incident wave amplitude: $\varepsilon = 0.534$			
Gauge location (m)	5.180	4.965	4.710

Table 4.1: Test 6 - Shoaling of solitary waves: LEGI experiment - Location of wave gauges for solitary waves shoaling on a 1:30 sloped beach (relative to the shoreline).

numerical results with time series of the free surface elevation at several wave gauges (the exact locations of the wave gauges are reported in Table 4.1).
Numerical results, obtained with $|\mathcal{T}_h| = 400$ and $k = 2$, are shown on Figure 4.9, together with the corresponding experimental data. We observe that for the 4 experiments, the corresponding shoaling and wave tranformations near the breaking points are very well reproduced.

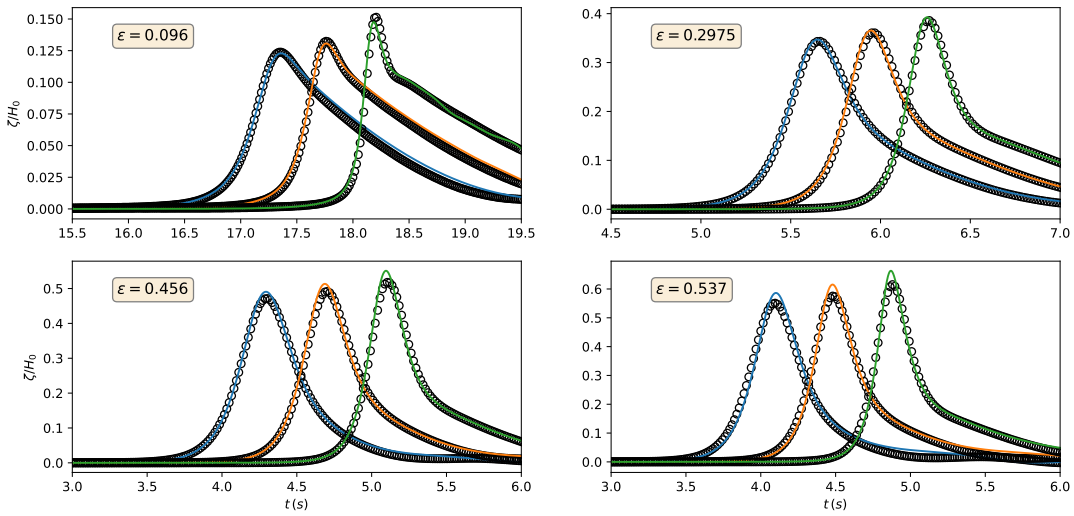


Figure 4.9: Test 6 - Shoaling of solitary waves: LEGI experiment: comparison between numerical (-) and experimental (o) time series of total free surface at three different locations before the breaking point.

The second test is based on an experimental set-up detailed in [75], for an incident solitary wave of relative amplitude $\epsilon = 0.2$, which propagates and breaks over a planar beach with a slope of $1 : 35$ in a computational domain of $85\,m$ long and a water level at rest $H_0 = 1\,m$.

Experimental data are provided as time series of the wave elevation at several gauges located along the wave flume. We show on Figure 4.10 the comparison between numerical results (obtained with $|\mathcal{T}_h| = 400$ and $k = 2$) and experimental data measured from five different wave gauges located at $x_1 = 20.96\,m, x_2 = 22.55\,m, x_3 = 23.68\,m, x_4 = 24.68\,m$, and $x_5 = 25.91\,m$, the last one being very close to the breaking point. We observe an excellent agreement between numerical and measured free surface elevation up to the breaking point.

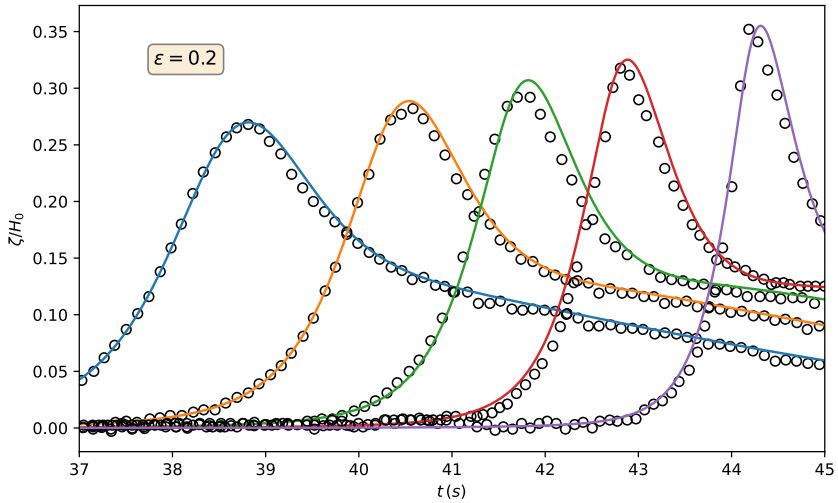


Figure 4.10: Test 7 - Shoaling of solitary waves: Grilli *et al.* experiment - Time series of the free surface elevation for the solitary wave propagating over the 1:35 sloping beach. (-) numerical results, (o) experimental data.

The third test allows to study the ability of the proposed discrete formulation to deal with the occurence of dry areas. We focus on the shoaling and run-up of a solitary wave over a beach with constant slope 1 : 19.85, following the experiments of [153]. The incident wave is supplied using (4.17), with a water level at rest $H_0 = 1m$ and $\varepsilon = 0.28m$. The mesh is set to $|\mathcal{T}_h| = 250$ elements and the polynomial order to $k = 2$. The resulting numerical results are compared with the experimental data at several times during the propagation (with a nondimensionalized time $t^* = t\sqrt{g/H_0}$) and we observe a very close agreement, as shown on Figure 4.11. In particular, the run-up is reproduced very well, and we do not have to artificially cancel the dispersive correction in the vicinity of dry areas.

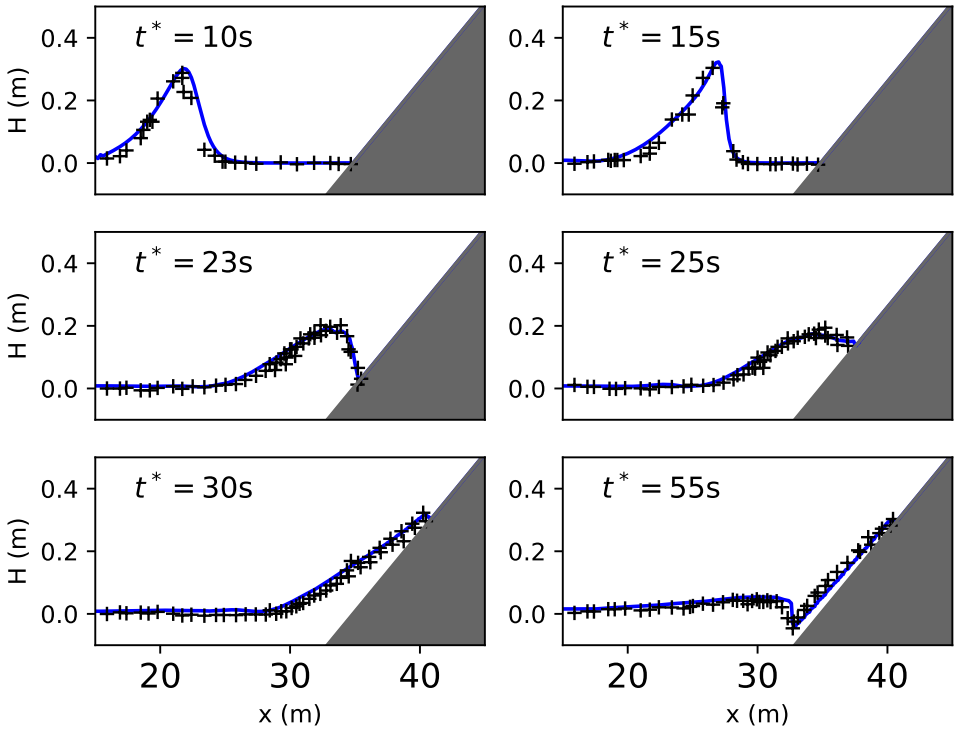


Figure 4.11: Test 8 - Shoaling of solitary waves: Synolakis *et al.* experiment - Free surface profiles (numerical results in solid lines, experimental data in cross) at several times during the propagation.

4.5 Conclusion

We introduce in this paper a new discontinuous Galerkin discrete formulation to approximate the solutions of Serre-Green-Naghdi (SGN) equations. A new non conforming discrete formulation belonging to the family of Symmetric Weighted interior Penalty discontinuous Galerkin methods (SWIP-DG) is introduced to accurately approximate the solutions of the second order elliptic operator occurring in the SGN equations in the surface horizontal $d = 1$ case. We show that the corresponding discrete bilinear form enjoys some consistency and coercivity properties. The global discrete formulation is extensively validated through an extended set of benchmarks, including some convergence studies for various polynomial orders of approximation and comparisons with experimental data for the reflexion of solitary waves over uneven topographies and nonlinear shoaling. Further studies will be devoted to the extension to SGN equations with vorticity based on the models of [101], to the surface horizontal $d = 2$ case, and to *a posteriori* limitations methods allowing to accurately handle the occurrence of dry areas within the framework of very high-order DG methods.

Chapter 5

Discontinuous Galerkin approximations of rotational SGN equations

This Chapter gathers the works initially submitted in the following paper:

Zefzouf, M. and Marche, F. Discontinuous Galerkin approximations of rotational SGN equations, submitted to *J. Comput. Phys.*, 2022.

5.1 Introduction

The modeling of the propagation and transformations of free surface waves in an incompressible, homogeneous and inviscid fluid can be achieved using the Euler equations supplemented with nonlinear boundary conditions at the surface and at the bottom. Such equations are very complex but, in the particular case of *shallow water* flows, simpler asymptotic expansions can be derived by vertically integrating the free surface Euler equations; see, e.g., [96] for a review. Introducing the typical water depth H_0, the typical wave length λ, the typical wave's amplitude a and the typical topography variations amplitude a_{bott}, we focus, in the following, on the *shallow water*

$$\mu \coloneqq \frac{H_0^2}{\lambda^2} \ll 1, \quad (\textit{dispersive parameter}) ,$$

and *fully nonlinear*

$$\varepsilon \coloneqq \frac{a}{H_0} = O(1), \quad (\textit{nonlinear parameter}) , \tag{5.1}$$

flow regime with no assumption on the topography variations:

$$\beta \coloneqq \frac{a_{\text{bott}}}{H_0} = O(1), \quad (\textit{bottom variation parameter}) . \tag{5.2}$$

When considering irrotational flows, the classical Nonlinear Shallow Water (NSW) equations can be derived by neglecting all the terms of order $O(\mu)$ in the asymptotic expansions, see for instance [95]. The NSW equations provide an accurate description of some important unsteady processes in the surf and swash zones. These equations, which form an hyperbolic system of conservation laws, have been widely studied both theoretically and numerically. However, these equations neglect the non-hydrostatic effects, which are needed for the study of wave transformations in the shoaling area. Keeping $O(\mu)$ terms and neglecting terms of size $O(\mu^2)$ and smaller, the relevant equations are the Serre-Green-Naghdi (SGN) equations, which were derived first by Serre [147], then by Green and Naghdi [74] for the two-dimensional case, and have been rigorously justified in [5].
In recent years, various numerical strategies have been proposed for the approximation of the SGN equations, mainly in the one dimensional case. We can mention Finite-Difference (FD) methods [20, 36], Finite methods [7], Finite-Volume (FV)-Volume WENO methods [29, 48], a pseudo-spectral (PS) method [63], continuous Finite-Element (FEM) methods [71, 118, 119], FV and FEM methods for hyperbolic relaxed approximation models [69, 77] or discontinuous Finite-Element (DG) approaches, possibly mixed with FEM in [51, 53, 60, 114, 127, 148]. For the two-dimensional case, fewer methods have been developed and, for the case of structured meshes, we can mention several FD methods [6, 163, 180], FV and hybrid FV-FD or WENO-FD methods [97, 103, 132, 149], a PS method for SGN equations in the the rotating case in [128], a central DG-FE method in [106] and a Hybridizable-DG (HDG) method in [144]. DG methods on unstructured simplicial meshes are considered in [59, 115]. It is also worth mentioning some works concerning non-hydrostatic models [2, 33], or the so called high-level SGN equations [183].

However, the SGN equations can only describe flow configurations where rotational effects are non existent or neglected. If one wants to take vorticity effects into account, then it is mandatory to describe the inner structure and vertical dependency of the velocity and pressure fields into the fluid domain. The addition of vorticity in weakly dispersive depth-integrated models has been

the topic of recent works and several attempts have been proposed in the literature to propose irrotational/rotational decompositions with various scalings. In [30], a model that includes vertical vorticity is proposed, in which the vertically dependent terms are suppressed by double integrating the equations. In [122], horizontal vorticity is directly included into the model, in the $d = 1$ case, relying on an approximate explicit solution of a separate vorticity transport equation. In [93], a SGN-like model that includes horizontal and vertical vorticity terms induced by the bottom-induced turbulent mixing is derived, while rotational effects are included in [179] through the use of polynomial basis functions to create velocity profiles which are substituted into the mass and momentum equations, keeping terms up to the desired asymptotic order. Let also mention some closely related recent works concerning surface wave and vorticity interactions in some specific configurations, like shear flows [80, 138], vortex patches [46] or wave breaking [89].
In [25], a rigorous derivation is proposed, starting from the free surface Euler equations, supplemented with an evolution equation for the vorticity field. As in the irrotational case, vertically averaged Euler equations can be derived and asymptotic descriptions of the pressure field and the "turbulent" terms in the fluid domain can be obtained under an assumption on the *vorticity strengh*, see [25] for details. As an incidence, the SGN equations in the presence of vorticity have to be supplemented with additional evolution equations on the second order turbulent tensor and the second order momentum of the variations of the shear velocity. Additional nonlinear terms involving these two quantities also appear in the momentum equation of this new SGN model.
One interesting conclusion arising from [25] is that the occurence of vorticity can be accounted for directly into the SGN equations, by extending the classical model with additional coupled evolution equations without any vertical dependency. And there is no need to solve the vorticity equation. The resulting SGN model with vorticity (SGNV equations in the following) is rigorously justified in [26], the existence and stability of solitary waves and peaked waves solutions are theoretically and numerically studied in [98] and a large time existence result has been proposed very recently in [79].
In the present work, we further investigate the construction of discrete formulations to approximate the solutions of the SGNV equations. Extending some of the authors previous works concerning the classical SGN equations, the SGNV model is reformulated as coupled nonlinear (pseudo) hyperbolic and elliptic problems, in which the non-hydrostatic terms and the vorticity terms, together with their interactions, appear as a purely algebraic source term in the NSW equations. This source term is computed as the solution of an auxiliary linear second order elliptic. With this reformulation of the model in hands, we observe that high-order DG methods appear as particularly well-suited for the approximation of the solutions of the rotational SGN equations. Indeed, DG methods exhibit several appealing features, such as *i.e.* local conservation, stability, arbitrary high-order approximations, geometrical flexibility, compact stencils and minimal inter-element communications. Beyond these general features, as already highlighted in [51], DG methods provide a unified discrete framework for the discretization of both the hyperbolic and elliptic operators, as well as for the highly nonlinear dispersive and vorticity terms occurring in the SGNV equations.
In what follows, we introduce a global DG discretization for the SGNV equations, which exhibits appealing properties. A suitable Symmetric Weighted interior Penalty DG (SWIP-DG) method, which enjoys a discrete coercivity property, is designed for the particular primal form of the auxiliary elliptic problem, allowing to deal with the discontinuous nature of the problem's coefficients in a consistent way and ensuring that the stability threshold on the penalty parameter is independent of the interface state values. Additionally, a robust Runge-Kutta DG (RK-DG) method is developed

for the hyperbolic part of the model. This method relies on an adapted HLLC Riemann solver especially designed to ensure the preservation of the convex set of admissible states at the discrete level, adapting the limitation strategy of [172].
The rest of this work is organized as follows: the next section is devoted to a description of the rotational SGN equations. The proposed new discrete formulation is introduced in third section and the numerical validations are provided in the last section.

5.2 Serre-Green-Naghdi equations with vorticity

5.2.1 The Serre-Green-Naghdi equations for irrotationnal flows

Denoting by d the horizontal dimension, we focus in this work on the one dimensional $d = 1$ case. Let x, z, and t denote, respectively, the horizontal, vertical, and time coordinates. We denote by $\zeta(t,x)$ the free surface elevation with respect to its rest state, by $-H_0 + b(x)$ a parametrization of the bottom's variations, by $H := H_0 + \zeta - b$ the water depth, and by $\eta = H + b$ the total free surface elevation, as shown in Figure 5.1.

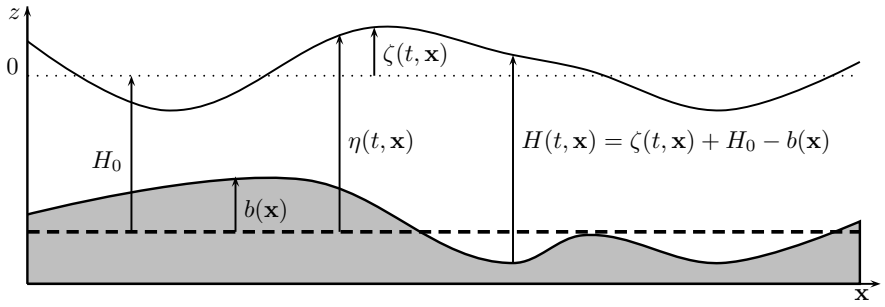


Figure 5.1: Free surface flow description and notations.

Denoting by u_{hor} the horizontal component of the velocity field in the fluid domain, we define the vertically averaged horizontal velocity $\bar{v} \in \mathbb{R}$ as

$$\bar{v} := \frac{1}{H}\int_{-H_0+b}^{\zeta} u_{\text{hor}}(t,x,z)dz,$$

and we denote by $q := H\bar{v}$ the corresponding horizontal momentum. The classical Serre–Green–Naghdi (SGN) equations, as reformulated in [20], read as follows:

$$\begin{cases} \partial_t \zeta + \partial_x(H\bar{v}) = 0, \\ \partial_t(H\bar{v}) + \partial_x(H\bar{v}^2) + \Big[1 + \mathbf{T}[H,b]\Big]^{-1}\Big(gH\partial_x\zeta + HQ_1[H,b](\bar{v})\Big) = 0, \end{cases} \tag{5.3}$$

where the linear operator $\mathbf{T}[H,b]\cdot$ and the quadratic form $Q_1[H,b](\cdot)$ are defined for all smooth

enough scalar-valued functions w by

$$\mathbf{T}[H,b]w \coloneqq H\mathcal{T}[H,b]\frac{w}{H}, \tag{5.4}$$

$$\mathcal{T}[H,b]w \coloneqq \mathcal{R}_1[H,b](\partial_x w) + \mathcal{R}_2[H,b](w\partial_x b), \tag{5.5}$$

$$\mathcal{Q}_1[H,b](w) \coloneqq -2\mathcal{R}_1[H,b]((\partial_x w)^2) + \mathcal{R}_2[H,b]((w\partial_x)^2 b). \tag{5.6}$$

where

$$\mathcal{R}_1[H,b]w \coloneqq -\frac{1}{3H}\partial_x(H^3 w) - \frac{H}{2}w\partial_x b, \qquad \mathcal{R}_2[H,b]w \coloneqq \frac{1}{2H}\partial_x(H^2 w) + w\partial_x b.$$

This formulation does not require the computation of third order derivatives and, as shown in the theoretical analysis of [5] and in our previous works [20, 29, 60], the presence of the operator $(1 + \mathbf{T}[H,b])^{-1}$ makes the model robust with respect to high frequency perturbations. In the flat bottom case, equations (5.3) admit solitary wave solutions of amplitude εH_0, which have known formulae in a closed form:

$$\eta(t,x) = H_0 + \varepsilon H_0 \ \mathrm{sech}^2\left(\kappa(x-ct)\right), \qquad q(t,x) = c\left(\eta(t,x) - H_0\right), \tag{5.7}$$

with $\kappa \coloneqq \sqrt{\frac{3\varepsilon}{4H_0^2(1+\varepsilon)}}$ and $c \coloneqq \sqrt{gH_0(1+\varepsilon)}$.

One of the main features of the SGN model is that it allows the description of $d+1$ dimensional waves by a set of d-dimensional equations: these equations are independent on the vertical variable z, leading to more mathematical simplicity and less computational time. The d-dimensional nature of the flow is inherited from the *irrotational* assumption, as the velocity field in the fluid domain derives from a scalar velocity potential Φ and, as remarked by Zakharov [176] and Craig-Sulem [43], the free surface $(d+1)$-dimensional Euler equations may then be reduced to an Hamiltonian system coupling the surface elevation ζ to the trace of Φ at the surface, denoted by ψ. Both ζ and ψ depend only on time and on the (d-dimensional) horizontal variable x. As the SGN equations are obtained by an asymptotic expansion of the Euler equations in terms of μ, it is no surprise that they are also d dimensional.

5.2.2 Serre-Green-Naghdi equations for rotational flows

The situation is very different in the presence of vorticity, since the dynamic of the vorticity $\boldsymbol{\omega} = \mathrm{curl}\,\mathbf{U}$ is fully $(d+1)$-dimensional. It indeed satisfies the following vorticity equation:

$$\partial_t \boldsymbol{\omega} + \mathbf{U}\cdot\nabla_{x,z}\boldsymbol{\omega} = \boldsymbol{\omega}\cdot\nabla_{x,z}\mathbf{U}. \tag{5.8}$$

The Zakharov-Craig-Sulem formulation has recently been generalized in [26] to the rotational case; this generalization couples the evolution of ζ and ψ as in the irrotational case but of course, the velocity field $\mathbf{U}$ does not derive from a scalar potential and ψ is defined such surface. This evolution is coupled to the evolution of the vorticity field which depends in general on all the space variables. One should therefore expect that $\nabla\psi$ is the projection onto (horizontal) gradient vector field of the horizontal component of the tangential velocity at the that generalizations of the SGN equations

in presence of vorticity have a full $(d+1)$-dimensional dependence in the space variables. It has however been shown recently in [25] that this is not the case (at least for small vorticity strength, for which the corresponding asymptotic models are fully justified). More precisely, the presence of the vorticity can be taken into account by supplementing the SGN equations with additional and coupled evolution equations, without having to explicitly solve the vorticity equation (5.8). Considering a general vorticity field

$$\text{curl}\,\mathbf{U} = (0,\omega,0)^T \quad \text{with} \quad \omega(t,x,z) = \partial_z v - \partial_x w$$

(and $\mathbf{U} = (v,0,w)^T$), the vorticity ω satisfies the scalar transport equation

$$\partial_t \omega + (v\partial_x + w\partial_z)\omega = 0, \tag{5.9}$$

in which the z dependence cannot be removed. Under a weak smallness assumption on the topography (that is assuming that $\varepsilon\beta\mu^{3/2} = \mathcal{O}(\mu^2)$), the proposed one-dimensional SGN system in the presence of vorticity may be formulated as follows:

$$\begin{cases} \partial_t H + \partial_x(H\bar{v}) = 0, & \text{(5.10a)} \\ (1+\mathbf{T}[H,b])[\partial_t(H\bar{v}) + \partial_x(H\bar{v}^2)] + gH\partial_x\zeta + HQ_1[H,b](\bar{v}) \\ \qquad\qquad + \partial_x(H^3\mathfrak{e}) + HC[H](H\mathfrak{v}^\sharp,\bar{v}) = 0, & \text{(5.10b)} \\ \partial_t(H\mathfrak{v}^\sharp) + \partial_x(H\bar{v}\mathfrak{v}^\sharp) = 0, & \text{(5.10c)} \\ \partial_t(H\mathfrak{e}) + \partial_x(H\bar{v}\mathfrak{e}) = 0, & \text{(5.10d)} \end{cases}$$

where:

1. the nonlinear interactions between the vertical dependence of the velocity field and the vertical dependence coming from the dispersive effects lead to the term $HC[H](H\mathfrak{v}^\sharp,\bar{v})$, which is defined as follows:

$$HC[H](H\mathfrak{v}^\sharp,\bar{v}) = -\frac{1}{6}\partial_x\left(2H^4\mathfrak{v}^\sharp\partial_x^2\bar{v} + \partial_x(H^4\mathfrak{v}^\sharp)\partial_x\bar{v}\right). \tag{5.11}$$

with

$$\mathfrak{v}^\sharp = \frac{v^\sharp}{H}, \quad v^\sharp = \frac{12}{H^3}\int_{-H_0+b}^{\zeta}(z+H_0-b)^2 v^*_{\text{sh}} \quad \text{and} \quad v^*_{\text{sh}} = -\int_z^\zeta \omega + \frac{1}{H}\int_{-H_0+b}^{\zeta}\omega. \tag{5.12}$$

Here, $v^\sharp$ is a second order momentum of the vorticity induced shear velocity, hence depending on ω. This term can be straightforwardly computed from its initial value by solving equation (5.10c).

2. the quantity $\mathfrak{e}$, appearing in the term $\partial_x(H^3\mathfrak{e})$, describes the self quadratic interaction of the vorticity induced shear inside the fluid domain and is defined as follows

$$\mathfrak{e} = \frac{E}{H^3} \quad \text{with} \quad E = \int_{-H_0+b}^{\zeta}(v^*_{\text{sh}})^2. \tag{5.13}$$

This term can also be straightforwardly computed from its initial value by solving equation (5.10d). Note that this quantity can be straightforwardly related to the *enstrophy* used in [137].

Remark 5.1. *A particular (and simpler) case of interest is the case of a constant vorticity, that is, when*

$$\text{curl}\,\mathbf{U} = (0,\omega,0)^T \quad \textit{with} \quad \omega(t,x,z) = \omega_0 = cst.$$

Indeed, there is no vertical dependency coming from the equation on the vorticity but the vorticity field induces a shear which, together with the dispersive effects, make the horizontal velocity depart from its vertical average. In this particular case, we observe that $H^3\mathfrak{e} = \frac{1}{12}H^3\omega_0^2$ *and* $H\mathfrak{v}^\sharp = H\omega_0$ *and the equation on* $\mathfrak{v}^\sharp$ *and* $\mathfrak{e}$ *reduces to the mass conservation equation. As a consequence, the previous system reduces to a system a two equations, as follows:*

$$\begin{cases} \partial_t H + \partial_x(H\bar{v}) = 0, \\ (1+\mathbf{T}[H,b])[\partial_t(H\bar{v}) + \partial_x(H\bar{v}^2)] + gH\partial_x\zeta + H\mathcal{Q}_1[H,b](\bar{v}) + \partial_x(\frac{H^3}{12}\omega_0^2) + HC[H](H\omega_0,\bar{v}) = 0. \end{cases} \tag{5.14}$$

Note that (5.14) can be related, up to a change of variable and algebraic manipulations, to the system introduced in [34].

Remark 5.2. *In [25], looking for an equation on* E*, a cascade of equations involving tensors (represented by scalar functions in dimension* 1*) of increasing order is obtained and one observes that the contribution of the fourth order and higher tensors are below the overall* $O(\mu^2)$ *precision of the model and can therefore be neglected. Hence, the (rigorously justified)* $O(\mu^2)$ *model with general vorticity derived in [25] reads as follows:*

$$\begin{cases} \partial_t H + \partial_x(H\bar{v}) = 0, \\ (1+\mathbf{T}[H,b])[\partial_t(H\bar{v}) + \partial_x(H\bar{v}^2)] + gH\partial_x\zeta + H\mathcal{Q}_1[H,b](\bar{v}) + \partial_x E + HC[H](v^\sharp,\bar{v}) = 0, \\ \partial_t v^\sharp + \bar{v}\partial_x v^\sharp + v^\sharp\partial_x\bar{v} = 0, \\ \partial_t E + \bar{v}\partial_x E + 3E\partial_x\bar{v} + \partial_x F = 0, \\ \partial_t F + \bar{v}\partial_x F + 4F\partial_x\bar{v} = 0, \end{cases} \tag{5.15}$$

where the third order term F *is defined as*

$$F = \int_{-H_0+b}^{\zeta} (v_{\text{sh}}^*)^3. \tag{5.16}$$

If F *is initially almost equal to zero, then the third order contributions remain negligeable and one can remove* F *from (5.15) to obtain the slightly simplified chosen model (5.10a)-(5.10d) which is numerically studied in this work.*

Further simplified models may be obtained under some particular flow regimes. In particular, lowering the asymptotic accuracy to $O(\mu^{3/2})$, one obtains

$$\begin{cases} \partial_t H + \partial_x(H\bar{v}) = 0, \\ (1+\mathbf{T}[H,b])[\partial_t(H\bar{v}) + \partial_x(H\bar{v}^2)] + gH\partial_x\zeta + H\mathcal{Q}_1[H,b](\bar{v}) + \partial_x(H^3\mathfrak{e}) = 0, \\ \partial_t(H\mathfrak{e}) + \partial_x(H\bar{v}\mathfrak{e}) = 0, \end{cases} \tag{5.17}$$

which reads as the classical SGN equations with an additional term $\partial_x(H^3\mathfrak{e})$ in the momentum equation and an additional evolution equation on $\mathfrak{e}$. This model may be related, up to the addition of dissipation-creation terms in the equation on $\mathfrak{e}$, to the models obtained in [89, 139], for which the time and space evolution of the enstrophy $\mathfrak{e}$ is used to model wave-breaking.

5.2.3 Reformulation of the SGNV equations

Assuming that H is bounded away from zero, it holds for any sufficiently smooth scalar-valued function v that:

$$(1+\mathbf{T}[H,b])v = (H+H\mathcal{T}[H,b])\frac{v}{H},$$

where

$$(H+H\mathcal{T}[H,b])w = \partial_x(-\kappa[H]\partial_x w) - \beta[H,\partial_x b]\partial_x w + \partial_x(\beta[H,\partial_x b]\, w) + \delta[H,\partial_x b]w,$$

and

$$\kappa[H] \coloneqq \frac{1}{3}H^3, \qquad \beta[H,\partial_x b] \coloneqq \frac{\sqrt{3}}{2}\kappa[H]^{\frac{1}{2}}\chi[H,\partial_x b], \qquad \delta[H,\partial_x b] \coloneqq \chi[H,\partial_x b]^2 + H, \tag{5.18a}$$

$$\chi[H,\partial_x b] = H^{\frac{1}{2}}\partial_x b. \tag{5.18b}$$

Provided that the exact solution is sufficiently regular, the SGN equations with vorticity (5.10) can be rewritten as follows

$$\begin{cases} \partial_t \mathbf{w} + \partial_x \mathbb{F}(\mathbf{w}) + \mathbb{D}(\mathbf{w},b) = \mathbb{B}(\mathbf{w},b), & \text{(5.19a)} \\ \partial_x(-\kappa[H]\partial_x \mathfrak{p}) - \beta[H,\partial_x b]\partial_x \mathfrak{p} + \partial_x(\beta[H,\partial_x b]\,\mathfrak{p}) + \delta[H,\partial_x b]\mathfrak{p} = \mathbb{Q}(\mathbf{w},b), & \text{(5.19b)} \end{cases}$$

with

$$\mathbf{w} = \begin{pmatrix} \zeta \\ H\bar{v} \\ H\mathfrak{v}^\sharp \\ H\mathfrak{e} \end{pmatrix}, \quad \mathbb{F}(\mathbf{w}) = \begin{pmatrix} H\bar{v} \\ \mathcal{F}(\mathbf{w}) \\ H\bar{v}\mathfrak{v}^\sharp \\ H\bar{v}\mathfrak{e} \end{pmatrix}, \quad \mathbb{B}(\mathbf{w},b) = \begin{pmatrix} 0 \\ -gH\partial_x b \\ 0 \\ 0 \end{pmatrix}, \quad \mathbb{D}(\mathbf{w},b) = \begin{pmatrix} 0 \\ H\mathfrak{p} - gH\partial_x\zeta - \partial_x(H^3\mathfrak{e}) \\ 0 \\ 0 \end{pmatrix}, \tag{5.20}$$

with

$$\mathcal{F}(\mathbf{w}) = H\bar{v}^2 + p(H,\mathfrak{e}), \tag{5.21}$$

$$p(H,\mathfrak{e}) = \frac{1}{2}gH^2 + H^3\mathfrak{e}, \tag{5.22}$$

and

$$\mathbb{Q}(\mathbf{w},b) = gH\partial_x\zeta + \partial_x(H^3\mathfrak{e}) + HQ_1[H,b](\bar{v}) + HC[H](H\mathfrak{v}^\sharp,\bar{v}). \tag{5.23}$$

Remark 5.3. *In practice, the numerical solution of* (5.19a)-(5.19b) *is sought in a bounded spatial domains (which reduce to line segments since we work in 1d). This issue of suitable boundary conditions for* (5.19a)-(5.19b) *is a completely open problem. In this work, in order to close* (5.19a)-(5.19b)*, we prescribe a set of boundary conditions that leads to stable computations:*

$$\partial_x\zeta_{|\partial\Omega} = 0, \tag{5.24}$$

$$\bar{v}_{|\partial\Omega} = 0, \tag{5.25}$$

$$\partial_x(H\mathfrak{v}^\sharp)_{|\partial\Omega} = 0, \tag{5.26}$$

$$\partial_x(H\mathfrak{e})_{|\partial\Omega} = 0, \tag{5.27}$$

$$\partial_x\mathfrak{p}_{|\partial\Omega} = 0. \tag{5.28}$$

Remark 5.4. *The state vector* $\mathbf{w}$ *is assumed to take values in a convex and open set* $\mathcal{U}$ *defined as*

$$\mathcal{U} = \{(H, H\bar{v}, H\mathfrak{v}^\sharp, H\mathfrak{e}) \in \mathbb{R}^4,\ H \geq 0, \mathfrak{e} \geq 0\}. \tag{5.29}$$

We emphasize that $\mathfrak{e}$ *is a non-negative quantity.*

Remark 5.5. *Focusing on the first-order and homogeneous part of* (5.19)*, which reads as*

$$\partial_t \mathbf{w} + \partial_x \mathbb{F}(\mathbf{w}) = 0,$$

the computation of $\mathbb{F}'(\mathbf{w})$ *shows that the corresponding system is strictly hyperbolic as soon as* $H > 0$*, with the following eigenvalues:*

$$\lambda_1 = \bar{v} - (gH + 3H^2\mathfrak{e})^{\frac{1}{2}}, \quad \lambda_2 = \lambda_3 = \bar{v}, \quad \lambda_4 = \bar{v} + (gH + 3H^2\mathfrak{e})^{\frac{1}{2}}.$$

5.3 Discrete formulations

In this section, we introduce a discontinuous Galerkin (DG) discrete formulation for the SGN equations with vorticity (5.19a)-(5.19b). Although we work here with $d = 1$, we keep the notation as close as possible to the classical one for DG methods in higher space dimensions; see, e.g., [50]. This is both to facilitate the reader familiar with DG methods, and to pave the way for the case $d = 2$, which we postpone to a future work.

5.3.1 Setting and notations

We consider an open segment $\Omega \subset \mathbb{R}$, with boundary $\partial\Omega$ (reduced to two vertices), and a mesh which reduced here in a partition $\mathcal{T}_h$ of Ω in open disjoint segments. We set $|\mathcal{T}_h|$ the number of mesh elements. A general element of $\mathcal{T}_h$ is denoted T, with a boundary ∂T, a length h_T, a barycenter x_T and unit outward normal n_T taking values in $\{-1, 1\}$ on ∂T. The partition is characterized by a meshsize $h := \max_{T\in\mathcal{T}_h} h_T$.

Mesh faces, reduced here to vertices, are collected in the set $\mathcal{F}_h = \mathcal{F}_h^{\mathrm{i}} \cup \mathcal{F}_h^{\mathrm{b}}$, where $\mathcal{F}_h^{\mathrm{i}}$ collects the internal vertices and $\mathcal{F}_h^{\mathrm{b}}$ the (two) boundary vertices. A general vertex of $\mathcal{F}_h$ is denoted by F, with an abscissa denoted by x_F, and h_F denote the minimum length of the mesh elements to which F belongs. For all $T \in \mathcal{T}_h$, $\mathcal{F}_T := \{F \in \mathcal{F}_h \mid F \subset \partial T\}$ denotes the set of vertices in ∂T and, for all $F \in \mathcal{F}_T$, n_{TF} is the unit normal to F pointing out of T. For any internal vertex $F \in \mathcal{F}_h^{\mathrm{i}}$, we choose an arbitrarily oriented but fixed unit normal n_F, and we set $\mathrm{n}_F := \mathrm{n}_{TF}$ for all boundary vertices $F \subset \partial T \cap \partial\Omega$. The maximum number of mesh faces composing the boundary of mesh elements is denoted by

$$N_\partial = \max_{T\in\mathcal{T}_h} \mathrm{card}(\mathcal{F}_T),$$

and we obviously have $N_\partial = 2$ in the present setting.

For any $k \geq 1$, we consider the space

$$\mathbb{P}^k(\mathcal{T}_h) := \left\{v \in L^2(\Omega) \mid v_{|T} \in \mathbb{P}^k(T)\ \ \forall T \in \mathcal{T}_h\right\}, \tag{5.30}$$

where $\mathbb{P}^k(T)$ denotes the space of polynomials in T of total degree at most k.

Considering a computational time $t_{\max} > 0$, we introduce a partition $(t^n)_{0\le n\le N}$ of $[0, t_{\max}]$ with $t^0 = 0$, $t^N = t_{\max}$ and $t^{n+1} - t^n =: \Delta t^n$. For any sufficiently regular scalar-valued function of time w, we let $w^n := w(t^n)$. Further details on the time marching algorithm are given in the following.

We introduce the following shortcut notations for smooth enough scalar-valued functions v, w:

$$(v,w)_\Omega := \int_\Omega v(x)w(x)dx, \quad (v,w)_T := \int_T v(x)w(x)dx \quad \forall T \in \mathcal{T}_h, \quad (v,w)_F := (vw)(x_F) \quad \forall F \in \mathcal{F}_h.$$

and we denote respectively by $\|v\|_\Omega = (v,v)_\Omega^{\frac{1}{2}}$, $\|v\|_T = (v,v)_T^{\frac{1}{2}}$ and $\|v\|_F = (v,v)_F^{\frac{1}{2}}$ the corresponding L^2 norms.
For all $T \in \mathcal{T}_h$, we denote p_T^k the L^2-orthogonal projector onto $\mathbb{P}^k(T)$ and $p_{\mathcal{T}_h}^k$ the L^2-orthogonal projector onto $\mathbb{P}^k(\mathcal{T}_h)$. Similarly, we denote I_T^k the element nodal interpolation into $\mathbb{P}^k(T)$. The corresponding nodal distributions in elements and edges are approximated optimal nodes introduced in [31], which have better approximation properties than equidistant distributions. The global $I_{\mathcal{T}_h}^k$ interpolation into $\mathbb{P}^k(\mathcal{T}_h)$ is obtained by gathering the local interpolating polynomials defined on each elements.

We also define the mesh elements and faces inner products as

$$(v,w)_{\mathcal{T}_h} := \sum_{T\in\mathcal{T}_h} (v,w)_T, \quad (\mu,\nu)_{\partial\mathcal{T}_h} := \sum_{T\in\mathcal{T}_h} (\mu,\nu)_{\partial T},$$

for $v, w \in L^2(\mathcal{T}_h)$ and $\mu, \nu \in L^2(\partial\mathcal{T}_h)$. Extensions to vector-valued functions are straightforward.

For any function $w_h \in \mathbb{P}^k(\mathcal{T}_h)$, $T \in \mathcal{T}_h$ and $F \in \mathcal{F}_T$, we conveniently set $w_T = w_{h|T}$ and w_{TF} (or w_F, in a more concise way, when no confusion is possible) refers to the trace of w_T on F. When fully discrete approximations are considered, w_T^n and w_F^n respectively refers to the values of w_T and w_F obtained at discrete time t^n. Similar shortcuts for vector-valued functions are straightforwardly obtained.

Let $\kappa, \beta, \delta \in L^\infty(\Omega)$ denote a uniformly bounded coefficients and set, for the sake of brevity, $\kappa_T := \kappa_{|T}, \beta_T := \beta_{|T}$ and $\delta_T := \delta_{|T}$ for all $T \in \mathcal{T}_h$. Following [52, 55], we define the jump and weighted average operators such that, for a sufficiently smooth function φ and an interior vertex $F \in \mathcal{F}_h^i$ such that $F \subset \partial T_1 \cap \partial T_2$ for distinct mesh elements T_1 and T_2,

$$[\![\varphi]\!] := \varphi_{|T_1} - \varphi_{|T_2}, \qquad \{\!\{\varphi\}\!\}_{\omega,F} := \omega_2\varphi_{|T_1} + \omega_1\varphi_{|T_2}, \quad \omega_i := \frac{\kappa_{T_i}}{\kappa_{T_1} + \kappa_{T_2}} \quad \forall i \in \{1,2\}. \tag{5.31}$$

In what follows, and when no confusion can arise, we omit the subscript F from both $[\![v]\!]_{\omega,F}$ and $\{\!\{v\}\!\}_{\omega,F}$. When $\kappa \equiv C$ in Ω for some real number $C > 0$, we have $\omega_1 = \omega_2 = \frac{1}{2}$, and also the subscript ω is omitted. We refer the reader to [50, Section 4.5] for a discussion on the role of weighted averages and harmonic means in the context of heterogeneous diffusion-like problems.

In what follows, we need discrete counterparts of the gradient and of the Laplacian applied to broken polynomial functions. For any $v_h \in \mathbb{P}^k(\mathcal{T}_h)$, we denote by $\nabla_h^k : \mathbb{P}^k(\mathcal{T}_h) \to \mathbb{P}^k(\mathcal{T}_h)$ the discrete gradient operator and by $\Delta_h^k : \mathbb{P}^k(\mathcal{T}_h) \to \mathbb{P}^k(\mathcal{T}_h)$ the discrete Laplace operator. We use the discrete operators already introduce in [51], whose definitions are recalled in Appendix A.

5.3.2 The semi-discrete problems

We focus in this section to the construction of a discrete formulation for the SGN equations with vorticity (5.19a)-(5.19b). Let $b_h \in \mathbb{P}^k(\mathcal{T}_h)$ denote a piecewise polynomial approximation of the topography parameterization b which can be obtained either by L^2-orthogonal projection (*i.e.* $b_h = \pi_h^k(b)$) or by interpolation (*i.e.* $b_h = \mathcal{I}_h^k(b)$). Note that any order of approximation may be used for the definition of b_h, and in what follows, we choose the same order k as for the primal variables, for the sake of simplicity, and the following shortcuts are introduced: $\nabla b_h = \nabla_h^k b_h$, $\Delta b_h = \Delta_h^k b_h$ and $\nabla^3 b_h = \nabla_h^k(\Delta_h^k b_h)$. The semi-discrete in space DG approximation of (5.19a)-(5.19b), supplemented by boundary conditions (5.24) reads:

Find $\mathbf{w}_h = (\zeta_h, \bar{v}_h, v_h^\sharp, \mathfrak{e}_h, \mathfrak{p}_h) \in (\mathbb{P}^k(\mathcal{T}_h))^5$ such that, for all $(\varphi_h, \psi_h) \in (\mathbb{P}^k(\mathcal{T}_h))^2$,

$$\big(\partial_t \mathbf{w}_h, \varphi_h\big)_{\mathcal{T}_h} + \big(\mathcal{A}_h(\mathbf{w}_h), \varphi_h\big)_{\mathcal{T}_h} = 0, \tag{5.32a}$$

$$a_h(\kappa[H_h], \beta[H_h, \nabla b_h], \delta[H_h, \nabla b_h]; \mathfrak{p}_h, \psi_h) = \big(\mathbb{Q}_h[H_h, b_h](\zeta_h, \bar{v}_h), \psi_h\big)_{\mathcal{T}_h}, \tag{5.32b}$$

where:

(i) The discrete bilinear form $a_h(\kappa, \beta, \delta; \cdot, \cdot)$ is defined on $\mathbb{P}^k(\mathcal{T}_h) \times \mathbb{P}^k(\mathcal{T}_h)$:

$$\begin{aligned} a_h(\kappa, \beta, \delta; v_h, w_h) \coloneqq & \sum_{T\in\mathcal{T}_h} \big(\kappa \partial_x v_h, \partial_x w_h\big)_T + \sum_{F\in\mathcal{F}_h} \xi\big(\frac{\gamma_{\kappa,F}}{h_F}[\![v_h]\!], [\![w_h]\!]\big)_F \\ & - \sum_{F\in\mathcal{F}_h} \Big(\big(\{\!\{\kappa \partial_x^h v_h\}\!\}_\omega, [\![w_h]\!]\big)_F + \big([\![v_h]\!], \{\!\{\kappa \partial_x^h w_h\}\!\}_\omega\big)_F\Big) \\ & - \sum_{T\in\mathcal{T}_h} \big(\beta v_h, \partial_x w_h\big)_T - \sum_{T\in\mathcal{T}_h} \big(\partial_x v_h, \beta w_h\big)_T \\ & + \sum_{F\in\mathcal{F}_h} \big(\big(\{\!\{\beta v_h\}\!\}_\omega, [\![w_h]\!]\big)_F + \big([\![v_h]\!], \{\!\{\beta w_h\}\!\}_\omega\big)_F\big) \\ & + \sum_{T\in\mathcal{T}_h} \big(\delta v_h, w_h\big)_T, \end{aligned} \tag{5.33}$$

with a κ-dependent penalty parameter $\gamma_{\kappa,F}$ defined as follows:

$$\gamma_{\kappa,F} \coloneqq \begin{cases} \frac{2\kappa_{T_1}\kappa_{T_2}}{\kappa_{T_1}+\kappa_{T_2}} & \text{if } F \in \mathcal{F}_h^{\mathrm{i}} \text{ is such that } F = \partial T_1 \cap \partial T_2, \\ \kappa_T & \text{if } F \in \mathcal{F}_h^{\mathrm{b}} \text{ is such that } F = \partial T \cap \partial\Omega. \end{cases}$$

In (5.33), ξ denotes a user-defined parameter sufficiently large to ensure coercivity (see [177] for details) and for a given function $v_h \in \mathbb{P}^k(\mathcal{T}_h)$ we have $(\partial_x^h v_h)_{|T} = \partial_x(v_{h|T})$.

(ii) The discrete nonlinear operator $\mathcal{A}_h$ in (5.32a) is defined by

$$\big(\mathcal{A}_h(\mathbf{w}_h), \varphi_h\big)_{\mathcal{T}_h} \coloneqq -\big(\mathbb{F}(\mathbf{w}_h), \partial_x^h \varphi_h\big)_{\mathcal{T}_h} + \big(\widehat{\mathbb{F}}\mathbf{n}, \varphi_h\big)_{\partial\mathcal{T}_h} + \big(\mathbb{D}_h, \varphi_h\big)_{\mathcal{T}_h} - \big(\mathbb{B}(\mathbf{w}_h, b_h), \varphi_h\big)_{\mathcal{T}_h}, \tag{5.34}$$

where the interface stabilizing fluxes contribution is defined as follows

$$\big(\widehat{\mathbb{F}}\mathbf{n}, \varphi_h\big)_{\partial\mathcal{T}_h} = \sum_{T\in\mathcal{T}_h} \sum_{F\in\mathcal{F}_T} \big(\widehat{\mathbb{F}}_{TF}\mathbf{n}_{TF}, \varphi_h\big)_F,$$

and $\widehat{\mathbb{F}}_{TF}$ is a numerical approximation of the normal face fluxes $\mathbb{F}(\mathbf{w}_h, b_h)\cdot\mathbf{n}_{TF}$ whose precise definition in postponed to Section 5.3.3 below. The discrete contribution of the dispersive correction

$$\big(\mathbb{D}_h, \varphi_h\big)_{\mathcal{T}_h} = \big(H_h\mathfrak{p}_h - gH_h\nabla_h^k(\zeta_h) - 3H_h^2\nabla_h^k(H_h)\mathfrak{e}_h - H_h^3\nabla_h^k(\mathfrak{e}_h), \varphi_h\big)_{\mathcal{T}_h}.$$

(iii) The discrete nonlinear operator $\mathbb{Q}_h[H_h, b_h]$ in (5.32b) is defined by

$$\mathbb{Q}_h[H_h, b_h](\zeta_h, \bar{v}_h) := gH_h\nabla_h^k(\eta_h) + 3H_h^2\nabla_h^k(H_h)\mathfrak{e}_h + H_h^3\nabla_h^k(\mathfrak{e}_h) + H_h\mathcal{Q}_{1h}[H_h, b_h](\bar{v}_h) + H_h\mathcal{C}_h[H_h](H_h v_h^\sharp, \bar{v}_h),$$

where, for any $w_h \in \mathbb{P}^k(\mathcal{T}_h)$,

$$\begin{aligned}\mathcal{Q}_{1,h}[H_h, b_h](w_h) := {} & 2H_h\nabla_h^k(H_h + \frac{b_h}{2})\nabla_h^k(w_h)^2 + \frac{4}{3}H_h^2\nabla_h^k(w_h)\Delta_h^k(w_h) \\ & + H_h\Delta_h^k(b_h)w_h\nabla_h^k(w_h) + \Big(\nabla_h^k(\eta_h)\Delta_h^k(b_h) + \frac{H_h}{2}\nabla_h^k(\Delta_h^k(b_h))\Big)w_h^2,\end{aligned}$$

and

$$\begin{aligned}H_h\mathcal{C}_h[H_h](u_h, w_h) := {} & -6H_h^2\nabla_h^k(H_h)u_h\Delta_h^k(w_h) - 2H_h^3\left(\nabla_h^k(u_h)\Delta_h^k(w_h) + u_h\nabla_h^k(\Delta_h^k(w_h))\right) \\ & - \left(6H_h\nabla_h^k(H_h)^2u_h + 3H_h^2\Delta_h^k(H_h)u_h + 6H_h^2\nabla_h^k(H_h)\nabla_h^k(u_h) + H_h^3\Delta_h^k(u_h)\right)\nabla_h^k(w_h) \\ & - \left(3H_h^2\nabla_h^k(H_h)u_h + H_h^3\nabla_h^k(u_h)\right)\Delta_h^k(w_h).\end{aligned}$$

5.3.3 Interface fluxes

We detail in this section the construction of an approximate interface fluxes $\widehat{\mathbb{F}}\mathbf{n}$ such that its restriction $\widehat{\mathbb{F}}_{TF}\mathbf{n}_{TF}$ to the face F of mesh element T is a numerical approximation of the normal face fluxes $\mathbb{F}(\mathbf{w}_h)\cdot\mathbf{n}_{TF}$ that allows to preserve the invariant domain $\mathcal{U}$.
Let $T \in \mathcal{T}_h$ and $F \in \mathcal{F}_T \cap \mathcal{F}_h^i$ (we only detail the case of interface here). Denote by $\mathbf{w}_F^-$ and $\mathbf{w}_F^+$, respectively, the *interior* and *exterior* traces of $\mathbf{w}_h$ on F with respect to the element T (that is if $F \subset \partial T \cap \partial T_e$ for a given neighboring element T_e, then $\mathbf{w}_F^-, \mathbf{w}_F^+$ are respectively the polynomial traces of $\mathbf{w}_T$ and $\mathbf{w}_{T_e}$ on F). We define the numerical flux function through the interface F as follows:

$$\widehat{\mathbb{F}}_{TF} = \mathbb{F}_h(\mathbf{w}_F^-, \mathbf{w}_F^+), \tag{5.35}$$

where $(\mathbf{w}_L, \mathbf{w}_R) \mapsto \mathbb{F}_h(\mathbf{w}_L, \mathbf{w}_R)$ is a numerical flux function consistent with the physical flux $\mathbf{w} \mapsto \mathbb{F}(\mathbf{w})$ and built upon an approximate Riemann solver of the HLLC type, see [16, 82]. More precisely, we consider an approximate Riemann solver at interface F consisting of 2 finite external wave-speeds λ_F^-, λ_F^+ and an additional intermediate wave $\lambda_F^\star$ (note that in the following, the subscript F may be avoided when no confusion is possible). We denote by $\mathbf{w}_L^\star$ and $\mathbf{w}_R^\star$ the intermediate states to the left and to the right of the wave $\lambda^\star$ respectively. The 3 wave speeds are therefore separating 4 constant states $\mathbf{w}_L$, $\mathbf{w}_L^\star$, $\mathbf{w}_R^\star$ and $\mathbf{w}_R$, leading to the following approximate solver:

$$\hat{\mathbf{w}}(\xi, \mathbf{w}_L, \mathbf{w}_R) = \begin{cases}\mathbf{w}_L & \text{if } \xi \le \lambda^-, \\ \mathbf{w}_L^\star & \text{if } \lambda^- \le \xi \le \lambda^\star, \\ \mathbf{w}_R^\star & \text{if } \lambda^\star \le \xi \le \lambda^+, \\ \mathbf{w}_R & \text{if } \lambda^+ \le \xi,\end{cases} \tag{5.36}$$

with $\xi = \frac{x-x_F}{t-t^n}$. Assuming that λ^- and λ^+ are given by some estimates, which are defined later, we need to define the 8 components of the 2 unknown intermediate states $\mathbf{w}_L^\star$ and $\mathbf{w}_R^\star$, and the intermediate wave speed $\lambda^\star$. To achieve this, we use the consistency condition for the discharge $H\bar{v}$, together with the jump conditions across each wave for the variables $H, H\mathfrak{v}^\sharp, H\mathfrak{e}$, leading to the following system:

$$\begin{cases} \lambda^-(H_L^\star - H_L) = H_L^\star \bar{v}_L^\star - H_L \bar{v}_L, \\ \lambda^\star(H_R^\star - H_L^\star) = H_R^\star \bar{v}_R^\star - H_L^\star \bar{v}_L^\star, \\ \lambda^+(H_R - H_R^\star) = H_R \bar{v}_R - H_R^\star \bar{v}_R^\star, \\ \lambda^-(H_L^\star \bar{v}_L^\star - H_L \bar{v}_L) + \lambda^\star(H_R^\star \bar{v}_R^\star - H_L^\star \bar{v}_L^\star) + \lambda^+(H_R \bar{v}_R - H_R^\star \bar{v}_R^\star) = H_R \bar{v}_R^2 - H_L \bar{v}_L^2 + \Delta p_{LR}, \\ \lambda^-(H_L^\star \mathfrak{v}_L^{\sharp,\star} - H_L \mathfrak{v}_L^\sharp) = H_L^\star \bar{v}_L^\star \mathfrak{v}_L^{\sharp,\star} - H_L \bar{v}_L \mathfrak{v}_L^\sharp, \\ \lambda^\star(H_R^\star \mathfrak{v}_R^{\sharp,\star} - H_L^\star \mathfrak{v}_L^{\sharp,\star}) = H_R^\star \bar{v}_R^\star \mathfrak{v}_R^{\sharp,\star} - H_L^\star \bar{v}_L^\star \mathfrak{v}_L^{\sharp,\star}, \\ \lambda^+(H_R \mathfrak{v}_R^\sharp - H_R^\star \mathfrak{v}_R^{\sharp,\star}) = H_R \bar{v}_R \mathfrak{v}_R^\sharp - H_R^\star \bar{v}_R^\star \mathfrak{v}_R^{\sharp,\star}, \\ \lambda^-(H_L^\star \mathfrak{e}_L^\star - H_L \mathfrak{e}_L) = H_L^\star \bar{v}_L^\star \mathfrak{e}_L^\star - H_L \bar{v}_L \mathfrak{e}_L, \\ \lambda^\star(H_R^\star \mathfrak{e}_R^\star - H_L^\star \mathfrak{e}_L^\star) = H_R^\star \bar{v}_R^\star \mathfrak{e}_R^\star - H_L^\star \bar{v}_L^\star \mathfrak{e}_L^\star, \\ \lambda^+(H_R \mathfrak{e}_R - H_R^\star \mathfrak{e}_R^\star) = H_R \bar{v}_R \mathfrak{e}_R - H_R^\star \bar{v}_R^\star \mathfrak{e}_R^\star, \end{cases} \tag{5.37}$$

where $\Delta p_{LR} = p(H_R, \mathfrak{e}_R) - p(H_L, \mathfrak{e}_L)$, and whose solution is given by

$$\lambda^\star = \frac{H_L \bar{v}_L(\lambda^- - \bar{v}_L) - H_R \bar{v}_R(\lambda^+ - \bar{v}_R) + \Delta p_{LR}}{H_L(\lambda^- - \bar{v}_L) - H_R(\lambda^+ - \bar{v}_R)}, \tag{5.38a}$$

$$\bar{v}_L^\star = \bar{v}_R^\star = \lambda^\star, \tag{5.38b}$$

$$H_L^\star = \frac{H_L(\lambda^- - \bar{v}_L)}{\lambda^- - \lambda^\star}, \qquad H_R^\star = \frac{H_R(\lambda^+ - \bar{v}_R)}{\lambda^+ - \lambda^\star}, \tag{5.38c}$$

$$\mathfrak{v}_L^{\sharp,\star} = \mathfrak{v}_L^\sharp, \qquad \mathfrak{v}_R^{\sharp,\star} = \mathfrak{v}_R^\sharp, \tag{5.38d}$$

$$\mathfrak{e}_L^\star = \mathfrak{e}_L, \qquad \mathfrak{e}_R^\star = \mathfrak{e}_R. \tag{5.38e}$$

Once the intermediate states are known, the corresponding fluxes can be computed as follows:

$$\mathbb{F}_h(\mathbf{w}_L, \mathbf{w}_R) = \begin{cases} \mathbb{F}(\mathbf{w}_L) \ \text{ if } \ 0 \le \lambda^-, \\ \mathbb{F}(\mathbf{w}_L) + \lambda^-(\mathbf{w}_L^\star - \mathbf{w}_L) \ \text{ if } \ \lambda^- \le 0 \le \lambda^\star, \\ \mathbb{F}(\mathbf{w}_R) + \lambda^+(\mathbf{w}_R^\star - \mathbf{w}_R) \ \text{ if } \ \lambda^\star \le 0 \le \lambda^+, \\ \mathbb{F}(\mathbf{w}_R) \ \text{ if } \ \lambda^+ \le 0. \end{cases} \tag{5.39}$$

5.3.4 Time discretization

Supplementing our formulation with an initial datum $\mathbf{w}(0,\cdot) = \mathbf{w}^0$, the time stepping is carried out using the explicit SSP-RK schemes of [73]. For $k < 3$, we consider SSP-RK schemes of order $(k+1)$. For instance, writing the semi-discrete equation (5.32a) in the operator form

$$\partial_t \mathbf{w}_h + \mathcal{A}_h(\mathbf{w}_h) = 0,$$

we advance from time level n to $(n+1)$ as follows with the third-order scheme as follows:

$$\begin{aligned}
\mathbf{w}_h^{n,1} &= \mathbf{w}_h^n - \Delta t^n \mathcal{A}_h(\mathbf{w}_h^n),\\
\mathbf{w}_h^{n,2} &= \frac{1}{4}(3\mathbf{w}_h^n + \mathbf{w}_h^{n,1}) - \frac{1}{4}\Delta t^n \mathcal{A}_h(\mathbf{w}_h^{n,1}),\\
\mathbf{w}_h^{n+1} &= \frac{1}{3}(\mathbf{w}_h^n + 2\mathbf{w}_h^{n,2}) - \frac{2}{3}\Delta t^n \mathcal{A}_h(\mathbf{w}_h^{n,2}),
\end{aligned}$$

where $\mathbf{w}_h^{n,i}$, $1 \le i \le 2$, are the intermediate stages, Δt^n is obtained from the CFL condition (5.40), and the discrete initial data $\mathbf{w}_h^0$ is defined either as the L^2-projection or interpolation on $(\mathbb{P}^k(\mathcal{T}_h))^2$ of $\mathbf{w}_0$. For $k \ge 3$, the five stages fourth order SSP-RK scheme of [150] is used (the details are omitted for the sake of simplicity). The corresponding time step Δt^n is computed adaptively using the following CFL condition (see [38]):

$$\Delta t^n = \frac{1}{2k+1} \min_{T\in\mathcal{T}_h}\Big(\frac{h_T}{\sigma_T}\Big). \tag{5.40}$$

with

$$\sigma_T := \max_{\partial T}\left(|\bar{v}_T| + \sqrt{gH_T + 3H_T^2\mathfrak{e}_T}\right).$$

5.3.5 Main properties

5.3.5.1 Positivity of the approximate Riemann solver

Let $T \in \mathcal{T}_h$, $F \in \mathcal{F}_T \cap \mathcal{F}_h^i$, $(\mathbf{w}_L, \mathbf{w}_R) \in \mathcal{U}^2$ and we consider the numerical flux $\mathbb{F}_h(\mathbf{w}_L, \mathbf{w}_R)$. We introduce the following wave-speed estimates:

$$\lambda^- = \bar{v}_L - \frac{s_L}{H_L}, \quad \lambda^+ = \bar{v}_R + \frac{s_R}{H_R}, \tag{5.41}$$

where s_L and s_R are 2 positive values to be defined in the following. Then (5.38a)-(5.38c) may be reformulated as follows:

$$\lambda^\star = \frac{s_L\bar{v}_L + s_R\bar{v}_R - \Delta p_{LR}}{s_L + s_R}, \tag{5.42}$$

$$\frac{1}{H_L^\star} = \frac{1}{H_L} + \frac{s_R(\bar{v}_R - \bar{v}_L) - \Delta p_{LR}}{s_L(s_L + s_R)}, \qquad \frac{1}{H_R^\star} = \frac{1}{H_R} + \frac{s_L(\bar{v}_R - \bar{v}_L) + \Delta p_{LR}}{s_R(s_L + s_R)}. \tag{5.43}$$

In what follows, assuming $(\mathbf{w}_L, \mathbf{w}_R) \in \mathcal{U}^2$, we show that a suitable choice of s_L and s_R ensures that the intermediate water heights $H_L^\star$ and $H_R^\star$ in the approximate Riemann solver remain positive, hence ensuring that $(\mathbf{w}_L^\star, \mathbf{w}_R^\star) \in \mathcal{U}^2$.

Proposition 5.6. *Consider the approximate Riemann solver (5.36)-(5.38), together with the wave-speed estimates (5.41). Let define s_L and s_R as follows:*

$$\text{if} \quad \Delta p_{LR} \ge 0, \quad \begin{cases} \dfrac{s_L}{H_L} = \sqrt{H_L(g + 3H_L\mathfrak{e}_L)} + \dfrac{3}{2}\Big(\dfrac{\Delta p_{LR}}{H_R\sqrt{H_R(g + 3H_R\mathfrak{e}_R)}} + \bar{v}_L - \bar{v}_R\Big)_+,\\[2ex] \dfrac{s_R}{H_R} = \sqrt{H_R(g + 3H_R\mathfrak{e}_R)} + \dfrac{3}{2}\Big(\dfrac{-\Delta p_{LR}}{s_L} + \bar{v}_L - \bar{v}_R\Big)_+. \end{cases} \tag{5.44}$$

$$\text{if} \quad \Delta p_{LR} \le 0, \quad \begin{cases} \dfrac{s_R}{H_R} = \sqrt{H_R(g + 3H_R\mathfrak{e}_R)} + \dfrac{3}{2}\Big(\dfrac{-\Delta p_{LR}}{H_L\sqrt{H_L(g + 3H_L\mathfrak{e}_L)}} + \bar{v}_L - \bar{v}_R\Big)_+, \\ \dfrac{s_L}{H_L} = \sqrt{H_L(g + 3H_L\mathfrak{e}_L)} + \dfrac{3}{2}\Big(\dfrac{\Delta p_{LR}}{s_R} + \bar{v}_L - \bar{v}_R\Big)_+. \end{cases} \tag{5.45}$$

Then the approximate Riemann solver (5.36)-(5.38) preserves the invariant domain $\mathcal{U}$:

$$\mathbf{w}_L, \mathbf{w}_R \in \mathcal{U} \quad \Rightarrow \quad \hat{\mathbf{w}}(\xi, \mathbf{w}_L, \mathbf{w}_R) \in \mathcal{U} \text{ for any value of } \xi.$$

Proof. We adapt the ideas of [22], initially introduced for the Suliciu relaxation schemes. We remark first that $(H, \mathfrak{e}) \to p(H, \mathfrak{e})$ satisfies the following properties:

$$\forall H, \mathfrak{e} > 0, \quad \partial_H(H\sqrt{\partial_H p(H, \mathfrak{e})}) > 0, \tag{5.46}$$

$$H\sqrt{\partial_H p(H, \mathfrak{e})} \underset{H\to\infty}{\to} \infty, \tag{5.47}$$

$$\partial_H(H\sqrt{\partial_H p(H, \mathfrak{e})}) \le \frac{3}{2}\sqrt{\partial_H p(H, \mathfrak{e})}, \tag{5.48}$$

and thus, there exists, for each value of $\mathfrak{e}$, an inverse function $\psi(., \mathfrak{e}) : (0, \infty) \to (0, \infty)$ such that

$$H\sqrt{\partial_H p(H, \mathfrak{e})} = s \;\Leftrightarrow\; H = \psi(s, \mathfrak{e}).$$

Note also that (5.48) entails $\partial_s\psi(s, \mathfrak{e}) \ge \dfrac{2\psi(s, \mathfrak{e})}{3s}$, and as $\partial_s(\psi(s, \mathfrak{e})s^{-\frac{2}{3}}) \ge 0$, we have:

$$\psi(\lambda s; \mathfrak{e}) \ge \lambda^{\frac{2}{3}}\psi(s, \mathfrak{e}), \ \forall \lambda \ge 1. \tag{5.49}$$

Step 1. We show that for any given $s_R > 0$, the choice

$$\frac{s_L}{H_L} = \sqrt{\partial_H p(H_L, \mathfrak{e}_L)} + \frac{3}{2}\Big(\frac{\Delta p_{LR}}{s_R} + \bar{v}_L - \bar{v}_R\Big)_+,$$

ensures that

$$\frac{1}{H_L^\star} = \frac{1}{H_L} + \frac{s_R(\bar{v}_R - \bar{v}_L) - \Delta p_{LR}}{s_L(s_L + s_R)} \ge \frac{1}{\psi(s_L, \mathfrak{e}_L)} > 0.$$

Indeed, if $s_R(\bar{v}_R - \bar{v}_L) - \Delta p_{LR} \ge 0$, we have $s_L = H_L\sqrt{\partial_H p(H_L, \mathfrak{e}_L)}$ and $H_L = \psi(s_L, \mathfrak{e}_L)$, giving the expected result. If $s_R(\bar{v}_R - \bar{v}_L) - \Delta p_{LR} < 0$, then it is equivalent to show that

$$1 - \frac{s_R}{s_L + s_R}\frac{X}{\sqrt{\partial_H p(H_L, \mathfrak{e}_L)} + \frac{3}{2}X} \ge \frac{H_L}{\psi(s_L, \mathfrak{e}_L)},$$

with $X = \frac{\Delta p_{LR}}{s_R} + \bar{v}_L - \bar{v}_R$. Introducing $\theta = \dfrac{\sqrt{\partial_H p(H_L, \mathfrak{e}_L)}}{\sqrt{\partial_H p(H_L, \mathfrak{e}_L)} + \frac{3}{2}X}$, a sufficient condition is

$$1 - \frac{2(1-\theta)}{3} - \frac{H_L}{\psi\Big(H_L(\sqrt{\partial_H p(H_L, \mathfrak{e}_L)} + \frac{3}{2}X), \mathfrak{e}_L\Big)} \ge 0. \tag{5.50}$$

Using (5.49), we see that (5.50) holds if we have $1 - \frac{2(1-\theta)}{3} - \theta^{\frac{2}{3}} \geq 0$, which is always true for $0 < \theta \leq 1$.

Note that the symmetric result holds: for all $s_L > 0$, the choice

$$\frac{s_R}{H_R} = \sqrt{\partial_H p(H_R, \mathfrak{e}_R)} + \frac{3}{2}\Big(\frac{-\Delta p_{LR}}{s_L} + \bar{v}_L - \bar{v}_R\Big)_+,$$

ensures that

$$\frac{1}{H_R^\star} = \frac{1}{H_R} + \frac{s_L(\bar{v}_R - \bar{v}_L) + \Delta p_{LR}}{s_L(s_L + s_R)} \geq \frac{1}{\psi(s_R, \mathfrak{e}_R)} > 0,$$

Step 2. Let assume $\Delta p_{LR} \geq 0$ and define s_L, s_L following (5.44). As $s_L \geq 0$, the symmetric result of the previous step directly ensures that $1/H_R^\star > 0$. Additionally, if $s_R(\bar{v}_R - \bar{v}_L) - \Delta p_{LR} \geq 0$, we obviously have

$$\frac{1}{H_L^\star} = \frac{1}{H_L} + \frac{s_R(\bar{v}_R - \bar{v}_L) - \Delta p_{LR}}{s_L(s_L + s_R)} \geq \frac{1}{H_L} > 0.$$

Now, if $s_R(\bar{v}_R - \bar{v}_L) - \Delta p_{LR} \leq 0$, as $s_R \geq H_R\sqrt{\partial_H p(H_R, \mathfrak{e}_R)}$, we have $s_L \geq \tilde{s_L}$, with

$$\frac{\tilde{s}_L}{H_L} = \sqrt{\partial_H p(H_L, \mathfrak{e}_L)} + \frac{3}{2}\Big(\frac{\Delta p_{LR}}{s_R} + \bar{v}_L - \bar{v}_R\Big)_+.$$

Using **Step 1**, we obtain

$$\frac{1}{H_L} + \frac{s_R(\bar{v}_R - \bar{v}_L) - \Delta p_{LR}}{\tilde{s_L}(\tilde{s_L} + s_R)} \geq \frac{1}{\psi(\tilde{s_L}, \mathfrak{e}_L)}.$$

As $\frac{-1}{s(s+s_R)}$ is an increasing function of $s > 0$, we have

$$\frac{1}{H_L^\star} = \frac{1}{H_L} + \frac{s_R(\bar{v}_R - \bar{v}_L) - \Delta p_{LR}}{s_L(s_L + s_R)} \geq \frac{1}{H_L} + \frac{s_R(\bar{v}_R - \bar{v}_L) - \Delta p_{LR}}{\tilde{s_L}(\tilde{s_L} + s_R)} \geq \frac{1}{\psi(\tilde{s_L}, \mathfrak{e}_L)} > 0.$$

We also observe that assuming $\mathfrak{e}_L, \mathfrak{e}_R \geq 0$, then according to (5.38e) we obviously have $\mathfrak{e}_L^\star, \mathfrak{e}_R^\star \geq 0$. □

5.3.5.2 Positivity of the lowest-order approximation

Now, we use the previous approximate Riemann solver to design some discrete formulations that preserve the positivity of H and $\mathfrak{e}$. We first consider the lowest-order fully discrete approximation (Finite-Volume).

Proposition 5.7. *The lowest-order numerical scheme, obtained by setting $k = 0$ and $\varphi_h = 1$ in (5.32a) with interface numerical fluxes built from the approximate Riemann solver (5.36), wave speed estimates (5.41)-(5.44)-(5.45) and a first-order Euler time discretization, preserves the invariant domain $\mathcal{U}$ under the following CFL-like condition:*

$$\Delta t^n = \min_{T\in\mathcal{T}_h}\Big(\frac{h_T}{\lambda_T}\Big), \quad \lambda_T := \max_{F\in\mathcal{F}_T}\left(|\lambda_F^-|, |\lambda_F^+|\right). \tag{5.51}$$

Proof. Let denote by $\bar{\mathbf{w}}_T^n$ the piecewise constant approximations (mean values) of $\mathbf{w}$ at discrete time t^n on mesh element T. Setting $k = 0$ and $\varphi_h = 1$ in (5.32a) and using a first-order Euler time discretization, the resulting Finite-Volume scheme reads as follows:

$$\frac{h_T}{\Delta t^n}(\bar{\mathbf{w}}_T^{n+1} - \bar{\mathbf{w}}_T^n) + \sum_{\substack{F\in\mathcal{F}_T \\ F\subset\partial T\cap\partial T_e}} \mathbb{F}_h(\bar{\mathbf{w}}_T^n, \bar{\mathbf{w}}_{T_e}^n)\mathbf{n}_{TF} + \int_T \mathbb{D}_T - \int_T \mathbb{B}(\mathbf{w}_T, b_T) = 0. \tag{5.52}$$

Assuming that for all $T \in \mathcal{T}_h$, $\bar{\mathbf{w}}_T^n \in \mathcal{U}$, Proposition 5.6 ensures that the associated approximate Riemann solver (5.36) associated with $\mathbb{F}_h(\bar{\mathbf{w}}_T^n, \bar{\mathbf{w}}_{T_e}^n)$ satisfies, at each interface x_F such that $F \subset \partial T \cap \partial T_e$:

$$\forall (t,x) \in (t^n, t^{n+1}] \times (x_T, x_{T_e}), \qquad \hat{\mathbf{w}}(\frac{x - x_F}{t - t^n}, \bar{\mathbf{w}}_T^n, \bar{\mathbf{w}}_{T_e}^n) \in \mathcal{U}.$$

Then, it is a classical result to show that for all $T \in \mathcal{T}_h$, $\bar{\mathbf{w}}_T^{n+1} \in \mathcal{U}$ under the CFL-like condition (5.54).

$$\Delta t^n \leq \min_{T\in\mathcal{T}_h}\Big(\frac{h_T}{\lambda_T}\Big), \quad \lambda_T := \max_{F\in\mathcal{F}_T} \left(|\lambda_F^-|, |\lambda_F^+|\right),$$

in which λ_F^- and λ_F^+ are the speed estimates obtained from (5.41)-(5.44)-(5.45). This final result relies on the fact that the topography and dispersive source terms do not contribute to the time evolution of H and $\mathfrak{e}$ and that the corresponding numerical schemes therefore updates values from a convex averaging of the states that appear in the approximate Riemann problem, see for instance [16, 22].

□

5.3.5.3 Positivity for higher-order approximations

Now, we consider an arbitrary order of approximation $k \geq 1$. Setting $\varphi_h = 1$ in (5.32a), using a first-order Euler time discretization and denoting by $\bar{\mathbf{w}}_T^n$ the mean values of $\mathbf{w}_h$ at discrete time t^n on mesh element T, the fully discrete formulation satisfied by the state vector averages reads as follows:

$$\frac{h_T}{\Delta t^n}(\bar{\mathbf{w}}_T^{n+1} - \bar{\mathbf{w}}_T^n) + \sum_{F\in\mathcal{F}_T} \mathbb{F}_h(\mathbf{w}_F^-, \mathbf{w}_F^+)\mathbf{n}_{TF} + \int_T \mathbb{D}_T - \int_T \mathbb{B}(\mathbf{w}_T, b_T) = 0, \tag{5.53}$$

where $\mathbf{w}_F^-, \mathbf{w}_F^+$ respectively stand for the interior and exterior traces of $\mathbf{w}_h$ on F, with respect to mesh element T. Following [172], let consider the τ-points Gauss-Lobatto quadrature rule $\{x_i^T,\ 1 \leq i \leq \tau\}$ on mesh element T (with $\tau \geq 2$), and the corresponding quadrature weights $\{\hat{w}_i,\ 1 \leq i \leq \tau\}$ such that $\sum_{i=1}^q \hat{w}_i = 1$. This quadrature rule allows to exactly compute integrals of polynomials up to degree $2\tau - 3$. In particular, choosing $\tau = \lceil (k+3)/2 \rceil$, we have:

$$\forall T \in \mathcal{T}_h, \quad \bar{\mathbf{w}}_T^n = \frac{1}{h_T}\int_T \mathbf{w}_T^n = \sum_{i=1}^{\tau} \hat{w}_i \mathbf{w}_T^n(x_i^T).$$

We have the following result:

Proposition 5.8. *Assume that for all $T \in \mathcal{T}_h$, $\bar{\mathbf{w}}_T^n \in \mathcal{U}$ and for all $i \in \{1,\dots,\tau\}, \mathbf{w}_T^n(x_i^T) \in \mathcal{U}$. Then the scheme (5.53), satisfied by the averaged values of the state vector, with interface numerical fluxes*

built from the approximate Riemann solver (5.36)*, and wave speed estimates* (5.41)-(5.44)-(5.45)*, preserves the invariant domain* $\mathcal{U}$ *under the following CFL-like condition:*

$$\Delta t^n \leq \hat{w}_1 \min_{T\in\mathcal{T}_h}\Big(\frac{h_T}{\lambda_T}\Big), \quad \lambda_T := \max_{F\in\mathcal{F}_T}\left(|\lambda_L^F|, |\lambda_R^F|\right). \tag{5.54}$$

Proof. Remarking that the dispersive source term $\int_T \mathbb{D}_T$ do not contribute to the first and fourth equations (respectively on H_h and $\mathfrak{e}_h$) in (5.53), the proof follows the lines of Proposition 3.2 in [172], taking benefits from the robustness of the lowest-order scheme established in Proposition 5.7. □

To enforce the conditions of this last Proposition, we need to modify H_h^n and $\mathfrak{e}_h^n$ so that for all $T \in \mathcal{T}_h$ and for all $i \in \{1,\dots,\tau\}$ we have $H_T^n(x_i^T) \geq 0$ and $\mathfrak{e}_T^n(x_i^T) \geq 0$. This can be achieved by using the high-order accuracy preserving limiter of [172] on both variables H_h^n and $\mathfrak{e}_h^n$. This consists in replacing, for each mesh element $T \in \mathcal{T}_h$, the polynomials H_T^n and $\mathfrak{e}_T^n$ by the following modified polynomials, before computing $\mathcal{A}_h(\mathbf{w}_h^n)$:

$$\hat{H}_T^n = \min\Big\{1, \frac{\bar{H}_T^n - \kappa}{\bar{H}_T^n - \min\limits_{1\leq i\leq\tau} H_T^n(x_T^i)}\Big\}(\bar{H}_T^n - H_T^n) + \bar{H}_T^n, \tag{5.55}$$

$$\hat{\mathfrak{e}}_T^n = \min\Big\{1, \frac{\bar{\mathfrak{e}}_T^n - \kappa}{\bar{\mathfrak{e}}_T^n - \min\limits_{1\leq i\leq\tau} \mathfrak{e}_T^n(x_T^i)}\Big\}(\bar{\mathfrak{e}}_T^n - \mathfrak{e}_T^n) + \bar{\mathfrak{e}}_T^n, \tag{5.56}$$

where $\bar{H}_T^n$ and $\bar{\mathfrak{e}}_T^n$ are respectively the mean values of H_T^n and $\mathfrak{e}_T^n$ on T and κ is a small threshold value (we set $\kappa = 1.0^{-10}$ in the numerical applications). This limitation process ensures the positivity at the required quadrature nodes, while preserving the mean values of the limited quantities, as well as the expected accuracy of the approximation.

Remark 5.9. *This analysis can be extended to high-order in time SSP-RK schemes, see Section 5.3.4, relying on the fact that the intermediate stages* $\mathbf{w}_h^{n,i}$ *are obtained as convex combinations of forward Euler sub-steps. As a consequence, the fully discrete formulations with a high-order SSP time discretization will still preserve the invariant domain* $\mathcal{U}$*. The limiters* (5.55) *and* (5.56) *should be applied at each stage of the RK method.*

5.3.5.4 Well-balancing for motionless steady states

Motionless steady states for equations (5.19a)-(5.19b) are defined by

$$\zeta = 0, \quad \bar{v} = 0, \quad \mathfrak{v}^\sharp = 0, \quad \mathfrak{e} = 0.$$

The preservation of motionless steady states may be achieved following one of the already existing approaches, the reader is referred for instance to [61, 172]. Note that such a well-balancing property for our SGN formulations may be inherited from the corresponding property obtained for the NSW equations provided that the discrete formulation (5.32b) associated with elliptic problems is well-defined. We choose not to recall the details of these reconstruction as it has been extensively applied and validated in some of our previous works, see for instance [59, 60].

5.4 Numerical validation and applications

In this section, we validate the discrete formulations of Section 5.3 through several benchmark problems. In all the test cases, the time step restriction is computed according to (5.40). Exploiting the symmetry of the discrete bilinear forms, the sparse linear systems are solved using a Cholesky methods. Of course, when the vorticity vanishes, we recover the classical SGN equations, and we directly focus on the validation of the model with nonzero vorticity.

5.4.1 Rotational solitary wave with constant vorticity

In the first test, we focus on the simplified case of constant vorticity. One can choose to solve the general system (5.19) or the simplified model (5.14) and of course, both provide exactly the same results. We compute the propagation of a rotational solitary wave over a flat bottom, in a domain of 200 m long. Following [98], the initial water height $H(0,x)$ is computed as the solution of

$$\frac{c}{3}\big(cH_0^2 - H_0\omega_0 H^2\big)H_x^2 = (H-H_0)^2\Big(c^2 - gH - \frac{H(H+2H_0)}{12}\omega_0^2\Big), \tag{5.57}$$

and the corresponding velocity is initialized as

$$\bar{v}(0,x) = c(1 - \frac{H_0}{H(0,x)}). \tag{5.58}$$

Still following the notations of [98], we have $\tilde{E}_\infty = \frac{1}{12}H_0\omega_0^2 > 0$, $v_\infty^\sharp = H_0\omega_0 > 0$ and the celerity $\underline{c}$ of the right solitary wave is given by

$$\underline{c} = \Big(gH_0(1+\varepsilon) + \frac{H_0^2(1+\varepsilon)(3+\varepsilon)}{12}\omega_0^2\Big)^{\frac{1}{2}}. \tag{5.59}$$

We set $\omega_0 = 0.3\,s^{-1}$, $\varepsilon = 0.1$ and the solitary wave is initially centred at $x_0 = 25\,m$. We compute the time evolution up to $t_{\max} = 40\,s$, with $|\mathcal{T}_h| = 200$ mesh elements, leading to a uniform meshsize $h = 1\,m$.

5.4.2 Rotational solitary wave with general vorticity

In the second test case, we consider the case of a general vorticity. Equations (5.19) admit two solitary wave solutions of opposite velocities given by

$$\pm\,\underline{c} = \pm\Big(gH_0(1+\varepsilon) + \frac{(1+\varepsilon)(3+\varepsilon)}{H_0}E_\infty\Big)^{\frac{1}{2}}, \tag{5.60}$$

and with different profiles. We set $E_\infty = 0.2\,m^3.s^{-2}$ and $v_\infty^\sharp = 1.6\,m.s^{-1}$, together with $\varepsilon = 0.1$, ensuring the existence of both left and right-going waves, leading to the profiles shown on the left of Figure 5.3 and Figure 5.4 respectively for the right-going and the left-going waves. The initial water height $H(0,x)$ is computed as the solution of

$$\frac{c}{3}\big(cH_0^2 - v_\infty^\sharp H^2\big)H_x^2 = (H-H_0)^2\Big(c^2 - gH - \frac{H(H+2H_0)}{H_0^3}E_\infty\Big), \tag{5.61}$$

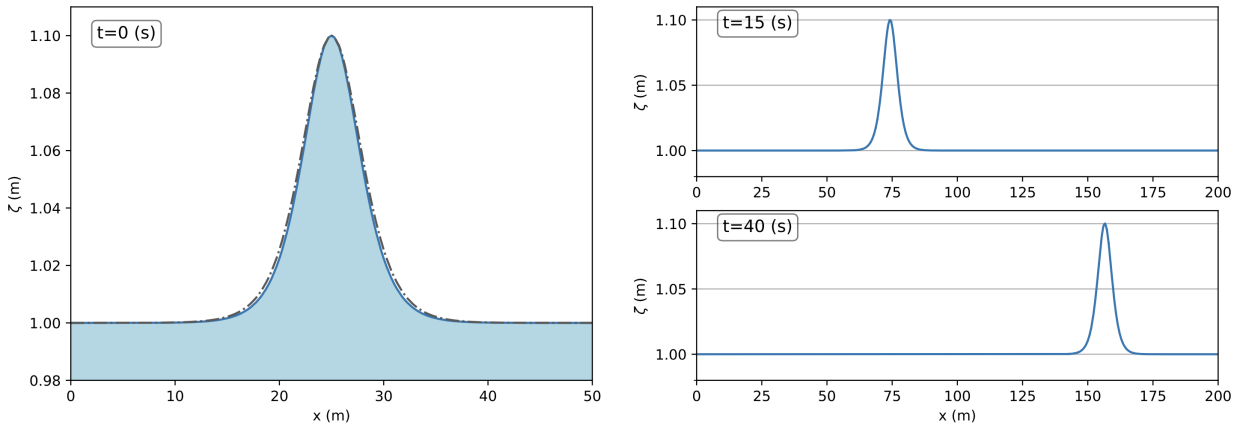


Figure 5.2: Rotational solitary wave with constant vorticity - On the left: initial free surface (in blue) and profile of the irrotational wave (in grey dot line). On the right: snapshot of the free surface at $t = 25\,s$ and $t = 40\,s$.

the corresponding velocity is initialized as in (5.58) and we set

$$\mathfrak{v}^\sharp(0,x) = \frac{H(0,x)}{H_0} v_\infty^\sharp, \qquad \mathfrak{e}(0,x) = \frac{H(0,x)^3}{H_0^3} E_\infty. \tag{5.62}$$

As in the previous case, the computational domain is $\Omega = [0, 200]$. The right-going wave is initially centred at $x = 50\,m$ and the left-going wave at $x = 150\,m$ and the propagation is computed up to $t_{\max} = 30\,s$. The time evolution of both right-going and left-going waves is shown on the right of Figure 5.3 and Figure 5.4 respectively. For these computations, we set $|\mathcal{T}_h| = 200$ and $k = 2$. We observe the preservation of the initial profiles, together with a very low numerical dissipation for the considered time interval.

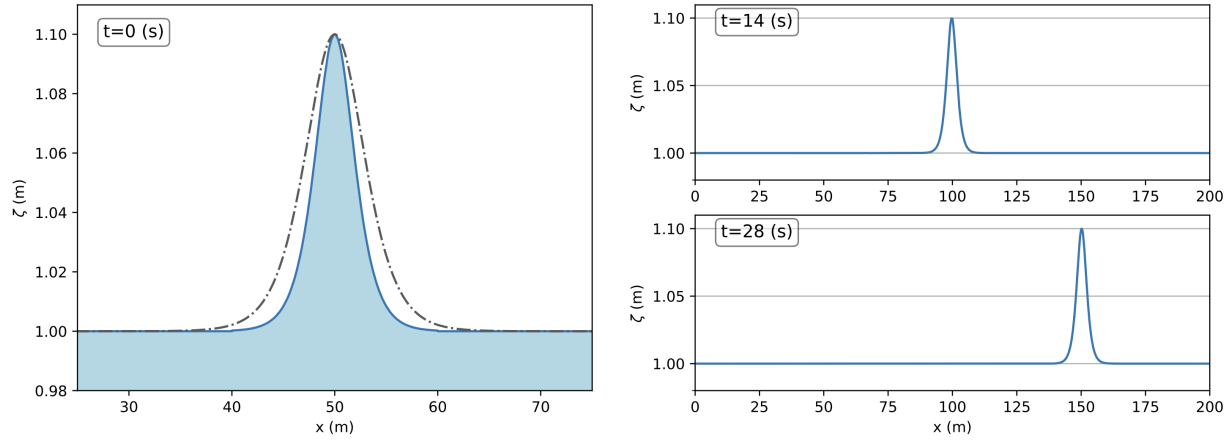


Figure 5.3: Rotational solitary wave with general vorticity: right-going wave - On the left: initial free surface (in blue) and profile of the irrotational wave (in grey dot line). On the right: snapshot of the free surface at $t = 14\,s$ and $t = 28\,s$.

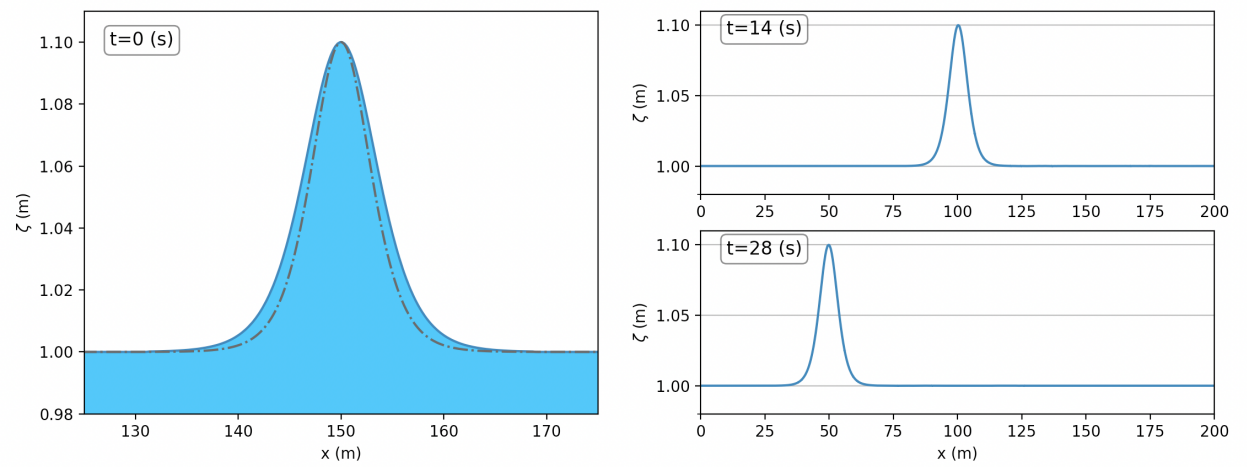


Figure 5.4: Rotational solitary wave with general vorticity: left-going wave - On the left: initial free surface (in blue) and profile of the irrotational wave (in grey dot line). On the right: snapshot of the free surface at $t = 14\,s$ and $t = 28\,s$.

We also perform a numerical convergence analysis relying on a sequence of refined meshes and a reference solution computed with $k = 5$ and $|\mathcal{T}_h| = 2000$. The L^2-error between the current numerical solution and this reference solution at $t = 0.1\,s$ is computed for $k = 2,3,4$ and the sequence of refined meshes. The resulting convergence rates for the water height are reported on Figure 5.5.

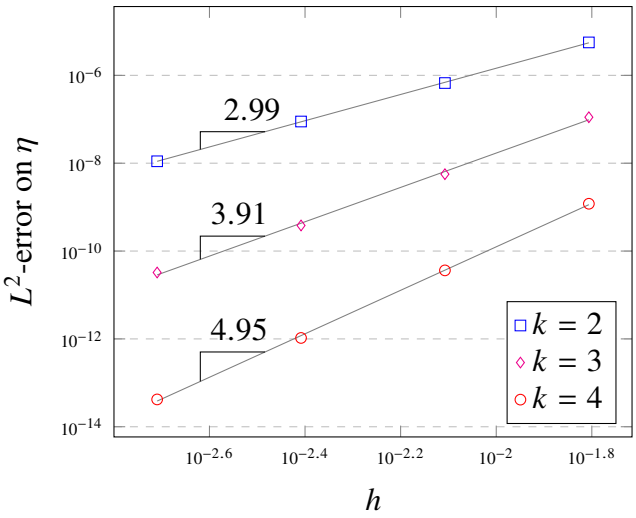


Figure 5.5: Test 1 - Rotational solitary wave propagation: L^2-errors for the water height η at $t = 0.1\,s$ vs. h, for polynomial orders $k = 2,3,4$.

5.4.3 Collision of rotational solitary waves

In the third test case, we simulate two rotational solitary waves (with general vorticity) of initial (relative) height $\epsilon = 0.2$, propagating in opposite directions in a channel of $400\,m$ long. The

collision of solitary waves is known to introduce additional challenges to the model by a sudden change of the nonlinear and frequency dispersion characteristics. Here, we add rotational effects and focus on their impact during the collision.

In a first computation, we set $v_\infty^\sharp = 0$ so that left-going and right-going solitary waves have similar profiles. We also set $E_\infty = 1.0\, m^3 s^{-2}$ and the flow variables are initialized with (5.58)-(5.61)-(5.62). The right-going solitary wave is initially centred at $x = 150\, m$ and the left-going wave is initially centred at $x = 250\, m$. The computation relies on $|\mathcal{T}_h| = 1200$ mesh elements and we set $k = 2$. The situation is qualitatively very similar to the irrotational case but: *i*) the speed $\underline{c}$ defined in (5.60) is larger than in the irrotational case, *ii*) the solitary waves becomes narrower as E_∞ increases. To highlight these differences, we show on Figure 5.6 several snapshots of the free surface elevation observed at several time during the propagation. The free surface of the corresponding solitary wave solution in the irrotational case is also plotted in orange for comparison purpose.

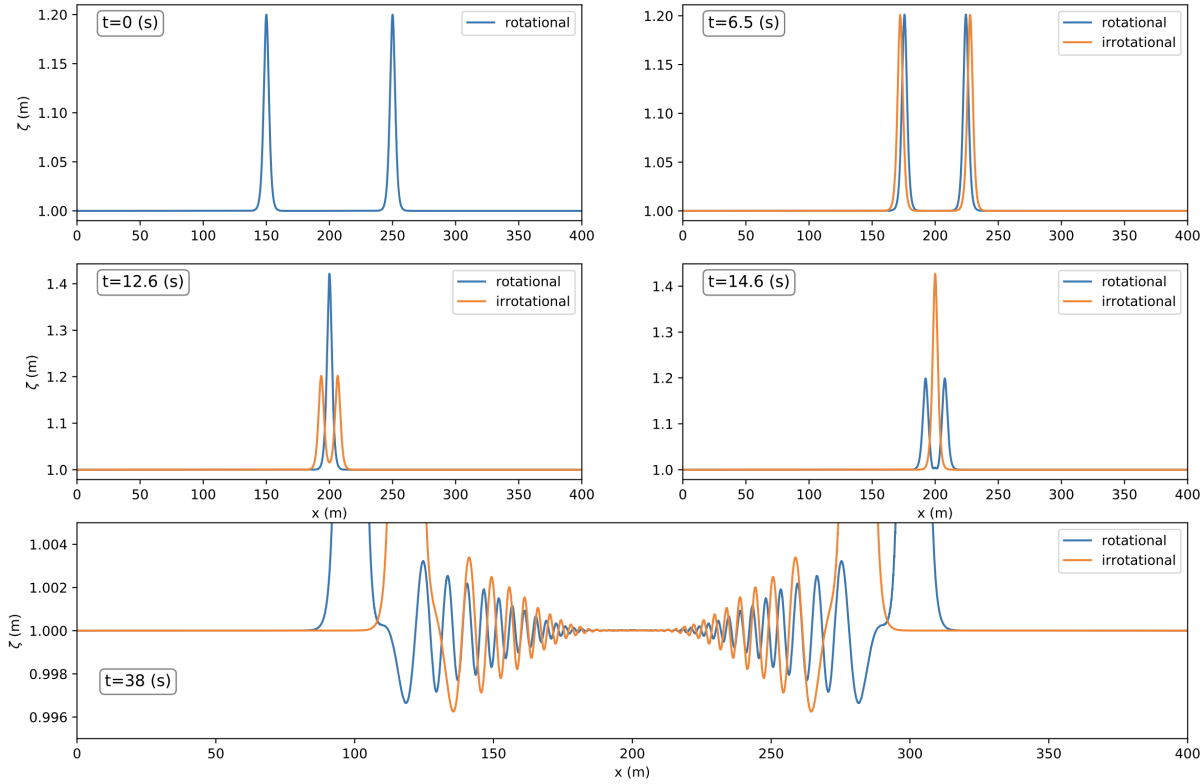


Figure 5.6: Collision of rotational solitary waves - Case $\varepsilon = 0.2$, $v_\infty^\sharp = 0\, ms^{-1}$ and $E_\infty = 1\, m^3 s^{-2}$ - Snapshots of the free surface at several times during the propagation. The rotational solitary waves are plotted in blue, the corresponding irrotational waves are plotted in orange.

In a second computation, we set $v_\infty^\sharp = 1.6\, ms^{-1}$ and $E_\infty = 0.2\, m^3 s^{-2}$, so that both waves exists but the right-going solitary wave has a narrower profile than the left-going one. Again, we set $|\mathcal{T}_h| = 1200$ and $k = 2$. The different profiles for right-going and left-going waves are expected to induce non-symmetric oscillations in the corresponding dispersive tails that are observed after the collision. And indeed, we show on Figure 5.7 some snapshots of the waves profiles during

the evolution, with a zoom on the dispersive tails observed after the collision, and we observe a particular modulation that shapes the dispersive tail of the right-going wave (which is the narrower wave). This oscillating tail also appears to be shorter than the one of the left-going wave, which is more comparable to the dispersive tail that is usually observed with irrotational flows. These two tests demonstrates the capability of the proposed discrete formulation to handle strong nonlinearity and dispersion in rotational solitary waves.

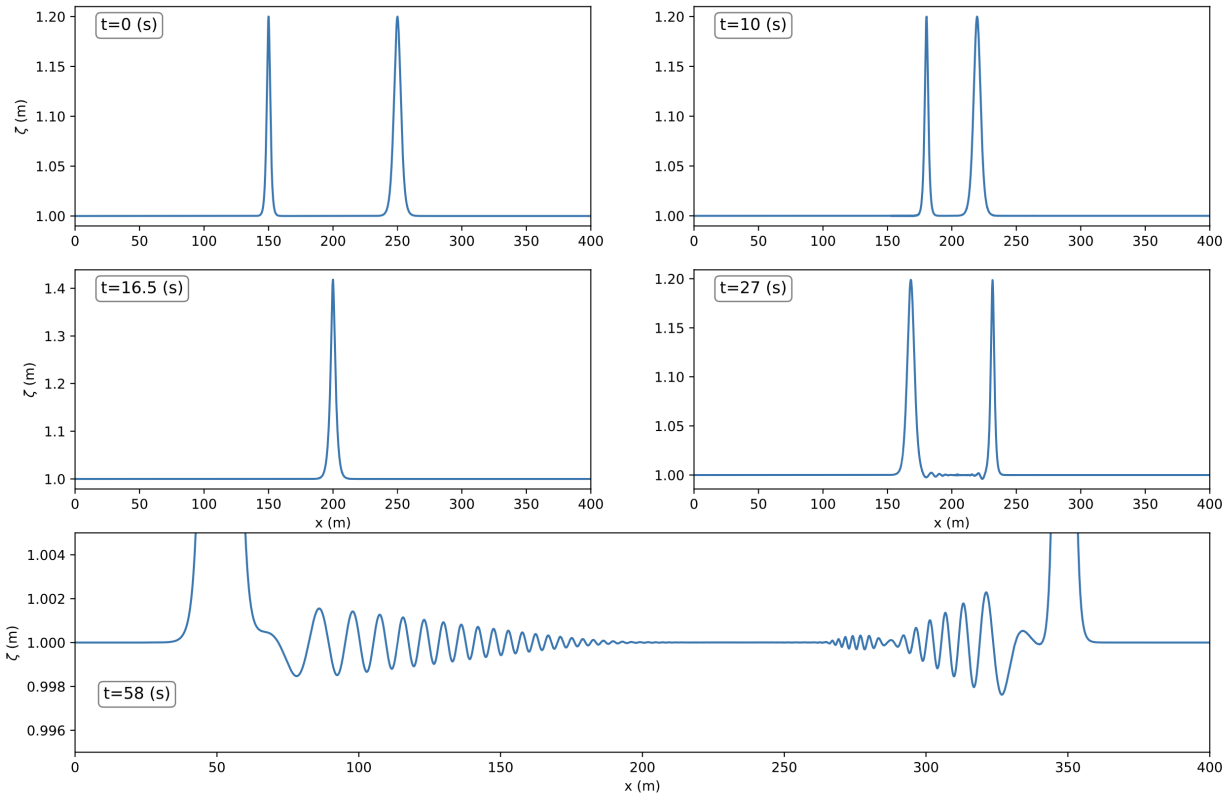


Figure 5.7: Collision of rotational solitary waves - Case $v_\infty^\sharp = 1.6\,ms^{-1}$ and $E_\infty = 0.2\,m^3s^{-2}$ - Snapshots of the free surface at several times during the propagation.

5.4.4 Shoaling of rotational solitary waves

In this subsection, we aim at qualitatively studying the shoaling of rotational solitary waves over a varying topography. As a first assessment, we reproduce the test initially proposed in [98] with a WENO method. We consider a $200\,m$ long channel with $H_0 = 1\,m$ and the topography is defined as follows

$$b(x) = \frac{H_0}{10}\left(1 + \tanh\left(\frac{x - x_c}{\lambda}\right)\right),$$

with $x_c = 100\,m$ and $\lambda = 20\,m$. A right-going rotational solitary wave corresponding to the choice $E_\infty = 0.2\,m^3s^{-2}$, $v_\infty^\sharp = -1.5\,ms^{-1}$ is initially centered at $x = 20\,m$ and propagates with an initial celerity $c = 3.53\,m\,s^{-1}$ (the celerity associated with the irrotational solitary wave of similar relative amplitude is $3.43\,m\,s^{-1}$). We show on Figure 5.8 some snapshots of the free surface at several times during the propagation. For comparison purpose, we also plot in light blue the corresponding free

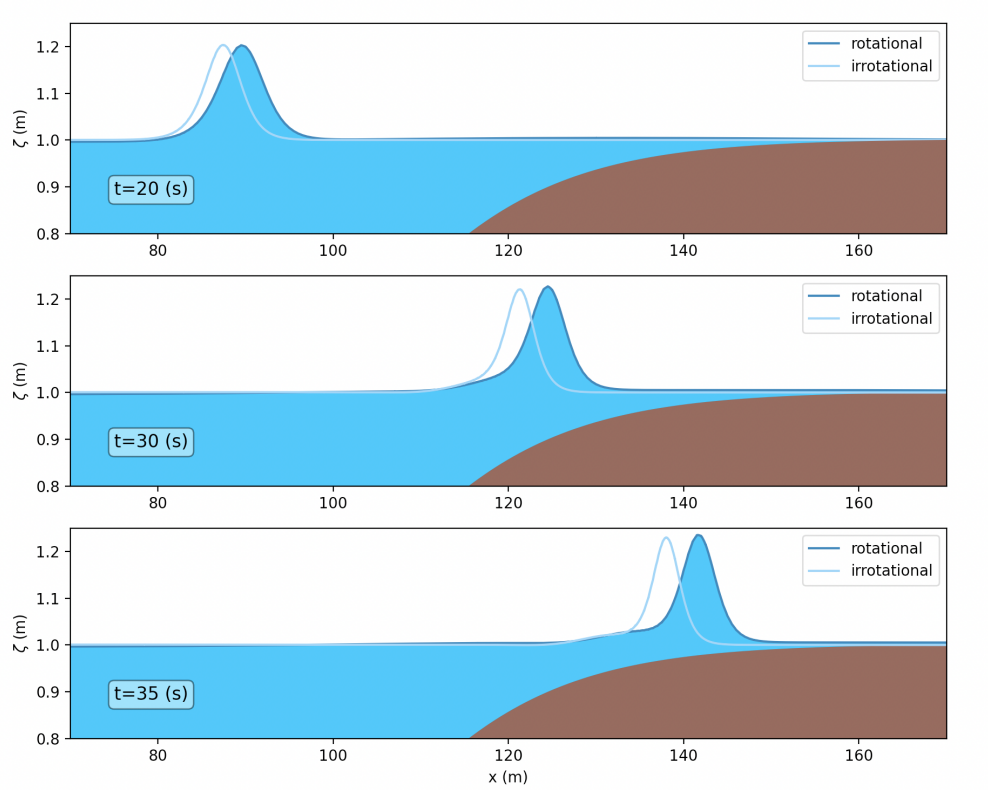


Figure 5.8: Shoaling of rotational solitary waves - Case $v_\infty^\sharp = -1.5\,ms^{-1}$ and $E_\infty = 0.2\,m^3s^{-2}$ - Snapshots of the free surface at times $t = 20\,s,\ 30\,s$ and $35\,s$.

surface of an irrotational solitary wave of similar relative amplitude.

To further investigate the influence of the rotational terms on wave shoaling, we place a wave gauge at $x = 140\,m$ and the corresponding time series of the free surface elevation for the rotational and irrotational waves are plotted on Figure 5.9. In a second test, we numerically reproduce the experimental set-up detailed in [75], for an incident solitary wave of relative amplitude $\epsilon = 0.2$, which propagates and breaks over a planar beach with a slope of $1 : 35$ in a computational domain of $85\,m$ long and a water level at rest $H_0 = 1\,m$.

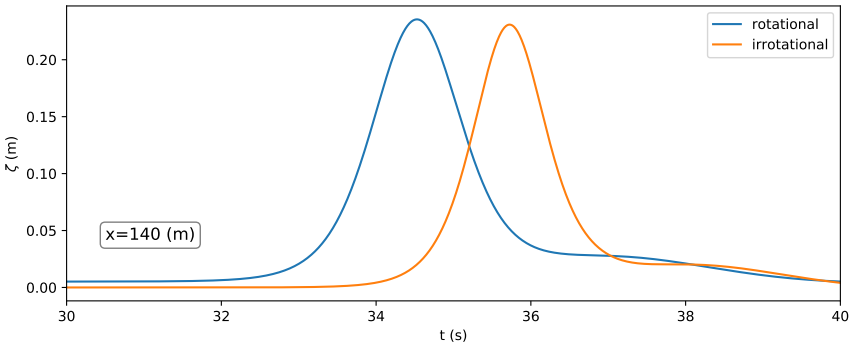


Figure 5.9: Shoaling of rotational solitary waves - Case $v_\infty^\sharp = -1.5\,ms^{-1}$ and $E_\infty = 0.2\,m^3s^{-2}$ - Time series of the surface elevation at $x = 140\,m$.

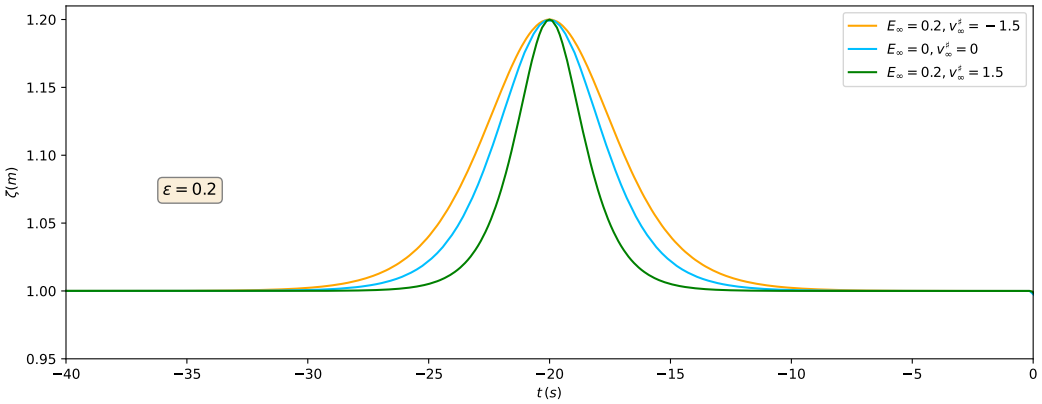


Figure 5.10: Shoaling of rotational solitary waves - Three different initial solitary waves for the experimental set-up of [75].

We perform the computations with three different solitary waves, corresponding to the following values: *i)* $v_\infty^\sharp = -1.5\,ms^{-1}$ and $E_\infty = 0.2\,m^3s^{-2}$, *ii)* $v_\infty^\sharp = 0\,ms^{-1}$ and $E_\infty = 0\,m^3s^{-2}$, *iii)* $v_\infty^\sharp = 1.5\,ms^{-1}$ and $E_\infty = 0.2\,m^3s^{-2}$. These three sets of values lead to the three initial wave profiles shown on Figure 5.10. Note that the blue wave profile is the solitary wave classically obtained in the irrotational case. We set $|\mathcal{T}_h| = 200$ and $k = 2$ and compute the waves propagation over the uneven bottom up to the breaking point. Numerical results are shown on Figure 5.11 as time series of the free surface measured from four different wave gauges located at $x_1 = 20.96\,m, x_2 = 22.55\,m, x_3 = 23.68\,m, x_4 = 24.68\,m$. We observe a slightly increase shoaling in the two situations involving a non-zero vorticity.

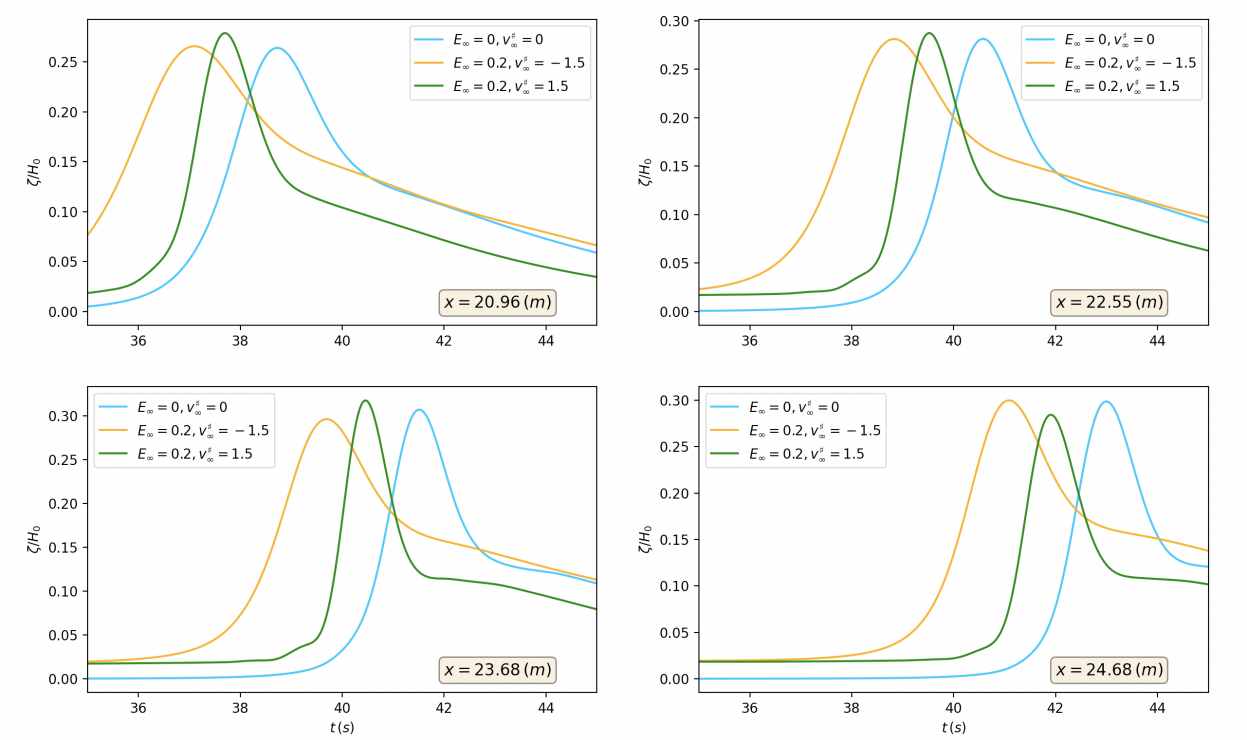


Figure 5.11: Shoaling of rotational solitary waves - Time series of the surface elevations at four locations along the channel.

5.4.5 Run-up of rotational solitary waves

To conclude this section, we focus on the ability of the proposed discrete formulation to deal with the occurence of dry areas. Considering the experimental set-up initially proposed in [153], we study the run-up of a rotational solitary wave over a beach with constant slope 1:19.85, in a $100\,m$ long domain. The incident wave is supplied using (5.61), with a water level at rest $H_0 = 1m$ and a relative amplitude $\varepsilon = 0.02\,m$. We recall that in this work, we do not introduce any mathematical and numerical treatment that may allow to consider the occurrence of wave-breaking in a stable way. We also recall that irrotational flows, $\varepsilon = 0.02\,m$ is the threshold amplitude which prevents wave-breaking from occurring. As weakly sheared flows are considered within equations (5.19) (as assumed in the derivation proposed in [25]), we observe that such a threshold value for non-breaking waves may reasonably also be used for the particular rotational flow under study in this test. For the solitary waves provided by (5.61), and for any given value of E_∞, positive values of $v_\infty^\sharp$ lead to narrower wave profiles. Our numerical investigations show that wave-breaking tends to occur slightly sooner for solitary waves with narrower profiles. Hence, we choose here to set $E_\infty = 0.2\,m^3\,s^{-2}$ and $v_\infty^\sharp = -0.2\,m\,s^{-1}$, as negative values for $v_\infty^\sharp$ lead to larger wave profiles. The mesh is set to $|\mathcal{T}_h| = 500$ elements and the polynomial order to $k = 2$. The solitary wave is initially centered at $x = 40\,m$. The wave propagation is computed up to $t = 30\,s$, after the wave run-up and reflection. The resulting numerical results are plotted on Figure 5.12. The computation is performed in a stable way and the preservation of the positivity of the water height and the second order moment is ensured. In particular, the run-up is computed in a stable way for this augmented

set of equations, without any spurious oscillations and we do not have to artificially cancel the dispersive correction in the vicinity of dry areas.

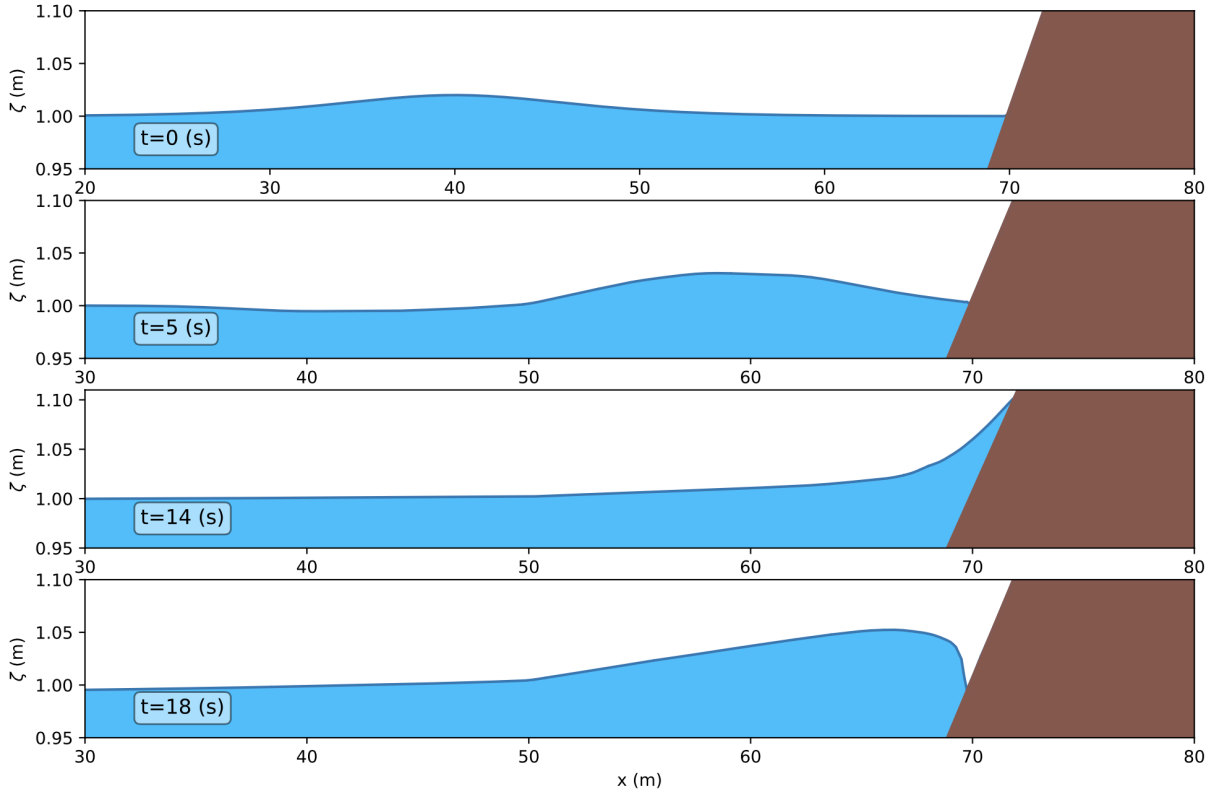


Figure 5.12: Run-up of rotational solitary waves - Case $\varepsilon = 0.02$, $E_\infty = 0.2\, m^3\, s^{-2}$ and $v_\infty^\sharp = -0.2\, m\, s^{-1}$ - Snapshots of the free surface at four times during the wave propagation.

Chapter 6

Conclusion et perspectives

Au cours de ces travaux, nous avons étudié et analysé des modèles d'écoulements de type Shallow water, à savoir, les équations de SGN avec et sans vorticity en 1d. La dérivation de ces équations est fournie dans le Chapitre 2, en détaillant les étapes de calcul fournies dans [25]. Nous avons ensuite proposé des schémas numériques capable d'approcher ces équations, en préservant les états d'équilibre au repos et produisant des hauteurs d'eau positives.

Nous avons dans un premier temps, étudié la construction d'une nouvelle formulation discrète de type Galerkin discontinue pour approcher la solution des équations SGN classiques dans un cadre horizontal unidimensionnel. Une nouvelle formulation discrète non conforme appartenant à la famille des méthodes Galerkin discontinues à pénalité intérieure symétrique pondérée (SWIP-DG) est introduite pour approcher avec précision les solutions de l'opérateur elliptique du second ordre apparaissant dans les équations SGN. La formulation discrète globale qui en résulte est ensuite validée par un ensemble étendu de cas test, y compris des études de convergence et des comparaisons avec des données tirées d'expériences. Le schéma présente l'avantage d'une formulation consistante, stable, coercive, et préserve les états d'équilibre au repos et elle est capable de produire des hauteurs d'eaux positives.

Nous nous sommes ensuite intéressé à l'étude des équations de SGN avec vorticité dérivées dans [25], ces équations SGN avec vorticité admettent une famille de solutions de types ondes solitaires. En prolongeant les travaux antérieurs développés pour l'étude des écoulements irrotationnels, nous avons reformulé les modèles comme un système pseudo-hyperbolique complété par des termes sources algébriques qui rende compte de la correction non hydrostatique et dispersive, ainsi que de l'interaction entre vorticité et effets dispersifs. Nous avons introduit une discrétisation DG globale pour les équations de SGN rotational, qui présente des propriétés intéressantes. Une méthode robuste de Runge-Kutta DG (RK-DG) est développée pour la partie hyperbolique du modèle. Cette méthode repose sur un solveur de Riemann HLLC adapté, spécialement conçu pour assurer la préservation de l'ensemble convexe d'états admissibles au niveau discret.

Concernant les perspectives, il est naturel de penser à considerer maintenant les extensions en

dimension 2 d'espace pour ces schémas. Aussi, il peut être intéressant d'utiliser le schéma proposé dans notre chapitre 5 pour les modèles de déferlement de [89, 137] et ainsi assurer la robustesse des schémas numériques pour ces modèles.

En outre, la question de la construction d'une méthode d'approximation pour les équations SGN à vorticité générale en gardant les termes du second ordre (5.15) est une question ouverte. Ces équations peuvent être reformulées ainsi:

$$\begin{cases} \partial_t H + \partial_x(H\bar{v}) = 0, & \text{(6.1a)} \\ (1 + \mathbf{T}[H,b])[\partial_t(H\bar{v}) + \partial_x(H\bar{v}^2)] + gH\partial_x\zeta + H\mathcal{Q}_1[H,b](\bar{v}) \\ \qquad + \partial_x(H^3\mathfrak{e}) + HC[H](H\mathfrak{v}^\sharp, \bar{v}) = 0, & \text{(6.1b)} \\ \partial_t(H\mathfrak{v}^\sharp) + \partial_x(H\bar{v}\mathfrak{v}^\sharp) = 0, & \text{(6.1c)} \\ \partial_t(H\mathfrak{e}) + \partial_x(H\bar{v}\mathfrak{e} + H^2\mathfrak{f}) + \partial_x(H^2)\mathfrak{f} = 0, & \text{(6.1d)} \\ \partial_t(H\mathfrak{f}) + \partial_x(H\bar{v}\mathfrak{f}) = 0, & \text{(6.1e)} \end{cases}$$

et nous voyons apparaitre deux difficultés supplémentaires: (i) le terme de flux "conservatif" dans l'équation d'évolution sur $\mathfrak{e}$ est modifié par rapport à la situation sans $\mathfrak{f}$, avec un nouveau terme en $\partial_x(H^2\mathfrak{f})$, (ii) il y a un terme *non-conservatif* en $\partial_x(H^2)\mathfrak{f}$ dans l'équation d'évolution sur $\mathfrak{e}$. La présence de ce terme non conservatif invalide la stratégie proposée ici pour assurer la positivité de $\mathfrak{e}$. Plus généralement, la question de la construction d'une formulation discrète pour ce système est intéressante. En oubliant provisoirement les termes dispersifs, et en ne gardant que les termes avec dérivées du premier ordre, pour lesquels nous pourrions être tenté de développer une méthode DG décentrée "hyperbolique", nous obtenons:

$$\begin{cases} \partial_t H + \partial_x(H\bar{v}) = 0, & \text{(6.2a)} \\ \partial_t(H\bar{v}) + \partial_x(H\bar{v}^2) + gH\partial_x\zeta + \partial_x(H^3\mathfrak{e}) = 0, & \text{(6.2b)} \\ \partial_t(H\mathfrak{v}^\sharp) + \partial_x(H\bar{v}\mathfrak{v}^\sharp) = 0, & \text{(6.2c)} \\ \partial_t(H\mathfrak{e}) + \partial_x(H\bar{v}\mathfrak{e} + H^2\mathfrak{f}) + \partial_x(H^2)\mathfrak{f} = 0, & \text{(6.2d)} \\ \partial_t(H\mathfrak{f}) + \partial_x(H\bar{v}\mathfrak{f}) = 0. & \text{(6.2e)} \end{cases}$$

Notons qu'en négligeant les termes en $\mathfrak{f}$ dans l'équation (6.2d), nous retrouvons le système étudié dans le chapitre précédent pour lequel le solveur de Riemann HLLC a été construit. Notons également que deux équations ont des termes non-conservatifs dans ce système: l'équation sur $H\bar{v}$ avec le terme classique en $gH\partial_x b$, et l'équation sur $H\mathfrak{e}$ avec le terme $\partial_x(H^2)\mathfrak{f}$ et qu'il est important d'essayer de traiter ce nouveau terme non-conservatif $\partial_x(H^2)\mathfrak{f}$ de façon appropriée afin d'essayer d'assurer la positivité de $\mathfrak{e}$.
Le système (6.2) peut maintenant s'écrire de manière plus compacte ainsi:

$$\partial_t \mathbf{w} + \partial_x \mathbb{F}(\mathbf{w}) = \mathbb{B}(\mathbf{w}, b), \tag{6.3}$$

avec

$$\mathbf{w} = \begin{pmatrix} \zeta \\ H\bar{v} \\ H\mathfrak{v}^\sharp \\ H\mathfrak{e} \\ H\mathfrak{f} \end{pmatrix}, \quad \mathbb{F}(\mathbf{w}) = \begin{pmatrix} H\bar{v} \\ \mathcal{F}(\mathbf{w}) \\ H\bar{v}\mathfrak{v}^\sharp \\ H\bar{v}\mathfrak{e} + H^2\mathfrak{f} \\ H\bar{v}\mathfrak{f} \end{pmatrix}, \quad \mathbb{B}(\mathbf{w}, b) = \begin{pmatrix} 0 \\ -gH\partial_x b \\ 0 \\ -\partial_x(H^2)\mathfrak{f} \\ 0 \end{pmatrix}, \tag{6.4}$$

with

$$\mathcal{F}(\mathbf{w}) = H\bar{v}^2 + p(H, \mathfrak{e}), \tag{6.5}$$

$$p(H, \mathfrak{e}) = \frac{1}{2} g H^2 + H^3 \mathfrak{e}. \tag{6.6}$$

Il est intéressant de constater que la matrice jacobienne $\mathbb{F}'(\mathbf{w})$ va maintenant dépendre aussi de $\mathfrak{f}$ et que ses valeurs propres aussi. Les premières études de l'algèbre associée à $\mathbb{F}'(\mathbf{w})$ montrent qu'il n'y a pas de formules explicites pour les valeurs propres, obtenues comme racines d'un polynôme de degré 5. Il est toutefois possible de fournir une description asymptotique de ces valeurs propres en fonction de μ, à la précision du modèle et de mettre ainsi en évidence la contribution de ce terme. Une piste de recherche pourrait ainsi être de construire un solveur de Riemann approché associé à ce système, en essayant de discrétiser convenablement le terme non-conservatif. Deux possibilités, au moins, peuvent être envisagées pour traiter ce terme non-conservatif: (i) proposer un modèle de relaxation adapté pour lequel ce terme est relaxé, (ii) traiter ce terme par une approche *path-conservative*.

Un autre thème de recherche nous ouvre certaines perspectives: nous travaillons sur des modèles asymptotiques de propagation d'ondes internes unidimensionnelles à l'interface entre deux couches de fluides non miscibles de densités différentes, sous hypothèse couvercle rigide et à fond plat [56, 58]. Un nouveau modèle de type Green-Naghdi dans le régime de Camassa-Holm (ou moyenne amplitude) est développé dans [57]. Ce modèle est pleinement justifié, dans le sens où il est cohérent, bien posé, et que ses solutions restent proches des solutions exactes du systèmes d'Euler complet avec des données initiales correspondantes. Le domaine de deux couches est infini dans l'espace horizontal variable (ici on travaille en d=1) et délimité en haut par un couvercle plat et rigide, et en bas par un fond plat. De plus, les fluides sont supposés homogènes, idéaux, incompressibles et irrotationnels. Ce modèle a été reformulé dans [23] pour améliorer sa dispersion fréquentielle et pour qu'il soit plus adapté à la résolution numérique, un schéma de splitting de second ordre a été developpé dans [23] pour la résolution du modèle de Green-Naghdi amélioré, où la partie hyperbolique du systéme est traité avec un schéma de volume finis d'ordre élevé et la partie de dispersion est traité avec une approache de différence finies. L'objectif de notre travail est de développé un schéma de type Galerkin discontinu d'ordre élevé pour l'approximation des solutions de modèle de Green-Naghdi amélioré en prolongeant nos travaux antérieurs.

Bibliography

[1] Michael B Abbott, Andrew D McCowan, and Ian R Warren. "Accuracy of short-wave numerical models". In: *Journal of Hydraulic Engineering* 110.10 (1984), pp. 1287–1301 (cit. on p. 16).

[2] N. Aissiouene et al. "A combined finite volume - finite element scheme for a dispersive shallow water system". In: *Networks and heterogeneous media* 11.2016 (2016), pp. 1–27 (cit. on pp. 13, 104).

[3] Vadym Aizinger and Clint Dawson. "A discontinuous Galerkin method for two-dimensional flow and transport in shallow water". In: *Advances in Water Resources* 25.1 (2002), pp. 67–84 (cit. on p. 15).

[4] F. Alcrudo and P. Garcia-Navarro. "A high-resolution Godunov-type scheme in finite volumes for the 2D shallow-water equations". In: *Internat. J. Numer. Methods Fluids* (1993) (cit. on p. 15).

[5] B. Alvarez-Samaniego and D. Lannes. "Large time existence for 3D water-waves and asymptotics". In: *Invent. math.* 171.3 (2008), pp. 485–541 (cit. on pp. 12, 74, 76, 77, 104, 107).

[6] J.S. Antunes do carmo, F.J. Seabra-Santos, and A.B. Almeida. "Numerical solution of the generalized Serre equations with the Mac-Cormack finite-difference scheme". In: *Int J Numer Methods Fluids* 16.725-738 (1993) (cit. on pp. 16, 75, 104).

[7] José S Antunes Do Carmo. "Boussinesq and Serre type models with improved linear dispersion characteristics: Applications". In: *Journal of hydraulic research* 51.6 (2013), pp. 719–727 (cit. on pp. 75, 104).

[8] Douglas N Arnold. "An interior penalty finite element method with discontinuous elements". In: *SIAM journal on numerical analysis* 19.4 (1982), pp. 742–760 (cit. on p. 15).

[9] Douglas N Arnold et al. "Unified analysis of discontinuous Galerkin methods for elliptic problems". In: *SIAM journal on numerical analysis* 39.5 (2002), pp. 1749–1779 (cit. on p. 15).

[10] E Audusse. "A multilayer Saint-Venant model: derivation and numerical validation". In: *Discrete Contin. Dyn. Syst. Ser. B* 5.2 (2005), pp. 189–214 (cit. on p. 13).

[11] E. Audusse, M.-O. Bristeau, and A. Decoene. "Numerical simulations of 3D free surface flows by a multilayer Saint-Venant model". In: *Internat. J. Numer. Methods Fluids* (2008) (cit. on p. 13).

[12] E. Audusse and M.O. Bristeau. “A well-balanced positivity preserving "second-order" scheme for shallow water flows on unstructured meshes”. In: *J. Comput. Phys.* 206.1 (2005), pp. 311–333 (cit. on p. 15).

[13] E. Audusse et al. “A fast and stable well-balanced scheme with hydrostatic reconstruction for shallow water flows”. In: *SIAM J. Sci. Comput.* 25.6 (2004), pp. 2050–2065 (cit. on p. 15).

[14] Garth A Baker. “Finite element methods for elliptic equations using nonconforming elements”. In: *Mathematics of Computation* 31.137 (1977), pp. 45–59 (cit. on p. 15).

[15] F. Bassi and S. Rebay. “A High-Order Accurate Discontinuous Finite Element Method for the Numerical Solution of the Compressible Navier–Stokes Equations”. In: *J. Comput. Phys.* 131 (1997), pp. 267–279 (cit. on p. 15).

[16] P. Batten et al. “On the choice of wavespeeds for the HLLC Riemann solver”. In: *J. Sci. Comput.* 18.6 (1997), pp. 1553–1570 (cit. on pp. 114, 119).

[17] C. Berthon and F. Marche. “A positive preserving high order VFRoe scheme for shallow water equations: a class of relaxation schemes”. In: *SIAM J. Sci. Comput.* 30.5 (2008), pp. 2587–2612 (cit. on p. 15).

[18] Maria Bjørnestad and Henrik Kalisch. “Shallow water dynamics on linear shear flows and plane beaches”. In: *Physics of Fluids* 29.7 (2017), p. 073602 (cit. on p. 13).

[19] P. Bonneton. “Modelling of periodic wave transformation in the inner surf zone”. In: *Ocean Engineering* 34.10 (2007), pp. 1459–1471 (cit. on p. 74).

[20] P. Bonneton et al. “A splitting approach for the fully nonlinear and weakly dispersive Green-Naghdi model”. In: *J. Comput. Phys.* 230.4 (2011), pp. 1479–1498 (cit. on pp. 75, 76, 80, 104, 106, 107).

[21] Philippe Bonneton et al. “Recent advances in Serre–Green Naghdi modelling for wave transformation, breaking and runup processes”. In: *European Journal of Mechanics-B/Fluids* 30.6 (2011), pp. 589–597 (cit. on p. 16).

[22] F. Bouchut. *Nonlinear stability of finite volume methods for hyperbolic conservation laws, and well-balanced schemes for sources*. Anglais. Frontiers in Mathematics. Birkhauser, 2004, p. 138 (cit. on pp. 117, 119).

[23] Christian Bourdarias, Stéphane Gerbi, and Ralph Lteif. “A numerical scheme for an improved Green–Naghdi model in the Camassa–Holm regime for the propagation of internal waves”. In: *Computers & Fluids* 156 (2017). Ninth International Conference on Computational Fluid Dynamics (ICCFD9), pp. 283–304 (cit. on p. 133).

[24] J Boussinesq. “Théorie des ondes et des remous qui se propagent le long d’un canal rectangulaire horizontal, en communiquant au liquide contenu dans ce canal des vitesses sensiblement pareilles de la surface au fond.” In: *Journal de Mathematiques Pures et Appliquees* 2 (1872), pp. 55–108 (cit. on p. 12).

[25] A. Castro and D. Lannes. “Fully nonlinear long-waves models in presence of vorticity”. In: *J. Fluid Mech.* 759 (2014), pp. 642–675 (cit. on pp. 17, 19, 105, 108, 109, 128, 131).

[26] A. Castro and D. Lannes. "Well-posedness and shallow water stability for a new hamiltonian formulation of the water waves equations with vorticity". In: *Indiana Univ. Math. J.* (2015) (cit. on pp. 105, 107).

[27] Angel Castro and David Lannes. "Fully nonlinear long-waves models in presence of vorticity". In: *arXiv preprint arXiv:1406.4096* (2014) (cit. on pp. 13, 36).

[28] Vincenzo Casulli. "Semi-implicit finite difference methods for the two-dimensional shallow water equations". In: *Journal of Computational Physics* 86.1 (1990), pp. 56–74 (cit. on p. 15).

[29] F. Chazel, D. Lannes, and F. Marche. "Numerical simulation of strongly nonlinear and dispersive waves using a Green-Naghdi model". In: *J. Sci. Comput.* 48 (2011), pp. 105–116 (cit. on pp. 16, 75, 76, 104, 107).

[30] Q. Chen. "Fully nonlinear Boussinesq-type equations for waves and currents over porous beds". In: *Journal of Engineering Mechanics* 132.2 (2006), pp. 220–230 (cit. on p. 105).

[31] Q. Chen and I. Babuska. "Approximate optimal points for polynomial interpolation of real functions in an interval and in a triangle". In: *Comput. Methods Appl. Mech. Engrg* 128 (1995), pp. 405–417 (cit. on pp. 81, 112).

[32] A. Chertock et al. "Well-balanced positivity preserving central-upwind scheme for the shallow water system with friction terms". In: *Int J Numer Methods Fluids* 78 (2015), pp. 355–383 (cit. on p. 15).

[33] D.Y. Choi, C.H. Wu, and C.-C. Young. "An efficient curvilinear non-hydrostatic model for simulating surface water waves". In: *Int J Numer Methods Fluids* 66 (2011), pp. 1093–1115 (cit. on p. 104).

[34] W. Choi. "Strongly nonlinear long gravity waves in uniform shear flows". In: *Phys. Rev. E* 68 (2003), p. 26305 (cit. on p. 109).

[35] Wooyoung Choi. "Strongly nonlinear long gravity waves in uniform shear flows". In: *Physical Review E* 68.2 (2003), p. 026305 (cit. on p. 13).

[36] R. Cienfuegos, E. Barthélemy, and P. Bonneton. "A fourth-order compact finite volume scheme for fully nonlinear and weakly dispersive Boussinesq-type equations. I: Model development and analysis". In: *Internat. J. Numer. Methods Fluids* 51.11 (2006), pp. 1217–1253 (cit. on pp. 16, 75, 104).

[37] B. Cockburn, S. Hou, and C.-W. Shu. "The Runge-Kutta local projection discontinuous Galerkin finite element method for conservation laws. IV. The multidimensional case". In: *Math. Comp.* 54.545–581 (1990) (cit. on p. 15).

[38] B. Cockburn and C.-W. Shu. "Runge-Kutta Discontinuous Galerkin Methods for Convection-Dominated Problems". In: *J. Sci. Comput.* 16.3 (2001), pp. 173–260 (cit. on pp. 61, 85, 116).

[39] B. Cockburn and C.-W. Shu. "The Local Discontinuous Galerkin method for time-dependent convection-diffusion systems". In: *SIAM J. Numer. Anal.* 141 (1998), pp. 2440–2463 (cit. on p. 15).

[40] B. Cockburn and C.-W. Shu. "TVB Runge-Kutta local projection discontinuous Galerkin finite element method for conservation laws. II. General framework". In: *Mathematics of Computation* 52 (1989), pp. 411–435 (cit. on p. 15).

[41] Bernardo Cockburn et al. "Superconvergence of the local discontinuous Galerkin method for elliptic problems on Cartesian grids". In: *SIAM Journal on Numerical Analysis* 39.1 (2001), pp. 264–285 (cit. on p. 15).

[42] Daniel Coutand and Steve Shkoller. "Well-posedness of the free-surface incompressible Euler equations with or without surface tension". In: *Journal of the American Mathematical Society* 20.3 (2007), pp. 829–930 (cit. on p. 20).

[43] W. Craig and C. Sulem. "Numerical simulation of gravity waves". In: *J. Comput. Phys.* 103 (1993), pp. 73–83 (cit. on p. 107).

[44] W. Craig et al. "Solitary water wave interactions". In: *Physics of fluids* 18.5 (2006) (cit. on p. 94).

[45] Walter Craig. "An existence theory for water waves and the Boussinesq and Korteweg-deVries scaling limits". In: *Communications in Partial Differential Equations* 10.8 (1985), pp. 787–1003 (cit. on p. 10).

[46] C.W. Curtis and H. Kalisch. "Interaction of a free surface with a vortex patch". In: *Wave Motion* 90 (2019), pp. 32–50 (cit. on p. 105).

[47] C. Dawson and J. Proft. "Coupling of continuous and discontinuous Galerkin methods for transport problems". In: *Comput. Methods Appl. Mech. Engrg* 191.3213-3231 (2002) (cit. on p. 15).

[48] M. Dehghan and M. Abbaszadeh. "The solution of nonlinear Green-Naghdi equation arising in water sciences via a meshless method which combines moving kriging interpolation shape functions with the weighted essentially non–oscillatory method". In: *Nonlinear science and numerical simulation* 68 (2018), pp. 220–239 (cit. on pp. 75, 104).

[49] D. A. Di Pietro and A. Ern. "Discrete functional analysis tools for discontinuous Galerkin methods with application to the incompressible Navier-Stokes equations". In: *Math. Comp.* 79.271 (2010), pp. 1303–1330 (cit. on p. 83).

[50] D. A. Di Pietro and A. Ern. *Mathematical Aspects of Discontinuous Galerkin Methods*. Vol. 69. Mathématiques and Applications. Springer, 2012 (cit. on pp. 15, 51–54, 81–83, 88, 89, 111, 112).

[51] D. A. Di Pietro and F. Marche. "Weighted interior penalty discretization of fully nonlinear and weakly dispersive free surface shallow water flows". In: *J. Comput. Phys.* 355 (2018), pp. 285–309 (cit. on pp. 16, 64, 75–77, 82, 84, 104, 105, 112).

[52] D. Di Pietro, A. Ern, and J.-L. Guermond. "Discontinuous Galerkin methods for anisotropic semi definite diffusion with advection". In: *SIAM J. Numer. Anal.* 46.2 (2008), pp. 805–831 (cit. on pp. 64, 81, 82, 112).

[53] H. Dong and M. Li. "A reconstructed central discontinuous Galerkin-finite element method for the fully nonlinear weakly dispersive Green-Naghdi model". In: *Applied Numerical Mathematics* 110 (2016), pp. 110–127 (cit. on pp. 75, 104).

[54] Jim Douglas and Todd Dupont. "Interior penalty procedures for elliptic and parabolic Galerkin methods". In: *Computing methods in applied sciences*. Springer, 1976, pp. 207–216 (cit. on p. 15).

[55] M. Dryja. "On discontinuous Galerkin methods for elliptic problems with discontinuous coefficients". In: *Comput. Methods Appl. Math.* 3.1 (2003), pp. 76–85 (cit. on pp. 81, 82, 112).

[56] Vincent Duchêne, Samer Israwi, and Raafat Talhouk. "A New Class of Two-Layer Green–Naghdi Systems with Improved Frequency Dispersion". In: *Studies in Applied Mathematics* 137.3 (2016), pp. 356–415 (cit. on p. 133).

[57] Vincent Duchêne, Samer Israwi, and Raafat Talhouk. "A New Fully Justified Asymptotic Model for the Propagation of Internal Waves in the Camassa–Holm Regime". In: *SIAM Journal on Mathematical Analysis* 47.1 (2015), pp. 240–290 (cit. on p. 133).

[58] Vincent Duchêne, Samer Israwi, and Raafat Talhouk. "Shallow water asymptotic models for the propagation of internal waves". In: *arXiv preprint arXiv:1306.1000* (2013) (cit. on p. 133).

[59] A. Duran and F. Marche. "A discontinuous Galerkin method for a new class of Green-Naghdi equations on unstructured simplicial meshes." In: *Appl. Math. Modelling* 45 (2017), pp. 840–864 (cit. on pp. 16, 17, 63, 67, 75, 85, 104, 120).

[60] A. Duran and F. Marche. "Discontinuous-Galerkin discretization of a new class of Green-Naghdi equations". In: *Commun. Comput. Phys.* 17.3 (2015), pp. 721–760 (cit. on pp. 63, 75, 76, 85, 104, 107, 120).

[61] A. Duran and F. Marche. "Recent advances on the discontinuous Galerkin method for shallow water equations with topography source terms". In: *Comput. Fluids* 101 (2014), pp. 88–104 (cit. on pp. 59, 84, 92, 120).

[62] Arnaud Duran and Fabien Marche. "Recent advances on the discontinuous Galerkin method for shallow water equations with topography source terms". In: *Computers & Fluids* 101 (2014), pp. 88–104 (cit. on p. 16).

[63] D. Dutykh et al. "Finite volume and pseudo-spectral schemes for fully-nonlinear 1D Serre equations". In: *Eur. J. Appl. Math.* 24 (2013), pp. 761–787 (cit. on pp. 75, 104).

[64] G.A. El, R.H.J. Grimshaw, and N.F. Smyth. "Unsteady undular bores in fully nonlinear shallow-water theory," in: *Phys. Fluids* 18 (2006) (cit. on p. 95).

[65] Kenneth Eriksson and Claes Johnson. "Adaptive finite element methods for parabolic problems I: A linear model problem". In: *SIAM Journal on Numerical Analysis* 28.1 (1991), pp. 43–77 (cit. on p. 15).

[66] Kenneth Eriksson and Claes Johnson. "Adaptive finite element methods for parabolic problems V: Long-time integration". In: *SIAM journal on numerical analysis* 32.6 (1995), pp. 1750–1763 (cit. on p. 15).

[67] Kenneth Eriksson, Claes Johnson, and Vidar Thomée. "Time discretization of parabolic problems by the discontinuous Galerkin method". In: *ESAIM: Mathematical Modelling and Numerical Analysis-Modélisation Mathématique et Analyse Numérique* 19.4 (1985), pp. 611–643 (cit. on p. 15).

[68] A. Ern and J.-L. Guermond. *Theory and practice of Finite Elements*. Vol. 159. Applied Mathematical Sciences. Springer, 2006 (cit. on p. 14).

[69] N. Favrie and S. Gavrilyuk. "A robust and rapid numerical method for dispersive models admitting a lagrangian : application to Serre-Green-Naghdi equations for long free surface gravity waves". In: *preprint* (2016) (cit. on pp. 75, 104).

[70] E.D. Fernandez-Nieto et al. "A hierarchy of dispersive layer-averaged approximations of Euler equations for free surface flows". In: *Communications in Mathematical Sciences* 16.5 (2018), pp. 1169–1202 (cit. on p. 13).

[71] A.G. Filippini, M. Kazolea, and M. Ricchiuto. "A flexible genuinely nonlinear approach for wave propagation, breaking and runup". In: *J. Comput. Phys.* 310 (2016), pp. 381–417 (cit. on pp. 75, 104).

[72] NC Freeman and RS Johnson. "Shallow water waves on shear flows". In: *Journal of Fluid Mechanics* 42.2 (1970), pp. 401–409 (cit. on p. 13).

[73] S. Gottlieb, C.-W. Shu, and Tadmor E. "Strong stability preserving high order time discretization methods". In: *SIAM Review* 43 (2001), pp. 89–112 (cit. on pp. 85, 115).

[74] A. E Green and P. M Naghdi. "A derivation of equations for wave propagation in water of variable depth". In: *Journal of Fluid Mechanics Digital Archive* 78.02 (1976), pp. 237–246 (cit. on pp. 12, 74, 104).

[75] S.T. Grilli et al. "Shoaling of solitary waves on plane beaches". In: *J. Wtrwy. Port Coast. and Oc. Engrg.* 120.6 (1994), pp. 609–628 (cit. on pp. 12, 99, 126, 127).

[76] Christian Grossmann, Hans-Görg Roos, and Martin Stynes. *Numerical treatment of partial differential equations*. Vol. 154. Springer, 2007 (cit. on p. 14).

[77] J.-L. Guermond et al. "Robust explicit relaxation technique for solving the Green-Naghdi equations". In: *J. Comput. Phys.* (2019) (cit. on pp. 75, 104).

[78] S. Guibourg. *Modélisation numérique et expérimentale des houles bidimensionnelles en zone cotière,* PhD Thesis, Université Joseph Fourier-Grenoble I, 1994 (cit. on p. 98).

[79] C. Guillopé, S. Israwi, and R. Talhouk. "Large-time existence for one-dimensional Green-Naghdi equations with vorticity". In: *Discrete Contin. Dyn. Syst. Ser. S* 14.8 (2021), pp. 2947–2974 (cit. on p. 105).

[80] P. Guyenne. "A high-order spectral method for nonlinear water waves in the presence of a linear shear current". In: *Computers and Fluids* 154 (2017), pp. 224–235 (cit. on p. 105).

[81] Emmanuel Hanert et al. "An efficient Eulerian finite element method for the shallow water equations". In: *Ocean Modelling* 10.1-2 (2005), pp. 115–136 (cit. on p. 15).

[82] A. Harten, P.D. Lax, and B. Van Leer. "On Upstream Differencing and Godunov-Type Schemes for Hyperbolic Conservation Laws". In: *SIAM Review* 25.1 (1983), pp. 35–61 (cit. on p. 114).

[83] Moritz Hauck et al. "Enriched Galerkin method for the shallow-water equations". In: *GEM-International Journal on Geomathematics* 11.1 (2020), pp. 1–25 (cit. on p. 15).

[84] T.R.J. Hughes and A. Brook. "Streamline upwind Petrov–Galerkin formulations for convection dominated flows with particular emphasis on the incompressible Navier–Stokes equations". In: *Comput. Methods Appl. Mech. Engrg* 32 (1982), pp. 199–259 (cit. on p. 14).

[85] S. Israwi. "Large time existence for 1D Green-Naghdi equations". In: *Nonlinear Analysis* 74.81-93 (2011) (cit. on pp. 74, 77).

[86] Pierre Jamet. "Galerkin-type approximations which are discontinuous in time for parabolic equations in a variable domain". In: *SIAM Journal on Numerical Analysis* 15.5 (1978), pp. 912–928 (cit. on p. 15).

[87] Robin Stanley Johnson. "A problem in the classical theory of water waves: weakly nonlinear waves in the presence of vorticity". In: *Journal of Nonlinear Mathematical Physics* 19.supp01 (2012), p. 1240012 (cit. on p. 13).

[88] D. Kay, V. Styles, and E. Sulli. "Discontinuous Galerkin finite element approximation of the Cahn-Hilliard equation with convection". In: *SIAM J. Numer. Anal.* 47.4 (2009), pp. 2660–2685 (cit. on p. 83).

[89] M. Kazakova and G. L. Richard. "A new model of shoaling and breaking waves: one-dimensional solitary wave on a mild sloping beach". In: *J. Fluid Mech.* 862 (2019), pp. 552–591 (cit. on pp. 17, 67, 71, 105, 109, 132).

[90] M. Kazolea, A.G. Filippini, and M. Ricchiuto. "A low dispersion finite volume/element method for nonlinear wave propagation, breaking and runup on unstructured meshes". In: *preprint* (2022) (cit. on p. 16).

[91] Christian Kharif and Malek Abid. "Nonlinear water waves in shallow water in the presence of constant vorticity: A Whitham approach". In: *European Journal of Mechanics-B/Fluids* 72 (2018), pp. 12–22 (cit. on p. 13).

[92] Christian Kharif, Malek Abid, and Julien Touboul. "Rogue waves in shallow water in the presence of a vertically sheared current". In: *Journal of Ocean Engineering and Marine Energy* 3.4 (2017), pp. 301–308 (cit. on p. 13).

[93] D.-H. Kim, P.J. Lynett, and S.A. Socolofsky. "A depth-integrated model for weakly dispersive, turbulent, and rotational fluid flows". In: *Ocean Modelling* 27 (2009) (cit. on p. 105).

[94] Alexander Kurganov. "Finite-volume schemes for shallow-water equations". In: *Acta Numerica* 27 (2018), pp. 289–351 (cit. on p. 15).

[95] D. Lannes. *The water waves problem: mathematical analysis and asymptotics*. Mathematical Surveys and Monographs 188. American Mathematical Society, 2013 (cit. on p. 104).

[96] D. Lannes and P. Bonneton. "Derivation of asymptotic two-dimensional time-dependent equations for surface water wave propagation". In: *Physics of fluids* 21 (2009), p. 016601 (cit. on pp. 74, 104).

[97] D. Lannes and F. Marche. "A new class of fully nonlinear and weakly dispersive Green-Naghdi models for efficient 2D simulations". In: *J. Comput. Phys.* 282 (2015), pp. 238–268 (cit. on pp. 16, 63, 75, 104).

[98] D. Lannes and F. Marche. "Nonlinear wave-current interactions in shallow water". In: *Stud. Appl. Math.* 136.4 (2016), pp. 382–423 (cit. on pp. 16, 105, 121, 125).

[99] David Lannes. *The water waves problem: mathematical analysis and asymptotics*. Vol. 188. American Mathematical Soc., 2013 (cit. on p. 74).

[100] David Lannes. "Well-posedness of the water-waves equations". In: *Journal of the American Mathematical Society* 18.3 (2005), pp. 605–654 (cit. on p. 10).

[101] David Lannes and Fabien Marche. "Nonlinear wave–current interactions in shallow water". In: *Studies in applied mathematics* 136.4 (2016), pp. 382–423 (cit. on pp. 13, 50, 51, 67, 101).

[102] P.D. Lax. *Hyberbolic Systems of Conservation Laws and the Mathematical Theory of Shock Waves*. SIAM, 1973 (cit. on p. 11).

[103] O. Le Métayer, S. Gavrilyuk, and S. Hank. "A numerical scheme for the Green-Naghdi model". In: *J. Comput. Phys.* 34.229 (2010), pp. 2034–2045 (cit. on pp. 75, 94, 95, 104).

[104] O. Le Métayer, S. Gavrilyuk, and S. Hank. "A numerical scheme for the Green–Naghdi model". In: *Journal of Computational Physics* 229.6 (2010), pp. 2034–2045 (cit. on p. 16).

[105] Randall J LeVeque et al. *Finite volume methods for hyperbolic problems*. Vol. 31. Cambridge university press, 2002 (cit. on p. 14).

[106] M. Li, L. Xu, and Y. Cheng. "A CDG-FE method for the two-dimensional Green-Naghdi model with the enhanced dispersive property". In: *J. Comput. Phys.* 399 (2019) (cit. on pp. 75, 104).

[107] Q. Liang and F. Marche. "Numerical resolution of well-balanced shallow water equations with complex source terms". In: *Advances in Water Resources* 32.6 (2009), pp. 873–884 (cit. on p. 78).

[108] M.S. Longuet-Higgins and R.W. Stewart. "Radiation stresses in water waves: a physical discussion, with applications". In: *Deep-Sea Research* 11 (1964), pp. 529–562 (cit. on p. 13).

[109] Lukas Lundgren and Ken Mattsson. "An efficient finite difference method for the shallow water equations". In: *Journal of Computational Physics* 422 (2020), p. 109784 (cit. on p. 15).

[110] G. Ma et al. "Non-hydrostatic modeling of wave interactions with porous structures". In: *Coastal Engineering* 91 (2014), pp. 84–98 (cit. on p. 13).

[111] Per A Madsen, Russel Murray, and Ole R Sorensen. "A new form of the Boussinesq equations with improved linear dispersion characteristics". In: *Coastal Engineering* 15.4 (1991), pp. 371–388 (cit. on p. 80).

[112] Per A Madsen and Ole R Sørensen. "A new form of the Boussinesq equations with improved linear dispersion characteristics. Part 2. A slowly-varying bathymetry". In: *Coastal engineering* 18.3-4 (1992), pp. 183–204 (cit. on p. 12).

[113] Ch G Makridakis and I Babuska. "On the stability of the discontinuous Galerkin method for the heat equation". In: *SIAM journal on numerical analysis* 34.1 (1997), pp. 389–401 (cit. on p. 15).

[114] L. Maojin et al. "High order well-balanced CDG-FE methods for shallow water waves by a Green-Naghdi model". In: *J. Comput. Phys.* 257, Part A.0 (2014), pp. 169–192 (cit. on pp. 75, 104).

[115] F. Marche. "Combined Hybridizable Discontinuous Galerkin (HDG) and Runge-Kutta Discontinuous Galerkin (RK-DG) formulations for Green-Naghdi equations on unstructured meshes". In: *J. Comput. Phys.* 418 (2021), p. 109637 (cit. on pp. 75, 104).

[116] V. Michel-Dansac. "A well-balanced scheme for the shallow-water equations with topography". In: *Computers and Mathematics with Applications* 72.3 (2016), pp. 568–593 (cit. on p. 15).

[117] J. Miles and R. Salmon. "Weakly dispersive nonlinear gravity waves". In: *J. Fluid Mech.* 157 (1985), pp. 519–531 (cit. on p. 12).

[118] D. Mitsotakis, B. Ilan, and D. Dutykh. "On the Galerkin/Finite-Element Method for the Serre Equations". In: *J. Sci. Comput.* 61.1 (2014), pp. 166–195 (cit. on pp. 16, 75, 94, 104).

[119] D. Mitsotakis, C.E. Synolakis, and M. McGuinness. "A modified Galerkin/finite element method for the numerical solution of the Serre-Green-Naghdi system". In: *Int J Numer Methods Fluids* (2016) (cit. on pp. 16, 75, 104).

[120] R. Mittal and G. Iaccarino. "Immersed boundary methods". In: *Annu. Rev. Fluid Mech.* 37 (2005), pp. 239–261 (cit. on p. 14).

[121] RM Moreira and JTA Chacaltana. "Vorticity effects on nonlinear wave–current interactions in deep water". In: *Journal of Fluid Mechanics* 778 (2015), pp. 314–334 (cit. on p. 13).

[122] R.E. Musumeci, I.A. Svendsen, and J. Veeramony. "The flow in the surf zone: a fully nonlinear Boussinesq-type of approach". In: *Coastal Engineering* 52 (2005), pp. 565–598 (cit. on p. 105).

[123] Rosaria E Musumeci, Ib A Svendsen, and Jayaram Veeramony. "The flow in the surf zone: a fully nonlinear Boussinesq-type of approach". In: *Coastal Engineering* 52.7 (2005), pp. 565–598 (cit. on p. 13).

[124] I.M. Navon. "Finite-element simulation of the shallow-water equations model on a limited-area domain". In: *Appl. Math. Modelling* 3 (1979) (cit. on p. 15).

[125] S. Noelle, Y. Xing, and C.-W. Shu. "High-order well-balanced finite volume WENO schemes for shallow water equation with moving water". In: *J. Comput. Phys.* 226.1 (2007), pp. 29–58 (cit. on p. 15).

[126] Okey Nwogu. "Alternative form of Boussinesq equations for nearshore wave propagation". In: *Journal of waterway, port, coastal, and ocean engineering* 119.6 (1993), pp. 618–638 (cit. on p. 12).

[127] N. Panda et al. "Discontinuous Galerkin methods for solving Boussinesq-Green-Naghdi equations in resolving non-linear and dispersive surface water waves". In: *J. Comput. Phys.* 273 (2014), pp. 572–588 (cit. on pp. 75, 104).

[128] J.D. Pearce and J.G. Esler. "A pseudo-spectral algorithm and test cases for the numerical solution of the two-dimensional rotating Green-Naghdi shallow water equations". In: *J. Comput. Phys.* 229 (2010), pp. 7594–7608 (cit. on pp. 75, 104).

[129] D Howell Peregrine. "Calculations of the development of an undular bore". In: *Journal of Fluid Mechanics* 25.2 (1966), pp. 321–330 (cit. on p. 16).

[130] D Howell Peregrine. "Interaction of water waves and currents". In: *Advances in applied mechanics* 16 (1976), pp. 9–117 (cit. on p. 13).

[131] D Howell Peregrine. "Long waves on a beach". In: *Journal of fluid mechanics* 27.4 (1967), pp. 815–827 (cit. on p. 12).

[132] S. Popinet. "A quadtree-adaptive multigrid solver for the Serre-Green-Naghdi equations". In: *J. Comput. Phys.* 302 (2015), pp. 336–358 (cit. on pp. 16, 75, 104).

[133] U. Putrevu and IB. ISvendsen. "Three-dimensional dispersion of momentum in wave-induced nearshore currents". In: *European Journal of Mechanics - B/Fluids* (1999), pp. 409–427 (cit. on p. 13).

[134] William H Reed and Thomas R Hill. *Triangular mesh methods for the neutron transport equation*. Tech. rep. Los Alamos Scientific Lab., N. Mex.(USA), 1973 (cit. on p. 15).

[135] M. Ricchiuto and A. Bollermann. "Stabilized residual distribution for shallow water simulations". In: *J. Comput. Phys.* 228 (2009), pp. 1071–1115 (cit. on p. 15).

[136] M. Ricchiuto and A.G. Filippini. "Upwind Residual discretization of enhanced Boussinesq equations for wave propagation over complex bathymetries". In: *J. Comput. Phys.* 271 (2014), pp. 306–341 (cit. on p. 94).

[137] G. L. Richard, A. Duran, and B. Fabrèges. "A new model of shoaling and breaking waves. Part 2. Run-up and two-dimensional waves". In: *J. Fluid Mech.* 867 (2019), pp. 146–194 (cit. on pp. 17, 67, 71, 75, 108, 132).

[138] G.L. Richard and S.L. Gavrilyuk. "Modelling turbulence generation in solitary waves on shear shallow water flows". In: *J. Fluid Mech.* 773 (2015), pp. 49–74 (cit. on p. 105).

[139] G.L. Richard and S.L. Gavrilyuk. "The classical hydraulic jump in a model of shear shallow-water flows". In: *J. Fluid. Mech.* 725 (2013), 492:521 (cit. on p. 109).

[140] Gaël Loic Richard and SL Gavrilyuk. "Modelling turbulence generation in solitary waves on shear shallow water flows". In: *Journal of Fluid Mechanics* 773 (2015), pp. 49–74 (cit. on p. 13).

[141] B. Rivière, M.F. Wheeler, and V. Girault. "A priori error estimates for finite element methods based on discontinuous approximation spaces for elliptic problems". In: *SIAM J. Numer. Anal.* 39.3 (2001), pp. 902–931 (cit. on p. 15).

[142] G. Russo. "Central schemes for conservation laws with application to shallow water equations". In: *Trends and applications of mathematics to mechanics : STAMM 2002*. Ed. by S. Rionero and G. Romano. Springer-Verlag Italia SRL, 2005, pp. 225–246 (cit. on p. 15).

[143] A.J.-C. de Saint-Venant. "Théorie du mouvement non-permanent des eaux, avec application aux crues des rivières et à l'introduction des marées dans leur lit". In: *C.R. Acad. Sci. Paris, Section Mécanique* 73 (1871), pp. 147–154 (cit. on pp. 11, 74).

[144] A. Samii and C. Dawson. "An explicit hybridized discontinuous Galerkin method for Serre–Green–Naghdi wave model". In: *Comput. Methods Appl. Mech. Engrg* 330 (2018), pp. 447–470 (cit. on pp. 75, 104).

[145] Dirk Schwanenberg and Jürgen Köngeter. "A discontinuous Galerkin method for the shallow water equations with source terms". In: *Discontinuous Galerkin Methods*. Springer, 2000, pp. 419–424 (cit. on p. 15).

[146] Fernando J Seabra-Santos, Dominique P Renouard, and André M Temperville. "Numerical and experimental study of the transformation of a solitary wave over a shelf or isolated obstacle". In: *Journal of Fluid Mechanics* 176 (1987), pp. 117–134 (cit. on p. 12).

[147] F Serre. "Contribution à l'étude des écoulements permanents et variables dans les canaux." In: *Houille Blanche* 8 (1953), pp. 374–388 (cit. on pp. 12, 74, 104).

[148] M.K. Sharifian, G. Kesserwani, and Y. Hassanzadeh. "A discontinuous Galerkin approach for conservative modelling of fully nonlinear and weakly dispersive wave transformations". In: *Ocean Modelling* (2018) (cit. on pp. 75, 104).

[149] F. Shi et al. "A high-order adaptive time-stepping TVD solver for Boussinesq modeling of breaking waves and coastal inundation." In: *Ocean Modelling* 43-44 (2012), pp. 36–51 (cit. on pp. 75, 104).

[150] R.J. Spiteri and S.J. Ruuth. "Non-linear evolution using optimal fourth-order strong-stability-preserving Runge-Kutta methods". In: *Math. Comput. Simulation* 62.1-2 (2003), pp. 125–135 (cit. on pp. 61, 85, 116).

[151] C.H. Su and C.S. Gardner. "Korteweg–de Vries equation and generalizations. III. Derivation of the Korteweg–de Vries equation and Burgers equation". In: *J. Math. Phys.* 10.3 (1969), pp. 536–539 (cit. on pp. 12, 74).

[152] Chau Hsing Su and Clifford S Gardner. "Korteweg-de Vries equation and generalizations. III. Derivation of the Korteweg-de Vries equation and Burgers equation". In: *Journal of Mathematical Physics* 10.3 (1969), pp. 536–539 (cit. on p. 12).

[153] C.E. Synolakis. "The runup of solitary waves". In: *J. Fluid. Mech.* 185 (1987), pp. 523–545 (cit. on pp. 100, 128).

[154] Costas Synolakis. "Standards, criteria, and procedures for NOAA evaluation of tsunami numerical models". In: (2007) (cit. on p. 97).

[155] GP Thomas. "Wave–current interactions: an experimental and numerical study. Part 2. Nonlinear waves". In: *Journal of Fluid Mechanics* 216 (1990), pp. 505–536 (cit. on p. 13).

[156] GP Thomas. "Wave-current interactions: an experimental and numerical study. Part 1. Linear waves". In: *Journal of Fluid Mechanics* 110 (1981), pp. 457–474 (cit. on p. 13).

[157] Sergey Tkachenko. "Analytical and numerical study of a dispersive shallow water model". PhD thesis. Aix-Marseille, 2020 (cit. on p. 95).

[158] Eleuterio F Toro. *Shock-capturing methods for free-surface shallow flows*. Wiley-Blackwell, 2001 (cit. on p. 14).

[159] T. Utnes. "A finite element solution of the shallow-water wave equations". In: *Appl. Math. Modelling* 14 (1990), pp. 20–29 (cit. on p. 15).

[160] Jayaram Veeramony and Ib A Svendsen. "The flow in surf-zone waves". In: *Coastal Engineering* 39.2-4 (2000), pp. 93–122 (cit. on p. 13).

[161] S. Vukovic. "ENO and WENO Schemes with the Exact Conservation Property for One-Dimensional Shallow Water Equations". In: *J. Comput. Phys.* 179.2 (2002), pp. 593–621 (cit. on p. 15).

[162] M. Walkley and M. Berzins. "A finite element method for the two-dimensional extended Boussinesq equations". In: *Internat. J. Numer. Methods Fluids* 39.10 (2002), pp. 865–885 (cit. on p. 96).

[163] G. Wei et al. "A fully nonlinear Boussinesq model for surface waves. Part 1. Highly nonlinear unsteady waves". In: *Journal of Fluid Mechanics* 294 (1995), pp. 71–92 (cit. on pp. 74, 75, 104).

[164] Ge Wei and James T Kirby. "Time-dependent numerical code for extended Boussinesq equations". In: *Journal of Waterway, Port, Coastal, and Ocean Engineering* 121.5 (1995), pp. 251–261 (cit. on p. 16).

[165] Mary Fanett Wheeler. "An elliptic collocation-finite element method with interior penalties". In: *SIAM Journal on Numerical Analysis* 15.1 (1978), pp. 152–161 (cit. on p. 15).

[166] J.M. Witting. "A unifed model for the Evolution of Nonlinear Water Waves". In: *J. Comput. Phys.* 56 (1984), pp. 203–236 (cit. on p. 80).

[167] S.B. Woo and P.L.-F. Liu. "A Petrov–Galerkin finite element model for one-dimensional fully non-linear and weakly dispersive wave propagation". In: *Int. J. Numer. Meth. Fluids* 37 (2001), pp. 541–575 (cit. on p. 16).

[168] Sijue Wu. "Well-posedness in Sobolev spaces of the full water wave problem in 2-D". In: *Inventiones mathematicae* 130.1 (1997), pp. 39–72 (cit. on p. 10).

[169] Sijue Wu. "Well-posedness in Sobolev spaces of the full water wave problem in 3-D". In: *Journal of the American Mathematical Society* 12.2 (1999), pp. 445–495 (cit. on p. 10).

[170] Y. Xing. "Exactly well-balanced discontinuous Galerkin methods for the shallow water equations with moving water equilibrium". In: *J. Comput. Phys.* 257 (2014), pp. 536–553 (cit. on p. 15).

[171] Y. Xing and X. Zhang. "Positivity-preserving well-balanced discontinuous Galerkin methods for the shallow water equations on unstructured triangular meshes". In: *J. Sci. Comput.* 57 (2013), pp. 19–41 (cit. on p. 92).

[172] Y. Xing, X. Zhang, and C.-W. Shu. "Positivity-preserving high order well-balanced discontinuous Galerkin methods for the shallow water equations". In: *Advances in Water Resources* 33.12 (2010), pp. 1476–1493 (cit. on pp. 85, 86, 106, 119, 120).

[173] Yulong Xing and Chi-Wang Shu. "High order well-balanced finite volume WENO schemes and discontinuous Galerkin methods for a class of hyperbolic systems with source terms". In: *Journal of Computational Physics* 214.2 (2006), pp. 567–598 (cit. on p. 15).

[174] Sung B Yoon and Philip L-F Liu. "Interactions of currents and weakly nonlinear water waves in shallow water". In: *Journal of fluid mechanics* 205 (1989), pp. 397–419 (cit. on p. 13).

[175] Hideaki Yosihara. "Gravity waves on the free surface of an incompressible perfect fluid of finite depth". In: *Publications of the Research Institute for Mathematical Sciences* 18.1 (1982), pp. 49–96 (cit. on p. 10).

[176] V.E. Zakharov. "Stability of periodic waves of finite amplitude on the surface of a deep fluid". In: *J. Appl. Mech. Tech. Phys* 2 (1968), pp. 190–194 (cit. on pp. 20, 107).

[177] M. Zefzouf and F. Marche. "A new Symmetric Interior Penalty Discontinuous Galerkin formulation for the Serre-Green-Naghdi equations". In: *submitted* (2022) (cit. on pp. 66, 113).

[178] X. Zhang and C.-W. Shu. "On maximum-principle-satisfying high order schemes for scalar conservation laws". In: *J. Comput. Phys.* 229.9 (2010), pp. 3091–3120 (cit. on pp. 85, 86).

[179] Y. Zhang et al. "Boussinesq-Green-Naghdi rotational water wave theory". In: *Coastal Engineering* 73 (2013), pp. 13–27 (cit. on p. 105).

[180] Y. Zhang et al. "Validation of Boussinesq–Green–Naghdi modeling for surf zone hydrodynamics". In: *Ocean Engineering* 111 (2016), pp. 299–309 (cit. on p. 104).

[181] Yao Zhang et al. "Rotational surf zone modeling for O (μ4) Boussinesq–Green–Naghdi systems". In: *Ocean Modelling* 79 (2014), pp. 43–53 (cit. on p. 13).

[182] Yao Zhang et al. "Validation of Boussinesq–Green–Naghdi modeling for surf zone hydrodynamics". In: *Ocean Engineering* 111 (2016), pp. 299–309 (cit. on p. 75).

[183] B.B. Zhao, W.Y. Duan, and R.C. Ertekin. "Application of higher-level GN theory to some wave transformation problems". In: *Coastal Engineering* 83 (2014), pp. 177–189 (cit. on p. 104).